Downloaded from orbit.dtu.dk on: May 02, 2024

DTU Library

CarboCell

a novel drug delivery system for the formulation of immunotherapeutics for cancer treatment

Chávez, Elizabeth Serrano

Publication date:
2022

Document Version
Publisher's PDF, also known as Version of record

Link back to DTU Orbit

Citation (APA):
Chávez, E. S. (2022). *CarboCell: a novel drug delivery system for the formulation of immunotherapeutics for cancer treatment*. DTU Health Technology.

General rights
Copyright and moral rights for the publications made accessible in the public portal are retained by the authors and/or other copyright owners and it is a condition of accessing publications that users recognise and abide by the legal requirements associated with these rights.

- Users may download and print one copy of any publication from the public portal for the purpose of private study or research.
- You may not further distribute the material or use it for any profit-making activity or commercial gain
- You may freely distribute the URL identifying the publication in the public portal

If you believe that this document breaches copyright please contact us providing details, and we will remove access to the work immediately and investigate your claim.

DTU Health Tech
Department of Health Technology

CarboCell: a novel drug delivery system for the formulation of immunotherapeutics for cancer treatment

PhD thesis

Elizabeth Serrano Chávez

Supervisors:

Jonas Rosager Henriksen
Anders Elias Hansen
Thomas Lars Andresen

March 2022

Preface

The work described in this PhD thesis is the result of three years of research conducted in the Colloids and Biological Interfaces (CBIO) group, which forms part of the Health Technology Department at the Technical University of Denmark (DTU). This work was performed from March 2019 to March 2022 under the main supervision of Associate Professor Jonas Rosager Henriksen and the support of Senior Researcher Anders Elias Hansen and Professor Thomas Lars Andresen as co-supervisors.

"Todos llevamos adentro una insospechada fuerza que emerge cuando la vida nos pone una prueba."

"We all have an unsuspected reserve of strength inside that emerges when life puts us to the test."

Isabel Allende

List of publications

The work conducted during this PhD project has resulted in two manuscripts and two patent applications.

Manuscripts:

I. **CarboCell, a novel delivery platform providing on-target sustained release of resiquimod prodrugs for effective intratumoral immunotherapy.**
Elizabeth Serrano-Chávez, Sophie B. Jensen, Martin Bak, Linda M. Bruun, Paul Kempen, Fredrik Melander, Anders E. Hansen, Jonas R. Henriksen, Thomas L. Andresen

II. **CarboCell combinatorial immunotherapy orchestrates sustained immune activation of the tumor microenvironment.**
Sophie B. Jensen, Elizabeth Serrano-Chávez, Trine B. Engel, Jennifer S. Jørgensen, Lars R. Petersen, Martin Bak, Linda M. Bruun, Paul Kempen, Fredrik Melander, Anders E. Hansen, Jonas R. Henriksen, Thomas L. Andresen

Patent applications:

I. **Dissacharide formulations for controlled drug release. Patent No. WO2020249801**
Thomas L. Andresen, Jonas R. Henriksen, Anders E. Hansen, Fredrik Melander, Elizabeth Serrano-Chávez, Linda M. Bruun.

II. **Prodrugs for prolonged sustained release and safety. Patent application**
Thomas L. Andresen, Jonas R. Henriksen, Anders E. Hansen, Martin Bak, Elizabeth Serrano-Chávez, Sophie B. Jensen, Anna Colliander.

Acknowledgements

My journey as a PhD student has been a true adventure, which would have not been the same without the help and support of many people. First, I would like to sincerely thank my main supervisor Associate Professor Jonas R. Henriksen for giving me the amazing opportunity to work in this project. Thank you for all your valuable guidance, support and all the enjoyable meetings and scientific discussions throughout the past three years. You always helped me to see there are no obstacles, but instead challenges and new opportunities and overall it has been a true pleasure to be a PhD student under your supervision. Special thanks go to my co-supervisor Senior Researcher Anders E. Hansen for all his feedback, guidance and help with the biological part of my project; I learned a lot from you and you always gave me new perspectives on the project. I would also like to thank my co-supervisor Professor Thomas L. Andresen for his valuable input and insights and for keeping an active research on the CarboCell.

I also owe many thanks to my colleagues at the CBIO group because they were an essential part to accomplish this work. A special thanks to PhD student Sophie B. Jensen for her valuable help in conducting practically all the *in vivo* studies presented in this thesis and for always sharing her data in a concise and timely manner. Moreover, I owe great gratitude to Researcher Fredrik Melander for being my mentor in the lab and introducing me to the world of the CarboCells; thank you for teaching me so many techniques and for your help with the cell assays regarding the R848 prodrugs. I would also like to thank Postdoc Linda M. Bruun for always providing me many carbohydrate esters and contrast agents for the CarboCell formulations, for all the help with the MALDI-TOF analysis and for answering my chemistry questions. Thanks also to Postdoc Martin Bak, who synthesized all the R848 prodrugs and for sharing his knowledge in chemistry with me. I would also like to express my gratitude to BSc student Emilie J. Petersen, who conducted most of the hydrophobic ion pairing experiments presented in this thesis. It was a pleasure to be your supervisor and thanks for your great attitude and all your hard work in the lab. Thanks to Associate Professor Paul Kempen for his help with the cryo-SEM imaging, the fruitful discussions and for organizing the “Food on a stick day!”. Additionally, thanks to PhD student Katrine Jønsson for teaching me several enzyme-based assays and for all our nice chats at the office. I would also like to thank PhD student Albert J. Fuglsang-Madsen for all the nice discussions about science, music and games in the lab, and for being my CarboCell buddy. Thanks also to PhD student Hólmfridur R. Halldórsdóttir for her support in several *in vivo* studies, I hope we can keep collaborating in the future. Furthermore, a special thank you to Laboratory Technicians Lene Hubert, Lotte Nielsen, Ole Kristoffersen and Helene Ringvig for their constant support in keeping things running in the lab. Overall, I want to thank all my colleagues at the CBIO group for the nice working environment and making workdays fun and enjoyable!

Moreover, I want to express my deepest gratitude to my all my friends and family. Your friendship and support throughout this journey that even included a global pandemic meant the world to me. A big shout out to my dearest friends Ugne, Ashton, Jakob, Rodrigo, Saúl and Ida for making Denmark feel as home. Importantly, I owe the most to my wonderful and loving boyfriend Edgar. There are not enough words to thank you for your tremendous support and love that goes beyond the last three years, I would have not made this without you – I love you. I would also like to express the most loving thank you to my dad, my brother and my little sister. You have always inspired me to give my best and I am grateful for your unconditional love and support. Last, but never least, I want to dedicate this work to my beloved mom, I know you would be very proud. This one is for you, thanks for giving me the wings to fly.

Abstract and thesis outline

Immunotherapy has emerged as a revolutionary cancer treatment and an encouraging alternative to traditional cancer therapies as surgical resection, radiotherapy and chemotherapy. Cancer immunotherapy is focused on generating and enhancing an anti-cancer immune response in the body of the patient that is both effective and durable. However, in the current clinical practice, only a small fraction of patients are respondent to cancer immunotherapy. Moreover, most of the immunotherapies are systemically administered, which is often associated with severe toxic effects particularly for therapies aimed at activating and bridging the innate and adaptive immune responses. Intratumoral administration can be a useful alternative strategy, but low injection reproducibility, rapid drug clearance from tumors and drug leakage into systemic circulation can negatively affect the therapeutic response and compromise patient safety.

We have developed the CarboCell drug delivery system to address the aforementioned challenges for intratumoral immunotherapy. CarboCell is comprised of three main components: (i) a carbohydrate ester, (ii) a co-solvent, and (iii) a solvent, which form a low viscosity fluid. Upon injection, CarboCell self-assembles as a highly viscous depot that acts as both drug reservoir and localization marker. CarboCell provides a sustained drug release that can enable continuous immune stimulation of the tumor microenvironment while minimizing systemic drug exposure, in addition to secure accurate and reproducible intratumoral injections. This project was focused on the formulation and delivery of Toll-like receptors 7/8 agonists, particularly resiquimod (R848), and the transforming growth factor-β (TGF-β) inhibitor RepSox, which are water-insoluble drugs. The present PhD thesis describes the characterization and formulation development of the CarboCell as well as its *in vivo* therapeutic efficacy in murine models.

In Chapter 2, the drug stability of R848 in the CarboCell was investigated. The chemical stability of R848 was evaluated in multiple CarboCell formulations, at different temperatures and in the presence of benzoic acid (BA) or trimethylamine. It was observed that R848 was susceptible to chemical modifications resulting from interactions with some carbohydrate esters. The type of carbohydrate ester played a key role in R848 stability, where non-reducing carbohydrates esters comprising benzoate groups promoted the stability of R848. Also, R848 was less reactive when adding BA to the formulation and upon storage at low temperatures (≤ 4°C). R848 showed excellent short-term stability in CarboCells comprising sucrose octabenzoate (SuBen), so SuBen was deemed as the main carbohydrate ester for subsequent formulations.

Chapter 3 contains a manuscript to be submitted to the Journal of Controlled Release, presented in its intended submission format. In such manuscript, the characterization, formulation and delivery of five novel R848 prodrugs is described. R848 and R848 prodrugs were formulated in various CarboCells

that were tested both *in vitro* and *in vivo*. CarboCell was able to provide sustained drug release, which could be tailored based on both the chemical composition of the CarboCell and drug hydrophobicity. Moreover, the incorporation of a novel computed tomography (CT) contrast agent named CLA-8 was evaluated. CLA-8 provided excellent CT contrast to the CarboCell depot thus highlighting the application of CarboCell as localization marker for image-guided injections and subsequent monitoring. Intratumoral injections with R848 and the R848 prodrugs were well tolerated and significantly increased the median survival time of mice bearing CT26 tumors.

Chapter 4 describes the simultaneous formulation and co-delivery of R848 and RepSox from CarboCells. The multi-drug therapy enhanced the therapeutic response in mice compared to the R848 monotherapy. Furthermore, the combination treatment induced both a local and systemic anti-cancer response. Moreover, an improved CarboCell formulation was developed in which the drug-releasing period was doubled. Thus, the interval between injections was extended from 7 to 14 days thus reducing by half the number of injections per treatment. By increasing the SuBen to co-solvent ratio in the CarboCell, the viscosity and hydrophobicity of the self-formed depot was increased resulting in an overall slower drug release. The results of the *in vivo* efficacy in mice for the extended release formulation were equivalent to those of the original CarboCell.

Chapter 5 comprises multiple characterization studies of numerous CarboCell compositions aimed at gaining further knowledge and understanding of the system. Overall, the data showed a correlation between viscosity, solvent diffusion and drug release. It was observed that the drug burst release was highly dependent on the amount and type of solvent in the CarboCell. In contrast, the long-term release profile was generally influenced by the type of carbohydrate ester and co-solvent as well as the ratio between them. In addition, two sterilization methods were tested: steam sterilization via autoclave and gamma irradiation. The latter was better at maintaining the chemical drug stability in the CarboCells; however, gamma irradiation also caused the modification of 3 to 5% of the CLA-8 in the formulation.

In Chapter 6, hydrophobic ion-pairing (HIP) was investigated as a formulation strategy to enable the solubilization of hydrophilic charged drugs in the CarboCell. The fluorescent dye indocyanine green (ICG), a hydrophilic anionic molecule, was used as a model molecule. HIP complexation of ICG with several co-ions was successfully done using the Bligh-Dyer method. The solubility of ICG in the CarboCell was significantly improved when formulated as a HIP complex. Furthermore, the release of ICG could be tailored depending on the type and concentration of the co-ion as well as the chemical composition of the CarboCell. Lastly, an *in vivo* test in rats showed that CarboCells containing ICG-HIP complexes might be used as markers for near-infrared (NIR) fluorescence imaging applications.

Dansk resumé

Immunterapi har vist sig at være en revolutionerende kræftbehandling og et lovende alternativ til traditionelle kræftbehandlinger som kirurgisk resektion, strålebehandling og kemoterapi. Kræftimmunterapi er fokuseret på at generere- og forstærke et anti-cancer immunrespons i patientens krop, som er både effektiv og holdbar. I den nuværende kliniske praksis er det dog kun en lille del af patienterne, der responderer på cancerimmunterapi. Desuden indgives de fleste immunterapier systemisk, hvilket ofte er forbundet med alvorlige toksiske bivirkninger, især for terapier, der sigter mod at aktivere- og bygge bro mellem de medfødte og adaptive immunresponser. Intratumoral indgivelse kan være en nyttig alternativ strategi, men lav injektionsreproducerbarhed, hurtig lægemiddelclearance fra tumorer og lægemiddellækage til systemisk cirkulation kan påvirke det terapeutiske respons negativt og kompromittere patientsikkerheden.

Vi har udviklet CarboCell-lægemiddelleveringssystemet til at løse de førnævnte udfordringer for intratumoral immunterapi. CarboCell består af tre hovedkomponenter: (i) en kulhydratester, (ii) et co-opløsningsmiddel og (iii) et opløsningsmiddel, som danner en væske med lav viskositet. Ved injektion former CarboCell sig som et meget viskøst depot, der fungerer som både lægemiddelreservoir og lokaliseringsmarkør. CarboCell giver en vedvarende lægemiddelfrigivelse, der muliggører kontinuerlig immunstimulering af tumormikromiljøet og samtidig minimerer systemisk lægemiddeleksponering, foruden at sikre nøjagtige og reproducerbare intratumorale injektioner. Dette projekt var fokuseret på formulering og levering af Toll-like receptorer 7/8 agonister, især resiquimod (R848), og den transformerende vækstfaktor-β (TGF-β) inhibitor RepSox, som er vanduopløselige lægemidler. Denne ph.d.-afhandling beskriver karakteriseringen, formuleringsudviklingen og den *in vivo* terapeutiske effekt i musemodeller.

I kapitel 2 blev lægemiddelstabiliteten af R848 i CarboCell undersøgt. Den kemiske stabilitet af R848 blev evalueret i flere CarboCell-formuleringer, ved forskellige temperaturer og i benzoesyre (BA) eller trimethylamin. Det viste sig at R848 var modtagelig for kemiske modifikationer som følge af interaktioner med nogle af kulhydratesterene. Typen af kulhydratester var dermed vigtigt for R848-stabiliteten, hvor ikke-reducerende kulhydratestere indeholdende benzoatgrupper fremmede stabiliteten af R848. R848 var også mindre reaktiv ved tilsætning af BA til formuleringen og ved opbevaring ved lave temperaturer (≤ 4°C). R848 udviste fremragende korttidsstabilitet i CarboCells indeholdende saccharoseoctabenzoate (SuBen), så SuBen blev anset for at være den bedste kulhydratester for CarboCell formuleringer af R848.

Kapitel 3 indeholder et manuskript, der indsendes til Journal of Controlled Release, præsenteret i det tilsigtede indsendelsesformat. I dette manuskript beskrives karakteriseringen, formuleringen og leveringen af fem nye R848 prodrugs. R848 og R848 prodrugs blev formuleret i forskellige CarboCells,

der blev testet både *in vitro* og *in vivo*. CarboCell var i stand til at levere vedvarende lægemiddelfrigivelse, hvor frigivelsesprofilen kunne skræddersyes baseret på den kemiske sammensætning af CarboCell og lægemidlets hydrofobicitet. Desuden blev inkorporeringen af et nyt computertomografi (CT) kontrastmiddel ved navn CLA-8 evalueret. CLA-8 gav fremragende CT-kontrast til CarboCell-depotet, hvilket fremhævede anvendelsen af CarboCell som lokaliseringsmarkør til billedstyrede injektioner og efterfølgende monitorering. Intratumorale injektioner med R848 og R848 prodrugs blev godt tolereret og øgede den gennemsnitlige overlevelsestid signifikant for mus med CT26-tumorer.

Kapitel 4 beskriver sam-formulering og samlevering af R848 og RepSox fra CarboCells. Multilægemiddelbehandlingen forbedrede den terapeutiske respons hos mus sammenlignet med R848-monoterapi. Desuden inducerede kombinationsbehandlingen både et lokalt og systemisk anti-cancer-respons. Derudover blev der udviklet en forbedret CarboCell-formulering, hvor lægemiddel-frigivelsesperioden blev fordoblet. Intervallet mellem injektioner blev således forlænget fra 7 til 14 dage, hvilket halverede antal injektioner per behandling. Ved at øge forholdet mellem SuBen og co-opløsningsmiddel i CarboCell, blev viskositeten og hydrofobiciteten af det selvdannede depot øget, hvilket resulterede i en samlet langsommere frigivelse af lægemiddel. Resultaterne af *in vivo*-effektiviteten hos mus for formuleringen med forlænget frigivelse var ækvivalente med resultaterne af den originale CarboCell.

Kapitel 5 omfatter flere karakteriseringsstudier af adskillige CarboCell-sammensætninger med det formål at opnå yderligere viden og forståelse af systemet. Samlet set viste data en sammenhæng mellem viskositet, opløsningsmiddeldiffusion og lægemiddelfrigivelse. Det blev observeret, at medicinsprængningsfrigivelsen var meget afhængig af mængden og typen af opløsningsmiddel i CarboCell. I modsætning hertil var den langsigtede frigivelsesprofil generelt påvirket af typen af kulhydratester og co-opløsningsmiddel samt forholdet mellem dem. Derudover blev to steriliseringsmetoder testet: dampsterilisering via autoklave og gammabestråling. Sidstnævnte var bedre til at opretholde den kemiske lægemiddelstabilitet i CarboCells af de testede stoffer; gamma-bestråling forårsagede imidlertid også modifikationen af 3 til 5 % af CLA-8 i formuleringen.

I kapitel 6 blev hydrofob ion-parring (HIP) undersøgt som en formuleringsstrategi for at muliggøre opløsning af hydrofile og ionisérbare lægemidler i CarboCell. Det fluorescerende farvestof indocyaningrøn (ICG), et hydrofilt anionisk molekyle, blev brugt som et modelmolekyle. HIP-kompleksering af ICG med flere modioner blev udført med succes ved hjælp af Bligh-Dyer-metoden. Opløseligheden af ICG i CarboCell blev væsentligt forbedret, når den blev formuleret som et HIP-kompleks. Ydermere kunne frigivelsen af ICG skræddersyes afhængigt af typen og koncentrationen af modion samt den kemiske sammensætning af CarboCell. Endelig viste en *in vivo*-test i rotter, at CarboCells indeholdende ICG-HIP-komplekser kan bruges som markører til nær-infrarød (NIR) fluorescensbilleddannelsesapplikationer.

Abbreviations

σ-SuBen	Sucrose benzoate manufactured by Sigma-Aldrich
π-Suben	Purified sucrose benzoate
ADA	Anti-drug antibody
APC	Antigen-presenting cell
ATC	Adoptive T cell transfer
AUC	Area under the curve
BA	Benzoic acid
BCG	Bacillus Calmette-Guérin
BENA	Benethamine
BenOH	Benzyl alcohol
CAR	Chimeric antigen receptor
CBIO	Colloids and Biological Interfaces
CC	CarboCell
CeO	Cerium oxide
CLA-8	Lactose octa para-iodobenzoate
CMC	Critical micelle concentration
COC	Cyclic olefin copolymer
COP	Cyclic olefin polymer
CT	Computed tomography
CTAB	Cetyltrimethyl ammonium bromide
CTLA4	Cytotoxic T lymphocyte antigen 4
DAMP	Danger-associated molecular pattern
DC	Dendritic cell
DDA	Dodecylamine
DDS	Drug delivery system
DHB	2,5-dihydroxy benzoic acid
DMSO	Dimethyl sulfoxide
ECM	Extracellular matrix
EDTA	Ethylenediaminetetraacetic acid
EPR	Enhanced permeability and retention
EtOH	Ethanol
Et-Myr	Ethyl myristate
Et-Pal	Ethyl palmitate
Et-Ste	Ethyl stearate
GTH	Glyceryl trihexanoate
GTO	Glyceryl trioctanoate
GRAS	Generally recognized as safe
HER2	Human epidermal growth factor receptor 2
HIP	Hydrophobic ion pairing
HPLC	High performance liquid chromatography
ICG	indocyanine green
ICH	International Council for Harmonization
ICI	Immune checkpoint inhibitor
IFN	Regulatory interferon
IGRT	Image guided radiation therapy
LacBen	Lactose octaisobutyrate
LCMS	Liquid chromatography – mass spectrometry
LOIB	Lactose octaisobutyrate
LOP	Lactose octapropionate
MeLOIB	Methoxy-LOIB
MeCN	Acetonitrile
MHC	Major histocompatibility complex

MRI	Magnetic resonance imaging
NIR	Near-infrared
NK	Natural killer
NMP	N-methyl-2-pyrrolidone
NMR	Nuclear magnetic resonance
PAMP	Pathogen-associated molecular pattern
PBS	Phosphate-buffered saline
PC	Propylene carbonate
PD1	Programmed cell death 1
PRR	Pattern-recognition receptor
PLA	Poly(lactic acid)
PLGA	Poly(lactic-co-glycolic acid)
PLGF2	Placental growth factor 2
RaBen	Raffinose octabenzoate
ROIB	Raffinose octaisobutyrate
ROS	Reactive oxygen species
R848-IBA	R848-isobutyrate
SAIB	Sucrose acetate isobutyrate
SEAP	Secreted embryonic alkaline phosphatase
SOIB	Sucrose octaisobutyrate
SuBen	Sucrose octabenzoate
T0	Time zero
TAA	Tumor-associated antigen
TCR	T cell receptor
TEA	Trimethylamine
TEAB	Tetraethyl ammonium bromide
TFA	Trifluoroacetic acid
TGF	Transforming growth factor
TGF-β	Transforming growth factor-β
TGF-BRI/II	TGF-β serine/threonine kinase receptors
TLR	Toll-like receptor
TLRa	Toll-like receptor agonist
TLR7/8a	Toll-like receptor 7/8 agonist
TME	Tumor microenvironment
TOAB	Tetraoctyl ammonium bromide
TOIB	Trehalose octaisobutyrate
T_{reg}	Regulatory T cells
UHPLC	Ultra high performance liquid chromatography
USP	United States Pharmacopeia
W/O	Water-in-oil
w/w	Weight/weight

Table of contents

Chapter 1. Introduction

1.1 Cancer and conventional cancer therapies

Cancer stands as the second most common cause of death in the world [1]. According to the International Agency for Research on Cancer, there were around 19 million new cancer cases and nearly 10 million cancer deaths in 2020 alone worldwide [2]. These numbers are only expected to increase overtime, with an estimate of more than 27 million new cancer cases by 2040 [1]. Cancer is a limiting factor on increasing life expectancy and a big financial load in every country around the globe [1], [2]. Thus, scientific research on new cancer therapeutic strategies are of great interest to cover the unmet need for effective therapies and overcome the cancer burden.

1.1.1 The biology of cancer

Cancer encompasses a group of diseases characterized by the uncontrolled growth of cells in any given tissue. Such abnormal cell proliferation is the result of a multistep process arising from genetic alterations [3], [4]. While there are more than 100 different cancer types, it has been proposed that the overall progression of a normal cell into a malignant cancer cell follows eight key physiological changes. These are referred to as cancer hallmarks and they describe the acquired capabilities of malignant cells [4], [5]. Originally, six hallmarks were suggested as the foundation for rationalizing the biology of cancer cells: self-sufficiency in growth signals, insensitivity to anti-growth signals, evasion of apoptosis, limitless replicative potential, sustained angiogenesis and tissue invasion and metastasis [4]. Later, the hallmarks were updated to include two additional capabilities, namely avoiding immune destruction and deregulating cellular energetics (Fig. 1) [5].

Altogether, the cancer hallmarks define the means by which cancer cells are able to survive, grow and disseminate in the body. In this process, two essential characteristics have been described as enablers of the cancer pathogenesis [5]. The first enabling factor is genomic instability, which causes random mutations that ultimately lead a normal cell to acquire abnormal cancer capabilities. The second enabling characteristic is tumor-promoting inflammation [5]; paradoxically, inflammatory immune cells can facilitate tumor growth by different mechanisms such as accelerating mutations by releasing reactive oxygen species [6]. While cancer cells constitute the foundation of the disease, the tumor microenvironment (TME), which consists of a heterogeneous population of cells (cancerous and non-cancerous), has also been listed as a key contributing factor to tumorigenesis [5]. The complex role of the TME will be described in detail later in the text.

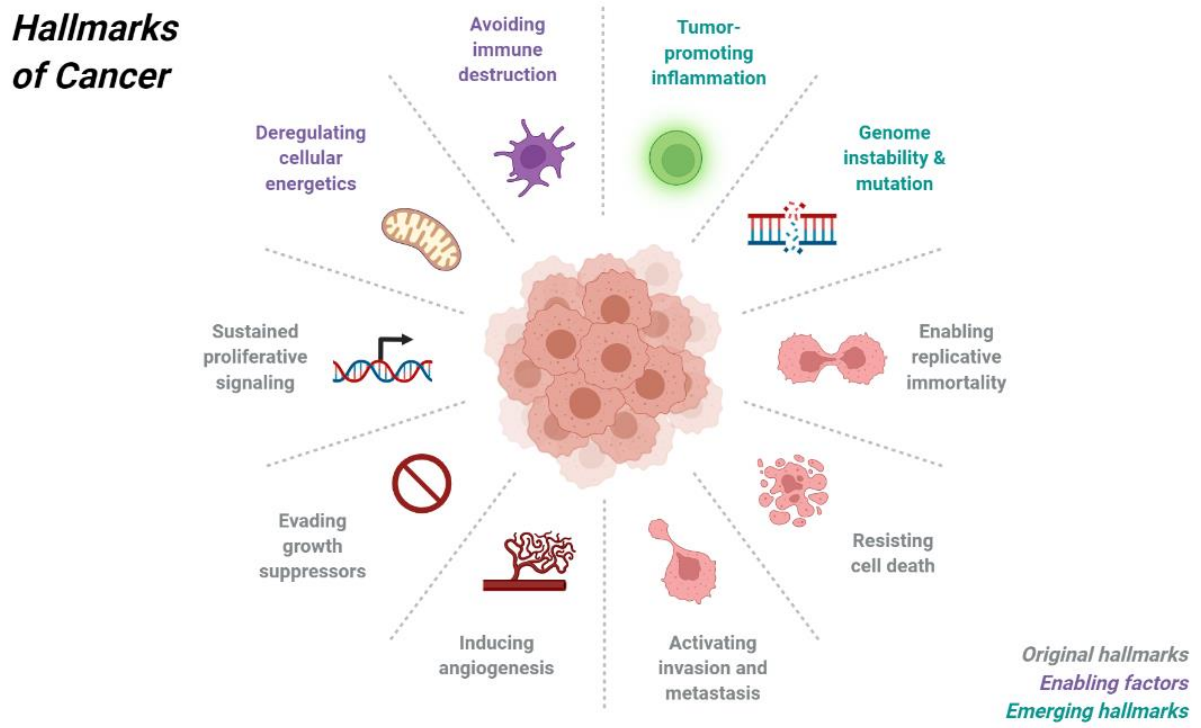

Figure 1. Hallmarks of cancer. Overview of the hallmarks of cancer and their enabling factors as described in [5]. (The illustration was created with Biorender.com).

1.1.2 Traditional cancer therapeutic strategies

Once cancer has been diagnosed, the treatment options depend on the cancer type, tumor location and the stage of progression [7]. Though cancer is a complex disease, three traditional treatment methods stand as the core cancer therapies: surgical resection, radiotherapy and chemotherapy [8]. These treatments can be applied as a stand-alone therapy or in combination. Nonetheless, despite their regular practice, these traditional therapies are often accompanied with limitations and side effects [8], [9].

Surgical resection is a preferred clinical treatment for many solid tumors. Throughout the years, the advancements in instrumentation and surgical techniques have improved the therapeutic outcome of surgery [10], [11]. In a successful surgical treatment, the complete cancerous tissue can be removed, which is curative as long as there is no metastatic disease. As an additional advantage, damage to the healthy tissue in the rest of the body is minimized [7]. Nevertheless, malignant tumors display highly invasive growth patterns, so there is a risk that residual cancer cells might remain in the surgical periphery. These residual cancer cells can serve as the basis for both cancer recurrence and progression, which increases mortality [11], [12].

Chemotherapy involves the administration of one or more drugs that kill the cancer cells by interfering with their cell cycle or metabolic activity [13], [14]. Chemotherapeutic drugs are often administered systemically, which can be beneficial for patients with unresectable tumors or metastatic cancer [9]. However, chemotherapeutic agents do not make clear distinctions between healthy and malignant tissue, so normal cells with fast division cycles (such as bone marrow cells and intestinal cells) are also

killed to some extent during the treatment. This translates into severe adverse effects in the cancer patient [8], [13]. Additionally, chemotherapy needs to be given in repeated intervals or cycles; and sometimes despite the constant systemic drug exposure, chemotherapeutic drugs can fail to reach a sufficient therapeutic concentration in the cancerous tissue [13].

In radiotherapy, cancer cells are killed through ionizing radiation. Radiotherapy relies on producing reactive oxygen species and damage to the DNA of cancer cells, which leads to cycle cell alterations and ultimately, apoptosis [15]. In contrast to chemotherapy, radiotherapy can be directed to a specific area in the body. Radiotherapy is usually delivered by an external beam, but radioactivity sources (e.g., radioactive metals) can also be directly implanted in tumors, a procedure referred as brachytherapy [15], [16]. Despite tremendous advances in irradiation technologies and instrumentation, side effects to normal tissue remain a challenge [8], [15], [17].

1.2 Cancer immunotherapy

According to the immune surveillance hypothesis, the immune system is on a constant lookout for genetically altered cells, just as it does for pathogens [18]. Thus, the immune system can sometimes recognize cancer cells as abnormal and raise an effective immune attack against them. This process occurs through a series of steps that has been referred to as the cancer-immunity cycle (Fig. 2) [19].

The cycle starts by the release of cancer-associated antigens produced by the cancer cell due its genomic alterations [20]. These antigens can then be captured by antigen-presenting cells (APCs) such as dendritic cells (DCs). The APCs process the antigens and present them to naïve T cells via the major histocompatibility complex (MHC), an event that occurs in lymphatic tissues. This causes the priming and activation of T cells, which acquire effector functions against the cancer-specific antigens. Next, the effector T cells migrate to the tumor site through the blood vessels and start infiltrating the tumor. Here, the T cells may be able to recognize the malignant cells and eliminate them, which causes a further release of antigens and cytokines, which fuels the immunity cycle. Hence, the repetition of the cycle amplifies and broadens the anti-cancer response [19], [20].

However, the cancer-immunity cycle is often hindered in cancer patients. Solid cancers represent a significant challenge for the immune system because they have multiple mechanisms to avoid immune-mediated detection and eradication [5]. Immunotherapy is therefore aimed at modulating the immune response to recognize and eliminate cancer cells.

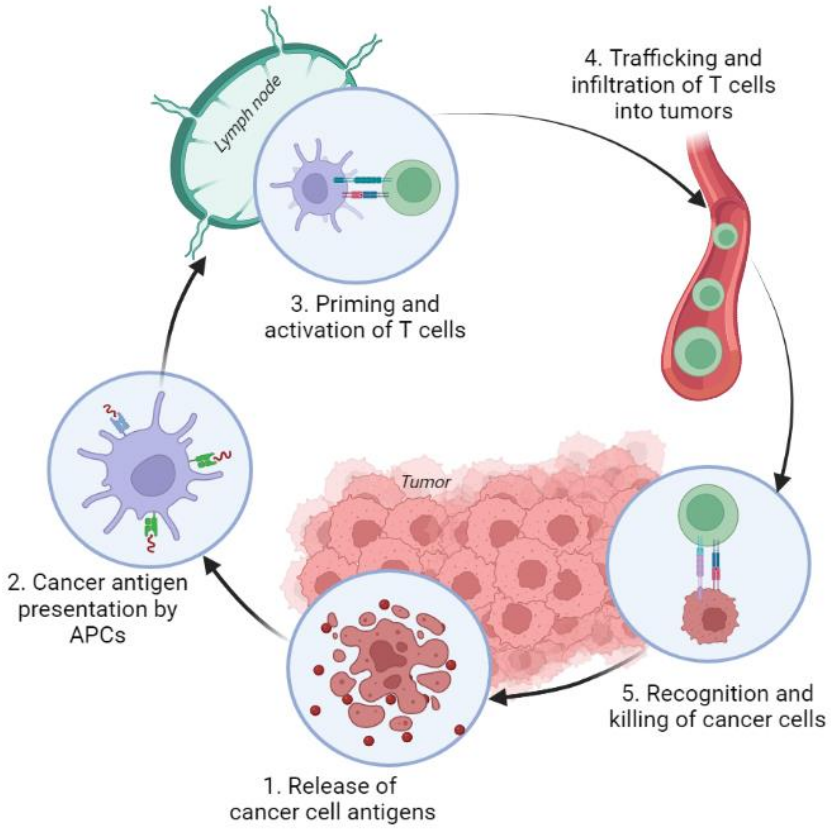

Figure 2. The cancer-immunity cycle. The immune response against cancer cells is produced through a multi-step process that starts with the detection of neo-antigens and finalizes with the elimination of tumor cells Abbreviation: APCs: antigen-presenting cells. (Illustration inspired by [19] and created with Biorender.com).

Over the last decades, immunotherapy has become a promising strategy in the fight against cancer [21]. In contrast to the traditional treatments, which focus on directly damaging the cancer cells, immunotherapy is focused on using the capacity of the immune cells to kill and eradicate cancer cells. In immunotherapy, the goal is to generate an anti-cancer immune response in the body of the patient that is both durable and effective [21], [22].

Examples of the most prominent cancer immunotherapies include immune checkpoint blockade, adoptive T cell transfer (ATC) and cancer vaccines [22]. Nonetheless, the arsenal of immunotherapeutic strategies is constantly growing [23]. The great diversity of factors involved in the cancer-immunity cycles gives a wide range of options for therapeutic targets [19], [21]. In the following sections, the immunotherapeutic strategies most relevant for this project will be described.

1.2.1 Immune checkpoint blockade

Before the immune system can exert an effect on cancer cells, T lymphocytes need to be activated. T cell activation requires the interaction between the lymphocytes and antigen-presenting cell (APC) [24]. Such interaction is facilitated in the lymphocytes by a surface protein complex denominated as the T cell receptor (TCR). The TCR is able to recognize antigens presented by an APC through the major histocompatibility complex (MHC). Besides antigen stimulation of the TCR, an additional co-stimulatory signal is needed. CD28 is a co-stimulatory receptor also present on the surface of T cells. The ligands

of CD28, CD80 and CD86, are found on the surface of APCs. Therefore, T cell activation occurs once the TCR binds to the antigen-MHC conjugate of the APC, while CD28 interacts with its respective co-stimulatory ligands (Fig. 3) [22], [24].

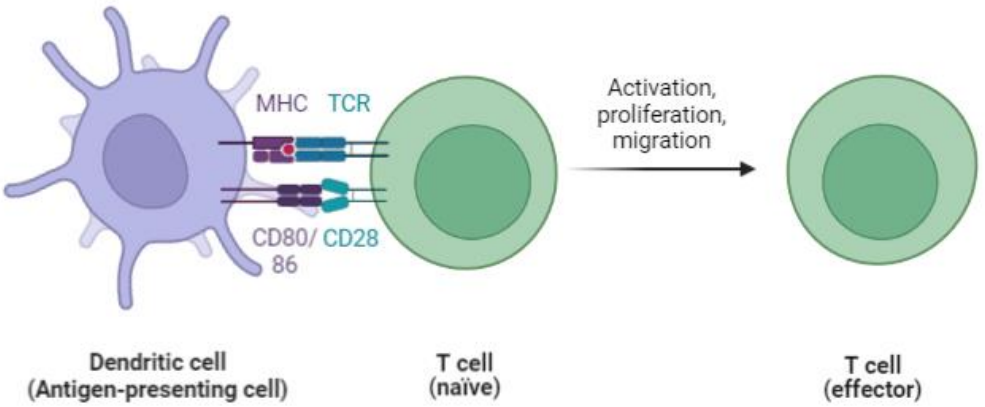

Figure 3. Activation of T cells. Scheme of T cell activation via the immunological conjugate formed between an APC and a naïve T cell. (Illustration created with Biorender.com).

In order to modulate the immune response and prevent hyperactivation, T cells possess inhibitory regulators that function as 'checkpoint molecules'. The most prominent examples of such molecules are cytotoxic T lymphocyte antigen 4 (CTLA4) and programmed cell death 1 (PD1) [25]. Each one has different biological functions, conducted at distinct parts of the body and at different time points in the lifespan of T cells. Thus, CTLA4 and PD1 have complementary roles, whose common objective is to ensure that the T cell responses are self-tolerant, but at the same time that they are effective enough to give protection against pathogens and neoplasia [22], [26].

Prior to activation, the expression of CTLA4 is very low in naïve T cells, in addition to being contained in intracellular vesicles. Early after activation, CTLA4 expression in T cells increases and CTLA4 moves to the cell surface, a process that mainly occurs within the lymphoid organs [22]. CTLA4 is a biochemically and structurally similar receptor as CD28. For this reason, CTLA4 can also bind to CD80/86, the same ligands as CD28. Nevertheless, an important difference is that CTLA4 has higher affinity to CD80/86 compared to CD28 [27]. Therefore, CTLA4 can burden the activation of T cells by directly antagonizing CD28 and preventing the interaction with the co-stimulatory molecules in APCs.

PD1 expression is also upregulated upon stimulation of the TCR. The ligands of PD1 are PD-L1 and PD-L2, which are constitutively expressed on APC [22]. Additionally, pro-inflammatory cytokines can induce the expression of PD-L1/2 in tumor cells. The interaction between PD1 and PD-L1/2, also called the PD1 axis, induces a negative regulation of T cells resulting in T cell exhaustion. In contrast to CTLA4, the inhibitory effects of the PD1 axis occur later after T cell activation, predominantly during the effector phase when T cells are confronted with cancer cells [24], [28].

Thus, an approach of cancer immunotherapy involves blocking CTLA4 and PD1 or their respective ligands using targeted antibodies (Fig. 4). Immune checkpoint blockade prevents inhibition of the T cell activation processes, thereby generating an enhanced T cell response that can lead to anti-tumor

effects [21], [26], [28]. This strategy has proven successful for various cancer types and several therapies targeting blockade of either CTLA4 or the PD1 axis have been already approved by regulatory authorities [29]. Beyond demonstrated improvements in overall survival, immune checkpoint blockade has the advantage of conveying lower toxicity than traditional treatments such as chemotherapy, which gives better quality-of-life to the patients [29], [30].

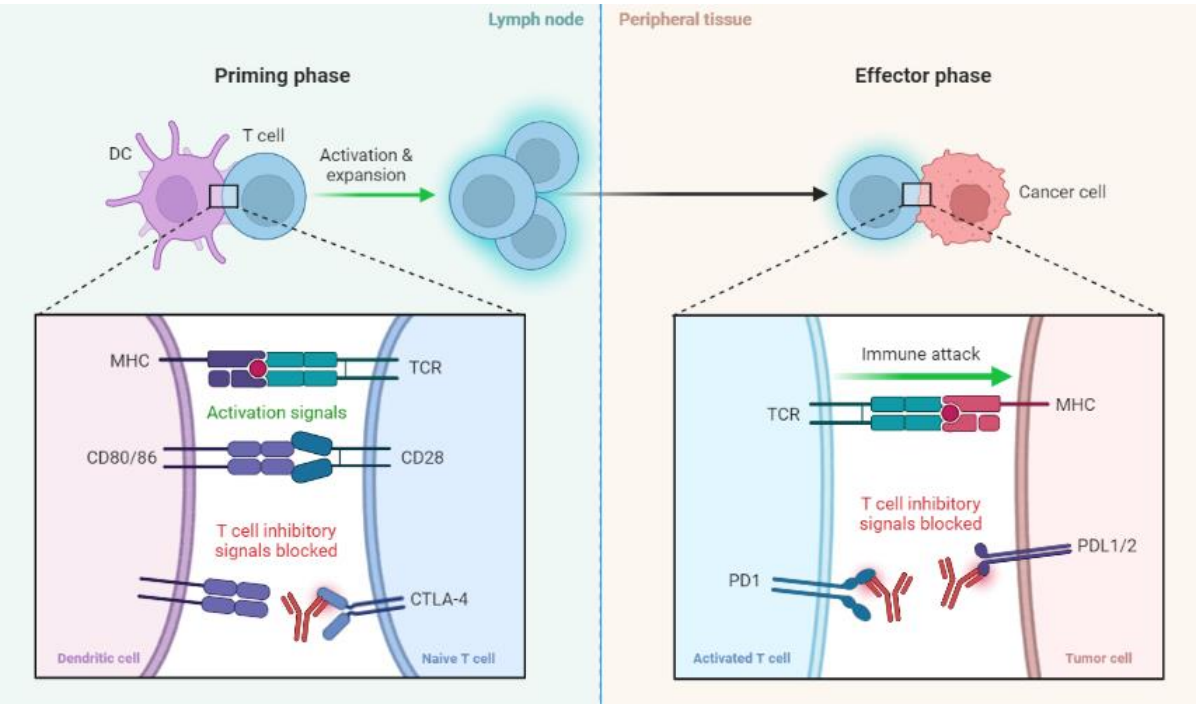

Figure 4. **Immune checkpoint blockade.** Mechanisms of the inhibition of CTLA4 and the PD1 axis through targeted antibodies in cancer immunotherapy. (Illustration created with Biorender.com).

Despite the positive therapeutic outcomes, long-term anti-cancer response has only been observed for a minority of patients [31], [32]. Immune checkpoint inhibitors (ICIs) target the adaptive arm of the immune system. However, in the majority of the cancer patients there is a very low or nonexistent adaptive immune response against cancerous tissue, which severely hinders the therapeutic efficacy of ICIs. In addition, the immunosuppressive TME hampers T cell infiltration, which is essential for an effective treatment with ICIs [33]–[35]. Importantly, the blockage of a fundamental immune checkpoint can unleash strong immune responses that can still lead to undesired side effects [36]. For instance, it has been estimated that 15-90% of patients treated with ipilimumab (an approved CTLA4 inhibitor) show immune-related side effects [37]. Moreover, between 15 and 30% of patients treated with inhibitors of CTLA4 or the PD1 axis suffer severe toxic effects [38]. In many cases, toxicity is associated with autoimmunity, which sometimes might be irreversible or life-threatening [32]. Furthermore, it has been reported that the combination therapy of CTLA4 and PD1 blockade provides an enhanced therapeutic efficacy. Unfortunately, the associated risk of severe toxicity is also higher [22].

1.2.2 Toll-like receptors

Toll-like receptors (TLRs) belong to the class of pattern-recognition receptors (PRRs), an evolutionarily highly conserved group of receptors [39]. TLRs play a critical part in the initiation of the immune response since they can recognize pathogen-associated molecular patterns (PAMPs), which are conserved motifs found across bacteria, viruses, fungi and protozoa. Examples of PAMPs include viral DNA and RNA as well as lipoproteins and peptidoglycans from bacterial cell walls [40]. Moreover, TLRs can recognize danger-associated molecular patterns (DAMPs), also known as alarmins. DAMPs are released by cells after injury or apoptosis. The recognition of PAMPs/DAMPs starts a downstream cascade that leads to the transcription of regulatory interferon (IFN) and pro-inflammatory cytokine genes [39], [41].

TLRs have been found in immune and non-immune cells, but more predominantly in the former. The expression of TLRs is very high in macrophages, dendritic cells and neutrophils [39], [42]. In a lower proportion, TLRs are also present in epithelial cells of the intestinal and respiratory tracts, probably as an additional antimicrobial defense. Hence, the function of TLRs is associated with the innate immune response and is aligned with the frontline defense of the host cell [40]. In addition, TLRs can also be expressed in a subset of activated T-cells. The stimulation of TLRs in T-cells can increase the proliferation of T-cells and cytokine production [39].

Until today, ten TLRs (TLR1-10) have been identified in humans [43]. TLR1, 2, 4, 5 and 6, are cell surface receptors and they recognize PAMPs/DAMPs present in the extracellular space. In contrast, TLR3, 7, 8 and 9, are intracellular receptors located on the surface of endosomes and lysosomes [41], [43]. The binding domain of the intracellular TLRs is found facing the interior of the organelles and they are specialized on the recognition of viral nucleic acids. The subsequent recognition of ligands occurs through processes such as autophagy [39], [42].

In recent years, the natural immunostimulatory power of TLRs have attracted great attention as a tool in cancer immunotherapy. More than a century ago, the first descriptions of a connection between microbial toxins and cancer regression were documented. Spontaneous tumor regressions were observed after streptococcal infections [44]. Then, repeated administration of Coley's toxins (heat-inactivated bacterial extracts of *Streptococcus pyogenes* and *Serratia marcescens*) cured a group of patients with sarcoma [45]. More recently, exceptional regressions of leukemia have been reported after bacterial or fungal infections [46]. In retrospective, it is likely that such anti-cancer responses were triggered by the activation of TLRs resulting from the presence of pathogenic toxins [40].

TLR agonists (TLRas) are being intensely investigated both as monotherapy and as adjuvants for cancer vaccines [47], [48]. The therapeutic use of TLRas relies mainly on their ability to initiate T cell immunity, which involves antigen uptake, processing and recognition by antigen-presenting cells (APCs) and ultimately the activation of T cells [41]. More specifically, the stimulation of TLRs in APCs triggers a multi-step process that results in enhanced phagocytosis, APC maturation and upregulation of MHC and co-stimulatory molecules, migration to draining lymph nodes, secretion of cytokines and antigen presentation to T cells [40].

Currently, there are three TLRas approved by the U.S. Food and Drug Administration (FDA). An attenuated strain of *Mycobacterium bovis*, referred to as Bacillus Calmette-Guérin (BCG) was initially developed as a tuberculosis vaccine, but is now indicated for treating bladder cancer. The other two therapies are monophosphoryl lipid A (TLR4 agonist) and imiquimod (TLR7 agonist) [41]. The great potential of targeting TLRs in cancer immunotherapy is reflected in the nearly 70 clinical trials involving TLR agonists that are currently on going [47], [49], [50].

In this project, the scope is mainly focused on the intratumoral delivery of TLR7/8 agonists (TLR7/8as) as immunotherapeutic agents. The combined stimulation of more than one TLR significantly improves the drug potency. For instance, the topical application of resiquimod (a TLR7/8a) had shown impressive effects on human cutaneous T cell lymphoma, whereas imiquimod (a TLR7 agonist) induced much lower response rates and immune activation levels. Such differences can be in part attributed to the ability of R848 to activate both TLR7 and TLR8 [51], [52]. Moreover, besides the previously enlisted effects of TLR activation, stimulation of TLR7/8 promotes anti-tumor activity also by angiogenesis inhibition as well as by natural killer (NK) cells-mediated cytotoxicity and apoptosis of tumor cells [53]–[55]. Enhanced immune responses have been observed when administering TLR7/8a as monotherapy and in combination with radiotherapy, chemotherapy or checkpoint inhibitors. Furthermore, anti-tumor effects have been triggered by TLR7/8a in several cancer types such as breast, pancreatic, head and neck cancer [56]–[59]. Overall, the dual stimulation of TLR7 and TLR8 may be optimal for activating and bridging the innate and adaptive immune response.

TLR7 and TLR8 are activated by single-stranded viral RNA, and imidazoquinolines, nucleosides analogues with a similar structure, have proven to be potent TLR7 or TLR7/8 agonists [41], [60]. Imidazoquinolines are a group of small synthetic molecules that include imiquimod, resiquimod and gardiquimod (Fig. 5) [60]. Despite their potent anti-tumor activity, the clinical application of TLR7/8as has proved challenging. Imidazoquinolines are poorly water-soluble, which limits their formulation in several dosage forms [48]. For instance, imiquimod, an FDA-approved molecule, is formulated in a cream and only delivered topically [40]. Moreover, the therapeutic efficacy of TLR7/8as is hindered by their poor pharmacokinetic profile. After intravenous injection or oral administration, TLR7/8a are quickly cleared from blood circulation causing a low bioavailability. Equally important, TLR7/8as can cause severe side effects after systemic administration such as autoimmunity and systemic inflammation [61], [62]. Toxic side effects can still be problematic even after local injection since, for example, resiquimod disperses from the injection site into blood circulation five minutes post-injection [63]. Thus, investigation of novel delivery strategies are of great interest to enhance the clinical performance of TLR7/8 agonists.

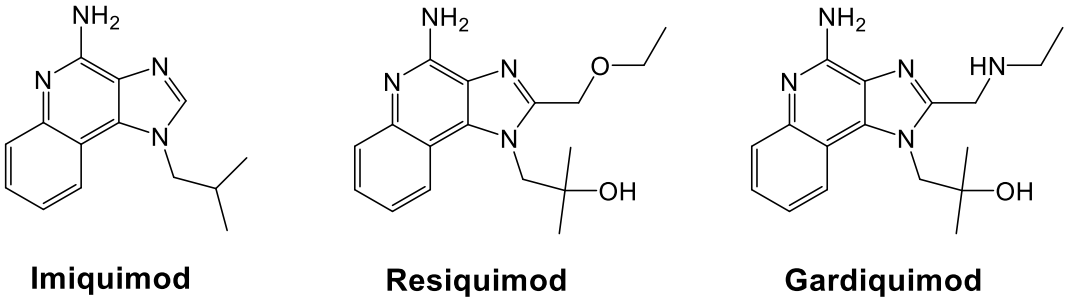

Figure 5. Imidazoquinolines. Chemical structures of the TLR7 agonist imiquimod and the TLR7/8 agonists resiquimod and gardiquimod, all members of the imidazoquinoline family.

1.2.3 Transforming growth factor-β inhibitors

A key factor to be considered in the implementation of cancer immunotherapy is the tumor microenvironment (TME) [5]. Solid cancers are not only a mass accumulation of malignant cells. Instead, the TME comprises both cancer and non-cancerous cells, the latter including immune cells (e.g., lymphocytes, macrophages), fibroblasts and adipocytes [64]. The TME is a dynamic environment with its own vasculature as well as scarce lymphatics. Moreover, a complex network communication is driven within the TME by cytokines and chemokines. All of this is surrounded by a modified extracellular matrix (ECM) that plays a critical role in the movement into and out of the TME [64], [65].

The complexity and heterogeneity of the TME represents a challenge to cancer treatment in general. Tumors has broadly been defined as “hot” or “cold” depending if they are immunogenic or immunosuppressive, respectively [66], [67]. An immunosuppressive TME counteracts the immune recognition of cancer cells, especially by effector T cells, and not surprisingly, it is generally associated with poor therapeutic outcomes [68]. Thus, strategies promoting the conversion of the immunosuppressive TME are valuable.

One of the most important molecules involved in regulating mechanisms of immunosuppression is transforming growth factor-β (TGF-β). TGF-β is a cytokine that can induce the expression of PD1 in cytotoxic T cells, which can reduce their effector function and hinder the overall anti-tumor response. Additionally, it has been shown that TGF-β is the master regulator of T cell polarization and effectively promotes the expansion of regulatory T cells (T_{reg}), which are known to have immunosuppressive effects [69]. Equally important, TGF-β has been associated with immune exclusion in several cancer types. Immune exclusion refers to a tumor phenotype in which effector T cells are not able to infiltrate the tumor. In this case, the access is restricted particularly by a peritumoral zone abundant in fibroblasts [70]. As the T cells stay in the tumor-surrounding area, they cannot interact with the tumor cells and cancer cells endure. It has been observed that inhibition of TGF-β can lead to conversion of the immune exclusion phenotype, thus allowing the infiltration of cytotoxic T cells into the tumor (Fig. 6) [69], [70].

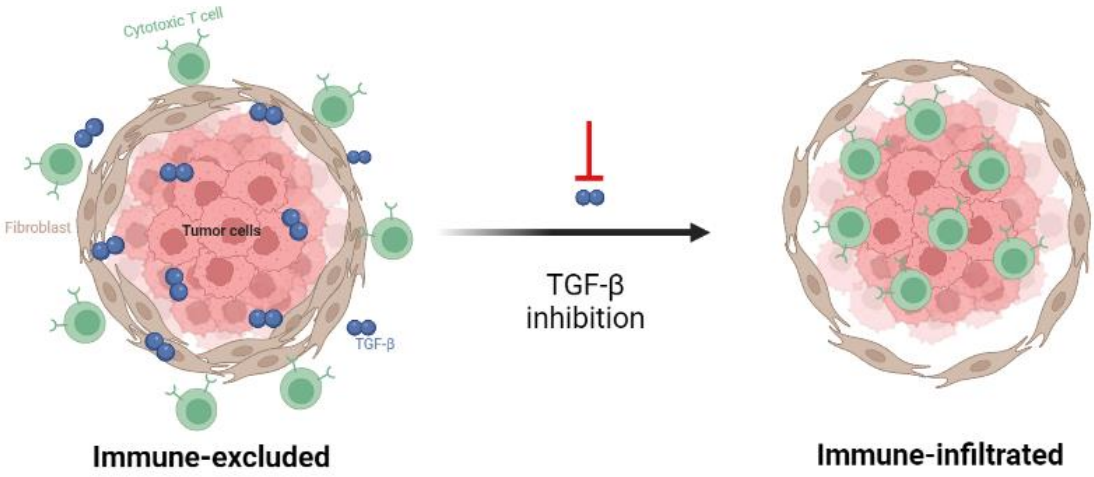

Figure 6. Effect of the inhibition of TGF-β in an immune excluded tumor. Cytotoxic T cells remain in the peripheral tumor area due to the effects of TGF-β and a fibroblast rich zone. Upon inhibition of TGF-B, cytotoxic T cells are able to infiltrate the tumor and exert their tumoricidal function. (Illustration created in Biorender.com and inspired by [69])

TGF-β can be inhibited in several ways during its signaling pathway [69], [71]. Briefly, TGF-β secreted into the extracellular space is cleaved by integrins into its active form as a TGF-β dimer. Next, the TGF-β dimer binds to TGF-β serine/threonine kinase receptors (TGF-BRI/II) present on the cell surface. This initiates an intracellular phosphorylation cascade that results in the transcription of diverse TGF-β target genes. There are four key points in the TGF-β pathway that can be prevented: (i) the transcription of TGF-β, (ii) the cleavage by integrins, (iii) the interaction between the TGF-β dimer and its receptor, and (iv) the intracellular signaling cascade. Anti-sense oligonucleotides are employed for strategy (i), blocking antibodies are used for strategies (ii) and (iii), while small molecule kinase inhibitors perform strategy (iv) [69], [71]. Inhibition of TGF-β has been investigated in combination with immune checkpoint blockade, particularly targeted to the PD1 axis, with successful therapeutic improvements [70], [72], [73]. Hence, TGF-β inhibition seems as a promising tool in immunotherapy, especially in combination with other immunotherapeutic agents. Nonetheless, due to the ubiquitous expression of TGF-β and its receptors in healthy tissues, the systemic administration of TGF-β inhibitors has also been associated with autoimmunity effects especially severe cardiac toxicity [74], [75]. In this project, the formulation and intratumoral delivery of RepSox, an inhibitor of the signaling cascade produced by TGF-BRI, will be investigated.

1.3 Drug delivery of immunotherapeutics

As of 2021, nearly twenty cancer immunotherapies have received FDA-approval and many more are currently in clinical trials [76], [77]. These immunotherapies can be classified in several categories including immune checkpoint inhibitors (ICIs), chimeric antigen receptor (CAR) T cell therapies and other immunomodulatory molecules such as co-stimulatory receptor antibodies, oncolytic viruses and cancer vaccines [22]. Overall, cancer immunotherapies have shown promising improvements and benefits when compared to conventional cancer treatments like chemotherapy.

Nevertheless, the clinical application of cancer immunotherapy is still confronting challenges associated with both efficacy and safety [36], [77]. In terms of efficacy, the proportion of patients that show a durable response to immunotherapy is relatively small (<20% for many indications), and it is difficult to predict if or how a patient will respond to the treatment [77], [78]. Regarding safety, each type of immunotherapy has a unique toxicity profile depending on its mechanism of action. But overall, autoimmunity effects are predominant and the side effects can range from mild organ-specific autoimmunity to potentially lethal events such as cytokine release syndrome [36], [79]. Adverse effects are usually correlated to the administered dose, so dose-limiting toxicities represent a challenge [22].

There is a need for novel strategies for the administration of immunotherapeutics in a safer and more controlled manner that concurrently improve their efficacy and broaden their application. Drug delivery platforms present valuable options since solely optimizing the dosing and administration schedule might not be sufficient [36]. The use of drug delivery systems (DDSs) have several advantages over the immunotherapeutic agents alone. In general, DDSs could improve the bioavailability of immunotherapeutics in cancerous tissue, provide more effective targeting and consequently, decrease off-target toxic effects [77]. When developing a drug delivery system for cancer immunotherapy, it is important to consider that the immune response is generated and built in the cancerous tissue and associated lymph nodes [80]. Thus, DDS can be designed to enable local and sustained delivery of drugs, and additionally, drug delivery might be triggered by specific stimuli such as pH, temperature and ultrasound [50], [81], [82]. As an added benefit, the formulation of immunotherapeutic agents into a DDS might give extra protection to the cargo until its delivery to the target cells or tissues [83].

Besides the drug delivery technology, the choice of administration route can have an effect on both the therapeutic efficacy and the toxicity profile of the treatment. In the current clinical practice, the majority of cancer immunotherapies have a systemic administration [77]. Nonetheless, local administration is becoming an attractive alternative to increase drug bioavailability while minimizing systemic toxicity [84]. Related to the latter, it is important to highlight that the cells that can respond to immunotherapy are not solely contained in the cancerous tissue, but rather are present throughout the body. In the following sections, the advantages and challenges of systemic and intratumoral administration of immunotherapy will be described as well as the most relevant drug delivery platforms within each route of administration.

1.3.1 Systemic immunotherapy

As previously highlighted, almost all of the currently approved cancer immunotherapies rely on intravenous (systemic) administration. Hence, the delivery of the immunotherapeutic agent to its target depends on systemic biodistribution. Systemic parenteral administration offers clear advantages such as practicality and extensive availability of the required clinical infrastructure [84]. While systemic administration is logical for treating hematological cancers, it might not be optimal for the treatment of solid tumors. In this case, the malignant target tissue is not as accessible as in skin or hematological cancers. Drug penetration from blood circulation into tumor tissue is usually limited, which leads to target under-occupancy and low therapeutic effect [68], [85]. In addition, systemic drug exposure can

cause overstimulation of immune cells, whose response is not necessarily targeted to the tumor thus leading to immune adverse effects [36].

While systemic administration is not specifically targeting tumor tissue, some drug formulations such as nanoparticles tend to naturally accumulate there. This is a phenomenon referred to as passive targeting or the permeability and retention (EPR) effect (Fig. 7A). The EPR effect describes a higher permeability of tumor vessels compared to vessels in healthy tissue, which facilitates the permeation of nanoparticles circulating in the blood stream into the tumor site [85]. Moreover, nanoparticles can accumulate at the tumor site because of the poor lymphatic clearance in tumors. Overall, the EPR effect can result in a higher local drug concentration and lower systemic toxicity [86], [87]. However, the EPR effect shows great variations between patients and across tumor types. Despite good results in pre-clinical models, once in clinical trials many nanomedicines do not display significant improvements over traditional cancer treatments [77]. According to a meta-analysis involving more than 100 studies of nanoparticle delivery, it was estimated that less than 1% of systemically administered nanoparticles actually arrived to the tumor [88].

As an alternative approach, nanoparticles and other drug delivery strategies have been designed to selectively target tumor cells or lymphoid organs, depending on the therapeutic agent [89]. In targeted delivery, the drugs are packed in delivery vehicles that facilitate crossing biological barriers or the therapeutic agents are chemically modified to purposely direct them to the target where they will elicit their function (Fig. 7B). Generally, overexpressed receptors in cancer cells are used as ligands for the drug delivery vehicle [85]. An example of the latter are drugs conjugated to tumor-targeted antibodies.

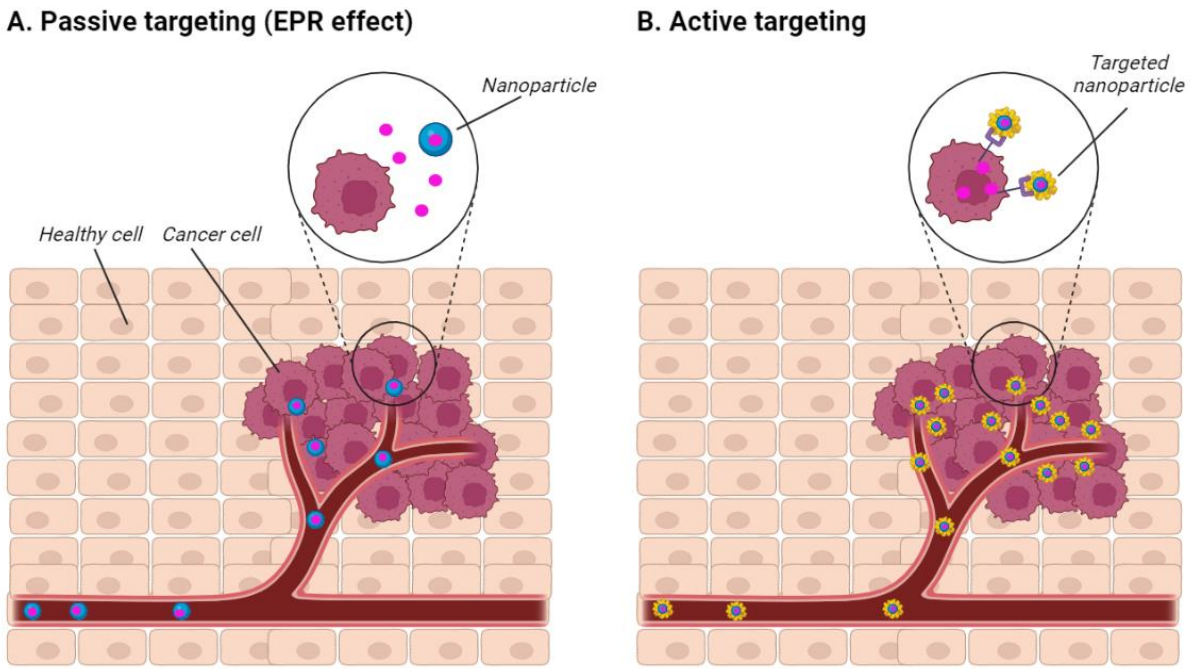

Figure 7. Delivery of therapeutic agents into tumors through two different mechanisms. (**A**) passive targeting (EPR effect) via characteristic leaky blood vessels and (**B**) active targeting, which employs functionalized nanoparticles or drugs directed towards specific receptors or ligands in tumor cells. (Illustration adapted from [77] and created with Biorender.com).

In one approach, a TLR7/8a was conjugated to a monoclonal antibody specific to human epidermal growth factor receptor 2 (HER2) (Fig. 8) [90], [91]. It is known that the gene of HER2 is prone to abnormal amplification and subsequent protein overexpression in some patients with breast and gastric cancer, making it an adequate cancer cell target [92]. In the exemplified study [91], a TLR7/8a was specifically designed to be linked to a HER2 antibody through a non-cleavable linker. The covalent linker was designed to prevent off-site cleavage of the TLR7/8a and the consequent systemic toxic effects that such molecule can cause [62]. Following systemic administration, a localized immune response was observed, which led to tumor clearance and immunological memory. Moreover, weight loss in mice was negligible and no signs of off-target toxicity were observed. Nevertheless, potency of the TLR7/8a-HER2 antibody conjugate depended directly on the expression level of HER2 on the target cells; so, a lower therapeutic efficacy was obtained for cancer models with low expression of HER2. This exemplifies that the therapeutic effect of tumor-targeted delivery technologies might be limited to specific subsets of cancer types. Furthermore, the authors acknowledged that, while unexplored, it is possible that the TLR7/8a-HER2 antibody conjugate generates anti-drug antibodies. The generation of anti-drug antibodies (ADAs) is particularly relevant for biological molecules like monoclonal antibodies because they can be mistakenly considered as foreign by the immune system. ADAs have been increasingly recognized as a relevant factor for evaluation since they can cause immune-related adverse effects [93].

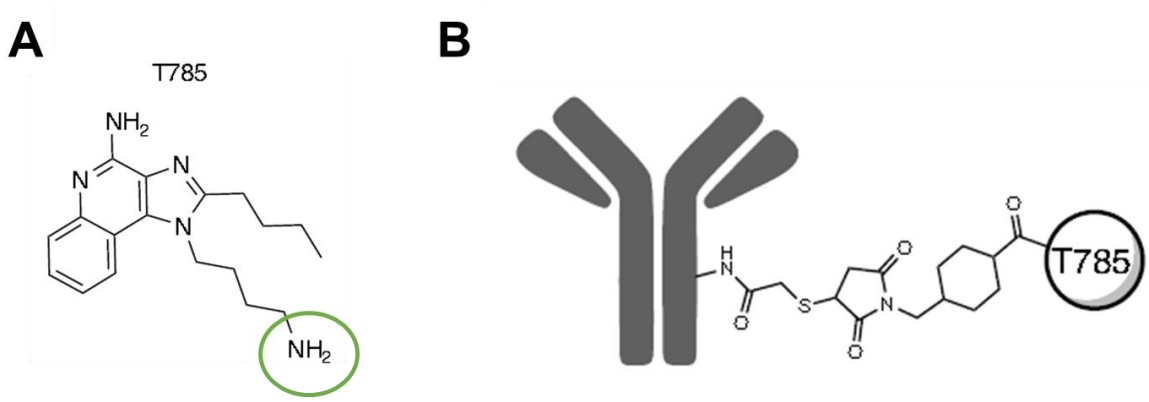

Figure 8. Delivery of a TLR7/8 agonist via conjugated antibody. (**A**) Chemical structure of the TLR7/8 agonist namely T785, highlighting the moiety used to for the covalent linker with the HER2 antibody. (**B**) Graphical representation of the TLR7/8a-HER2 antibody conjugate. (Illustration adapted from [91]).

1.3.2 Intratumoral immunotherapy

Intratumoral administration is a promising approach for improving therapeutic efficacy and broaden the application of cancer immunotherapies to solid tumors. As mentioned before, the TME represents a challenging barrier for the penetration of systemically administered immunotherapeutics. Such obstacle can be circumvented by directly injecting the drugs into the tumor. Consequently, the local drug concentration and bioavailability are increased, so therapeutic doses can be reached with a lower administered dosage [84]. From an economic standpoint, a reduced dosing is also an attractive advantage [94]. Intratumoral immunotherapy minimizes systemic drug exposure, which considerably

decreases the risk of off-target immune activation and related adverse effects [95]. In addition, this enables the intratumoral administration of combined immunotherapeutics with synergistic effects, which otherwise would cause severe toxic effects [96].

1.3.2.1 The abscopal effect and in situ cancer vaccination

Intratumoral immunotherapy also has the potential of generating systemic immune anti-cancer responses, a phenomenon known as abscopal effect, which can also be useful for metastatic cancers. The abscopal effect describes that after local stimulation, the immune system is able to attack distant tumors that were not in direct contact with the immunotherapeutic agent (Fig. 9) [89]. In order for T cells to elicit an efficacious response against tumors, two phases need to be completed: the T cell priming phase (i.e., the creation of anti-cancer T cells) and the effector phase, in which cytotoxic T cells kill the cancer cells. Regarding the former, local stimulation by TLR7/8 can enhance antigen uptake and presentation by APCs, a process necessary for T cell priming. Moreover, after intratumoral injection, immunostimulatory drugs can also travel to the tumor draining lymph nodes where they can further aid the priming of T cells [32], [89]. Subsequently, activated T cells can be distributed through lymphatics and blood circulation thereby arriving to remote tumor tissues where they effect a cytotoxic function. This *in situ* priming might be especially beneficial for ICIs targeted to the PD1 axis, which relies on a pre-exisiting antitumor immunity. It is hypothesized that non-respondent patients to ICIs lack a preceding T cell priming [32].

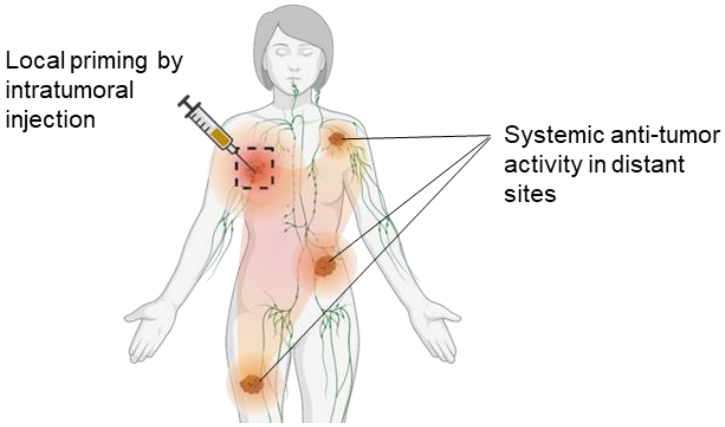

Figure 9. Graphical representation of the abscopal effect. A systemic anti-cancer response can be elicited by the immune system after local stimulation with immunotherapeutic agents. (Illustration taken from [32] and created with Biorender.com).

Furthermore, in intratumoral immunotherapy, the tumor of the patient is used as its own vaccine to generate an immune response towards cancer cells, allowing an effective response despite cancer heterogeneity [32]. An intrinsic characteristic of cancer is that cancer cells gradually accumulate genetic mutations over time. Accordingly, the offspring clones of a single cancer cell can display different genomic profiles, which generates various polyclonal sub-populations (Fig. 10). This causes heterogeneity both within the tumor and between patients [97]. An *in situ* vaccination refers to the process in which tumor-associated antigens (TAAs) present at the tumor site are used to produce an

adaptive immune response. Generally, malignant cell antigens are released after apoptosis of cancer cells, which are taken and then presented by APCs to prime T cells. This cycle can be stimulated and enhanced by immunoregulatory drugs. In contrast to conventional vaccines, specific antigens do not need to be identified or isolated [98]. The cancerous tissue can be considered as the source of the vaccine antigen, while the immune activating agents (e.g., TLRas) act as the adjuvant. Therefore, intratumoral immunotherapy can promote an antitumor immune response against several cancer targets to better tackle the naturally heterogeneous tumors.

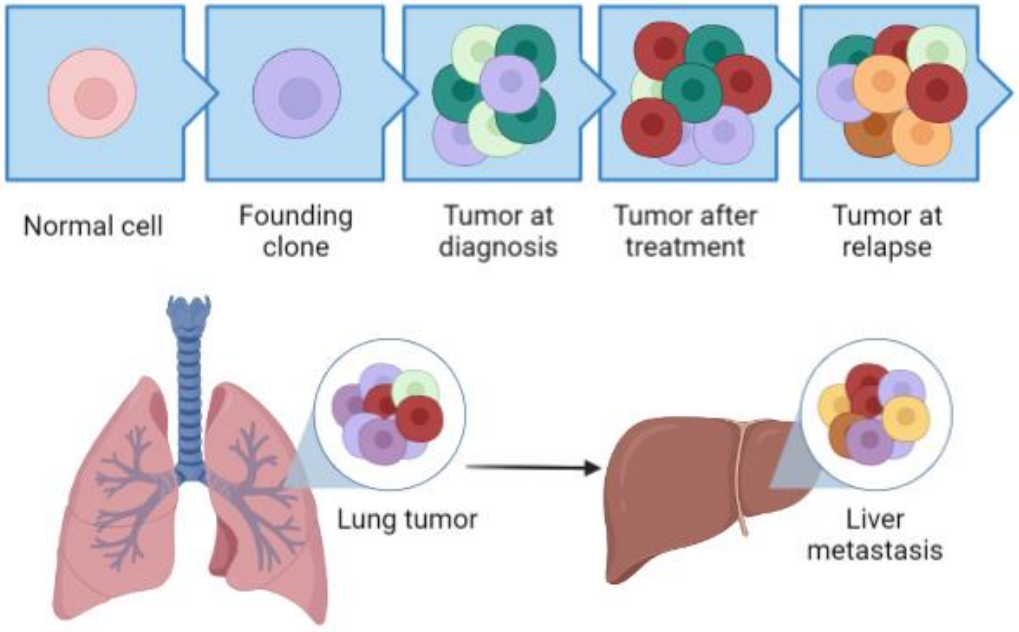

Figure 10. **Heterogeneity of cancer.** Example of lung cancer showing the gradual generation of subclonal populations of cancer cells and their diversity in different tumors. (Illustration inspired by [97] and created with Biorender.com).

1.3.2.2 Intratumoral drug delivery

While intratumoral administration can minimize drug exposure, it does not necessarily mean that the drugs will be retained at the tumor site. After intratumoral injection of free immunotherapeutics, these can still reach the systemic circulation via the leaky blood vessels of the tumor. If such leakage to blood circulation is excessive, the intratumoral treatment might not be effective and might even resemble the toxicity caused by intravenous administration [36]. A frequent approach to prevent undesired systemic exposure is to chemically modify immunotherapeutic drugs to improve their retention in the tumor after injection [77]. An example in this category is 3M-052, a synthetic TLR7/8a derived from the imidazoquinolines family, which was designed to contain a C18 lipid tail. The high lipophilicity of 3M-052 promoted its preferential retention at the tumor site. Moreover, the lipid moiety in 3M-052 allows its incorporation in liposomes, which provides an additional drug delivery strategy [99], [100]. In a similar example, another TLR7/8a was PEGylated to ensure that the drug will remain at the tumor [101]. In both cases involving chemically modified TLR7/8a, an enhanced induction of antitumor activity was observed, while the drug concentration in the systemic circulation remained low. In another approach,

ICIs were linked to a peptide derived from placental growth factor 2 (PLGF2), which is known to have great affinity for proteins in the tumor ECM. After intratumoral administration, the ICI-PLGF2 conjugates remained in the tumor area and promoted an improved anti-cancer effect in both local and distant tumors. As expected, the tested conjugates showed less toxic effects than the free ICIs [102].

Nonetheless, intratumoral administration by itself does not provide constant stimulation of the TME. Immune cells present in the TME are very plastic, meaning that they are unceasingly modifying their phenotype and functional characteristics. Therefore, continuous immune stimulation is optimal to prime or enhance their immune response [103]. For this purpose, platforms of sustained release are necessary. For instance, Montanide ISA 51 is a water-in-oil (W/O) emulsion that is formed by a mixture of mineral oil with the surfactant mannose mono-oleate [104]. An ICI against CTLA-4 was formulated in the Montanide ISA 51 emulsion, which resulted in the slow local release of the ICI. When compared to systemic administration of the free ICI, a lower dosage in the Montanide ISA 51 emulsion was needed to achieve the same therapeutic efficacy [105]. Although no severe systemic toxicity was described in the exemplified study, it has been reported that Montanide ISA 51 can cause adverse effects in the injection site. This observation highlights the importance of using biocompatible materials for drug delivery formulations [104].

Injectable scaffolds represent another option for sustained drug delivery. Since large preformed implantable scaffolds often require invasive surgical procedures for its colocation, alternative systems and materials have been investigated such as gelatin and alginate hydrogels. These materials have a low viscosity and are highly deformable besides being able to self-assemble upon injection [106]. For this reason, they are suitable for parenteral administration.

A relevant example for this project are hydrogels, whose formulation comprises a cross-linked polymer network capable of absorbing and retaining vast water amounts. These characteristics make hydrogels physically similar to tissues and it is one of the reasons why they display great biocompatibility. Moreover, hydrogels are tunable materials; so, features as stiffness and porosity can be optimized according to the application. The mesh size (i.e., the open spaces within the polymer network) is usually the main factor dictating drug diffusion and release kinetics. Moreover, due to its polymeric network, hydrogels can provide protection to their cargo to prevent premature degradation [107]. An example of a hydrogel applied to cancer immunotherapy is given by a system named TransCon™, in the TLR7/8a resiquimod is given with the purpose of stimulating inflammation and activation of cytotoxic T cells [108]–[110]. In this delivery system, the TLR7/8a is transiently bound to the hydrogel via a patented linker. At specific pH and temperature, the linker is auto-cleaved causing the release of the TLR7/8a. Importantly, before this step the TLR7/8a is considered a prodrug as it remains inactive while linked to the hydrogel. The auto-cleavage occurs at a known rate, thereby releasing the drug in a sustained manner. Once the drug is released, the hydrogel is degraded into smaller polymers followed by renal clearance. As with previous examples, systemic drug exposure is very low and effective antitumor activity has been observed.

An additional hydrogel system shows the potential of combination therapies. In this case, a hydrogel was designed to deliver sustained release of both a chemotherapeutic and an ICI targeted to PD-L1 [111]. Combination therapies can be especially beneficial for patients displaying tumors with low immune activation for which an immune monotherapy may not be sufficient to elicit an anti-cancer response [22]. In the aforementioned study, a hydrogel was fabricated that degrades upon contact with reactive oxygen species (ROS), which are present at the TME at various concentrations. The drugs were bound to the hydrogel via a ROS-reactive linker and they were released with distinct kinetics; due to its lower molecular weight, the chemotherapeutic gemcitabine was released first, followed by the ICI (a monoclonal antibody). By first releasing gemcitabine, cancer cells are killed, which may release tumor-associated antigens. Afterwards, the ICI aids in stimulating an antitumor response. An approach such as the ROS-activated hydrogel can help to minimize the side effects associated to intravenous administration of the aforementioned combination therapies.

A common criticism brought upon intratumoral immunotherapy is the feasibility of the injection to the tumor [32]. Nonetheless, such concern is not well substantiated since it has been demonstrated that image-guided intratumoral injections are generally safe and they can be done in a great variety of organs. For instance, aspiration biopsies are performed basically across all malignancies using both fine and large needles [112]. However, challenges remain in terms of reproducibility and precision of the injections. It has been suggested that therapeutic efficacy of intratumoral immunotherapy might be influenced by variations in the operator and the injection technique, resulting in a lack of repeatability [113]. This technical factor represents a critical concern especially for the execution of clinical trials in which more than one institution is involved. Discouraging efficacy results might be observed because of intra- and inter-operators variability rather than because of the actual efficacy of the treatment [84]. Therefore, standardized methods to determine if an injection was adequate or suboptimal are much needed.

1.4 The CarboCell drug delivery platform

1.4.1 Background: in situ forming depots

As previously exemplified, *in situ* forming depots are a particularly appealing drug delivery platform for intratumoral administration and sustained drug release. Over the last decades, several materials have been investigated to form such delivery systems including natural and synthetic polymers like alginate and poly (lactic-co-glycolic acid) (PLGA), respectively [114], [115]. These materials have the advantage of being biocompatible and biodegradable, so their implantation *in vivo* is generally well tolerated. *In situ* forming depots are fluids with a low viscosity, which facilitates their injection through thin needles. Once injected, the formulation experiences chemical and/or physical changes that result in the formation of a semisolid or solid depot [114].

Depending on the mechanisms of depot formation, the *in situ* forming technologies can be catalogued as cross-linked systems or phase separation systems [114]. An example of the former are hydrogels

(as previously described with the TransCon™ system), as they rely on physical or chemical cross-linking to produce their characteristic network structure [107], [109]. In the phase separation systems, PLGA-solvent mixtures have been investigated as delivery platforms such as the FDA-approved Eligard™ technology. Nonetheless, safety concerns still exist regarding the toxicity of these formulations due to their high amount of organic solvent (e.g., > 50% of N-methyl-2-pyrrolidone (NMP)) and the acidic degradation products from PLGA [116], [117].

Non-polymeric formulations based on sucrose acetate isobutyrate (SAIB) represent a remarkable example of phase separation systems. SAIB is a fully esterified derivative of sucrose with very high hydrophobicity (Fig. 11A). SAIB presents as an odorless clear fluid with a high viscosity, which exceeds 100000 mPa·s [118]. According to the FDA, SAIB is generally recognized as safe (GRAS), supporting its use for oral consumption as a food additive. Thus, SAIB is regarded as biodegradable and biocompatible [119]. When SAIB is mixed with small amounts (10-35% of volume) of organic solvents, the viscosity of the resulting fluid dramatically decreases to the range of 50-200 mPa·s enabling its injection through small needles [118]. For this purpose, several pharmaceutically accepted solvents can be used such as ethanol (EtOH) and dimethyl sulfoxide (DMSO). Once the formulation is injected, the solvent diffuses away forming a solid or highly viscous liquid from which the drug is gradually released. Due to this solvent efflux, the self-formed depot acquires a viscosity over 100000 mPa·s [114], [118], [119].

SAIB-based systems have been used for the sustained release of several small molecules, microparticles and peptides [120]–[122]. It has been found that the drug release kinetics depend on the type of solvent as well as on the ratios of SAIB and solvent in the composition, making it a very flexible system. Noticeably, it has been reported that the solvent efflux rate influences the bust release, where a fast diffusion of the solvent out from the system caused a higher burst release [121]. However, the SAIB/solvent mixtures in general tend to have a high burst release since there is a lag between injection and the self-formation of the depot. To lower the burst release, polymers like PLGA and poly (lactic acid) (PLA) have been incorporated into the SAIB system at concentrations not higher than 10%. The polymers created a shell surrounding the depot, which slowed down the drug diffusion and lowered the burst release [117]. The components of the SAIB system are commercially available and the preparation of the formulation is simple, which makes it an attractive technology for scale-up manufacturing [114]. The SAIB system is licensed to DURECT with the trade name SABER™. In 2021, SABER™-bupivacaine (POSIMIR™) was approved by the FDA as an injectable solution for post-surgical pain reduction.

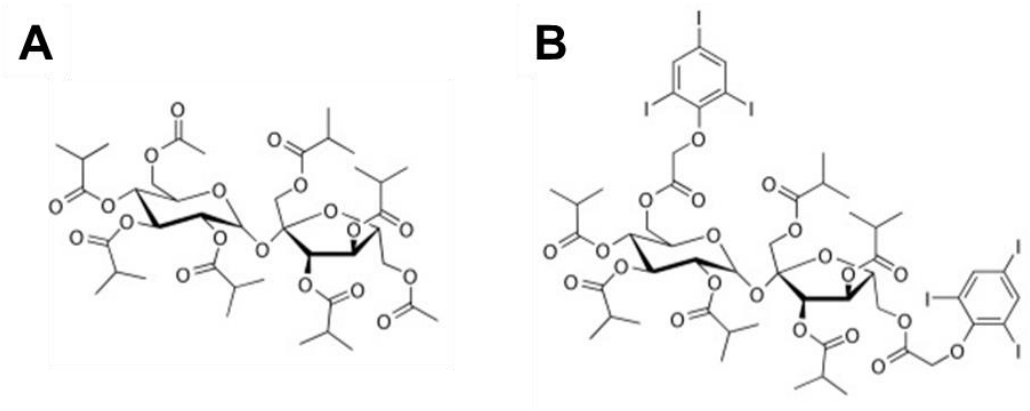

Figure 11. **SAIB and xSAIB.** Chemical structure of (**A**) SAIB and the (**B**) CT contrast agent xSAIB.

In the context of cancer treatment, the SAIB system has served as inspiration for developing fiducial markers for image guided radiation therapy (IGRT). In clinical practice, radiopaque markers such as gold seeds are implanted in the tumor or its surrounding area to optimize the precision of IGRT. Despite providing great radiographic contrast, the insertion of the implants can be an invasive procedure [123]. For instance, serious complications like pneumothorax and bleeding has been reported in around 30-70% of lung cancer patients requiring solid gold implants [124]–[127]. Furthermore, such implants can move from its original location over time, which has a negative effect on subsequent IGRT precision [125], [126]. To solve these issues, PEGylated gold nanoparticles were formulated in a SAIB/EtOH/PLA (75:20:5) system to serve as an easily injectable fiducial marker [119]. To test the system, the formulation was injected subcutaneously in mice and monitored over a period of 12 weeks. It was found that the formed depot showed stability in geometry, volume and computed tomography (CT) contrast, making it a promising technology for further evaluation. In a related approach, an iodine-rich CT contrast agent derived from SAIB, referred to as xSAIB, was developed (Fig. 11B). xSAIB can be easily incorporated into a SAIB-based formulation, which results in a liquid fiducial marker for improving IGRT and for surgical guidance. This technology is patented by Nanovi under the name of BioXmark®. BioXmark® has been clinically tested in several cancer types and it has demonstrated excellent and durable visibility in various imaging modalities including fluoroscopy, ultrasound and CT. Besides being well tolerated, BioXmark® does not migrate after its injection and no related complications have been reported [128]–[130].

1.4.2 The CarboCell system

CarboCell is an *in situ* forming depot formulation developed in the Colloids and Biological Interfaces (CBIO) group designed for an easy parenteral administration in soft tissues and to provide local and sustained drug release. Prior to injection, CarboCell is a clear homogeneous fluid with a low viscosity (<1000 mPa·s), which facilitates its injection using small-gauge needles. After injection in aqueous media or tissue, solvent efflux promotes the formation of a highly viscous self-assembling scaffold at the site of injection from which drug is released in a sustained manner.

The composition of CarboCell comprises three main elements: (i) a carbohydrate ester, (ii) a co-solvent, and (iii) a solvent. Carbohydrate esters are highly hydrophobic molecules and they represent the major constituent of CarboCell acting as the matrix of the formulation (40-70 weight/weight (w/w)%). Over the past years, multiple carbohydrate esters have been developed in the CBIO group. Mono-, di- or trisaccharides have been functionalized with various short ester groups (e.g., acetic, propionic and isobutyric esters) in a uniform manner or by combining different ester groups in the same individual sugar (Fig. 12). Thus, we count with a large group of carbohydrate esters, each one with unique physico-chemical properties that can influence the physical characteristics of CarboCell as well as the drug release kinetics [131].

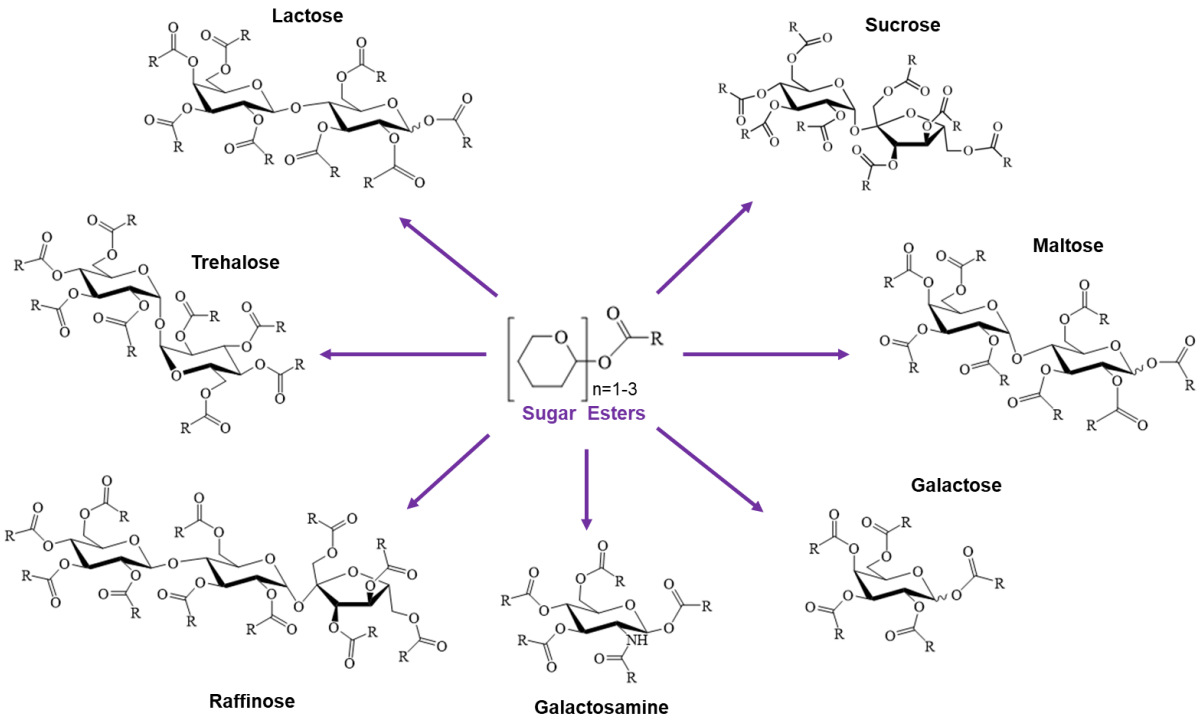

Figure 12. Chemical structure of some of the carbohydrate esters synthesized in the CBIO group. R represents methyl, ethyl, isopropyl or benzoate groups. The individual carbohydrates can have the same or different ester groups. (illustration adapted from [131]).

The co-solvents are triglycerides such as glyceryl trioctanoate (GTO) and glyceryl trihexanoate (GTH), which comprise 15-30 w/w% of the CarboCell composition. The addition of triglycerides improves the injectability of the formulation and modulates its softness both before and after injection. Once CarboCell is injected and the solvent diffuses out of the system, the formed depot is composed of the carbohydrate and the co-solvent since the triglycerides are also poorly mixable with water. The amount and type of co-solvent in the formulation influence the physical characteristics of the CarboCell; and the ratio between the carbohydrate ester and the co-solvent is of particular importance as it dictates the viscosity of the self-formed depot and consequently the drug release profile.

Solvents are chosen based on their ability to solubilize the carbohydrate ester and co-solvent mixtures and logically, pharmaceutically accepted solvents are preferred. Solvents used in the CarboCell system include EtOH, DMSO, propylene carbonate (PC) and benzyl alcohol (BenOH), and they constitute 10-30 w/w% of the formulation. The type and proportion of solvent particularly affects the viscosity of the CarboCell prior injection. Moreover, the solvents present different polarities, which influence their diffusion rate out of the CarboCell. As previously described for SAIB-based systems, the solvent efflux rate has a direct effect on the burst release [121].

Due to the hydrophobic nature of its components, water-insoluble molecules can be easily incorporated in CarboCell without the need of any chemical modifications. Over the last 25 years, an estimated 70 to 80% of novel small molecules drug candidates have been described as poorly soluble in water [132]. Water-insoluble molecules represent a challenge especially for liquid-based formulations for parenteral administration. Therefore, CarboCell provides a practical solution for the formulation of the increasing number of hydrophobic drugs. Moreover, multiple drug molecules can be simultaneously formulated in the CarboCell, allowing for the implementation of combination therapies.

The preparation of CarboCell is a straighforward process (Fig. 13). Briefly, the components are weighed in the corresponding ratios and then the mixture is subjected to ultrasonication at high temperatures (70 -80 °C) for approximately 1.5 - 2 h. Within this period, the mixture is occasionally vortexed to promote solubilization of the components and the process ends when obtaining a clear homogeneous solution. Next, the CarboCell is added on top of a previously prepared drug aliquot until achieving the required drug concentration. This new mixture is heated at 35 - 45 °C and homogenized using a magnet stirrer. This is considered an easy and gentle drug loading procedure, which helps in maintaining the integrity of the drug in the formulation. The simplicity of the preparation of CarboCell is advantageous as it might also facilitate its scale-up production.

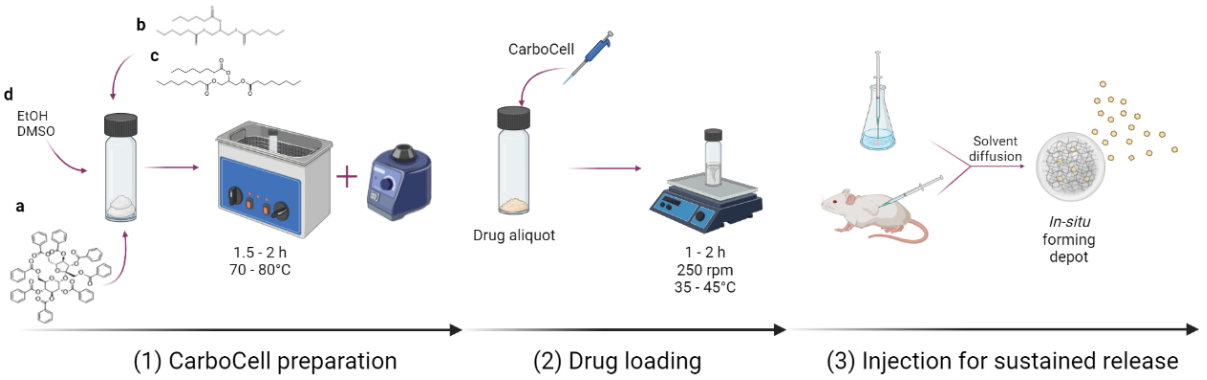

Figure 13. Schematic illustration of the preparation and function of the CarboCell drug delivery system. (**1**) The carbohydrate ester (e.g., (a) SuBen), co-solvents (e.g., (b) GTH or (c) GTO), and the corresponding (d) solvent (e.g., EtOH, DMSO) are proportionally weighed followed by sonication and vortexing to mix them and form a homogeneous clear solution. (**2**) CarboCell is added to a vial containing the previously aliquoted drug, which then is heated and mixed using a magnetic stirrer until the drug is fully dissolved. (**3**) After in-vitro or in-vivo injection, the solvent diffuses out of the CarboCell that results into an in-situ forming depot from which the drug is released in a sustained manner. (Illustration created with Biorender.com)

As previously mentioned, the self-formed CarboCell scaffold acts as a drug reservoir from which the drug is gradually released in a sustained manner. In the context of intratumoral immunotherapy, this is especially beneficial as the constant stimulation of the TME is ensured. The localized delivery also minimizes systemic drug exposure thereby preventing the associated toxic effects. Additionally, the drug molecules are protected within the CarboCell depot prior their release, thus avoiding premature drug degradation or clearance.

Importantly, CarboCell is intrinsically visible through magnetic resonance imaging (MRI) and ultrasound. The multimodal visibility of CarboCell was thoroughly demonstrated in a study conducted in our group, which additionally shows that additives such as CT contrast agents, UV-vis and near-infrared (NIR) fluorescence dyes can be straightforwardly incorporated to the formulation [133]. The visibility of CarboCell can allow live image-guided intratumoral injections and subsequent validation of the injection precision. This feature addresses the concern of low reproducibility when performing intratumoral injections as well as the correlated variability in therapeutic outcomes. Due mainly to the dramatic increase of viscosity upon injection, the CarboCell depot remains positionally stable after injection allowing its monitoring over time. Moreover, the visualization of the CarboCell scaffold can help in planning the optimum positions of injections as determined by combined anatomical and functional imaging [112], [134], [135].

1.5 General project overview and objectives

In spite of the advances and promising clinical results of cancer immunotherapy, there are still efficacy- and toxicity-related challenges hindering its broad application. For instance, therapy with CAR T cells has shown a good performance for hematological cancers, but it is not as effective for treating solid tumors [136]. In the case of ICIs, they rely on an anti-cancer adaptive immune response, which is low or absent in most of the cancer patients. Also, the systemic administration of ICIs is commonly associated with immune-related adverse effects, which in some cases might be irreversible [137].

In this project, we investigated the CarboCell system in synergy with small molecules targeted to reverse the immunosuppressive TME and activate the anti-cancer response. Following intratumoral delivery, the CarboCell system enables a continuous stimulation of the TME through the localized sustained release of the immunomodulatory drugs with minimal systemic exposure. CarboCell uses the tumor as a source of antigens expressed across multiple cancer cell clones. Thus, the CarboCell treatment initiates intratumoral immune activation, recruitment of immune cells and priming of T cells for a systemic polyclonal antitumor response, thereby addressing intra- and inter-tumoral heterogeneity.

The main class of immunomodulatory drugs used in this project were TLR7/8as. TLR7/8as have the ability of initiating an innate immunity response by inducing immune stimulatory cytokines and enhancing tumor antigen presentation by APCs. Consequently, the priming of T cells is facilitated, which is a fundamental step for the inhibition of tumor growth by the adaptive immune system. Therefore, TLR7/8as create a link between innate and adaptive immunity [138].

Resiquimod (R848), a synthetic small molecule and TLR7/8a, was the mainly featured drug molecule throughout the project. R848 belongs to the imidazoquinolines family like imiquimod, an FDA-approved immunotherapeutic. While R848 is able to produce a 50- to 100-fold higher cytokine response than imiquimod, its clinical application has been impeded mainly because of the severe toxicity caused after systemic administration [62], [139], [140]. The intratumoral administration of R848 in the CarboCell can prevent systemic exposure and toxicity, while promoting an enhanced antitumor response. Moreover, R848 is poorly soluble in water and this represents a challenge for its formulation as exemplified by imiquimod, whose administration is limited as a topical cream [48]. Here, CarboCell offers a solution for the formulation of hydrophobic molecules like R848.

Moreover, after injection, CarboCell´s self-assembling scaffold remains stable in position and it is visible through several image guidance modalities. Such feature can allow clinicians to validate the accuracy of the injection thereby improving injection reproducibility, a current concern for intratumoral administration. To further enhance the visibility of the CarboCell, in this project the incorporation of a CT contrast into the CarboCell formulation was also investigated.

The overall objective of this project was to aid in advancing the clinical translation of the CarboCell system for intratumoral immunotherapy with a focus on drug formulation and development. For this purpose, the general aims included:

- ☐ To characterize the physical and chemical properties of the CarboCell system, including the validation of drug stability in the formulation
- ☐ To investigate the correlation between the physico-chemical properties of CarboCell and drug release kinetics *in vitro* and *in vivo*
- ☐ To validate the efficacy and safety of CarboCell in synergy with immunomodulatory drugs in pre-clinical mice models
- ☐ To investigate formulation strategies that enable the incorporation of a wider range of drug molecules into the CarboCell system

Numerous CarboCell formulations were prepared and investigated throughout this project and to facilitate the results presentation, each chapter contains its own table detailing the CarboCell compositions used in the specific chapter. The reader must remember that the name identifiers of each CarboCell are different between chapters.

Chapter 2.
Investigation on the stability of R848 in various CarboCell formulations

2.1 Background

Drug stability is a critical quality attribute in any pharmaceutical formulation. According to the United States Pharmacopeia (USP), drug stability is defined as “the extent to which a drug substance or product retains, within the specified conditions, the same properties and characteristics that it possessed at the time of its manufacture”. As part of the regulatory requirements, ensuring drug stability is a fundamental part during the drug formulation development since it has a direct impact on the therapeutic efficacy of the drug product as well as on the safety of the patients [141].

Drug molecules can be susceptible to multiple forms of chemical decomposition during its processing, storage and until its use [141], [142]. As described in the International Council for Harmonization (ICH) guidelines, a drug impurity is a new chemical entity that is not the originally defined drug substance [143]. Chemical reactions, for example hydrolysis and oxidative degradation, might generate impurities in the drug formulation that even in small amounts can be detrimental in several ways [144]. The presence of undesired chemical entities may cause changes in the physical properties of the formulation (e.g., color, odor), generate incompatibility between components of the formulation and limit its shelf life. More importantly, impurities might lead to a decreased therapeutic effect and, or alternatively, cause unwanted toxicological effects. Thus, the formulation development process involves physical and chemical characterization of the drug product that helps in identifying the components that either promote or negatively affect the stability of the drug molecule. In this regard, it is important to highlight that drug instability can also be triggered by external environmental factors such as light and temperature. [142], [144].

The influence of pharmaceutical ingredients on drug stability is a key evaluation aspect during formulation development. In the context of the CarboCell system, carbohydrate esters represent the major component in the formulation. Previously, a wide variety of carbohydrate esters has been synthesized in the CBIO group as derivatives of mono-, di- and trisaccharides (Fig. 12). One way to classify these sugars is as reducing and non-reducing. A reducing carbohydrate refers to a sugar that contains a free aldehyde or ketone group and consequently can act as a reducing agent. Following this principle, all monosaccharides are then classified as reducing sugars. In contrast, non-reducing sugars lack a free aldehyde or ketone, meaning that they cannot donate electrons to other molecules [145].

Regarding disaccharides, the distinction between reducing and non-reducing carbohydrates is indicated by the anomeric carbons in the molecule. The anomeric carbon is a stereocenter and refers to the carbon derived from the carbonyl group in the straight chain configuration of the sugar, i.e., before it reacts with its own hydroxyl group. Depending on the direction of the hydroxyl group in the anomeric carbon, two different molecules (α or β anomers) can result from the cyclization of the sugar. At equilibrium, both anomers exist in solution and they can interconvert by mutarotation, a process that refers to the change between the open chain and cyclic form of a carbohydrate. Nevertheless, mutarotation can only occur if the anomeric carbon is free or, in other words, is not involved in any bond [145]. For instance, in sucrose and trehalose, the anomeric carbons of their two forming monosaccharides are implicated in the glycosidic bond. Therefore, these sugars are not able to convert to its open chain form and are classified as non-reducing carbohydrates. In the case of maltose and lactose, just one out of their two anomeric carbons is implicated in the glycosidic bond; consequently, the free anomeric carbon enables mutarotation so the sugar can switch between the cyclic and open chain configuration (Fig. 14).

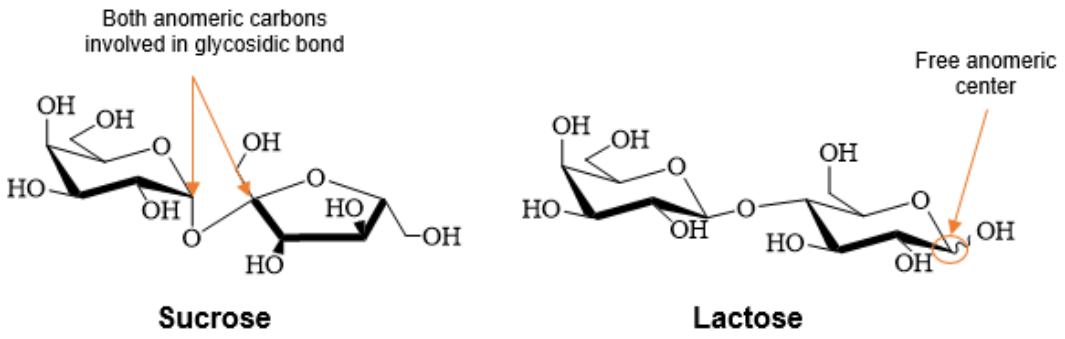

Figure 14. Anomeric carbons in sucrose and lactose. Both anomeric carbons in sucrose are involved in the glycosidic bond, whereas lactose has one free anomeric center. Therefore, mutarotation cannot occur in sucrose, but it does in lactose resulting in the formation of anomers.

Previously in our group, lactose octaisobutyrate (LOIB) was the carbohydrate ester used in one of the lead formulations of CarboCell under investigation. This formulation also included the drug molecule R848. R848 in such LOIB-based CarboCell had undergone several preclinical tests and during this period, UV-vis spectroscopy was the main analytical method to determine the concentrations of R848 in experiments such as *in vitro* drug release studies. Despite its practicality, one of the disadvantages of UV-vis spectroscopy is that is not a selective method because it cannot discriminate between the molecule of interest and other chemical entities that absorb light at the same wavelength [146]. When switching to high performance liquid chromatography (HPLC), a highly selective analytical method, chromatograms from release media samples showed the presence of not only R848 but also an unknown molecule. Hereafter, an investigation began to determine the source of the impurity and identify the factors that triggered its formation.

2.2 Objectives

It is essential that CarboCell-R848 formulations advancing on the development pipeline have an adequate stability. In this project, the stability of R848 was investigated in multiple CarboCell formulations with the following objectives:

- ☐ To identify potential impurities derived from R848 in the CarboCell
- ☐ To evaluate the effect of temperature as well as the addition of acidic and basic compounds on the stability of R848 in the CarboCell
- ☐ To investigate the effect of various carbohydrate esters on the stability of R848, specifically on regards to their anomeric center
- ☐ To determine adequate conditions for enhancing drug stability in the CarboCell system

2.3 Results and discussion

Identification of impurities in R848-CarboCell

One of the main CarboCell formulations formerly investigated in the group consisted of LOIB:GTO:EtOH (82.5:7.5:10 w/w%) with 1.2 mg/g R848, further referred to as R2 CarboCell (CC). Preliminary HPLC analyses had suggested the presence of impurities in the CarboCell. So initially, to evaluate the stability of R848, the R848-R2 formulation was incubated at 37°C and the integrity of R848 was monitored over time. Additionally, an *in vitro* drug release study was done to identify the molecules being released from the CarboCell.

At 320 nm, a wavelength specific for R848, the HPLC chromatograms from both the release media and the CarboCell revealed an additional peak corresponding to a chemical entity other than R848 (Fig. 15A). To determine the mass of the molecules, the samples were analyzed by liquid chromatography-mass spectrometry (LC-MS). The measured m/z values were 315.1 and 385.3 (Appendix II-S2). The former value was confirmative for R848, whose exact mass is 314.2. The higher m/z value of the unidentified molecule suggested that R848 had acquired an additional moiety. The difference between the m/z values of both molecules was 70.2; thus, by examining the chemical structure of the components of the CarboCell (LOIB, GTO and EtOH), it was found that the additional mass corresponded to the isobutyrate group in the esterified carbohydrate. Next, to determine the chemical structure of the newly formed molecule, the samples were analyzed by nuclear magnetic resonance (NMR). Hence, the mass and chemical structure of the modified R848 was confirmed, and this molecule was named R848-isobutyrate (R848-IBA) (Fig. 15C).

Furthermore, the analysis of R2 CC after incubation at 37°C showed that the amount of R848-IBA in the formulation increased gradually over time. After 14 days, around 80% of R848 had converted to R848-IBA (Fig. 15D). When analyzing the release media from R2 CC, it was observed that the fraction of R848-IBA also increased steadily. At 14 days post-injection, approximately 40% of the total drug released corresponded to R848-IBA (Fig. 15E). The presence of R848-IBA could compromise the

reliability of the results from previous and subsequent preclinical tests since the potency and toxicity profile of R848-IBA are unknown.

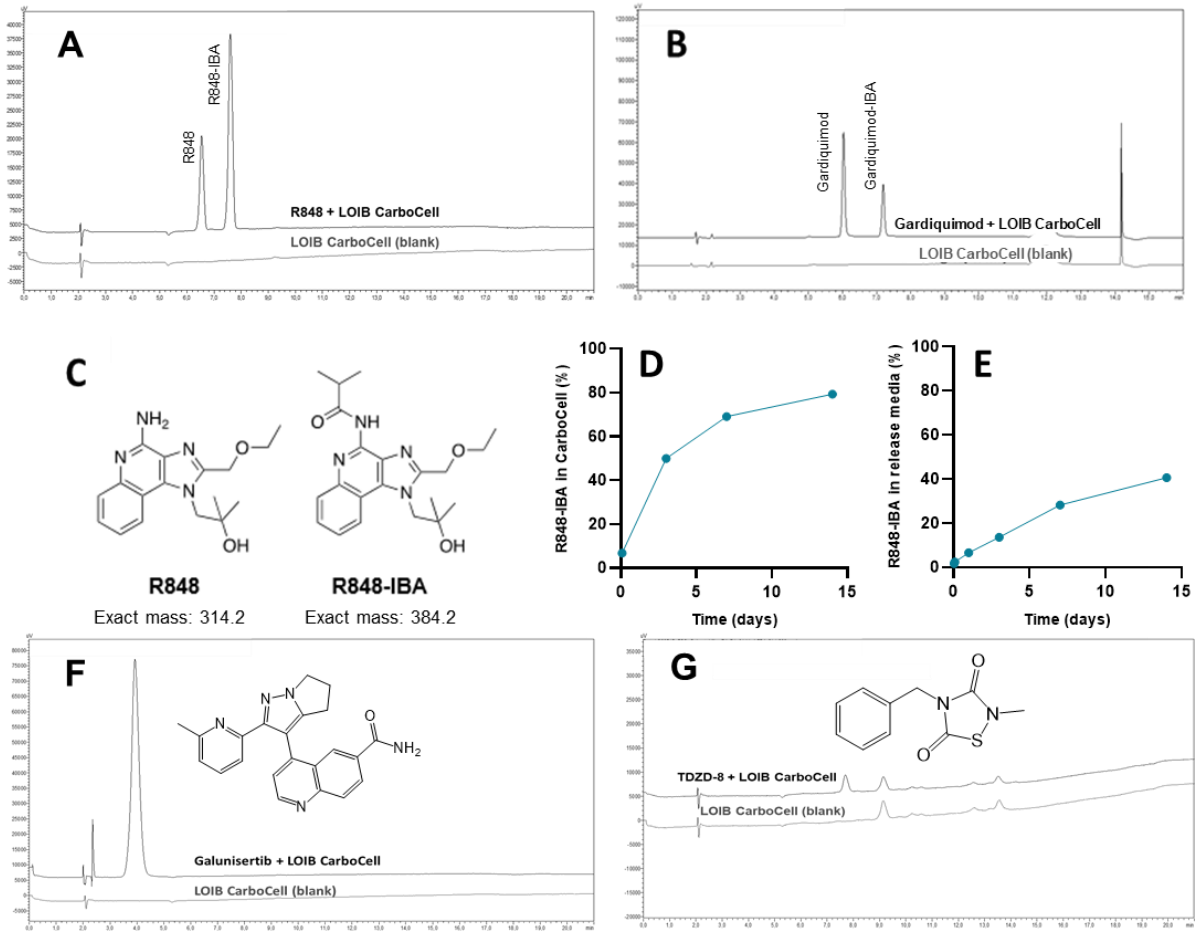

Figure 15. Instability of the imidazoquinolines R848 and gardiquimod in LOIB-based CarboCells. (**A**) Representative HPLC chromatograms of R2 CarboCell containing R848 versus a blank CarboCell; the sample was taken after incubation for 7 days at 37°C. (**B**) Representative HPLC chromatograms of the release media from a R2 CarboCell containing gardiquimod versus a blank CarboCell; the sample was taken after incubation for 14 days at 37°C. (**C**) Chemical structures of R848 and R848-IBA, which was detected in LOIB-based formulations. (**D, E**) Percentage of R848-IBA detected at 37° C in (**D**) R2 CarboCell and the (**E**) release media after its injection of PBS. (**F-G**) HPLC chromatograms of (**F**) galunisertib (UV at 320 nm) and (**G**) TDZD-8 (UV at 260 nm) after incubation for 14 days in R2 CarboCell compared to a blank CarboCell; the chemical structure of each molecules are shown in the corresponding chromatogram. The AUC of R848 and R848-IBA was measured by HPLC (UV detection at 320 nm) and the reported values correspond to the AUC percentage of R848-IBA in a given sample (n=2). Abbreviations: AUC: area under the curve.

Next, gardiquimod, another TLR7/8a from the imidazoquinolines family was also formulated in R2 CC to evaluate if drug instability in such CarboCell was specific to R848. Like in the formulation containing R848, a chemical entity besides gardiquimod was detected in both the R2 CC and the release media (Fig. 15B). An LC-MS analysis of the samples showed that the difference in the m/z values of the two detected compounds was also 70.2 Therefore, it was established that gardiquimod was also prone to acquire an isobutyrate moiety from LOIB.

The addition of the isobutyrate group occurs in the primary quinoline amine of both R848 and gardiquimod, so two additional molecules with different chemical structures (galunisertib and TDZD-8) were tested in R2 CC to assess if there was a correlation between drug instability and its chemical structure. After incubation at 37°C for 14 days, no additional drug-derived molecules were detected in

neither galunisertib nor TDZD-8 formulations. The chemical structure of TDZD-8 does not share any features with the imidazoquinolines (Fig. 15G). Galunisertib has a quinoline group and a primary amine though in different configurations than R848 and gardiquimod, regardless, galunisertib was not prone to chemical modifications within R2 CC. This suggested that imidazoquinolines are particularly unstable in the R2 CC formulation; and it is probable that drug substances from other structure classes will be less reactive in LOIB-based CarboCells.

Effect of temperature, acids and bases on R848 stability

Subsequently, we wanted to investigate if the presence of acidic and basic compounds as well as temperature would influence the stability of R848 when formulated in R2 CC. To evaluate the former, benzoic acid (BA) and trimethylamine (TEA) were added to R848-R2 CC and incubated at 37°C. We were particularly interested in the effect of BA, since LOIB powder might contain undetectable traces of acid residues from the synthesis process, which might be catalyzing the formation of R848-IBA.

It was found that when adding BA, the equilibrium of the reaction forming R848-IBA was shifted. In the presence of BA, a reaction equilibrium was reached after 3 days at 37°C, afterwards the percentage of R848-IBA in R2 CC remained constant at around 18%. Contrastingly, when adding TEA the reaction equilibrium was reached after 14 days with approximately 80% of R848-IBA present in R2 CC. Moreover, the trend of the R848 conversion observed in the R2 CC with TEA was comparable to the regular R2 CC formulation, so the addition of TEA did not have an apparent effect on the formation rate of R848-IBA (Fig. 16B). We hypothesize that the aromatic amines in R848 act as base catalysts for the acylation of its primary amine. Thus, due to the addition of BA, the greater amount of protons will make the aromatic amines in R848 to be more protonated, which hinders their reactivity so the acylation of the amine in R848 occurs at a lower degree. Moreover, since BA actually shifted the reaction equilibrium favoring the preservation of R848, it is unlikely that acid traces, if any, in the LOIB material are causing the modification of R848. While the addition of acid might help improving the stability of R848, a high amount of acid might have a negative effect upon CarboCell injection as it may cause irritation or inflammation at the injection site.

To study the effect of temperature on drug stability, R2 CC was stored at 4°C and 37°C and the drug fraction corresponding to R848-IBA was determined after 5 days. It was found that around 15% of R848-IBA was present in the formulation at 4°C, whereas R848-IBA accounted for nearly 70% of the total drug substance at 37°C (Fig. 16A). Thus, at 4°C there was a decrease of approximately 5-fold in the conversion rate of R848. Not surprisingly, a lower temperature slowed down the reaction kinetics leading to a reduced formation of R848-IBA. In the case of unstable drugs, it is a very common strategy to set low storage temperatures (ranging from -80°C to 4°C) to avoid unwanted degradation and extend the shelf life of the drug product [147]. Nevertheless, a R848 conversion of circa 15% after only 5 days is still not adequate enough to define the drug as stable in R2 CC, especially when considering that the minimum shelf life for a drug product to be commercially viable is 2 years [148].

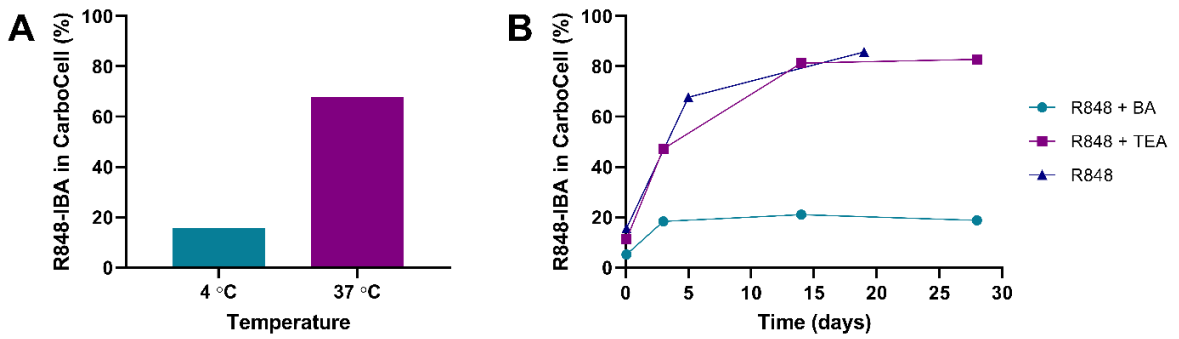

Figure 16. Effect of temperature, BA and TEA on the stability of R848 in a LOIB-based CarboCell. (**A**) Percentage of R848-IBA in R2 CarboCell after 5 days at either 4°C or 37°C. (**B**) Percentage of R848-IBA in CarboCells following addition of BA or TEA and incubation at 37°C. The AUC of R848 and R848-IBA was measured by HPLC (UV detection at 320 nm) and the reported values correspond to the AUC percentage of R848-IBA in a given sample.

Effect of carbohydrate esters on R848 stability

Since it had been determined that R848-IBA was derived from R848 reacting with an isobutyrate moiety from LOIB, next we wanted to investigate if drug instability could be prevented by using other carbohydrate esters. Hence, non-reducing carbohydrate esters (SAIB, SOIB, ROIB, SuBen and RaBen) and reducing carbohydrate esters (LOIB, LOP and LacBen) were used as the matrix of several CarboCell compositions (the full name of the sugar esters can be found in Table 1 and their chemical structure in Fig. 17). Additionally, a CarboCell composed only of LOIB and EtOH (CC1) was prepared to discard that GTO was promoting the conversion of R848. The stability of R848 at 37°C in the multiple CarboCells was monitored over time.

Table 1. Overview of the composition of the evaluated CarboCell formulations expressed as weight percent (w/w%). Abbreviations: LOIB: lactose octaisobutyrate, LOP: lactose octapropionate, SAIB: sucrose acetate isobutyrate, SOIB: sucrose octaisobutyrate, ROIB: raffinose octaisobutyrate, TOIB: trehalose octaisobutyrate, SuBen: sucrose octabenzoate, RaBen: raffinose octabenzoate, LacBen: lactose octaisobutyrate, MeLOIB: methoxy-LOIB, GTO: glyceryl trioctanoate, EtOH: ethanol.

CarboCell	Chemical components (w/w%)											
	LOIB	*LOP*	*SAIB*	*SOIB*	*ROIB*	*TOIB*	*SuBen*	*RaBen*	*LacBen*	*MeLOIB*	*GTO*	*EtOH*
R2 CC	82.5	-	-	-	-	-	-	-	-	-	7.5	10
CC1	82.5	-	-	-	-	-	-	-	-	-	17.5	-
CC2	-	82.5	-	-	-	-	-	-	-	-	7.5	10
CC2	-	-	82.5	-	-	-	-	-	-	-	7.5	10
CC4	-	-	-	80	-	-	-	-	-	-	10	10
CC5	-	-	-	-	80	-	-	-	-	-	10	10
CC6	-	-	-	-	-	80	-	-	-	-	10	10
CC7	-	-	-	-	-	-	60	-	-	-	25	15
CC8	-	-	-	-	-	-	-	60	-	-	25	15
CC9	-	-	-	-	-	-	-	-	60	-	25	15
CC10	-	-	-	-	-	-	-	-	-	82.5	7.5	10

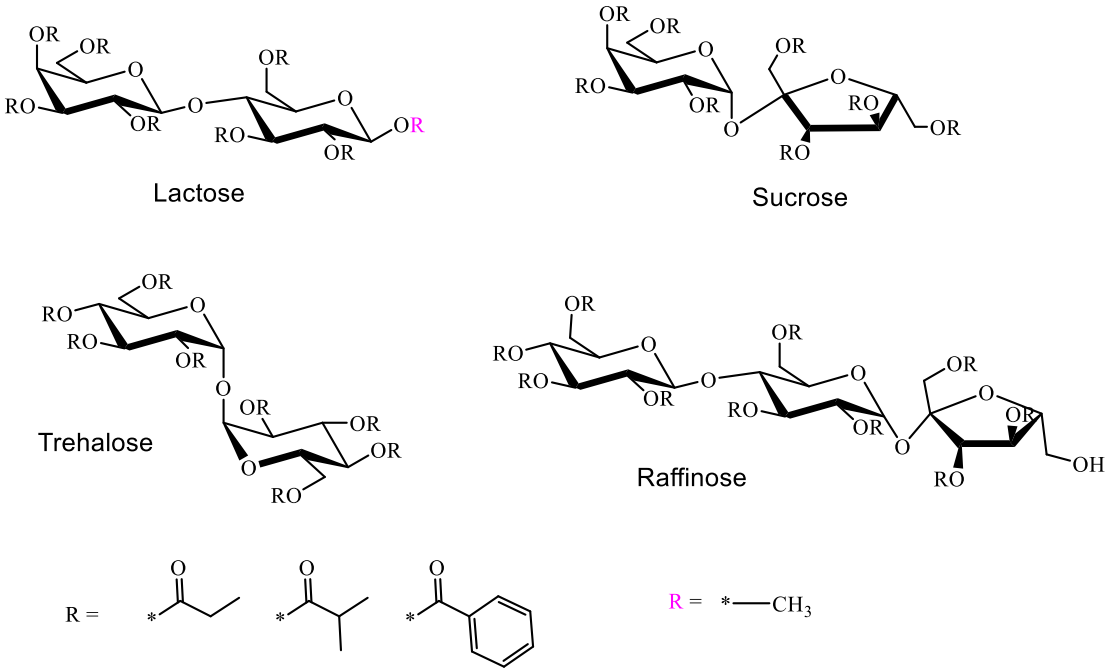

Figure 17. Chemical structure of the tested carbohydrate esters. The carbohydrates can be uniformly functionalized with different moieties. The functionalization to block the anomeric center in the lactose esters is highlighted in pink. The chemical structure of SAIB is shown in Fig. 11.

A similarly high fraction of R848-IBA was detected in LOIB-based formulations irrespective of the presence of GTO. Thus, it was determined that GTO did not influence the modification of R848. An equally high percentage of modified R848 was found in the LOP CarboCell, however, in this case R848 acquired a propionate group from LOP as confirmed by LC-MS (Fig. 15C, Appendix II-S3). Interestingly, both LOP and LOIB are ester derivatives of lactose, a reducing sugar possessing a free anomeric center (Fig. 18A). In contrast, CarboCells composed of non-reducing carbohydrate esters showed a noticeably lower degree of R848 conversion (Fig. 18B). From the non-reducing sugars group, SAIB was the one that displayed a higher reactivity towards R848. Unlike the other carbohydrate esters, SAIB is not uniformly esterified as it contains mixed acetate and isobutyrate esters. However, in SAIB samples only R848-IBA was detected (Fig. 18C), so apparently R848 did not acquire an acetate group from SAIB. Alternatively, if R848 did acquired an acetate group from SAIB, the resulting molecule might have converted back to R848. These results suggested that R848 is more stable in formulations comprising non-reducing carbohydrate esters. However, using reducing carbohydrate esters might still be desirable because mixtures of anomers tend to be less prone to crystallization, which can enhance their solubility in different solvents and co-solvents [131].

Remarkably, R848 maintained its chemical integrity in CarboCells comprising SuBen, RaBen and LacBen, meaning that no R848-derived molecules were detected throughout the study (Fig. 18A, B). R848 was stable regardless of the anomeric centers in the carbohydrate esters. SuBen and RaBen are non-reducing sugars with occupied anomeric centers, while LacBen is classified as a reducing carbohydrate due to its free anomeric center. SuBen, RaBen and LacBen are fully esterified with benzoate groups. Therefore, we hypothesize that the bulkiness of the benzoate moieties present in the

aforementioned sugars cause steric hindrance, which impedes the reactivity with R848 [149]. This might also explain why SAIB was more reactive with R848 than SOIB, ROIB and TOIB; some of the isobutyrate groups in SAIB may experience less steric hindrance because SAIB also has acetate groups, which are smaller, less bulky functional groups. Hence, both the anomeric center and the steric bulk of the moieties in the carbohydrate esters have an influence in the stability of R848 in the CarboCell. Nonetheless, it is expected that R848 would have an enhanced stability in formulations in which the carbohydrate esters, either reducing or non-reducing, contain benzoate groups.

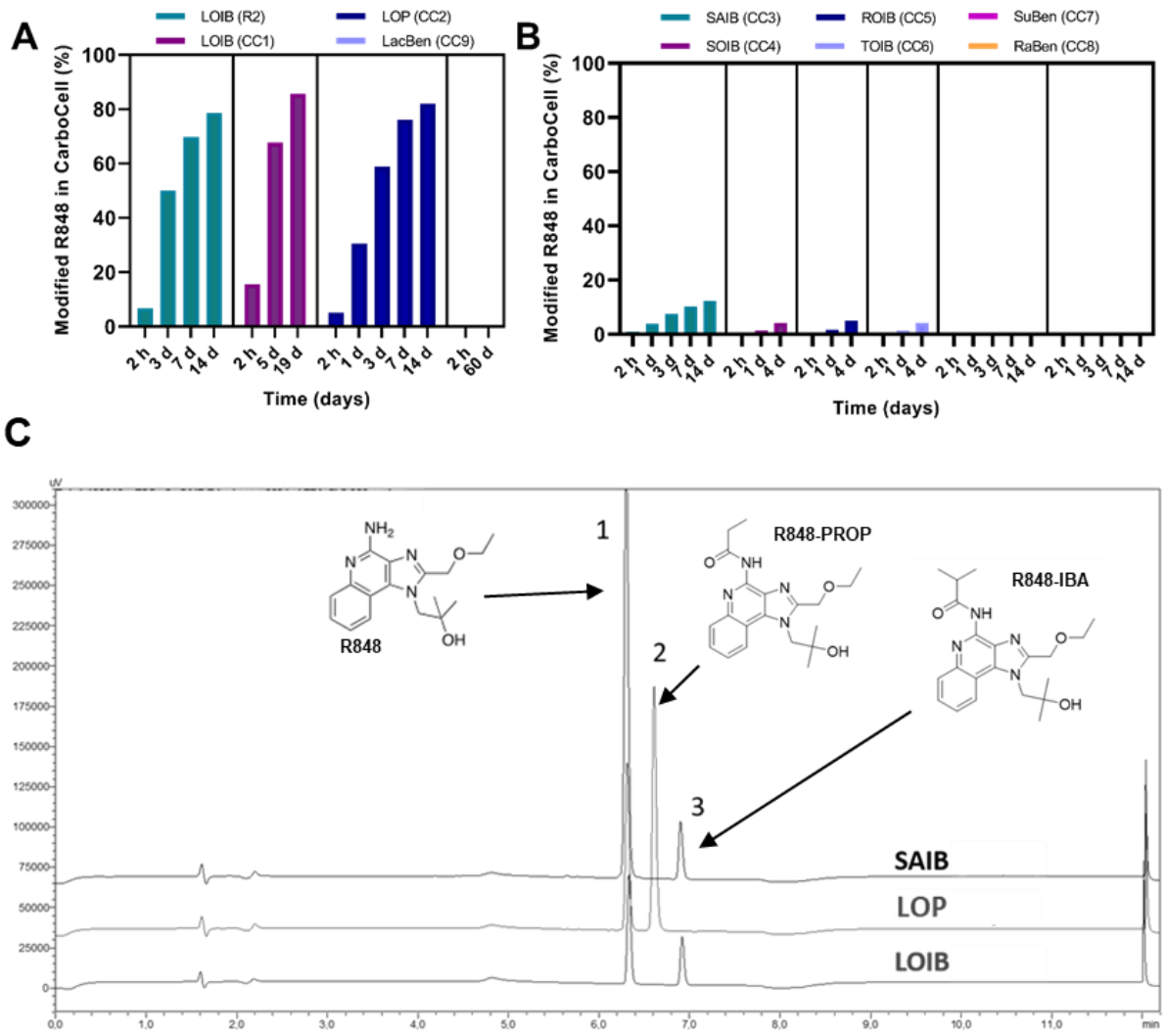

Figure 18. Effect of different carbohydrate esters on the stability of R848. (**A**) Percentage of modified versions of R848 detected over time in the CarboCells containing carbohydrate esters derived from a reducing sugar (lactose) as matrix. (**B**) Percentage of modified versions of R848 detected over time in the CarboCells containing carbohydrate esters derived from non-reducing sugars (sucrose, trehalose and raffinose). (**C**) HPLC chromatograms of the release media from three different CarboCell formulations (from top to bottom: F3, F2 and R2) taken after 7 days; the identity of each peak was confirmed by LC-MS and the corresponding chemical structure is shown in the image. All formulations were incubated at 37C. The AUC of R848 and R848-IBA was measured by HPLC (UV detection at 320 nm) and the reported values correspond to the AUC percentage of R848-IBA in a given sample; data points correspond to single measurements. Note: the percentage of modified R848 in LacBen, SuBen and Raben-based formulations is not included as R848 maintain 100% integrity throughout the study.

To further evaluate the influence of the anomeric center in the stability of R848, the isobutyric acid on the anomeric center of LOIB was substituted with a methoxy ether thereby creating a novel carbohydrate ester referred to as methoxy-LOIB (MeLOIB). Ester bonds are more reactive than ether

bonds, as the former contains a carbonyl group that is susceptible to a nucleophilic attack. Hence, a lower reactivity of MeLOIB was expected. R848 was then formulated in a MeLOIB-based CarboCell and incubated at 37°C. After 2 months, R848 did not display signs of instability. All the chromatograms from this formulation only showed a single peak for R848 and none of its modified versions were detected (Fig. 19). This suggests that by blocking the anomeric center in reducing carbohydrate esters, long-term stability of R848 might be achieved as the reactivity towards R848 was abolished. Furthermore, the anomeric center might be blocked in other reducing sugars through a methoxy ether, ethyl ether, or other ether linked groups.

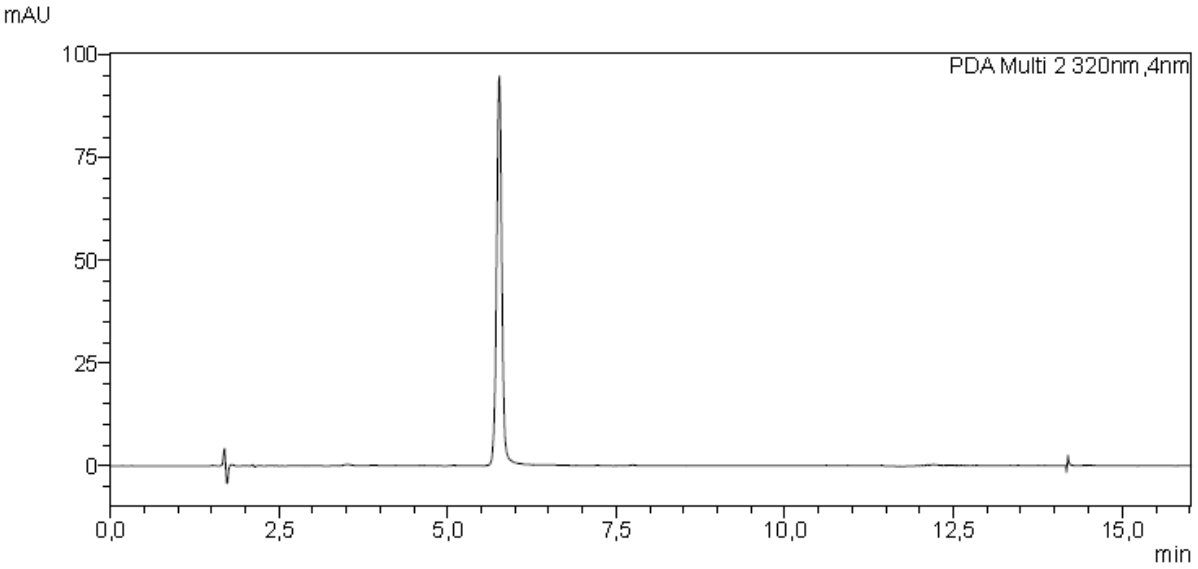

Figure 19. Representative HPLC chromatogram of a CarboCell formulation containing R848 as an intact molecule. R848 is considered stable since no modified versions of the molecule are detected (i.e., no additional peaks are observed) (UV detection at 320 nm).

Stability of R848 in SuBen-based CarboCells

According to the previous results, R848 is expected to have high long-term stability in CarboCells formulated with non-reducing carbohydrate esters containing benzoate groups. For this reason, it was decided to select SuBen as the leading carbohydrate ester for subsequent R848-CarboCell formulations. Another reason for choosing SuBen is that this is a commercially available chemical. Besides SAIB, all the formerly used carbohydrate esters had to be synthesized in house. Thus, SuBen being supplied by Sigma-Aldrich is a more convenient and practical option. However, it was noticed that such SuBen was not pure despite the label claiming >99% purity. The HPLC from a SuBen standard solution revealed that more than one chemical entity was present in the material (Fig. 20A). The sample was then analyzed by matrix-assisted laser desorption/ionization-time of flight (MALDI-TOF) MS and three less esterified forms of SuBen were detected. Hence, besides sucrose octabenzoate (SuBen), the material from Sigma-Aldrich contained sucrose hepta-, hexa-, and pentabenzoate (Appendix II-S4). This finding highlights the importance of verifying the quality of purchased materials before use.

Since the presence of benzoate groups is key to enhance the stability of R848, we needed to investigate if having less esterified SuBen derivatives in the formulation would affect the reactivity of R848. For this purpose, the SuBen powder from Sigma-Aldrich (from now referred to as σ-SuBen) was purified to obtain solely the fully esterified carbohydrate, which was denoted as π-SuBen (Fig. 20B). Next, CarboCells with either σ- or π-SuBen were prepared (CC7). The short-term stability of CarboCell in these formulations was evaluated at 4°C and 37°C. After 14 days, R848 remained chemically stable in both CarboCells at either temperature. Again, no R848-derived molecules were detected in any of the HPLC chromatograms (Fig. 19).Given that the two SuBen materials did not cause apparent differences in the stability of R848, it was decided to continue using σ-SuBen as the matrix of CarboCell.

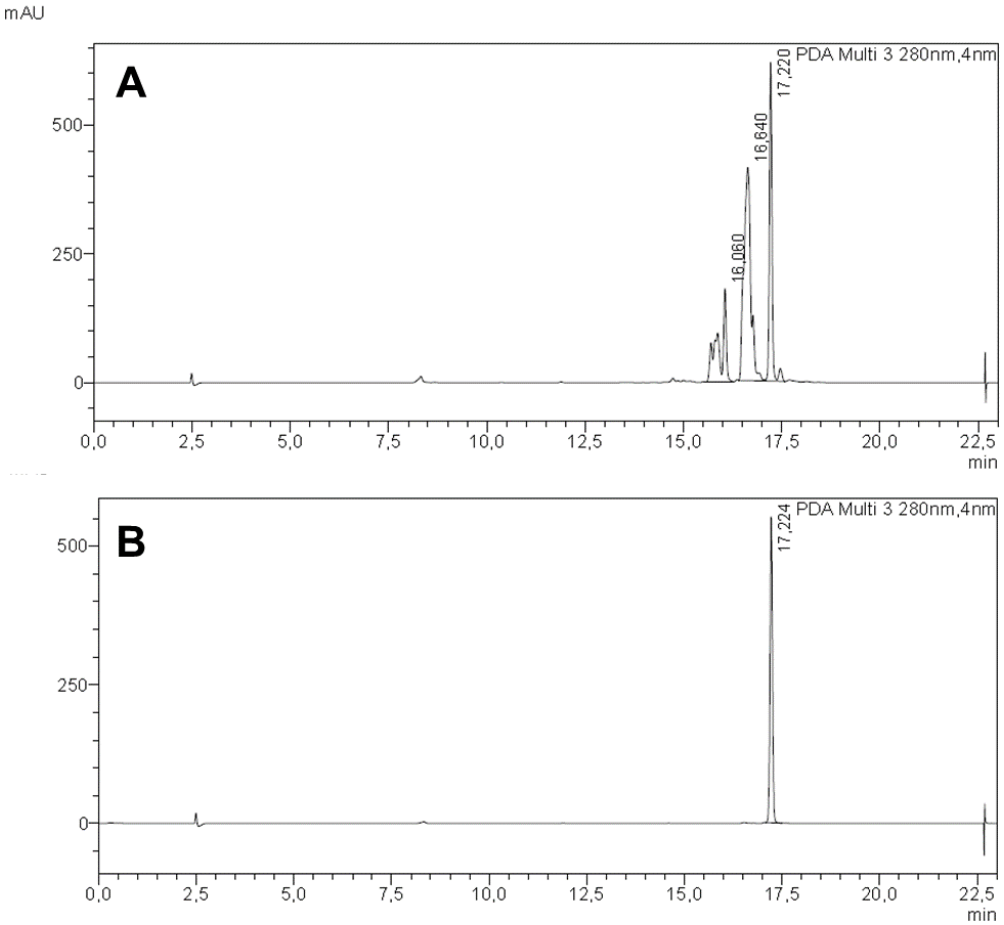

Figure 20. σ-SuBen and π-SuBen. HPLC chromatograms of 1 mg/mL standard solutions of (**A**) σ-SuBen and (**B**) π-SuBen. The fully esterified sucrose (octabenzoate) has a retention time of 17.2 min.

To validate that R848 would be stable for longer periods, R848 in a CarboCell comprising σ-SuBen was prepared and incubated at 4°C and 37°C for more than 3 months. Additionally, an *in vitro* drug release study of the aforementioned formulation was done to verify that R848 would not be modified upon injection of the CarboCell. The drug release study lasted 7 weeks, after which the amount of R848 in the release media as well as the R848 amount left inside the self-formed depot was determined by HPLC. As expected, only R848 was detected in both the release media and the self-formed depot. Since the mass of injected CarboCell was known, it was possible to calculate how much R848 was

initially in the self-formed depot. After adding the amounts of released R848 and what was left in the depot, the sums matched the originally injected amount of R848 (100.9 ± 0.2%) (Table 2). This result confirmed that neither degradation nor modification of R848 had occurred. Moreover, after 23 weeks at 4°C and 37°C, the HPLC chromatograms confirmed that R848 maintained its chemical integrity (Fig. 19). Therefore, it was concluded that σ-SuBen CarboCells confer high stability to R848. Even though long-term stability studies need to be done, the observed results are encouraging to suggest that this CarboCell formulation might achieve a shelf life of at least 2 years likely even at room temperature.

Table 2. Results from the in vitro R848 release study with σ-SuBen CarboCell. The amount of released R848 and R848 left in the self-formed depot were determined 7 weeks post-injection. The addition of these values resulted in the calculated amount of total R848.

Injection Nr.	Injected amount of R848 (µg)	R848 released (µg)	R848 left in the depot (µg)	Calculated amount of total R848 (µg)
1	129.7	81.8	49.1	130.9
2	127.4	80.1	48.1	128.2
3	127.1	81.8	46.7	128.5

2.4 Concluding remarks and future perspectives

Drug stability is a fundamental attribute that needs to be investigated and ensured in any pharmaceutical formulation. The presence of impurities or degradation products from the drug not only affects the integrity and quality of the formulation, but it can also have a negative effect on the therapeutic efficacy and safety of the treatment. Thus, as a critical aspect during formulation development, the stability of R848 in the CarboCell was evaluated.

R848 was found to undergo a chemical modification when formulated in CarboCells in which LOIB was the carbohydrate matrix. The chemical reaction between LOIB and R848 resulted in the addition of an isobutyrate group from LOIB in the primary amine of R848. The conjugation of HPLC, LC-MS and NMR analysis allowed the identification of such R848 derivative namely R848-IBA. The same chemical modification was observed for gardiquimod, but not for other drug substances out of the imidazoquinoles family. Moreover, both an acidic environment and low temperature shifted the reaction equilibrium resulting in a lower formation of R848-IBA. These conditions should be kept in mind as strategies to enhance the stability not only of R848, but also for other drug molecules in future CarboCell formulations.

Furthermore, the stability of R848 was considerably lower in CarboCells comprising reducing carbohydrate esters. The lack of a free anomeric center in non-reducing carbohydrate esters was deemed as a key feature to reduce the reactivity towards R848. The importance of the anomeric center was demonstrated by blocking the anomeric center in LOIB via the addition of a methoxy group in the anomeric carbon. In this case, the formation of R848-IBA was abolished and R848 was preserved intact. Nonetheless, R848 was chemically stable in formulations where the carbohydrate esters contained

benzoate groups irrespective of the sugars being reducing or non-reducing, suggesting that steric hindrance can prevent modifications to R848. Hence, non-reducing sugars with benzoate groups were considered as the best option to ensure the stability of R848 in the CarboCell. R848 was stable in both π-SuBen and σ-SuBen, and σ-SuBen was chosen as the main carbohydrate esters for future formulations in part due to its commercial availability. Remarkably, R848 showed excellent short-term stability in a SuBen-based CarboCell after *in vitro* injection and when incubated at 4°C and 37°C thereby making it a promising formulation for further development, a topic that will also be discussed in Chapter 4. Moreover, even though the analysis were focused on drug chemical stability, no changes in the physical characteristics of the formulation were observed throughout the studies; specifically, all formulations remained clear, homogeneous solutions free of any visible particles and with no apparent differences in fluidity.

While the obtained results are very encouraging, in the future, supplementary stability studies still need to be performed. Besides long-term studies, CarboCells should be subjected to stress conditions to which it might be exposed during its life cycle. This includes, for example, higher temperatures and specific relative humidity values. In this project, the stability of R848 was evaluated by measuring the area under the curve (AUC) proportions in the HPLC chromatograms between R848 and any derived chemical entity. The monitoring of drug stability might be optimized by validating an HPLC method to quantify the actual concentration of R848 in the formulation. Besides serving as quality control, such approach also helps ensuring that R848 is not being degraded into undetectable compounds. Moreover, even though reducing carbohydrate esters like LOIB and LOP promoted the modification of R848, this does not mean that such instability effects will be necessarily observed in other drug molecules. Therefore, stability needs to be assessed on a case-by-case basis. Lastly, in an attempt to overcome the stability challenges presented by R848, the R848-derivatives identified in these studies served as inspiration to develop R848 prodrugs. In these molecules, the primary amine of R848 was protected from possible interactions with the carbohydrate esters in CarboCell, but once released they would act as R848. These novel molecules will be discussed in the following chapter.

2.5 Materials and methods

Chemicals

All chemicals were purchased from Sigma Aldrich, Merck unless stated otherwise. Ethanol (absolute), acetonitrile (MeCN) and dimethyl sulfoxide (DMSO) were purchased from VWR Chemicals. R848 was purchased from AmBeed and gardiquimod from InvivoGen. TDZD-8 and galunisertib were purchased from Selleckchem. LOIB was obtained from Carbosynth and purified in house. All the other carbohydrate esters, except σ-SuBen (Sigma Aldrich) and SAIB (kindly provided by Nanovi A/S), were synthesized in the CBIO group [150].

Preparation of CarboCell

CarboCell formulations were prepared by mixing the carbohydrate esters (SuBen, LacBen, RaBen, etc.) with GTO and EtOH. The different compositions are indicated in weight percent in Table 1, and the corresponding amount of compound was weighed into one vial. The mixture was placed in an ultrasonication bath at 70-80°C for 1-2 hours and occasionally vortexed to generate homogenous solutions, namely CarboCells, which were stored at 4 °C until further use. Drug molecules were incorporated into the formulation by proportionally adding CarboCell on top of a previously freeze-dried drug aliquot, until reaching a drug concentation of 1.2 mg/g. CarboCells were subjected to magnetic stirring at 40-50 °C until the drug was completely dissolved.

HPLC method

HPLC analyses were done using a Shimadzu Nexera-i HPLC instrument with a PDA detector. The samples were injected (5 µL) onto a Waters Terra RP18 column (5µm, 4.6x150mm, temperature 25 °C) at a flow rate of 0.8 mL/min. The solvent system consisted of mobile phase A (5% MeCN, 0.1% trifluoroacetic acid (TFA) in water) and mobile phase B (0.1% TFA in MeCN). Chromatographic separation was achieved using a gradient of 0 to 100% phase B in 15 min. Ultraviolet detection at 260 nm, 280 nm or 320 nm was used to identify the specified compounds.

LC-MS method

Samples were analyzed in an ACQUITY UPLC instrument coupled with a QDa detector. Samples (5 µL) were injected onto a Waters BEH C18 column (2.1 µm, 2.1x50mm, temperature 40°C) at a flow rate of 0.4 mL/min. The solvent system consisted of mobile phase A (5% MeCN, 0.1% FA in water) and mobile phase B (0.1% FA in MeCN). Chromatographic separation was achieved using a gradient of 0 to 100% phase B in 6 min.

In vitro drug release

50 µL of each tested CarboCell were individually injected in 8-mL glass vials containing 2 mL of phosphate-buffered saline (PBS). The vials were incubated at 37 °C and at each sampling point 1 mL of PBS was taken. 1 mL of fresh buffer was added immediately to the vial to replace the taken sample. The samples were then analyzed by HPLC (UV detection at 320 nm, gradient of 0-50% phase B in 5 min) and the AUC of R848 and modified versions of R848 was measured. When applicable, at the end of the release study, the PBS was carefully removed from the vials and 1 mL of MeCN was added to dissolve the CarboCell. A sample from the dissolved CarboCell was analyzed by HPLC to determine the drug concentration left in the depot.

Evaluation of stability

For stability assessments only at 37°C, drug loaded CarboCells were placed in the incubator immediately after preparation. When evaluating stability at 4°C and 37°C, drug loaded CarboCells were divided by half and transferred to new glass vials; then each vial was placed in the fridge or the incubator, accordingly. Irrespectively, at the specified sampling points around 50 µL of CarboCell were taken and dissolved in 1 mL of MeCN prior analysis by HPLC or LC-MS. To evaluate the effect of pH, CarboCells containing 1.2 mg/g R848 were prepared as previously described. Three formulations were obtained by adding either benzoic acid (BA), triethylamine (TEA) or none. The CarboCells were incubated at 37°C and samples were taken as aforementioned. In this project, drug stability was assessed by determining the fraction of other chemical species, besides the drug and the formulation components, present in the CarboCell. The AUC values of R848 and any other chemical entities, namely modified versions of R848, were measured at 320 nm and stability was reported as the percentage AUC corresponding to the R848-derived chemical species.

Characterization of σ-SuBen and π-SuBen

π-SuBen was obtained by purifying σ-SuBen (powder from Sigma-Aldrich). The material was purified by distillation followed by washing and drying in vacuuo. The resulting octaacylated sugar (a fine white powder) was characterized by MALDI-TOF and NMR. σ-SuBen and π-SuBen were weighed in individual glass vials to prepare 10 mg/mL stock solutions in MeCN. The solutions were diluted 10-fold and then they were analyzed by HPLC using the aforementioned method.

NMR

NMR spectra were recorded on a Varian Mercury 400 MHz Spectrometer. 1H and 13C NMR were recorded at 400 and 100 MHz, respectively. Chemical shifts (δ) are reported in ppm relative to the solvents signal peak. For R848-IBA: ^{1}H NMR (400 MHz, DMSO-d_6) δ ppm: 10.01 (s, 1H), 8.53 (dd, J = 8.4, 1.4 Hz, 1H), 7.93 (dd, J = 8.3, 1.4 Hz, 1H), 7.62 (ddd, J = 8.3, 6.9, 1.3 Hz, 1H), 7.54 (ddd, J = 8.3, 6.9, 1.4 Hz, 1H), 5.23 – 4.54 (m, 5H), 3.55 (q, J = 7.0 Hz, 2H), 3.13 (hept, J = 6.8 Hz, 1H), 1.38 – 1.06 (m, 15H). ^{13}C NMR (101 MHz, DMSO-d_6), δ (ppm): 175.54, 143.15, 135.48, 128.61, 126.78, 124.23, 121.55, 116.82, 65.26, 64.65, 54.75, 33.88, 27.42, 19.18, 14.75.

MALDI-TOF MS

The analysis was performed on Bruker Autoflex TOF/TOFTM (Bruker Daltonics GmbH) in reflector mode. A matrix consisting of 2,5-dihydroxy benzoic acid (DHB) (60 mg/mL), sodium trifluoroacetate (1 mg/mL) in methanol was used for the mass spectra in positive mode. Shots: 100 and frequency: 1000.

Chapter 3.
Manuscript: CarboCell, a novel delivery platform providing on-target sustained release of resiquimod prodrugs for effective intratumoral immunotherapy

Elizabeth Serrano-Chávez[a], Sophie Bjørn Jensen[a], Martin Bak[a], Linda Maria Bruun[a], Paul Kempen[a], Fredrik Melander[a], Anders Elias Hansen[a], Thomas Lars Andresen[a], Jonas Rosager Henriksen[a]

[a] *Colloids and Biological Interfaces Group, Dept. of Health Technology, Technical University of Denmark, Produktionstorvet, Building 423, 2800, Kgs. Lyngby, Denmark.*

3.1 Abstract

The systemic administration of immunotherapies, especially those targeted to reverse the immunosuppressive tumor microenvironment (TME) and activate the anti-cancer response, present a high risk of severe toxic effects. While intratumoral administration is a practical alternative strategy, low injection reproducibility remains a challenge that can negatively affect the therapeutic outcome. We have developed the CarboCell drug delivery system to allow for safe and continuous immune stimulation of the TME and secure accurate and reproducible intratumoral injections. CarboCell is a low viscosity fluid that is easily injected through thin needles. After injection, CarboCell self-forms a highly viscous scaffold that acts as both drug reservoir and localization marker. Validation and monitoring of injections can be done due to the intrinsic visibility of CarboCell in standard clinical imaging technologies. In the present paper, the versatility of the CarboCell system was evaluated by solubilizing water insoluble TLR7/8 agonists in different CarboCell formulations. Drug release profiles showed sustained drug release, that could be tailored based on both the drug hydrophobicity and the chemical composition of CarboCell. CarboCells releasing TLR7/8 agonists were demonstrated to be well-tolerated and provided therapeutic efficacy in a syngeneic murine cancer model. Thus, CarboCell proves to be a promising platform for intratumoral immunotherapy that addresses the key challenges for intratumoral drug delivery technologies.

Key words: *immunotherapy, intratumoral delivery, systemic toxicity, hydrophobic drugs, Toll-like receptor agonists, resiquimod*

Highlights

- CarboCell provides optimal sustained intratumoral release of hydrophobic immunostimulatory drugs
- Drug release rate can be tailored based on the chemical composition of CarboCell and the hydrophobicity of the drug
- The viscosity of CarboCell increases drastically upon injection making it positionally stable at the injection site
- The image properties of CarboCell secures injection accuracy and validates location for evaluation of therapeutic performance
- By providing a sustained release of TLR7/8 agonists, CarboCell triggers an effective anti-cancer response

3.2 Introduction

While immunotherapy has established itself as a revolutionary cancer treatment, significant toxicological challenges are still hindering its full potential [79], [151]. In the clinical setting, the vast majority of cancer immunotherapies involve the systemic administration of immunomodulatory drugs [77]. Despite its practicality, systemic administration of immunotherapeutics can cause serious adverse effects such as cytokine release syndrome, autoimmunity and nonspecific inflammation [62], [152], [153]. Systemic administration is specially challenging for therapies aimed at activating and bridging the innate and adaptive immune responses [52]. Clinical trials pursuing innate immune activation and reversing the immunosuppressive tumor microenvironment (TME) have reported acute systemic toxicity before reaching therapeutic activity in cancerous tissue [52], [62]. Thus, alternative strategies for the polarization of the TME to improve the therapeutic response are of high interest.

In the context of solid tumors, intratumoral administration is a simple strategy to limit the toxic effect of immunostimulatory drugs aimed at activating the innate phases of the immune response [84]. Intratumoral injections reduce systemic drug exposure, permit a high local drug concentration and even higher doses of immunotherapeutics can be better tolerated [95]. Importantly, intratumoral immunotherapy can generate both a local and a systemic immune response, a phenomenon referred to as abscopal effect [32], [154]. Nevertheless, after intratumoral injection of free immunotherapeutics, the drugs will rapidly leak to blood circulation and therefore still cause systemic toxicity and lack therapeutic activity [155], [156]. Furthermore, the immune cells in the TME are very plastic and responsive, so their continuous stimulation is biologically optimal [103]. Hence, to reduce the risk of systemic toxicity and enable a sustained local drug activity several drug delivery systems have been investigated including liposomes [50], [100], emulsions [157], [158], hydrogels [108], [159], [160] and nanoparticles [161], [162].

However, an often-overlooked challenge of intratumoral immunotherapy is to ensure accurate and reproducible drug deposition [84], [112]. It has been suggested that variations on the injection technique and operator can influence the treatment efficacy [112], [113]. While image guidance can facilitate

needle placement, the *in situ* distribution of the injected solution is hardly controlled. Thus, unless a contrast agent or dye is injected, it is not possible to monitor or confirm a successful injection (i.e., on-target and without leakage) [113].

The CarboCell system was developed to improve drug retention in tumors and secure injection precision and reproducibility. CarboCell furthermore allows for image-guided injection and validation to ensure on-target delivery of immunotherapeutics in addition to providing sustained drug release for continuous immune stimulation. CarboCell is a liquid formulation, which upon injection forms a self-structuring, highly viscous scaffold that acts as both a drug reservoir and a localization marker. Due to the fast and extreme increase on the viscosity of CarboCell upon injection, the CarboCell is positionally stable at the injection site [133], [163]. CarboCell is visible across clinical imaging technologies including ultrasound, magnetic resonance imaging (MRI) and computed tomography (CT), as previously demonstrated in a study using a comparable formulation [133]. Thus, clinicians can accurately locate CarboCell and confirm the precision of the injection.

CarboCell consists of three main components: (i) a carbohydrate ester that acts as the matrix of the formulation, (ii) fluidizing agents (triglycerides) and (iii) a solvent. The chemical composition of CarboCell can be modified to modulate the drug release kinetics and achieve the desired release rate of the particular drugs incorporated in the formulation. In comparison to other drug delivery technologies such as hydrogels [100], [111], CarboCell is a non-polymeric system that does not require any cross-linking or chemical modifications to the drugs. In addition, CarboCell facilitates the solubilization of water-insoluble drugs, which are generally challenging to formulate and administer.

Here, the versatility of the CarboCell system is shown by formulating resiquimod (R848) and novel R848 prodrugs with varying physico-chemical properties. Resiquimod is a toll-like receptor 7/8 agonist (TLR7/8a) with potent immune activating and anti-tumor activity [60]. The clinical application of R848 has, however, been challenged by adverse effects occurring when R848 is systematically administered [62]. Moreover, R848 is poorly water-soluble and this limits its administration through conventional routes [48]. Also, to further enhance the visibility of CarboCell during and after image-guided injections, a novel iodinated carbohydrate ester (CLA-8) was incorporated into CarboCell as a CT contrast agent. CarboCells were characterized *in vivo* and *in vitro*, and the therapeutic efficacy of CarboCell delivering TLR7/8 agonists was demonstrated in mice models bearing colon cancer tumors.

3.3 Materials and methods

Chemicals

All chemicals were purchased from Sigma Aldrich, Merck unless stated otherwise. Ethanol (absolute), acetonitrile (MeCN) and dimethyl sulfoxide (DMSO) were purchased from VWR Chemicals. Resiquimod (R848) was purchased from AmBeed. R848 prodrugs (R848-IBA, R848-BA, R848-C4, R848-C8, and R848-C12) and CLA-8 were synthesized as described in the supplementary material and methods. Sucrose octabenzoate (SuBen) was acquired from Sigma Aldrich, but prior to use the material was purified by distillation followed by washing and drying in vacuuo.

Animal handling

All experimental procedures were approved by the Danish Experimental Animal Inspectorate. All female BALB/c Jrj mice were obtained at 6 weeks of age from Janvier and allow to acclimatize for one week prior to entering studies.

In vitro potency test

RAW-Blue™ cells (InvivoGen) were used as TLR reporter cells and the activity induction by R848 and R848 prodrugs was measured by QUANTI-Blue™ detection solution (InvivoGen). Cell culture and the colorimetric assay were done according to the manufacturer´s protocol to test solutions of the different drugs in PBS (diluted from drugs stock solutions in DMSO) with increasing concentrations (0.004 – 10 μM). UV quantification was done using a Tecan Spark® Multimode Microplate Reader.

Preparation of CarboCells

CarboCells were prepared by weighing each component in the amount corresponding to the weight percent (or weight ratio) of each formulation, unless otherwise stated (Table 1). Then the mixtures were put in an ultrasonication bath at 70-80 °C for 1.5 – 2 h, and occasionally vortexed until a clear, homogeneous solution was obtained. To incorporate the drugs (R848 and R848 prodrugs) into CarboCell, aliquots of each drug were prepared and CarboCell was added proportionally to each aliquot to obtain the required drug concentration. R848 (1.2 mg/g), R848-IBA (1.47 mg/g), R848-C4 (1.47 mg/g) and R848-C8 (1.68 mg/g) were formulated in equimolar concentrations, unless otherwise stated. The drugs were then dissolved through magnetic stirring at 40-50°C. CarboCells were stored in sealed glass vials at -20°C and thawed at room temperature before use.

Table 3. Composition of the main CarboCell formulations shown as weight percent (w/w%)

Component	Type	Composition (w/w %)		
		CC1	*CC2*	*CC3*
Sucrose octabenzoate (SuBen)	Carbohydrate ester	52.5	60	50
CLA-8	CT contrast agent	-	-	10
Glyceryl trioctanoate (GTO)	Co-solvent	25	-	-
Glyceryl trihexanoate (GTH)	Co-solvent	-	20	20
Propylene carbonate (PC)	Solvent	22.5	-	-
Dimethyl sulfoxide (DMSO)	Solvent	-	20	20

Viscosity of CarboCell

All viscosity measurements were done using an EMS-1000 viscometer set at 1000 rpm. The measuring time varied depending on temperature and viscosity range. All tested CarboCell formulations were unloaded (i.e., did not contain drug molecules).

Basal viscosity

1 mL of CC1, CC2 and CC3 formulations were individually pipetted into the instrument´s corresponding glass tube and a 1.2 mm aluminum sphere was placed inside the tube. Viscosities were determined at 25, 37 and 50 °C with measurement times between 5 s and 1 min.

Viscosity of simulated depots

CC1, CC2 and CC3 formulations were prepared, but substituting PC or DMSO with ethanol because ethanol is a more volatile solvent. 1 mL of each of the resulting formulations were pipetted into a glass tube and a 4.7 mm aluminum sphere was added. To evaporate the ethanol and simulate complete solvent efflux, the tubes (without lid) were placed in a vacuum oven at 100°C at a reduced pressure (0-200 mbar) for 24 hours. The samples were equilibrated to room temperature and then viscosity was measured at 37 and 50°C, with measurement times between 5 and 45 min.

Viscosity as function of solvent diffusion

CarboCells containing the same proportion of different solvents (SuBen: co-solvent (GTH/GTO): solvent (DMSO/PC) (60:20:20)) were prepared. 0.5 mL of each formulation were placed inside a glass tube and a 4.7 mm aluminum sphere was added. The samples were incubated at 37°C for 2 h and then 5 mL of PBS were carefully added on top of the CarboCell in each tube. After 24 h 2 mL of PBS were removed and replaced with fresh buffer; afterwards this procedure was repeated every 5-7 days. Viscosity was measured at different time points at 37°C, with measuring times between 10 s and 5 min. Every 2-3 days, 2 mL of PBS were removed and replaced with fresh buffer.

UHPLC method

The analysis were performed in a Shimadzu Nexera-X UHPLC with a PDA detector using the following settings, unless otherwise stated. Samples were injected (5 µL) onto a Waters Terra XBridge BEH C8 column (2.5 µm, 4.6x75mm, temperature 25 °C) at a flow rate of 0.8 mL/min. The solvent system consisted of mobile phase A (5% MeCN, 0.1% TFA in water) and mobile phase B (0.1% TFA in MeCN). The gradient was 0% B for 1 min, 0 to 100% B in 5 min, 100% B for 1.5 min, 100% B to 0% B in 0.5 min, 0% B for 1 min.

In vitro release study

R848, R848-IBA, R848-C4 and R848-C8 were formulated in CC1 and CC3 CarboCells. Then 50 µL of each CarboCell formulation were individually injected in 8-mL glass vials containing 2 mL of PBS. The vials were incubated at 37 °C and at each sampling point 1 mL of PBS was taken. 1 mL of fresh buffer was added immediately to the vial to replace the taken sample. The samples were then analyzed by UHPLC (UV detection at 240 nm) and the concentration of drug in the release media was calculated through a standard curve.

In vivo release study

R848, R848-IBA, R848-C4 and R848-C8 were formulated in CC3 CarboCell. For each CarboCell, 50 µL were injected subcutaneously (s.c.) in female BALB/c Jrj mice (mice were anesthetized using ~3-5% sevoflurane during injections). At each sampling point, mice were euthanized and the CarboCell depots were collected. Such depots were immediately dissolved in 1 mL DMSO and incubated at room temperature overnight. The samples were then filtered using 0.45-µm pore, nylon syringe filters and diluted eight times prior analysis. As reference, 10 µL of each CarboCell (non-injected) were dissolved in 1 mL DMSO. All samples were then analyzed by UHPLC (but with 2.5 extra min at 100% B).

The drug release percentage was determined by ratiometric analysis. The AUC values of R848 (320 nm), R848 prodrugs (320 nm), and CLA-8 (280 nm) were measured to calculate the AUC ratios of drugs/CLA-8 in all samples. The percentage of released drug was calculated by comparing the AUC ratio of R848 and R848 prodrugs/CLA-8 in the collected CarboCells versus the corresponding ratios in the reference (non-injected) CarboCell (equation 1). In addition, prodrug stability in the injected depot is reported as the AUC percentage (at 320 nm) of the corresponding prodrug in a given sample.

$$Drug\ released\ (\%) = 100 - 100 * \left(\frac{AUC\ of\ sample\ (drug\ /CLA\text{-}8)}{AUC\ of\ reference\ (drug\ /CLA\text{-}8)}\right) \quad \text{(Equation 1)}$$

Cryo-SEM imaging

In addition to the samples collected from the *in vivo* therapy study, CarboCell CC3 was prepared (without drug loading). 50 µL of CC3 were injected in a plastic mold containing 6 mL of PBS and incubated at 37°C for 14 days. Every 2-3 days, 2 mL of PBS were removed and replaced with fresh buffer.

CarboCell samples were adhered to SEM stubs with a 50:50 mixture of colloidal graphite powder (Agar Scientific) and Tissue-Tek OCT compound (Ted Pella) and plunge frozen in liquid nitrogen. Frozen samples were then loaded onto a Leica EM VCT 100 Cryo Transfer Shuttle and transferred to a Leica EM MED020 freeze fracture and high vacuum coating system. Samples were fractured, sublimated for 5 min at -90°C and sputter coated with 6 nm of carbon/platinum. After coating, samples were transferred via the VCT 100 Cryo Transfer Shuttle under vacuum and at -140°C to the Thermo Scientific Quanta 3D FEG FIB/SEM for subsequent SEM imaging. Imaging was performed at high vacuum at -140ºC with an accelerating voltage of 2 kV at the center for integrated microscopy at the University of Copenhagen.

Determination of IL-6 concentration in mice serum

Female BALB/c Jrj mice were injected with R848, R848-IBA, R848-C4 and R848-C8 dissolved either in PBS, 8% DMSO or in CC3 CarboCell. R848 and R848 prodrugs solutions in PBS, 8% DMSO were prepared with a dosing concentration of 2 and 4 mg/kg; 500 µL of solution were injected i.p. in mice and blood was collected after 3 h. 50 µL of each CarboCell were injected s.c. and blood samples were taken 4 h post-injection. After collection, all blood samples were left undisturbed at room temperature for 15-30 min to allow the blood to clot. The samples were centrifuged at 3000 rpm for 15 min at 4 °C and the resulting supernatant (serum) was immediately transferred into clean polypropylene tubes and stored at -80°C until analysis. To determine the concentration of IL-6, an ELISA assay was done using a Mouse IL-6 DuoSet ELISA kit from R&D Systems (Cat #: DY406-05) and following the instructions from the manufacturer.

CT scan imaging

CC3 CarboCell was prepared as well as two additional formulations containing 5% and 15% of CLA-8 (SuBen:CLA-8:GTH:DMSO (55:5:20:20), SuBen:CLA-8:GTH:DMSO (45:15:20:20)); none of the CarboCells were drug loaded. 100 µL of each formulation were injected subcutaneously in the thigh of female BALB/c mice. CT scan images of the mice were obtained one hour after injection using a microCT scanner (Ultra-High Resolution U-CT^{UHR}, MiLabs NL). In addition, glass vials (without lid) containing the different CarboCell formulations were also CT scanned.

In vivo mouse therapy study

CT26 cells were obtained from ATCC and were maintained in RPMI 1640 medium supplemented with 10% fetal bovine serum (Biowest, VWR) and 1% penicillin-streptomycin. Cells were kept in a humidified tissue culture incubator at 37°C with 5% CO2 and were subcultured when confluent using Trypsin-

Ethylenediaminetetraacetic acid (EDTA) (0.25%) (Thermo Fisher Scientific) to remove adherent cells. CT26 tumors were established in 7 weeks old female BALB/c Jrj mice (3 x 10^5 CT26 cells/tumor). The mice were inoculated by s.c. injection of CT26 cells in 100 µL of serum-free medium. Tumors had a mean size of 117 mm^3 when starting the treatments (day 15 post-inoculation).

R848, R848-IBA, R848-C4 and R848-C8 were formulated in CC3 CarboCell at concetrations equimolar to 3 mg/kg R848. All CarboCell injections had a volume of 50 µL and were injected intratumorally. Mice received four injections at 7-day intervals with CarboCells containing theTLR7/8 agonists starting at day 15 post-inoculation. Mice were anesthetized by ~2-3% isoflurane during injections. Tumor size (volume = length x $width^2/2$) and bodyweight were measured 2-3 times/week. Mice were sacrificed when tumors reached 1500 mm^3. Mice were terminated from studies in case of ulcerations, failure to thrive, respiratory distress or weight loss >15%.

The study was finalized 90 days post-inoculation and CarboCell depots from the surviving mice were collected for cryo-SEM imaging. The depots were frozen immediately after collection and stored at -80°C until analysis.

Statistical analyses

When required, statistical analyses were performed on GraphPad Prism 9. The correspondingly used statistical test is specified in figure legends. A p-value ≤0.05 was deemed as statistically significant.

3.4 Results and discussion

Characterization of R848 prodrugs

R848, a TLR7/8 agonist and member of the imidazoquinolines family, is a drug capable of activating an innate immune response and inducing a potent anti-tumor activity [60]. Nevertheless, the formulation and administration of R848 is limited due to its poor water solubility and severe systemic toxicity [48], [62]. Thus, R848 is considered an excellent candidate to demonstrate the application of the CarboCell system. Furthermore, a set of five different R848 prodrugs were synthesized with the expectation of reducing drug toxicity in addition to investigate alternative ways to lower the initial release and exemplify the diversity of drug molecules that can be formulated in the CarboCell. The R848 prodrugs were generated by introducing diverse acyl groups in the primary quinoline amine of R848 (Fig. 21A). The introduced moieties vary in molecular size, structure, and hydrophobicity and so do the resulting R848 prodrugs.

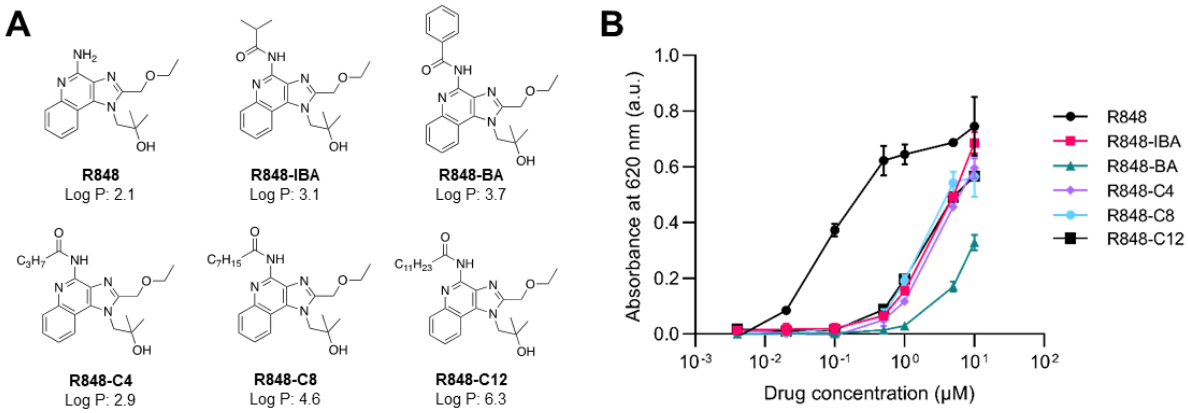

Figure 21. Resiquimod (R848) and R848 prodrugs and their stimulation of TLR 7/8 receptors in RAW-Blue cells. (**A**) Chemical structures and log P values of R848 and the prodrugs. (**B**) RAW-Blue cells were incubated for 24 h at 37ºC with increasing concentrations of R848 and R848 prodrugs. Response was evaluated by measuring the samples' SEAP-induced color with absorbance at 620 nm. Data points are presented as the mean ± SD (n=2).

The hydrophobicity of R848 and the R848 prodrugs, indicated by their log P values, is particularly useful to assess the ability of CarboCell to solubilize and release water-insoluble drugs. The log P value of each drug molecule was estimated using ChemAxon® software (Fig. 21A). Moreover, the solubility in water of R848, R848-IBA, R848-C4 and R848-C8 was experimentally determined and it correlated with their estimated log P values (Appendix III-S5). Therefore, the calculated log P values were considered as adequate hydrophobicity indicators.

The potency of the R848 prodrugs was then evaluated through a RAW-Blue colorimetric assay, in which R848 served as a reference. RAW-Blue cells express endogenous TLR7 and TLR8 and additionally, they are transfected with a secreted embryonic alkaline phosphatase (SEAP) reporter gene. Upon agonist stimulation of TLR7/8, the production and subsequent secretion of SEAP is induced. Consequently, the concentration of SEAP in the detection medium correlates with the activation of the TLRs [164]. All R848 prodrugs could induce TLR7/8 activation, with R848-BA showing the lowest activity induction. However, the parent compound R848 was at least 10-times more potent than most of the R848 prodrugs (Fig. 21B).

The lower *in vitro* potency observed for the R848 prodrugs might be explained by the position in which the acyl groups were added. Studies with imidazoquinoline analogues have shown that substitutions in the primary amine of the quinoline moiety can lead to a total loss of activity [164]. Also, it has been observed that such primary quinoline amine is implicated in crucial hydrogen bonds taking place in the TLR7/8 binding pockets [165], [166]. Therefore, it is likely that the R848 prodrugs are displaying partial TLR7/8 agonist activity because the conditions in the RAW-Blue assay are not optimal for full activation of the prodrugs and their primary quinoline amine is still partially blocked. Nevertheless, it was decided not to include R848-BA in further studies due to its considerably lower potency.

Before proceeding to the incorporation of R848 prodrugs into CarboCells, their stability in possible solvents of the formulation was evaluated. DMSO, PC, ethanol and benzyl alcohol are solvents that can be part of the CarboCell system. After incubation in the different solvents, the R848 prodrugs showed

high stability in DMSO and PC (Appendix III-S6). It was decided not to include neither ethanol nor benzyl alcohol as part of the following CarboCell formulations since in these solvents the prodrugs were activated into R848 in less than 48 h.

Viscosity evaluation of CarboCell

The CarboCell system has three main constituents: (i) a carbohydrate ester, (ii) fluidizing agents (also referred to as co-solvents or triglycerides) and (iii) a solvent. Prior to injection, CarboCell is a clear, homogeneous liquid with low viscosity (Fig. 22D). Upon injection in aqueous media or in tissue, the water-miscible solvent diffuses out from the system causing CarboCell to form an *in situ*, highly viscous and stable scaffold (Fig. 22E). The viscosity before injection governs the injectability of the formulation, whereas the viscosity of the self-formed depot influences drug diffusion and release. Hence, several experiments were performed to investigate the correlation between viscosity and the chemical composition of CarboCell before and after injection.

To characterize the basal viscosity of CarboCell, three main CarboCell formulations (CC1, CC2 and CC3 – Table 3) were prepared and their viscosity prior injection was measured at different temperatures. The viscosity of all CarboCells was inversely correlated with temperature as higher temperatures caused a decrease in viscosity. While there was no significant difference in the viscosity of the tested formulation at the individual temperatures, it appears that the CarboCell containing PC (CC1) tends to have a lower viscosity (Fig. 22A). At 25°C, the viscosity of the CarboCells was in the range of 900 – 1500 m Pa·s, which is considered adequate for injection through small-gauge needles [133]. This is particularly advantageous, as it has been reported that decreasing needle size lowers the morbidity risk associated with intratumoral injections [167].

To estimate the change of viscosity of CarboCell upon injection, complete solvent efflux from the CarboCells was simulated. The DMSO and PC fractions in CC1, CC2 and CC3 were substituted with ethanol as it is more volatile and then placed in a vacuum oven to evaporate ethanol. Therefore, the measured viscosity corresponds to the mixture of the carbohydrate esters and triglycerides fractions, mimicking the *in situ*-formed depots. At physiological temperature, CC1 had a 100-fold increase in viscosity, while both CC2 and CC3 showed a 200-fold viscosity increase (Fig. 22B). It has been reported that low viscosity fluids can leak from the injection pinhole due to the high pressure inside the tumor [168], [169]. Thus, such a high viscosity of the CarboCell scaffold is advantageous as it ensures that CarboCell remains in a stable position after injection.

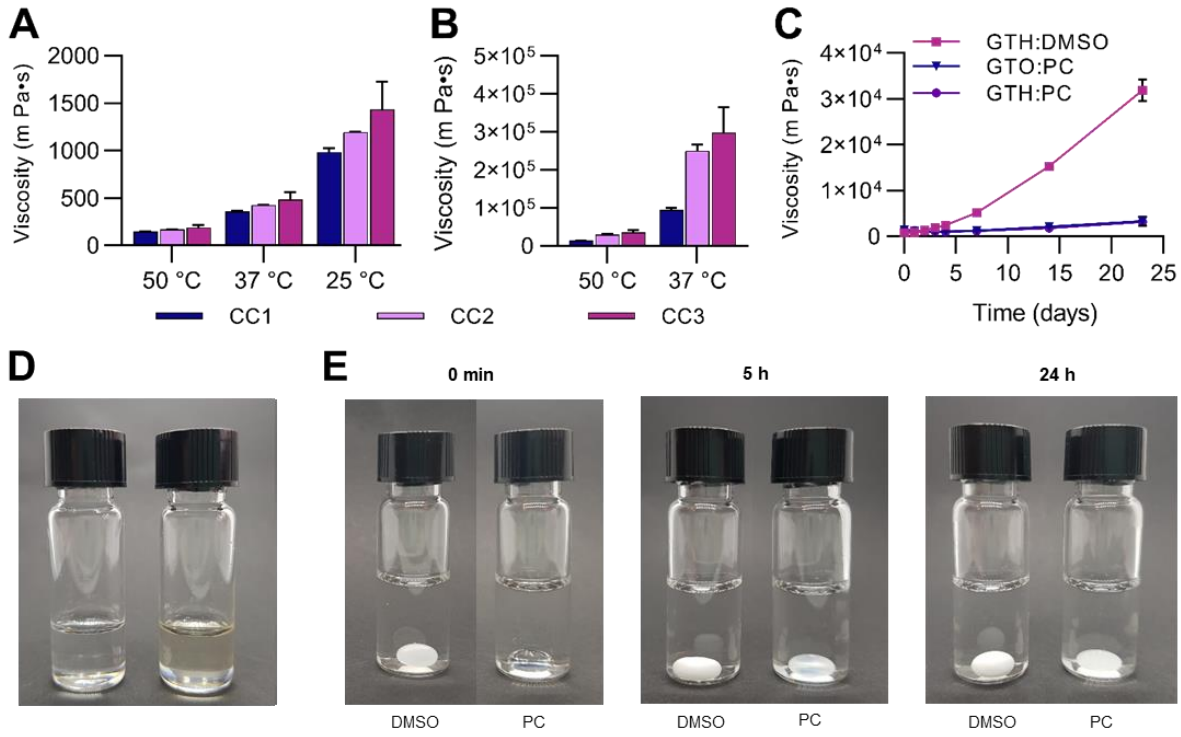

Figure 22. Viscosity of CarboCell formulations as a function of temperature and solvent diffusion. (**A**) Viscosity of CC1, CC2 and CC3 measured at three different temperatures right after preparation. (**B**) Viscosity of CarboCells measured at 50 and 37 °C after simulating solvent efflux. Homologous CC1. CC2 and CC3 formulations were prepared in which PC or DMSO were replaced by ethanol in the same proportion; ethanol was then evaporated in a vacuum oven and viscosity was measured. (**C**) Viscosity over time at 37°C of CarboCell formulations containing the same proportion of different solvents (SuBen: co-solvent (GTH/GTO): solvent (DMSO/PC) (60:20:20)). CarboCells (approx. 0.5 mL) were placed into viscosity tubes and PBS was added on top to promote solvent diffusion. Data points are presented as the mean ± SD (n=3). (**D**) CC1 and CC3 formulations after preparation. (**E**) Pictures of 50 µL of CarboCell injected in 2 mL PBS at different time points showing the difference in depot formation as each solvent (DMSO, PC) diffuses out at different rates. The injected formulations correspond to SuBen:GTH:DMSO (60:20:20) and SuBen:GTO:PC (60:20:20).

To investigate the effect of the type of co-solvent and solvent on the viscosity, three formulations with the same proportions but different co-solvents (GTH or GTO) and solvents (DMSO or PC) were prepared. Formulations with the combination of GTO:DMSO were excluded as these components are not mixable. PBS was added on top of sample tubes containing the CarboCells to simulate a gradual solvent release (Appendix III-S6). The CarboCell containing DMSO showed a more pronounced and faster increase in viscosity than both formulations containing PC. After 3 weeks at 37°C, the viscosity of the DMSO-based formulation had increased more than 40-fold, compared to only a 2-fold increase in the PC-based CarboCells (Fig. 22C). As CarboCell is injected, a phase separation occurs. In this process, the solvent diffuses into the aqueous phase followed by the formation of a very viscous *in situ* depot comprising the carbohydrate ester and the co-solvent fractions. The rate at which the solvent diffused out from CarboCell was correlated to the hydrophilicity of the solvents. DMSO has a higher affinity for water than PC as indicated by their log P values (-1.40 and 0.79, respectively). Additionally, it has been suggested that a higher intrinsic viscosity of the solvents might promote a faster diffusion into aqueous media [121]. Thus, both the higher intrinsic viscosity of DMSO and its lower log P may contribute to its quicker release from the system. The faster diffusion of DMSO compared to PC caused

a steeper increase in viscosity, which might indicate a faster phase separation process in the CarboCells containing DMSO.

Next, formulations containing SuBen:GTH:DMSO (60:20:20) and SuBen:GTH:PC (60:20:20) were injected in PBS to visually evaluate the CarboCell self-forming scaffolds. The DMSO-based CarboCell turned opaque immediately after injection, while its PC counterpart remained clear and translucent. Gradually, the PC-based CarboCell became opaque over time (Fig. 22E). These observations further confirm that DMSO promotes a faster solidification of the CarboCell compared to PC. A fast solidification is desired as this can lower the burst release and assist the quick positioning of CarboCell in the injection site [117], [133].

In vitro drug release from CarboCell

To evaluate the ability of CarboCell to solubilize water-insoluble immunostimulatory drugs, R848 and the R848 prodrugs were solubilized in equimolar concentration in CC1, CC2 and CC3. All drug molecules were easily incorporated into the CarboCells and no signs of drug precipitation were observed during the course of the studies. Next, R848 and R848 prodrugs formulated in CC1 and CC3 were used to investigate the effect of drug properties and the chemical composition of CarboCell on the *in vitro* release kinetics.

CC1 and CC3 were injected in PBS and their cumulative release was measured over 3 weeks. In both formulations, R848 and the prodrugs showed a sustained release profile. R848 had the fastest release followed by R848-IBA, R848-C4 and R848-C8 in that order (Fig. 23A, B). When ranking the tested molecules according to their water solubility (from less to more hydrophobic), the resulting sequence is R848 > R848-IBA > R848-C4 > R848-C8. This indicates that drug release is highly influenced by the hydrophobicity of the drug molecules. After the solvent diffuses out to the aqueous buffer, the remaining CarboCell components form a very hydrophobic and viscous scaffold [120]. The more hydrophobic a drug molecule is, it will have a higher affinity for the *in situ* scaffold. Likewise, a lower solubility of the drug in water will lower its partitioning from the CarboCell to the aqueous media, which contributes to a slower release. In addition, the high viscosity of the self-formed depot represents a diffusion barrier that also influences the release kinetics [170]. Overall, CarboCell offers the potential benefit of simultaneously formulating two or more drug molecules with different hydrophobicity, each one releasing at a different rate. For instance, this is an attractive approach when combining chemotherapeutics with immunomodulatory drugs, where a fast cytotoxic effect is desired along with a slower sustained immunostimulation [111].

In both CC1 and CC3, a low burst release was observed. After 24 h, R848 had a release of around 20% and the burst release of the prodrugs lowered as the hydrophobicity of the molecules increased. Having a low burst release is fundamental for tolerability and maintaining a prolonged release period [120], [171]. Moreover, CC1 and CC3 displayed similar drug release profiles despite their different chemical composition, which underlines the flexibility of the CarboCell system.

For the subsequent *in vivo* studies, it was decided to continue with CC3 as the lead formulation since this contains the CT contrast agent CLA-8. Moreover, while the prodrugs showed high stability in PC, their stability was considerably reduced when formulated in CC1 (Appendix III-S7, S8). In contrast, the R848 prodrugs showed good long-term stability in CC3 (Appendix III-S9).

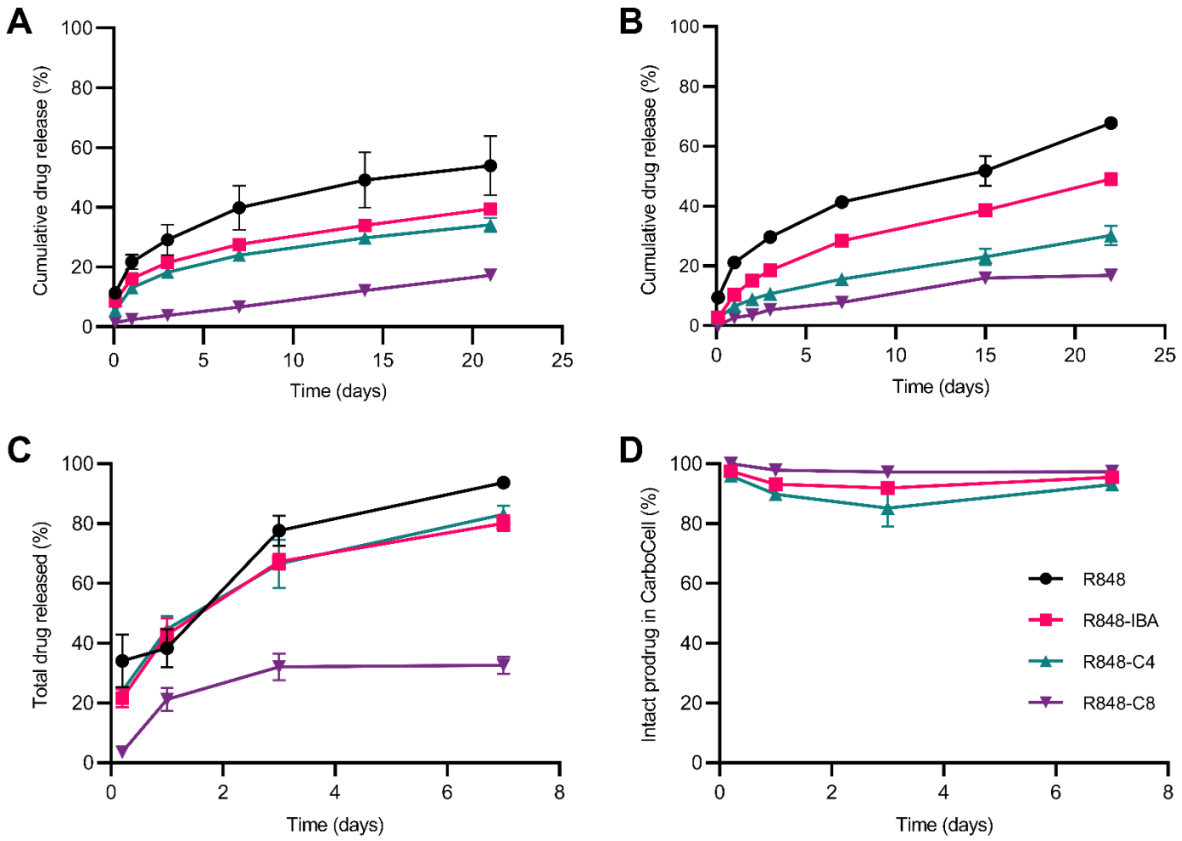

Figure 23. *In vitro* and in *vivo* release profiles of R848, R848-IBA, R848-C4 and R848-C8 from CarboCells. (**A-B**) *In vitro* cumulative drug release of R848 and R848 prodrugs in PBS from formulation (**A**) CC1 and (**B**) CC3 incubated at 37°C over a 3-week period. The drug concentration in the release media at each time point was quantified by UHPLC. (**C**) Percentage of R848 and prodrugs released from CC3 after s.c. injection in mice. At each sampling point, the injected depot was collected and the percentage of drug left in the depot was calculated by ratiometric analysis. (**D**) Percentage of intact prodrug (R848-IBA, R848-C4 and R848-C8) present in the CarboCell CC3 depots collected from the s.c. injections in mice. The AUC of R848 and the prodrugs was measured by UHPLC (UV detection at 320 nm) and the reported values correspond to the AUC percentage of prodrug in a given sample. In all formulations, the concentration of R848 was 1.2 mg/g and the prodrugs (R848-IBA, R848-C4, R848-C8) had equimolar concentrations (1.47 mg/g, 1.47 mg/g, and 1.68 mg/g, respectively). Data points are presented as the mean ± SEM (n= 3-5).

In vivo drug release from CarboCell

CC3 containing equimolar concentrations of R848 and R848 prodrugs was injected subcutaneously in mice for comparison to *in vitro* release studies. All CarboCell depots were easily identified at the site of injection and the amount of drug left in the depots was used to calculate the percentage of released drug. A similar trend the *in vitro* profiles was observed, with R848 having the fastest release followed by R848-IBA, R848-C4, and the slowest for R848-C8 (Fig. 23C). However, 7 days post-injection the percentage of total drug released was 2 to 5-fold higher in mice than in PBS. Alike observations were

obtained when injecting CC1 intratumorally (Appendix III-S10). Nonetheless, CC3 provided sustained release of all drug molecules for at least a week.

Moreover, the percentage of intact product in the collected CarboCell depots was determined to assess the *in vivo* stability of the R848 prodrugs. In average, more than 85% of the drug molecules found in the injected CarboCells corresponded to intact prodrugs (Fig. 23D). This suggests that CC3 provides a protective environment that prevents premature activation of the prodrugs even when injected in tissue.

Cryo-SEM imaging of CarboCell

The morphology of CarboCells injected both *in vitro* and *in vivo* was investigated by cryo-SEM imaging to obtain an insight into possible effects on drug release. Inter-connected water pores were observed in the inner part of the CC3 scaffold, highlighted here in the *in vitro* sample (Fig. 24C, D). While there were no apparent differences in the core of the CarboCell, major distinctions between *in vitro* and *in vivo* injections were associated with the surface of the CarboCells scaffolds. There were more water pores near the surface of the CarboCell injected in PBS compared to the *in vivo* depots (Fig. 24A, E). In addition, honeycomb structured pores were observed in the inner edge of the CarboCell after injection in tissue (Fig. 4F-H). These structures were present in most of the surface; however, they were not uniformly distributed and showed varying depth and size. Thus, while the surface of *in vivo*-injected CarboCell showed a reticular appearance, the surface of its *in vitro* counterpart was smoother. The honeycomb structures might be formed because of the direct contact with tissue, which along with movement, exerts a higher pressure on the CarboCell causing a change in morphology. The increased porosity in the surface might facilitate a higher drug release and might be one of the causes of the differences between the *in vitro* and *in vivo* drug release profiles.

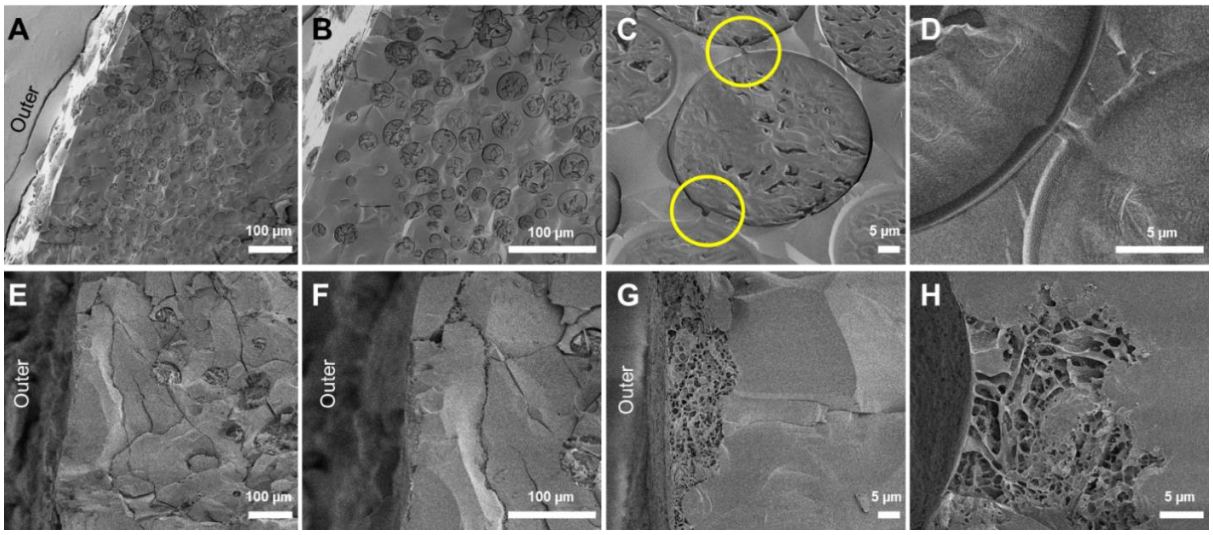

Figure 24. Cryo-SEM images of CC3 depots formed after in vitro and in vivo injections. (**A-D**) CC3 depot injected in PBS and collected after 14 days of incubation at 37°C: (**A, B**) Cross-section of CarboCell showing the inner structure of the depot; (**C, D**) Pores formed inside the CarboCell depot connected through channels. (**E-H**) CC3 depot injected i.t. in a mouse and collected 3 months post-injection: (**E, F**) Cross-section of CarboCell showing the inner structure of the depot; (**G-H**) Honeycomb structure formed in the surface of the depot

In vivo systemic toxicity of R848 and R848 prodrugs

A key challenge for intratumoral drug delivery systems is to control the initial burst release. If the burst release is not controlled or is too high, a large drug dose is released, which can lead to local or systemic toxic effects [171]. To investigate the correlation between burst release and systemic toxicity, CC3 loaded with R848 and the prodrugs was injected s.c. in mice and the IL-6 concentration in serum was measured after 4 h. The immunostimulatory drugs followed the same release pattern as noted before, where the highest burst release was observed for R848 (34 ± 9%) and the lowest for R848-C8 (4 ± 1%) (Fig. 25A). Likewise, the IL-6 concentration in serum decreased as the burst release was lower (Fig. 25B). Thus, this shows a direct correlation between the amount of released drug and the potential for induction of systemic toxicity.

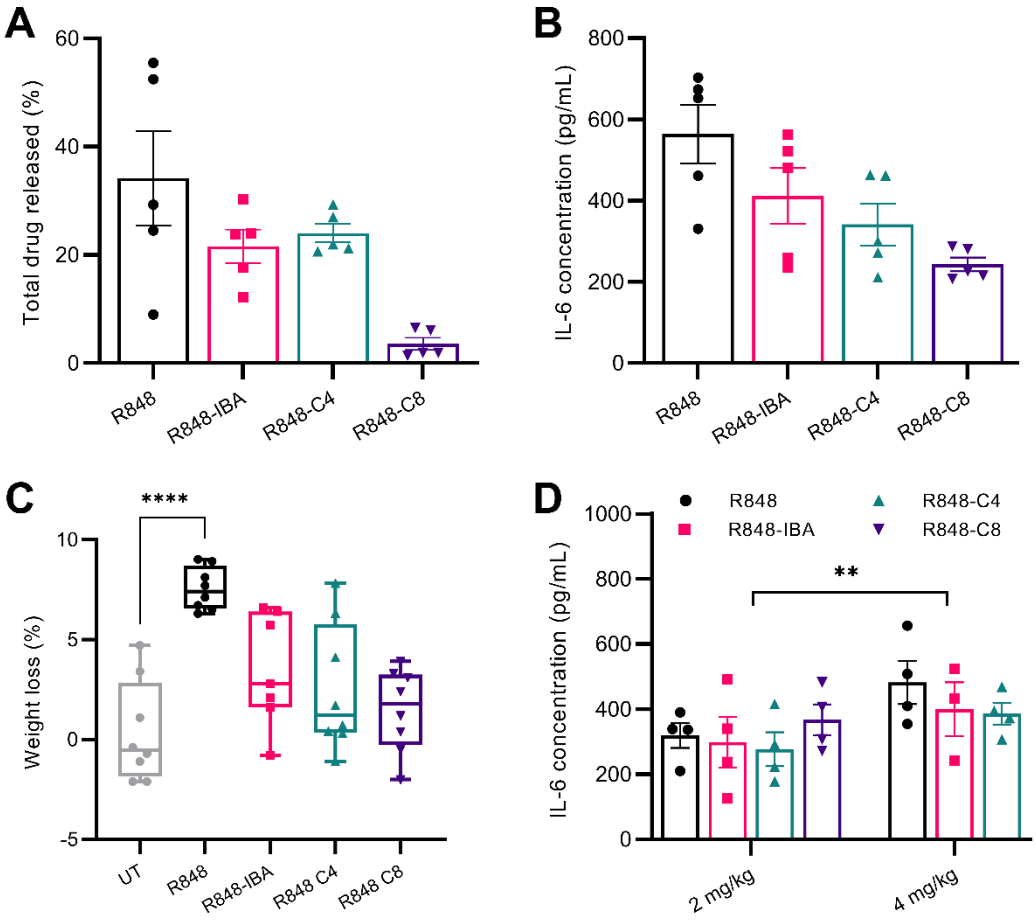

Figure 25. Correlation between initial burst release and a marker of systemic toxicity (IL-6) induced by R848 and R848 prodrugs. (**A**) Percentage of total drug released from CC3 4 h after s.c. injection in mice. The injected depot was collected and the percentage of drug left in the depot was calculated by ratiometric analysis. (**B**) Concentration of IL-6 in mice serum collected 4 h after s.c. injection of CC3. (**C**) Percentage of weight loss in mice 24 h after i.t. injection of CC3 presented as a box and whiskers plot (n=8). (**D**) Concentration of IL-6 in mice serum collected 3 h after i.p. injection of 500 µL of PBS, 8% DMSO solutions with drug concentrations equivalent to 2 or 4 mg/kg. In the studies involving CarboCell injections, the concentration of R848 was 1.2 mg/g and the prodrugs (R848-IBA, R848-C4, R848-C8) had equimolar concentrations (1.47 mg/g, 1.47 mg/g, and 1.68 mg/g, respectively). Data points are shown as mean ± SEM (n=4-5), unless otherwise stated. Statistical analyses: one-way ANOVA one-way ANOVA with Dunnett´s multiple comparisons test.

To evaluate the systemic toxicity after intratumoral administration, CC3 was injected intratumorally in mice carrying CT26 tumors and bodyweight was measured 24 h after injection. Overall, weight loss was below 10% for all treatments, which suggests the absence of acute toxicity [172]. In accordance to the previously observed trends, the greater weight loss was observed in mice receiving R848. Nonetheless, there were no significant differences in the weight loss of the mice treated with R848 prodrugs, neither when compared with the untreated control (Fig. 25C).

Intraperitoneal (i.p.) injections of free immunostimulatory drug solutions were done in mice to validate that the observed differences were due to the type of release rather than the intrinsic drug toxicity. The injected doses corresponded to 2 and 4 mg/kg, and the IL-6 concentration in serum was measured after 3 h. No significant differences in IL-6 concentration were observed between R848 and the prodrugs. Nevertheless, the higher drug dose caused a significant increase in IL-6 concentration (Fig. 25D). This confirms that the controlled release provided by CarboCell, specifically a low burst release, can reduce and limit systemic toxic effects. Such feature could be especially useful to minimize systemic toxicity in combination therapies, where the administration of more than one immunostimulatory drug could pose a higher risk of adverse effects [36].

CLA-8 as a novel CT contrast agent

Image guidance modalities such as ultrasonography and radiography, including fluoroscopy and CT, can improve and facilitate intratumoral injections in a wide variety of tissues and organs. Nevertheless, the accuracy and reproducibility of intratumoral injections remain a challenge [112], [113]. To guide and confirm accurate intratumoral injections, a novel iodinated carbohydrate ester, CLA-8, was synthesized that could be easily incorporated into CarboCell and act as a CT contrast agent.

One-to-one (1:1) substitutions of sucrose octabenzoate with CLA-8 could be done in CC3 without a significant effect in neither the viscosity nor the drug release kinetics (Fig. 22A, Appendix III-S11). CT images of CarboCells containing 5, 10 and 15% CLA-8 were obtained before and after s.c. injections in mice to evaluate the visibility of the formulations. It was observed that the measured Hounsfield unit (HU) values increased when increasing the CLA-8 content. Accordingly, the HU values of the non-injected formulations were, in ascending order, 1685 HU, 2275 HU and 2885 HU (Fig. 6A). More importantly, after injection in mice, all CarboCell scaffolds showed and excellent visibility due to full retention of the CT contrast. Moreover, the self-formed depots remained stable in the injection site without spreading to surrounding tissue (Fig. 6B-D). Thus, the great visibility of CarboCell can allow live image guidance during injections besides enabling the validation of a safe and accurate injection. The positional stability of CarboCell offers an advantage as therapeutic effect can be negatively influenced by variability in injections [112], [113]. Moreover, the visualization of the CarboCell scaffold can be further useful to clinicians to plan the optimum position of the injections according to combined anatomical and functional imaging [112], [134].

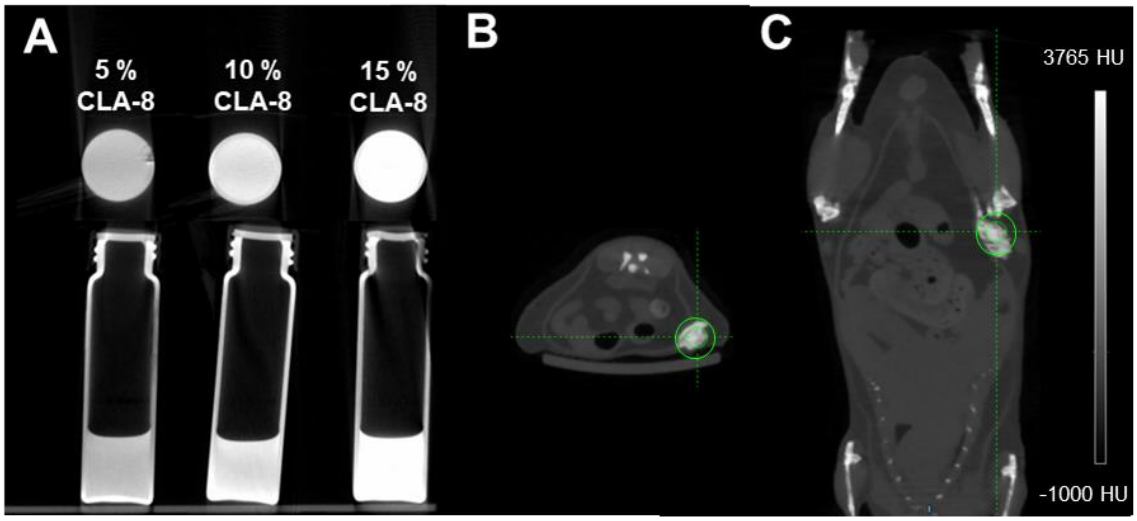

Figure 26. CT scan images of non-injected and injected CarboCell formulations containing 5, 10 or 15% (w/w%) of the contrast agent CLA-8. (**A**) Top and lateral view of glass vials containing approximately 2 g of CarboCells with varying amounts of CLA-8. (**B**) Axial and (**C**) coronal and views of 200 µL of CC3 subcutaneously injected in the thigh of a mouse.

Therapeutic efficacy of CarboCell with TLR7/8 agonists

Reversing the immunosuppressive tumor microenvironment (TME) is key to secure that a strong and effective innate and adaptive anti-cancer response can be generated [173], [174]. To achieve this, constant stimulation of the TME is optimal [60]. To demonstrate the synergy between CarboCell and TLR7/8 agonists, mice bearing CT26 tumors were treated with the lead formulation CC3. The dosing schedule was adjusted according to the observations from the *in vivo* drug release profile (Fig. 25C); thus, mice were injected once a week for four weeks.

The treatments with R848 and the R848 prodrugs were well tolerated, and they increased the median survival time (MST) compared to the untreated control (Fig. 27). R848 had the highest MST (>90 days), followed by R848-C4 (79 days), R848-IBA (69 days) and R848-C8 (35 days). Such sequence suggests that the increase in MST is directly correlated with the amount of drug released into the tumor (Fig. 25C). For instance, R848-C8, the slowest releasing drug, had a lower MST than R848-C4 even though both molecules have similar *in vitro* potency and comparable acyl groups. As polarization of the TME requires constant stimulation by immunomodulatory drugs, the better therapeutic effect of R848 is probably because its higher burst release induces a more acute inflammation. Nonetheless, R848-C4 delivered by CC3 is a promising alternative to R848. R848-C4 displayed a lower burst release and still promoted an effective anti-cancer response. Hence, R848-C4 may have a better tolerability in humans compared to R848. Moreover, the concentration of R848-IBA in CC3 can be increased, so that the absolute amount of delivered R848-C4 equals the one of R848. Such adjustment might further enhance the therapeutic effect of R848-C4.

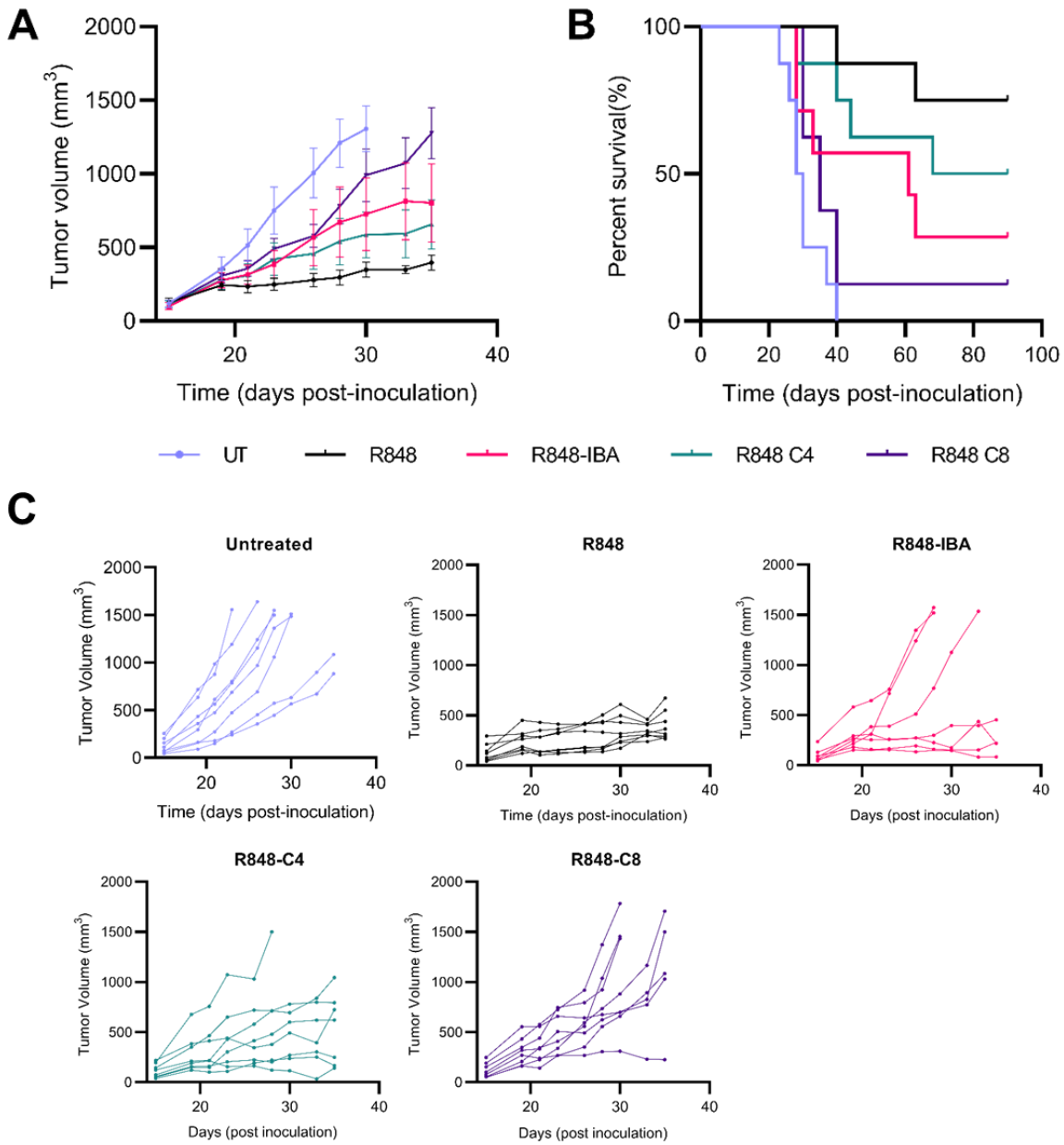

Figure 27. Evaluation of the therapeutic efficacy of R848 and R848 prodrugs formulated in CC3. Mice bearing CT26 tumors were treated weekly four times with a dose of 3 mg/kg R848 or the molar equivalent of each prodrug. Untreated (UT) mice did not receive any injection and were included as control group. (**A**) Mean tumor volume for control and treatment groups (n= 8 ± SEM). (**B**) Kaplan-Meyer plot of mice survival for treatment groups and controls. (**C**) Individual tumor growth for each treatment group.

Overall, we demonstrated that CarboCell could provide continuous stimulation of the TME by the sustained release of TLR7/8 agonists, which led to anti-tumor activity and improved survival of the mice models without any adverse toxic effects. Most recently, the clinical potential of intratumoral immunotherapy is exemplified in a current clinical trial involving the delivery of R848 via a cross-linked hydrogel (NCT04799054) [108]. Early results have shown that the intratumoral, sustained delivery of R848 engaged a robust immune response in tumor tissue and systemic anti-cancer responses have also been observed [175]. The good therapeutic effect obtained with CarboCell solely releasing TLR7/8 agonists are encouraging for future possible applications of CarboCells releasing multiple drugs or in

combination with other immunomodulatory drugs and therapies. As previously introduced, combination immunotherapies can be particularly toxic due to the exacerbated activation of the immune system [36]. CarboCell can aid on reducing such toxic effects and therefore enable further development and application of combinatorial treatments. While the formulation of multiple drugs in CarboCell still needs to be explored, the versatility and adaptability of the system makes CarboCell a promising drug delivery platform for further development in cancer immunotherapy.

3.5 Conclusion

We have developed and characterized CarboCell, a drug delivery system that allows safe and precise intratumoral administration of drugs aimed at activating the innate immune response and triggering an effective anti-cancer response. CarboCell was easily injectable due to its low viscosity. Once injected, the viscosity of CarboCell increased 100 to 200-fold due to solvent diffusion. The formulation included CLA-8, a novel carbohydrate ester that provided excellent CT contrast to the CarboCell scaffold. Hence, CarboCell is an excellent localization marker to validate accurate and reproducible intratumoral injections, which may be of central importance for evaluation clinical trial performance. As injection variability and low reproducibility is correlated to lower therapeutic outcomes, CarboCell offers an encouraging approach to enhance therapeutic response for intratumorally administered immunotherapy. Poorly water-soluble R848 and R848 prodrugs with a wide range of physico-chemical properties were effortlessly solubilized in several CarboCell formulations, demonstrating the versatility of the system. The drug release rate from CarboCell depended on both hydrophobicity of the drug and the chemical composition of CarboCell, which can be straightforwardly modified. Also, the low burst release provided by CarboCell was advantageous on minimizing systemic toxicity after both subcutaneous and intratumoral injection. The intratumoral administration of TLR7/8 agonists through CarboCell was well tolerated in mice and without observed toxicity even after repeated injections. Encouragingly, the synergistic treatment of CarboCell with TLR7/8 agonists showed an improved MST in mice bearing CT26 tumor models compared to the untreated control. Additionally, R848-C4 was identified as a potential alternative to R848 due to its low initial release, which may enhance its tolerability in humans. Thus, the safety and high adaptability of the CarboCell system makes it a promising delivery strategy also for other immunostimulatory drugs as monotherapy or in combinatorial treatments.

Chapter 4.
CarboCell for an extended sustained release of R848 and RepSox

4.1 Background

Scientific evidence throughout the years has shown how the cellular and non-cellular components of the TME play a fundamental role in tumor initiation, growth and metastasis as well as on its response to treatment [5], [80]. Due to the increasing understanding on the importance of the TME in cancer biology, a rising strategy in cancer treatment is to target the TME [176]. Nonetheless, the TME is a very complex entity and multiple factors and mechanisms are involved in shaping its characteristics. For this reason, a multi-targeted therapeutic approach can be beneficial to reverse the immunosuppressive status of the TME [80], [177].

TGF-β is a potent cytokine known for being a major facilitator of an immunosuppressive environment in established tumors thereby promoting tumor growth and invasion. TGF-β exerts multiple effects, which can suppress or alter the function of immune cells from both the innate and adaptive immune system. For instance, it has been demonstrated that TGF-β can reduce the number and activity of NK cells as wells as hinder the maturation and cytokine production of APCs [178], [179]. In addition, TGF-β dampens the activity of cytotoxic T cells and mediates the survival of T_{reg} cells. High levels of TGF-β have been found in a variety of tumors and due to its central role in immunosuppression and tumor progression, the inhibition of TGF-β has been considered an attractive target for immunotherapy [71], [178], [180]. Nonetheless, TGF-β has fundamental functions beyond the tumor site, which complicates the systemic administration of TGF-β inhibitors [74]. TGF-β and its receptors are ubiquitously expressed in healthy tissues and paradoxically, TGF-β has a tumor suppression function in premalignant lesions by inhibiting cell proliferation. Nevertheless, during tumor progression, the cancer cells turn insensitive to the anti-growth effects of TGF-β. It is until then that TGF-β becomes a tumor-promoting cytokine, which additionally can induce metastasis [69], [181]. Besides an unintentional inhibition of the tumor-suppression function of TGF-β, the systemic administration of TGF-β inhibitors has been associated with autoimmunity effects including severe cardiac toxicity [74], [75]. Hence, the intratumoral administration of TGF-β inhibitors is advantageous to preserve the normal functions of TGF-β in non-cancerous tissues and avoid undesired toxicities.

In this project, we investigated the formulation of R848 (a TLR7/8a formerly described) and RepSox, a potent TGF-β inhibitor, in CarboCells (Fig. 28). RepSox is a small molecule capable to inhibit the signaling pathway from the TGF-β type 1 receptor (TGFβRI) and like R848, RepSox is a water-insoluble

molecule (log P = 2.5) that can be straightforwardly incorporated in the CarboCell. Previously, the combination of a TLR7 agonist and a TGF-β inhibitor administered as free drugs has shown to promote tumor apoptosis and an increase in the number of T cells infiltrating the tumor [182]. Such combination had also proven successful in our group, where treatment with a CarboCell containing R848 (3 mg/kg) and a TGF-β inhibitor (either SD-208 or RepSox at 20 mg/kg) along with radiotherapy produced a favorable anti-tumor response in mice [183]. To bypass radiotherapy, we decided to increase the dose of R848 to further stimulate the activation of the innate immune system and enhance the immune response cycle. Thus, we evaluated the therapeutic efficacy of the CarboCell treatment in synergy with R848 (7.5 mg/kg) and RepSox (20 mg/kg) in murine cancer models.

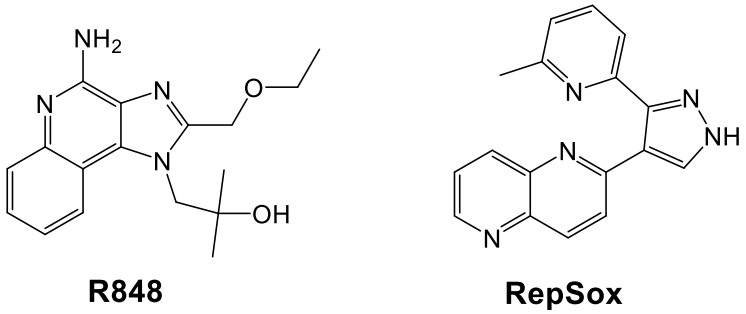

Figure 28. Chemical structures of R848 and RepSox.

Regarding the formulation of CarboCell, as presented in Chapter 2, SuBen is the preferred carbohydrate ester to maintain the drug stability of R848. Therefore, a SuBen-based CarboCell formulation was chosen as starting point, which will be referred to as N1 CC. The N1 CC formulation had been previously investigated in our group and consists of SuBen:GTO:EtOH:PLA (60:25:15:0.5). PLA, a water insoluble polymer, was originally included as an additive to prevent a high burst release as exemplified by other delivery systems using SAIB [118], [122].

As demonstrated in Chapter 3 and by previous research in our group [150], [183], the current dosing regimen of CarboCell consists of one intratumoral injection per week during four weeks, giving a total of four injections per treatment. One of the goals of this project was to adjust the release kinetics of CarboCell to extend the interval between injections from 7 to 14 days thereby decreasing the number of injections per treatment. Reducing the frequency of injections can improve patient compliance as well as lower the risk of bleeding, organ injury and undesired dissemination of cancer cells associated with repeated needle puncture [95], [112]. To obtain a formulation with an extended sustained release, in addition to changing the ratio of the CarboCell components, alternative co-solvents with different hydrophobicity were explored namely fatty acid ethyl esters (FAEEs) (Fig. 29). Within this optimization process, we also wanted to remove PLA from the original N1 CC formulation. Simplifying the formulation not only facilitates preparation and quality control, but also eliminates a possible source of impurities that might compromise the stability of the drug product. Furthermore, it is desired that the CarboCell contains a CT contrast agent to have the previously discussed benefits associated with an improved visibility of the CarboCell scaffold. For this purpose, lipiodol and CLA-8 (introduced in Chapter 3) were

evaluated. Lipiodol consists of a mixture of iodine with FAEEs of poppy seed oil and it is a radiopaque contrast agent approved by the FDA for several imaging procedures such as lymphangiography [184]. Since lipiodol is a water-insoluble fluid, it is a compatible component to include in the CarboCell.

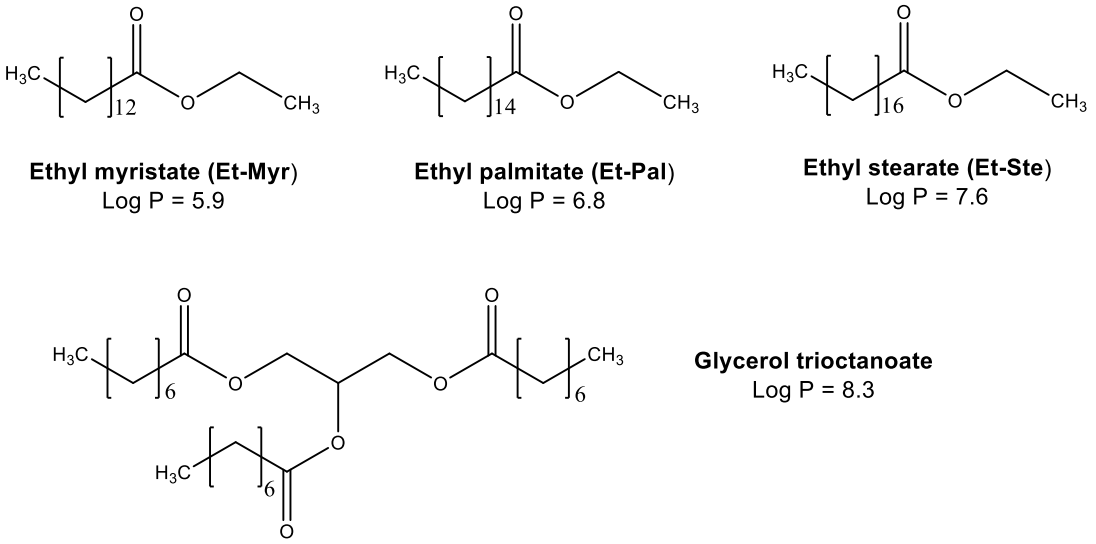

Figure 29. CarboCell co-solvents. Chemical structure and log P values of the different tested co-solvents.

4.2 Objectives

As synergistic drug combinations are advantageous in cancer immunotherapy, this project focused on investigating the combination of R848 and RepSox in the CarboCell system with the following objectives:

- ☐ To show that multiple drugs can be formulated in the CarboCell system and be released in a sustained manner
- ☐ To produce a CarboCell formulation with an extended period of sustained drug release, specifically to prolong the interval between *in vivo* injections to 14 days
- ☐ To demonstrate that CarboCell treatment with R848 (a TLR7/8 agonist) and RepSox (a TGF-β inhibitor) can elicit an anti-tumor immune response in murine models
- ☐ To incorporate a CT contrast agent into the CarboCell and investigate its effect on release kinetics and drug stability
- ☐ To evaluate the short-term drug stability in the selected CarboCells

4.3 Results and discussion

Therapeutic efficacy of CarboCell with R848 and RepSox

To evaluate the anti-cancer effect of R848 (7.5 mg/kg) and RepSox (20 mg/kg), mice bearing established tumor models were treated with N1 CC containing solely R848 or the combination of R848 and RepSox. The treatment consisted of one intratumoral injection per week for four weeks. The tested groups were compared to an untreated control.

The higher concentration of R848 was easily dissolved in the CarboCell together with RepSox, which demonstrates the ease of preparation and versatility of the CarboCell system. Despite the higher R848 dose, both treatments were well tolerated with no signs of severe toxicity. The treatment of CT26 tumor models with CarboCell either as monotherapy or with the drug combination increased the MST by at least 26 days compared to the untreated group. Moreover, the treatment with R848 and RepSox showed a higher MST than the treatment solely with R848, including 5/8 mice being complete responders. The MST for the monotherapy and the combination therapy were 50 and >110 days, respectively (Fig. 30). In addition, similar trends were observed in mice carrying EMT-6 tumors (Appendix IV-S12).

It has been demonstrated that the oral administration of R848 causes serious toxicity [62]. Regarding TGF-β inhibitors, their systemic administration is also known to cause severe effects, particularly cardiotoxicity [75], [185]. For instance, treatment with galunisertib (a small molecule structurally similar to RepSox) requires a specific intermittent dosing schedule (14 days on/14 days off), otherwise it causes potentially lethal cardiotoxicity and damages to the gastrointestinal and skeletal system [186], [187]. Moreover, while it is known that immunotherapy with multiple drugs can improve therapeutic efficacy, there is a higher associated risk of serious adverse effects [188], [189]. Thus, it is encouraging that the combination treatment of CarboCell with R848 and RepSox showed a better therapeutic response than the monotherapy without affecting its tolerability even after repeated, sustained dosing. The observed results might also suggest that there is neglilible drug spillover into systemic circulation, indicating that the drugs are well contained within the CarboCell scaffold displaying an on-target delivery.

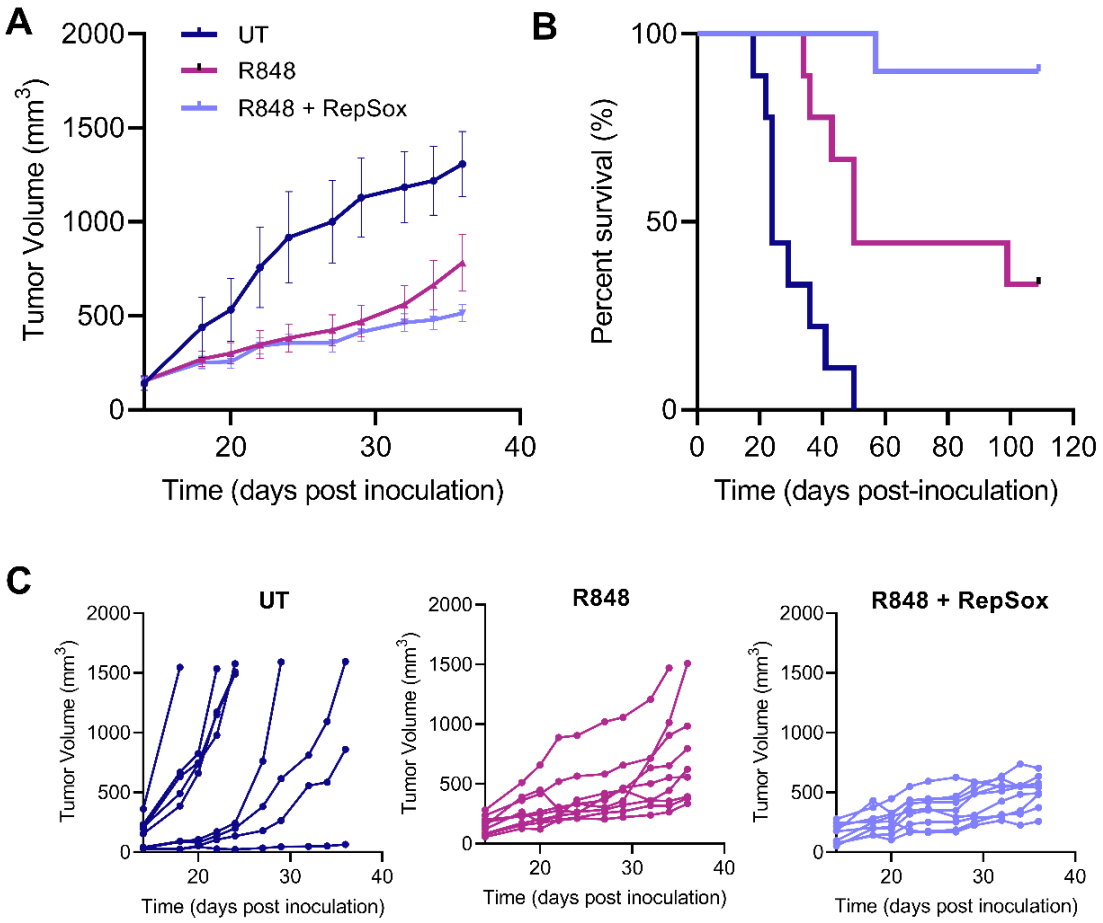

Figure 30. Evaluation of the therapeutic efficacy of R848 (7.5 mg/kg) and R848 + RepSox (7.5 mg/kg + 20 mg/kg) formulated in N1 CC. Mice bearing CT26 tumors were treated weekly four times with each CarboCell. Untreated (UT) mice did not receive any injection and were included as control group. (**A**) Mean tumor volume for control and treatment groups (n= 9 ± SEM). (**B**) Kaplan-Meyer plot of mice survival for treatment groups and controls. (**C**) Individual tumor growth for each treatment group. Note that the drug concentrations in N1 CC were 3 mg/g R848 or 3 mg/g R848 + 8 mg/g RepSox. Abbreviations: UT=untreated.

Next, we tested the ability of the CarboCell treatment to elicit a systemic anti-tumor response, also known as abscopal effect. For this purpose, mice bearing two separate CT26 tumors were treated with the dosing schedule previously described; however, the injections were done only in one tumor. As expected, the multi-drug treatment showed a higher MST than the untreated group (23 and >95 days, respectively). Remarkably, tumor progression was delayed or reduced in the non-injected lesions of mice treated with the multi-drug CarboCell thereby showing induction of an abscopal effect (Fig. 31, Appendix IV-S13). These results further underlines the clinical potential of CarboCell since triggering a systemic anti-tumor response can be beneficial for the treatment of metastatic cancer including undetected micrometastasis [32].

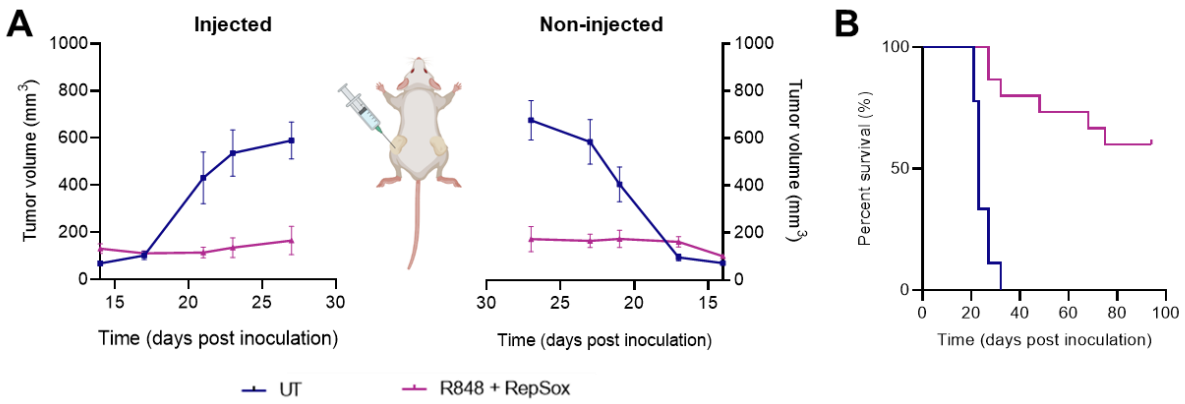

Figure 31. Evaluation of the abscopal effect. Mice bearing CT26 tumors were treated weekly four times with the N1 CC containing R848 and RepSox (7.5 mg/kg and 20 mg/kg, respectively), though only one tumor was injected. (**A**) Mean tumor growth of injected and non-injected tumors (n= 9-15 ± SEM). (**B**) Kaplan-Meyer plot of mice survival for treatment group and the untreated (UT) control.

Formulation development of CarboCell for extended drug release

As introduced earlier, it is desired to prolong the drug-releasing period of the CarboCell to reduce the frequency of injections and also, to incorporate a contrast agent for an enhanced visibility of the CarboCell scaffold. To address both purposes, it was decided to use lipiodol (ethiodized oil) as an alternative co-solvent to GTO due to its hydrophobicity and radiopaque properties.

Table 4. Overview of the composition of the CarboCell formulations evaluated in Chapter 4 expressed as weight percent (w/w%). Abbreviations: SuBen: sucrose octabenzoate, GTO: glyceryl trioctanoate, Et-Myr: ethyl myristate, Et-Pal: ethyl palmitate, Et-Ste: ethyl stearate, EtOH: ethanol, PLA: poly (lactic acid), CLA-8: lactose octa para-iodobenzoate.

CarboCell formulation	**Chemical components (w/w%)**								
	SuBen	*GTO*	*Lipiodol*	*Et-Myr*	*Et-Pal*	*Et-Ste*	*EtOH*	*PLA*	*CLA-8*
N1 CC	60	25	-	-	-	-	15	0.5	-
CC1	60	25	-	-	-	-	15	-	-
CC2	60	-	25	-	-	-	15	-	-
CC3	62.5	-	-	22.5	-	-	15	-	-
CC4	57.5	-	-	27.5	-	-	15	-	-
CC5	62.5	-	-	-	22.5	-	15	-	-
CC6	60	-	-	-	25	-	15	-	-
CC7	57.5	-	-	-	27.5	-	15	-	-
CC8	62.5	-	-	-	-	22.5	15	-	-
CC9	57.5	-	-	-	-	27.5	15	-	-
CC10	62	21	-	-	-	-	17	-	-
CC11	63	17	-	-	-	-	20	-	-
CC12	60.5	17	-	-	-	-	20	-	2.5
CC13	58	17	-	-	-	-	20	-	5
CC14	53	17	-	-	-	-	20	-	10

Following the composition of N1 CC, gardiquimod was incorporated in CarboCells containing either GTO or lipiodol as co-solvents, resulting in formulations CC1 and CC2, respectively (Table 4). The substitution of GTO with lipiodol caused a 3.7-fold reduction in the *in vitro* release of gardiquimod after 14 days. However, it was observed that the drug was stopped being released from the CarboCell after only 72 h post-injection (Fig. 32B). A similar trend is expected to occur with R848 as both molecules are structurally similar. Lipiodol is composed of iodine with FAEEs of poppy seed oil, but its exact structure is unknown, which might complicate subsequent quality control of CarboCell formulations. Thus, inspired by the composition of poppy seed oil [190], [191], individual FAEEs were then chosen as co-solvents (Fig. 29).

The FAEEs were incorporated in CarboCells in the ratios shown in Table 4, resulting in the formulations CC3 to CC9. Et-Myr and Et-Pal formed clear homogeneous CarboCells; however, Et-Ste could not be solubilized instead forming a white and extremely viscous mixture. Et-Ste presents as a solid and has an average melting point of 33°C [192], the highest of all tested co-solvents. Such physico-chemical properties might make it ineffective as fluidizer in the CarboCell system at the tested ratios. Regarding the release kinetics of R848, replacing GTO with Et-Myr did not cause a substantial change in the drug release profile. In contrast, the formulations containing Et-Pal (CC5 and CC7) showed approximately a 6-fold reduction in R848 release after 7 days (Fig. 32A). Unlike the CarboCell with lipiodol, R848 kept being released from CC5 and CC7 over time, but still in very small amounts.

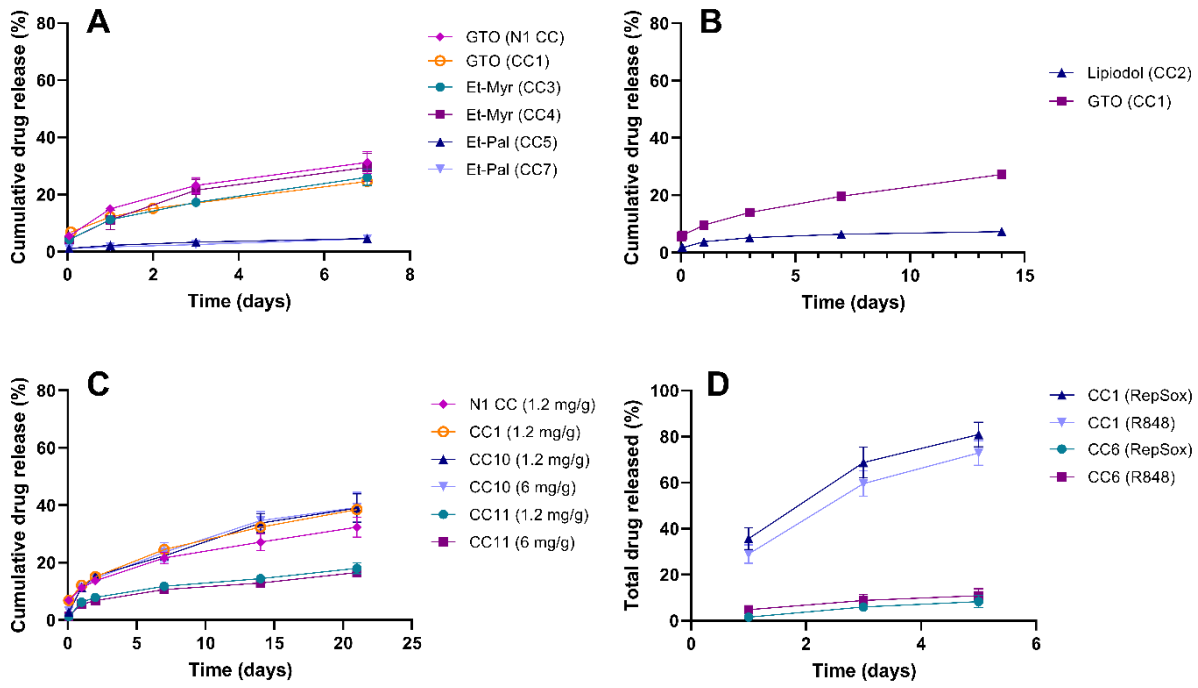

Figure 32. *In vitro* and *in vivo* drug release in formulations with varying co-solvents. (**A**) In vitro release of R848 from CarboCells with different fatty acid ethyl esters as co-solvents. (**B**) In vitro release of gardiquimod from formulations containing either lipiodol or GTO as co-solvents. (**C**) In vitro release of R848 in formulations with different SuBen/GTO ratios. (**D**) In vivo release of R848 and RepSox from CarboCells containing either Et-Pal (CC4) or GTO (CC9) as co-solvents. Data is presented as mean ± SEM (n= 3-4).

As shown in Chapter 3 (Fig. 23), drug release tends to be higher *in vivo* than *in vitro*. Therefore, CarboCells with GTO (CC1) and Et-Pal (CC6) were injected s.c. in mice to evaluate the release profile of R848 and RepSox. There were no significant differences between R848 and RepSox and after 5 days, the average drug release was around 8-fold lower when using Et-Pal as co-solvent. Nevertheless, only around 10% of the drugs had been released from CC6 and it is uncertain if a considerably higher percentage will be released further over time (Fig. 32D). Unlike GTO, Et-Pal contains a single aliphatic chain, which might facilitate its packing in a stable array that limits the diffusion of the drugs. The closer intermolecular interactions expected from the geometry of Et-Pal are reflected in its higher melting point [193]. The average melting point of Et-Pal is 24°C, while the one of GTO is 10°C [192]. Moreover, the average melting point of Et-Myr is 12°C, close to the one of GTO, which might also explain why both of these co-solvents caused similar *in vitro* drug release profiles.

As a next approach, it was decided to change the carbohydrate ester to co-solvent ratio. Once the CarboCell is injected, the solvent diffuses out of the system and the resulting self-formed depot consists of the carbohydrate ester and co-solvent fractions. We hypothesized that by increasing the hydrophobicity of the depot, water-insoluble drug molecules will have stronger interactions with the scaffold thereby delaying their release. As SuBen is more hydrophobic than GTO (estimated log P values of 15.3 and 8.3, respectively), the proportion of GTO was reduced to obtain a depot with higher hydrophocity, i.e., a higher SuBen to GTO ratio. Also, we hypothesized that decreasing the proportion of GTO in the formulation will increase the viscosity of the self-formed depot. A higher viscosity represents a barrier for drug diffusivity, which can delay drug release [170], [194]. Hence, the *in vitro* release of R848 was tested in CarboCell formulations with SuBen/GTO ratios of 2.4 (N1 CC and CC1), 3.0 (CC10) and 3.7 (CC11) (Table 4). In addition, CC10 and CC11 were prepared with two different R848 concentrations to evaluate if drug concentration influenced the release profile.

The formulations having a SuBen/GTO ratio of 2.4 and 3.0 displayed comparable drug release kinetics. Noticeably, CC11 showed an approximate 2-fold reduction in drug release when compared to the aforementioned formulations. Moreover, the drug concentration did not affect the percentage of released drug over time (Fig. 32C). Although the viscosity of the final depot of N1 CC and CC11 was not estimated, other CarboCell formulations have shown a higher depot viscosity when increasing the SuBen to co-solvent ratio, supporting our hypothesis (Appendix IV-S14). The 2-fold drug release reduction observed for CC11 suggested that the interval between injections could be doubled. Consequently, a higher drug loading in the CarboCell would be required to achieve the same absolute drug amount released from the depot. This should not be problematic as the *in vitro* studies showed that the drug release profile was not influenced by drug concentration. These results were encouraging to proceed to *in vivo* testing with CC11 as the lead formulation for prolonged sustained release.

In vivo evaluation of CarboCell for extended drug release

To compare the findings from the *in vitro* drug release studies, the initial N1 CC and CC11 containing different concentrations of R848 and RepSox were injected s.c. in mice. As previously observed for the *in vitro* experiments, the drugs concentration did not affect the relative release profile of neither formulation. For each formulation, the same percentage of drugs had been released over time irrespective of the drug concentration. After 7 days, more than 90% of the drugs had been released from N1 CC, whereas only around 50% had been released from CC11 (Fig. 33A, B). Furthermore, when analyzing the released amount of the individual drugs, it was observed that the same drug quantities were released from N1 CC and CC11 containing a double drug concentration (Fig. 33C, D). Such findings support that CC11 with 6 mg/g R848 and 16 mg/g RepSox can be administered bi-weekly and provide the same immune stimulation as the originally tested N1 CC formulation.

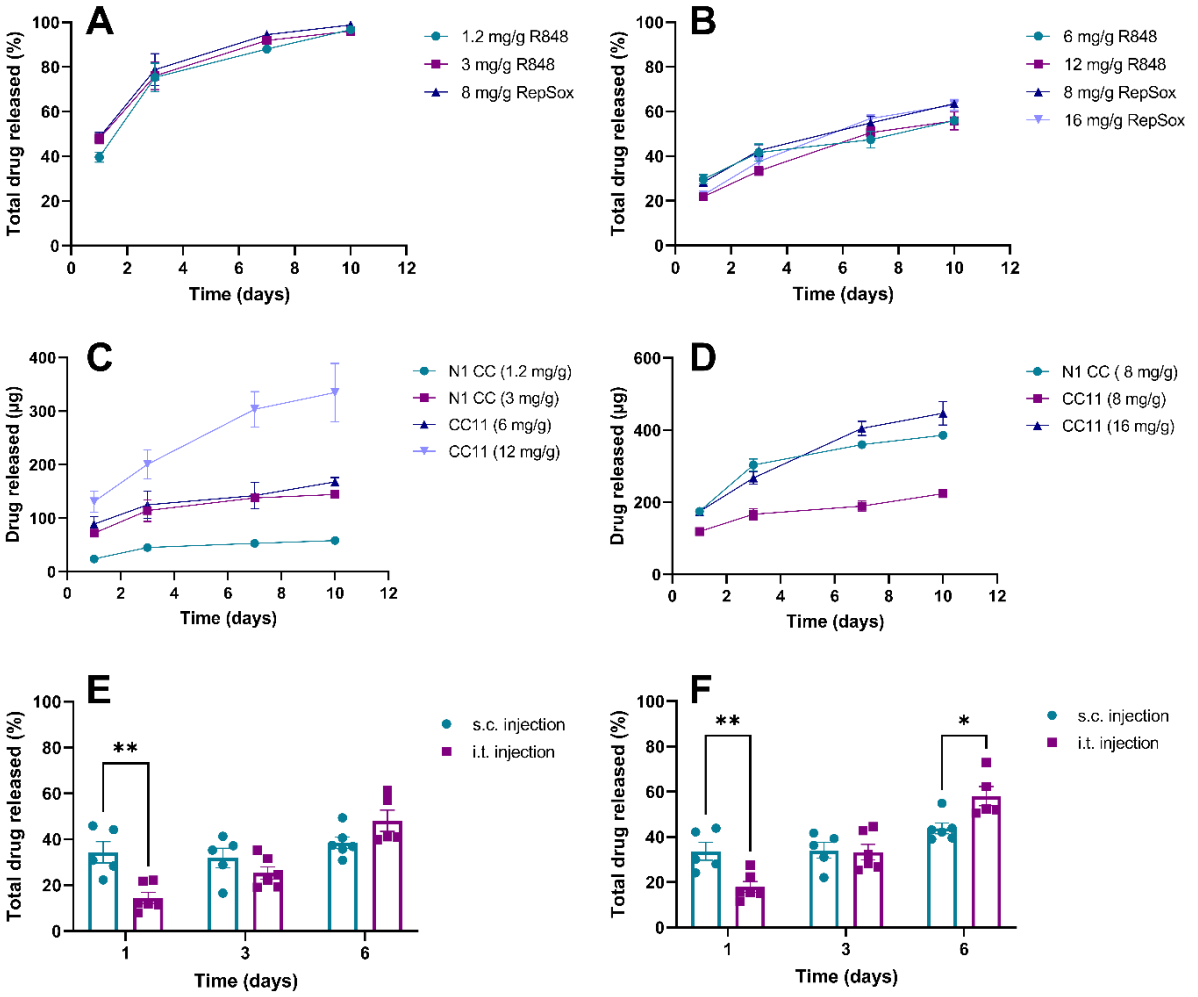

Figure 33. In vivo drug release profiles from N1 CC and CC11. (**A-B**) Percentage of drug released from formulations (**A**) N1 CC and (**B**) CC11 containing varying concentrations of R848 and RepSox after s.c. injection in mice. (**C-D**) Total amount of (**C**) R848 and (**D**) RepSox released after s.c. injection of N1 CC and CC11 containing different drug concentrations. (**E-F**) Comparison of the percentage of (**E**) R848 and (**F**) RepSox released after either s.c. or i.t. injection of CC11 formulated with 6 mg/g R848 and 16 mg/g RepSox. Data is presented as mean ± SEM (n=5-6). The statistical analysis on (**E-F**) was a two-way ANOVA with Ŝidák multiple comparions (* $p \leq 0.05$, ** $p \leq 0.01$).

Then, to further investigate the *in vivo* drug release kinetics, CC11 was injected either s.c. or i.t. in mice. Interestingly, the burst release was significantly lower when the CarboCell was injected i.t (Fig. 33E, F). One of the main challenges for the intratumoral drug delivery systems is to control the burst release since a high release of drug can lead to local or even systemic toxicity. Therefore, the low burst release observed for the i.t. injection of CarboCell represents an advantage to minimize the risk of systemic spillover and the associated toxic effects. As described in Chapter 3, the morphology of the CarboCell can change depending on the pressure and conditions surrounding the CarboCell, which might explain the observed differences between s.c. and i.t. injections. Although the mean percentage of drug released was slightly higher for the i.t. injections after 6 days, the difference in release kinetics after this point were not determined thereby it is unknown if there would be a negative effect on therapeutic efficacy, which was tested next.

To evaluate the therapeutic efficacy of the formulation for extended drug release, mice bearing MC38 tumors were treated with either weekly injections of N1 CC (3 mg/g R848 + 8 mg/g RepSox) or biweekly injections of CC11 (6 mg/g R848 + 16 mg/g RepSox). Additionally, an empty CarboCell (N1 CC) was included in the study to ensure that the CarboCell was not influencing the therapeutic outcome. Again, both treatments were well tolerated. As expected, the treatments with N1 CC and CC11 could limit tumor progression in more than 50% of the mice and both therapies showed a MST >80 days (Fig. 34). Moreover, there were no apparent differences between the mice injected with the empty CarboCell and the untreated group, which suggests that the CarboCell depot by itself does not exert neither a toxic nor a therapeutic effect (MST = 23 days). Overall, these results confirmed that we successfully developed a CarboCell formulation that requires less frequent injections without compromising the therapeutic effect.

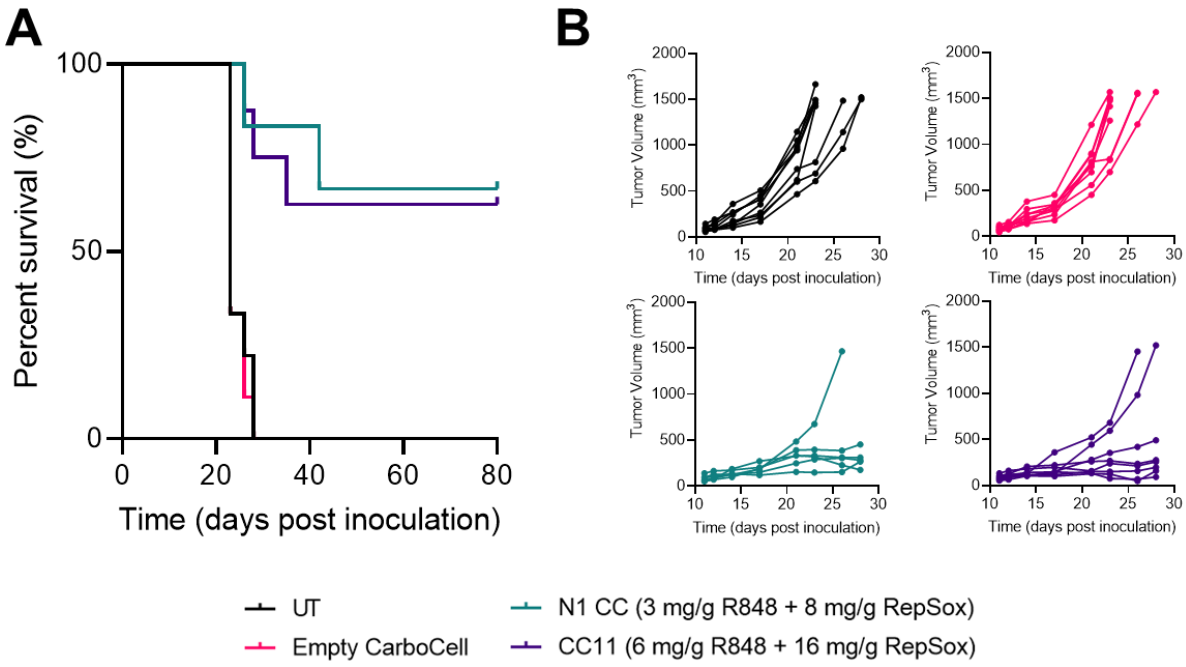

Figure 34. In vivo evaluation of the therapeutic efficacy of CarboCell for extended drug release. Mice bearing MC38 tumors were treated weekly four times (empty CarboCell (N1 CC) and N1 CC) or biweekly two times (CC11). (**A**) Kaplan-Meyer plot of mice survival for treatment group and control (n=6-9). (**B**) Individual tumor growth curves. Abbreviations: UT:untreated.

Incorporation of a CT contrast agent

As previously described, CarboCell is intrinsically visible across imaging technologies as ultrasound and MRI. To further expand the imaging properties of CarboCell, we decided to incorporate the CT contrast agent CLA-8 into the newly developed formulation for extended release. Since CLA-8 is an iodinated carbohydrate ester, SuBen could be substituted with CLA-8 in a one-to-one (1:1) ratio. Formulations with 2.5, 5 and 10% CLA-8 were prepared (CC12 – CC14, Table 4). However, after preparation, a phase separation was observed in the CarboCell containing 10% CLA-8 (CC14). CLA-8 is poorly soluble in EtOH and this might explain why CLA-8 could be solubilized in the CarboCell only at 2.5% and 5%. In contrast, CLA-8 is highly soluble in DMSO and as shown in Chapter 3, CLA-8 was easily solubilized up to a concentration of 15% in a formulation containing DMSO as solvent.

While the viscosity of CC12 (2.5% CLA-8) and CC13 (5% CLA-8) was the same, the addition of CLA-8 increased the viscosity of the CarboCells by no more than 10% when compared to CC11 (0% CLA-8) (Fig. 35A). Hereafter, the *in vitro* release of R848 from the aforementioned formulations was evaluated. According to a two-way ANOVA, there were no significant differences in the cumulative R848 release between the tested CarboCells ($p > 0.05$) (Fig. 35B). To confirm that the addition of CLA-8 would not influence the *in vivo* drug release profile and consequently, the therapeutic efficacy, mice bearing CT26 tumors were treated with CC11, CC12 and CC13 containing both R848 and RepSox. As expected, there were no substantial differences in the therapeutic response generated by the tested formulations (Appendix IV-S16). Thus, including up to 5% CLA-8 in the extended release CarboCell did not have an effect on the drug release kinetics nor on the efficacy of the treatment.

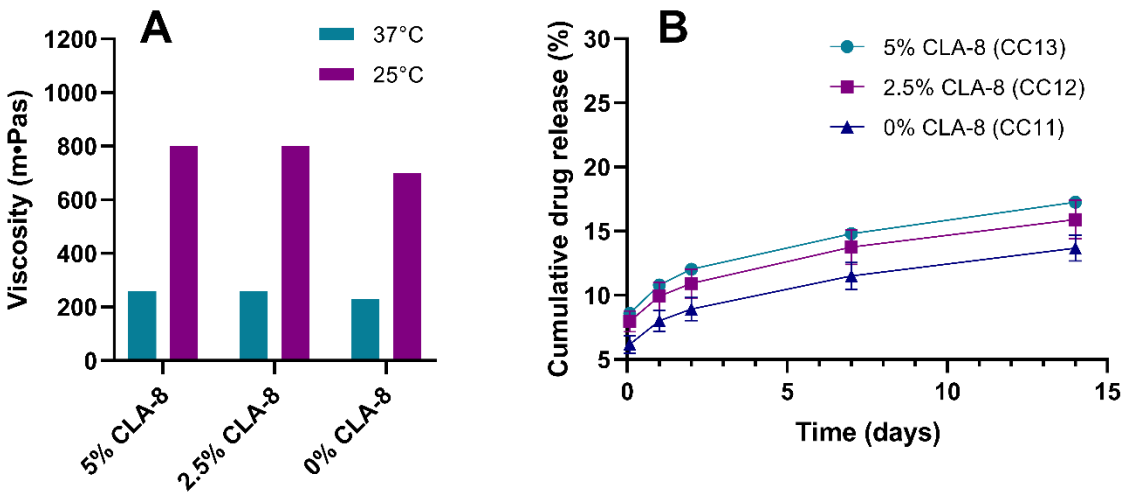

Figure 35. In vitro evaluation of CarboCells containing CLA-8. (**A**) Viscosity of CarboCells comprising 0, 2.5 or 5% CLA-8 (CC11, CC12 and CC13, respectively) measured at 25°C and 37°C. (**B**) In vitro release of R848 from CarboCells comprising 0, 2.5 or 5% CLA-8 (CC11, CC12 and CC13, respectively). Data is presented as (**A**) single measurements (n=1) or as (**B**) mean ± SEM (n=3).

Stability assessment of CarboCell with R848 and RepSox

Evaluating the stability of a drug product is a key aspect during the formulation development process. Comprehensive stability tests should comprises different stages ranging from the preparation of the drug product until its use to ensure the quality of the formulation. In this project, we investigated the short-term drug stability in CC11, CC12 and CC13 upon storage at two different temperatures and after sterilization, an essential process to protect the health of the patients. Sterilization was done via autoclave and the high temperatures to which the formulations are exposed during this process may trigger undesired chemical reactions affecting the stability of the drug [195].

As explained in Chapter 2, we know that R848 has a tendency to react with the acyl groups from the carbohydrate esters. Therefore, we were able to predict the possible modifications that could occur to R848 in the presence of SuBen and CLA-8 (Fig. 36). Although RepSox does not share the imidazoquinoline structure, it contains a pirazole group that, due to its adjacent nitrogen atoms, may make RepSox susceptible to the same chemical modifications as R848. In the case of RepSox, a modification in its pirazole group would likely affect its activity since such moiety is involved in hydrogen bond interactions with key residues in the binding pocket of TGFβRI [187], [196].

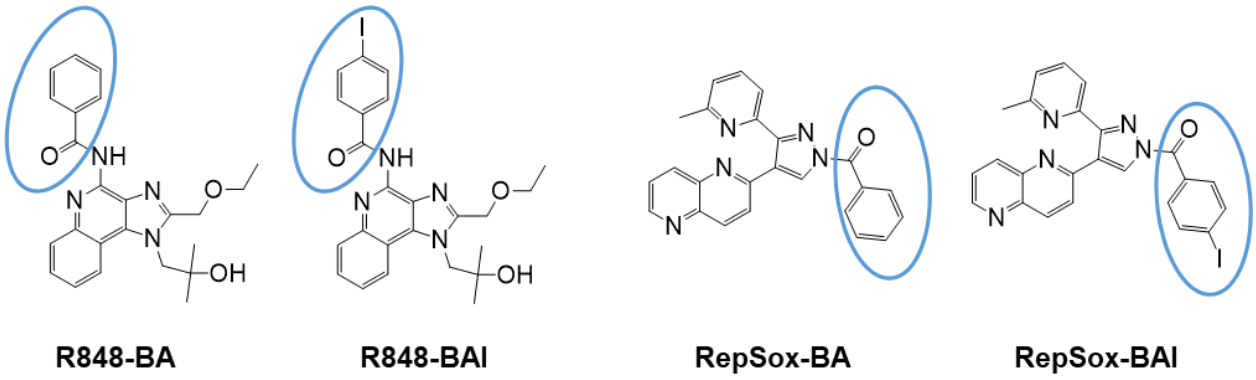

Figure 36. Potential drug modifications in CarboCells. Chemical structures of the molecules that might result from the interaction between the drug substances with the carbohydrate matrix SuBen and the CT contrast agent CLA-8 (-BA and –BAI modifications, respectively). The possible added moieties are circled in blue.

Since we previously showed that the reactivity of R848 is enhanced at higher temperatures, we chose to store the CarboCells at low temperatures (4°C and -20°C) and the drug stability after 3 months was evaluated. In the absence of CLA-8, both R848 and RepSox remained as intact molecules and no modified versions were detected at either temperature. For CC12 and CC13, only R848-BAI was detected in a percentage lower than 0.3% (Table 5). The amount of R848-BAI was slightly higher in CC13, which correlates to the higher percentage of CLA-8 in such formulation. As expected, drug stability was higher at -20°C. The CarboCells were opaque and likely frozen after being taken out of the freezer, but they turned clear and fluid again after less than 10 min at room temperature. Such phenomenon was not observed for the CarboCells stored at 4°C.

Table 5. Stability of CarboCells comprising 0, 2.5 or 5% CLA-8. Stability was measured after autoclaving the CarboCells and after 3 months of incubation at 4°C and -20°C. The formulations contained 6 mg/g R848 and 16 mg/g RepSox. The stability is reported as the percentage AUC corresponding to each potential modified drug substance (n= 3 ± SD); if the molecule was not detected, the result was reported as 0.0. Abbreviations: T0: time zero.

Molecule	0% CLA-8 (CC11)				2.5 % CLA-8 (CC12)				5 % CLA-8 (CC13)			
	T0	*Post auto-clave*	*4°C*	*-20°C*	*T0*	*Post auto-clave*	*4°C*	*-20°C*	*T0*	*Post auto-clave*	*4°C*	*-20°C*
RepSox-BA	0.0	0.0	0.0	0.0	0.0	0.0	0.0	0.0	0.0	0	0.0	0.0
RepSox-BAI	0.0	0.0	0.0	0.0	0.0	0.0	0.0	0.0	0.0	0.0	0.0	0.0
R848-BA	0.0	0.3 ± 0.0	0.0	0.0	0.0	0.3 ± 0.0	0.0	0.0	0.0	0.3 ± 0.0	0.0	0.0
R848-BAI	0.0	0.0	0.0	0.0	0.0	0.7 ± 0.1	0.1± 0.1	0.0	0.0	2.1 ± 0.1	0.3 ± 0.0	0.1± 0.1

Regarding the sterilization process, none of the potential RepSox-derived molecules were detected in any of the CarboCells after autoclaving (Table 5, Appendix IV-S16). Nonetheless, R848-BA was equally detected in all formulations, but in a very small percentage (0.3%). R848-BAI was formed in CC12 and CC13 resulting from a reaction between R848 and the iodinated benzoate moiety in CLA-8. The identity of R848-BAI was confirmed by LC-MS (m/z= 545.1) and the amount of R848-BAI increased when increasing the concentration of CLA-8 in the CarboCell. Due to the lower amount of CLA-8, CC12 might present a lower risk for drug instability than CC13. Moreover, CC11 and N1 CC had shown excellent long-term drug stability at 4°C; after 9 and 13 months, respectively, less than 0.1% of modified drug molecules have been detected (Appendix IV-S17, S18). Therefore, it is likely that similar results will be observed for long-term stability studies of CC12. Thus, CC12 was determined as a promising formulation to advance on the development pipeline.

4.4 Concluding remarks and future perspectives

We demonstrated that the CarboCell system allows easy and simultaneous formulation of multiple drugs. R848 and RepSox were solubilized in a straightforward manner in multiple CarboCell formulations without needing to adjust the preparation method nor dose. Moreover, the multi-target approach of the CarboCell combining R848 (a TLR7/8a) and RepSox (a TGF- inhibitor) showed an improved therapeutic response in mice compared to the monotherapy treatment with R848. Noticeably, no signs of acute toxicity were observed although the tested drug substances are known to produce serious adverse effects following systemic administration. This highlights the ability of CarboCell to provide on-target drug delivery with presumably negligible spillover to systemic circulation. Importantly, the aforementioned treatment was able to induce a systemic immune response, where an anti-cancer effect was also observed in non-injected cancerous tissue. Thus, the promising and synergistic effect of CarboCell with the R848 and RepSox combination was confirmed.

Furthermore, an improved CarboCell was developed that allowed for a doubling of the drug-releasing period compared to the original N1 CC both *in vitro* and *in vivo*. A slower drug release was achieved by increasing the SuBen/GTO ratio, which we assumed increased the hydrophobicity and viscosity of the self-formed depot and delayed the drug partitioning into the aqueous phase and tissue. In addition, this

change allowed to remove PLA as a low burst was achieved, thus simplifying the formulation. The newly developed CC11 formulation permitted to increase the interval between injections from 7 to 14 days thereby reducing by half the number of injections per treatment. This improvement can increase patient compliance, improve the quality-of-life of patients during treatment and reduce the risk of organ injury or dissemination of cancer cells that might be connected to frequent intratumoral injections. Moreover, the CT contrast agent CLA-8 was successfully incorporated in the formulation for extended release up to a concentration of 5%. Including CLA-8 in the CarboCell did not affect the drug release kinetics nor the therapeutic effect. Nonetheless, the CarboCell containing 2.5% CLA-8 (CC12) might represent a lower risk to drug instability since CLA-8 was seemingly found to be reactive with R848. Although long-term stability testing is still required, good drug stability is expected when storing the CarboCell at 4°C and -20°C.

Since many factors are involved in the cancer-immunity cycle, there are numerous potential therapeutic targets [19]. Although in this project we only incorporated two drugs in the CarboCell, it is very likely that more drug molecules can be incorporated into the drug delivery system. As CarboCell has the potential to reduce drug spillover, several drugs may be co-delivered with a minimized risk of systemic toxicity but with the possibility of an enhanced therapeutic response. Such approach would be interesting to investigate in the future. Moreover, a next step to improve the formulation would be to further extend the drug-releasing period to ultimately reduce the dosing to a single injection and amplify the previously discussed benefits.

4.5 Materials and methods

Chemicals

All chemicals were purchased from Sigma Aldrich, Merck unless stated otherwise. Ethanol (absolute), acetonitrile (MeCN) and dimethyl sulfoxide (DMSO) were purchased from VWR Chemicals. R848 was purchased from AmBeed and RepSox from Selleckchem. Note that SuBen from Sigma Aldrich was not purified prior use (thus the material is referred to as σ-SuBen). CLA-8 was synthesized as described in Appendix III.

Preparation of CarboCell

CarboCell formulations were prepared by mixing σ-SuBen with the co-solvents (GTO, Et-Myr, Et-Pal, Et-Ste, lipiodol), EtOH and PLA, if applicable. The different compositions are indicated in weight percent in Table 4, and the corresponding amount of each compound was weighed into one vial. The mixture was placed in an ultrasonication bath at 70-80°C for 1-2 hours and occasionally vortexed to generate homogenous solutions, namely CarboCells, which were stored at 4 °C until further use. Drug molecules were incorporated into the formulation by proportionally adding CarboCell on top of a previously freeze-dried drug aliquot, until reaching the desired drug concentration. CarboCells were subjected to magnetic stirring at 40-50 °C until the drug was completely dissolved.

Mice and cell lines

All experimental procedures were approved by the Danish Experimental Animal Inspectorate. Female mice were obtained at 6 weeks of age (BALB/c or C57BL/6 from Janvier and Charles River). CT26 and EMT-6 cells were obtained from ATCC. MC38 cells were obtained from Kerafast. CT26 and MC38 cells were maintained in RPMI 1640 medium (GibcoTM, Thermo Fisher Scientific or Sigma-Aldrich, Merck). EMT-6 cells were maintained in DMEM (GibcoTM, Thermo Fisher Scientific). All media were supplemented with 10% foetal bovine serum (GibcoTM, Thermo Fisher Scientific or Biowest, VWR) and 1% penicillin-streptomycin (GibcoTM, Thermo Fisher Scientific or Sigma-Aldrich, Merck). All cell lines were kept in a humidified tissue culture incubator at 37°C with 5% CO2. Cells were subcultured when confluent and Trypsin-EDTA (0.25%) (Thermo Fisher Scientific) was used to remove adherent cells.

In vivo mouse therapy study

Tumors were established in 7-9 weeks old female BALB/c (3 x 105 CT26 cells/tumor, 5 x 105 EMT-6 cells/tumor) or C57BL/6 (3 x 105 MC38 cells/tumor) mice. The mice were inoculated by subcutaneous injection of cancer cells in 100 µL of serum-free medium.

Tumors had a mean size between 87-150 mm^3 before starting the treatments (8-14 days post-inoculation). All CarboCell injections had a volume of 50 µL and were injected intratumorally. Mice received four injections at 7-day intervals (N1 CC) or two injections at 14-day intervals (CC11, CC12, CC13). The drug concentration in each CarboCell is specified in the corresponding figure legends. Mice were anesthetized by ~3-5% sevoflurane during injections. Tumor size (volume = length x $width^2/2$) and bodyweight was measured 2-3 times/week. Mice were euthanized once tumors reached a size between 1000 mm^3 and 1500 mm^3 depending on the study. Mice were terminated from studies in case of ulcerations, failure to thrive, respiratory distress or weight loss >15%.

UHPLC method

HPLC analyses were done using a Shimadzu Nexera-X UHPLC instrument with a PDA detector. The samples were injected (5 µL for samples in DMSO/MeCN or 40 µL for samples in PBS) onto a Waters Terra BEH C8 column (2.5µm, 4.6x75mm, temperature 25°C) at a flow rate of 0.8 or 1 mL/min (for samples in DMSO/MeCN or in PBS, respectively). The solvent system consisted of mobile phase A (5% MeCN, 0.1% TFA in water) and mobile phase B (0.1% TFA in MeCN). For *in vitro* drug release studies and analysis of samples dissolved in MeCN, chromatographic separation was achieved using a gradient of 0 to 100% phase B in 5 min followed by 2.5 min at 100% B. For analysis of samples dissolved in DMSO (i.e., containing CLA-8), the employed gradient was 0 to 100% phase B in 5 min followed by 4 min at 100% B. Ultraviolet detection at 280 nm or 320 nm was used to identify the specified compounds.

In vitro drug release

50 µL of each tested CarboCell were individually injected in 8-mL glass vials containing 2 mL PBS, for which the exact amount of injected CarboCell was weighed. The vials were incubated at 37 °C and at each sampling point 1 mL of PBS was taken. 1 mL of fresh buffer was added immediately to the vial to replace the taken sample. The samples were then analyzed by HPLC (UV detection at 320 nm) and the concentration of drug in the release media was calculated via a standard curve. The cumulative drug release was calculated as shown below (equations 2 and 3):

$$Cumulative\ drug\ release\ (\%) = \frac{\sum_{i=1}^{\infty} m_i}{m_{tot}} * 100\% \qquad \text{(Equation 2)}$$

where

$$m_i = C_i V_{tot} - C_{i-1}(V_{tot} - V_s) \qquad \text{(Equation 3)}$$

and m_{tot} is the total amount of drug contained in the injected CarboCell, m_i is the amount of drug released at time i, C_i is the measured drug concentration at time i, V_{tot} is the total volume of the solution (2 mL), V_s is the sample volume (1 mL).

In vivo release study

For each CarboCell, 50 µL were injected subcutaneously (s.c.) in female BALB/c Jrj mice or intratumorally (i.t.) in female BALB/c Jrj mice bearing CT26 tumors (inoculated as described in the *in vivo* therapy section); mice were anesthetized using ~2% isoflurane during injections. At each sampling point, mice were euthanized and the CarboCell depots were collected. Such depots were immediately dissolved in 1 mL MeCN (samples without CLA-8) or DMSO (samples with CLA-8) and incubated at room temperature overnight. The samples were then filtered using 0.45-µm pore, nylon syringe filters and diluted eight times prior analysis. As reference, 10 µL of each CarboCell (non-injected) were dissolved in 1 mL MeCN or DMSO, as described before. All samples were then analyzed by UHPLC.

The drug release percentage was determined by ratiometric analysis. The AUC values of R848 and RepSox (320 nm), SuBen and CLA-8 (280 nm) were measured to calculate the AUC ratios of drugs/SuBen or drugs/CLA-8 in all samples. The percentage of released drug was calculated by comparing the AUC ratios in the collected CarboCells versus the corresponding ratios in the reference (non-injected) CarboCell (equation 1). The use of SuBen as internal reference to calculate total drug release was validated as described in Appendix I.

Viscosity measurement

Viscosity measurements were done using an EMS-1000 viscometer set at 1000 rpm. The measuring time varied depending on temperature and viscosity range. 1 mL of each tested formulations (without containing drug molecules) were individually pipetted into the instrument´s corresponding glass tube

and a 1.2 mm aluminum sphere was placed inside the tube. Viscosities were determined at 25 and 37°C with measurement times between 10 s and 1 min.

Evaluation of stability

Immediately after preparation, drug loaded CarboCells were evenly divided in three sets. One set was subjected to a steam autoclave process, whereas the remaining vials where incubated at either 4°C or -20°C. At the specified sampling points around 50 µL of CarboCell were taken and dissolved in 1 mL of MeCN (formulations without CLA-8) or DMSO (formulations with CLA-8) prior analysis by UHPLC or LC-MS. The AUC values of R848 and RepSox as well as any drug-derived molecules, namely modified versions of R848, were measured at 320 nm and stability was reported as the percentage AUC corresponding to the R848- or RepSox-derived chemical entities.

LC-MS method

Samples were analyzed in an ACQUITY UPLC instrument coupled with a QDa detector. Samples (5 µL) were injected onto a Waters BEH C18 column (2.1 µm, 2.1x50mm, temperature 40°C) at a flow rate of 0.4 mL/min. The solvent system consisted of mobile phase A (5% MeCN, 0.1% FA in water) and mobile phase B (0.1% FA in MeCN). Chromatographic separation was achieved using a gradient of 0 to 100% phase B in 6 min.

Statistical analyses

When required, statistical analyses were performed on GraphPad Prism 9. The correspondingly used statistical test is specified in figure legends. A p-value ≤0.05 was deemed as statistically significant.

Chapter 5.
Extended characterization of the CarboCell system

5.1 Background

Characterization testing is useful to understand the physical and chemical properties of the CarboCell platform. A comprehensive understanding of the CarboCell formulation can expedite future formulation development activities and facilitate a smooth transition to later stages in the development pipeline. For instance, a thorough knowledge on the CarboCell system can be helpful to formulate new drug molecules and optimize release profiles more rapidly thereby saving costs and time.

Therefore, to extend our knowledge on the CarboCell technology, this chapter was focused on testing the effect of the different CarboCell components on parameters as viscosity and drug release kinetics. The importance of the drug release kinetics of CarboCell has been described in previous chapters. The evaluation of the viscosity included tests both before injection and after simulating injection and solvent diffusion out from the CarboCell. Viscosity is a key factor for parenteral administration as it is directly correlated to syringeability and injectability. The formers describes the easiness of withdrawal from vial to syringe, whereas the latter refers to how a formulation performs during injection including the injection force and evenness of flow [197]. Inadequate syringeability and injectability can negatively affect patient compliance and, alternatively, cause difficulties for clinicians performing the injections thereby hindering the clinical use of a formulation [198], [199].

Sterility, i.e., the absence of any microbes, is another key attribute that needs to be considered during drug product development of injectable formulations. Thus, sterilization is a fundamental process for the patient safety since it destroys all forms of pathogenic microorganisms that might be present in the drug product [200]. Generally, the sterilization step is performed once the product has been filled in its primary packaging, which is referred to as terminal sterilization. Several sterilization methods exist including dry heating, membrane filtration, steam sterilization, exposure to radiation, and gas sterilization. Choosing the most adequate sterilization method depends on the physico-chemical characteristics of both the drug substance and the pharmaceutical formulation [201]. In this project, the sterilization of the CarboCell via gamma irradiation and steam sterilization (from now also referred to as autoclaving) was investigated.

During steam sterilization, the product is exposed to heat as saturated steam under pressure. Under these conditions, microorganisms are killed due to the irreversible denaturation of enzymes and cell

components. Steam sterilization is generally carried out in an autoclave, where the most typical conditions are 121°C at 2 atm for 15 min. Depending on the formulation, the time, pressure and temperature can be adjusted to optimize the efficacy of sterilization [200]. Autoclaving is a widespread sterilization method; however, it might not be suitable for heat-sensitive drug substances or materials due to the high temperatures involved in the process [202]–[204].

Gamma irradiation is a very common method for pharmaceutical sterilization. In this method, gamma rays are emitted as result of the decay of radioactive materials such as cobalt-60 (^{60}Co) or cesium-137 (^{137}Cs). Such high-energy radiation generates electron disruptions (ionization), which breaks down the DNA of microorganisms. Thus, the pathogens are killed or their reproduction is inhibited [205]. The factors that can influence the sterilization process include the dose rate and the absorbed radiation dose, where the latter can be precisely measured using dosimeters placed along the items being sterilized [206], [207]. Gamma irradiation is considered an isothermal process, so it represents an effective alternative for the sterilization of drug products that are thermos-labile. Moreover, the high penetration power of gamma irradiation enables the sterilization of products in their final packaging [204]. However, gamma irradiation can cause alterations to the active ingredient and other materials. Radiation might promote fragmentation of covalent bonds as well as production of free radicals; this may result on modifications of the physico-chemical characteristics of the formulation, degradation of the drug molecule and production of impurities [204], [207]. Another consideration is that sterilization via gamma irradiation requires specialized instrumentation and infrastructure [201]. Although gamma irradiation does not induce radioactivity in the sterilized materials, this method requires a radioactive source that needs to be specially handled and disposed of. Inadequate handling and disposal of radioactive materials can represent a potential hazard for the environment and the staff in charge of the instrumentation [200], [201].

5.2 Objectives

In this project, R848 was the main model molecule used for the CarboCell characterization studies. Thus, to deepen our understanding on the variables influencing drug release from the CarboCell and generate useful knowledge for future formulation developments, the following objectives were established:

- ☐ To investigate the correlation between viscosity, solvent efflux and drug release from the CarboCell
- ☐ To investigate how different CarboCell components influence drug release. Particularly, to evaluate the effect of various solvents, co-solvents and two types of SuBen (σ-SuBen and π-SuBen)
- ☐ To evaluate the effect of different injection volumes in drug release kinetics
- ☐ To test two sterilization methods, autoclave and gamma irradiation, and evaluate their effect on the stability of CarboCells

5.3 Results and discussion

To aid presenting the correlation between the different CarboCells formulations and their tested properties, each section contains its own table detailing the CarboCell compositions used in the corresponding study.

Effect of solvent diffusion on the viscosity of CarboCell

After CarboCell is injected, the solvent diffuses out from the CarboCell into the surrounding media, which induces a phase separation and the formation of a highly viscous depot at the injection site. Solvent diffusion kinetics play a key role in the formation of the depot and the rate at which its viscosity changes over time. As described in Chapter 4, the viscosity of the self-formed depot influences the drug release kinetics. Hence, we were interested in evaluating how the diffusion of different solvents affects the viscosity of the CarboCell as a function of time. For this purpose, CarboCells were placed in a glass tube, which was then covered with PBS to promote solvent release into the aqueous media and their viscosity was measured over a 2-week period (Appendix III-S6A). Multiple CarboCell formulations were prepared and the tested co-solvents included GTO and GTH, whereas the solvents were PC, EtOH and DMSO (Table 6).

Table 6. CarboCell compositions used to study the effect of solvent release on viscosity.

CarboCell formulation	**Chemical components (w/w%)**					
	σ-SuBen	*GTO*	*GTH*	*PC*	*EtOH*	*DMSO*
CC1	60	20	-	20	-	-
CC2	60	-	20	20	-	-
CC3	60	20	-	-	20	-
CC4	60	-	20	-	20	-
CC5	60	-	20	-	-	20

The different solvents had a clear effect on the viscosity change of the CarboCell. The formulations that had EtOH as solvent displayed a faster increase in viscosity followed by the CarboCells containing DMSO and PC, in that order. When compared to the initial viscosity, the viscosity at day 14 was in average 210-fold, 20-fold, and 1.3-fold higher for the CarboCells with EtOH, DMSO and PC, respectively. Furthermore, the use of either GTH or GTO as co-solvents did not have an impact on the solvent diffusion kinetics (Fig. 37A, B). PC was the solvent with the slowest diffusion into the buffer and this is further exhibited in Fig. 37C. It is observed that after 48 h CC2, a CarboCell containing PC, was still clear and translucent, while formulations comprising EtOH or DMSO (CC4 and CC5, respectively) had undergone a visible phase separation.

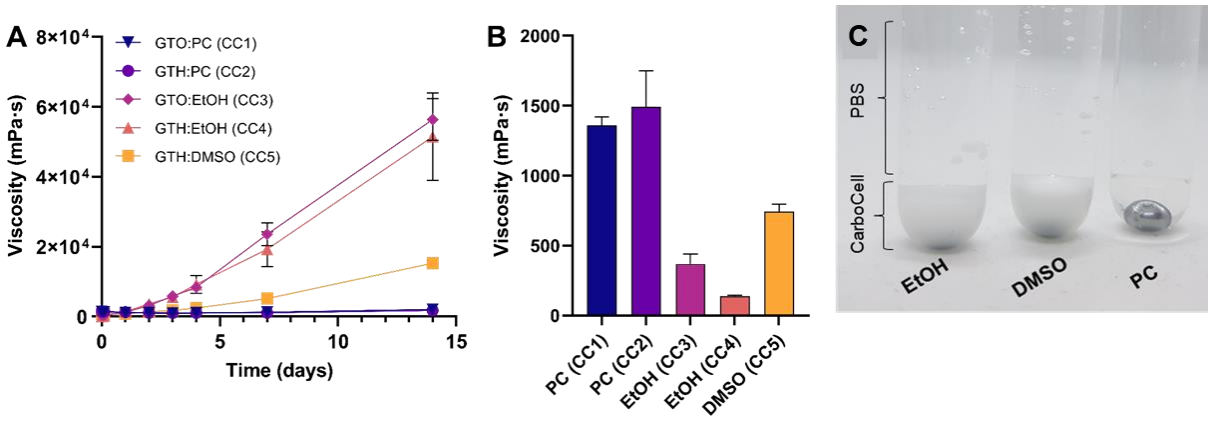

Figure 37. Effect of solvent release on CarboCell viscosity. (**A**) Viscosity at 37°C of various CarboCells measured as a function of solvent release over time. (**B**) Viscosity of the CarboCells at time zero measured at 37°C. (**C**) Picture of formulations CC4, CC5 and CC2 (from left to right) in the viscosity tube after 48 h of incubation at 37°C, where PBS is on top of the CarboCells and the aluminum sphere used to measure the viscosity is only visible in the formulation containing PC. Data is shown as mean ± SEM (n=3).

In Chapter 2, it was suggested that the rate at which solvents diffused out from the CarboCell depended on their hydrophobicity. A more hydrophilic solvent (low log P) would partition into the water phase faster than a solvent with a higher log P. While such hypothesis could be applied to DMSO and PC (log P values of -1.40 and 0.79, respectively), it was not the case for EtOH. Despite having a log P of -0.16, EtOH was the solvent with the fastest diffusion as shown by the steep increase in viscosity. Additionally, it has been reported that the miscibility of the solvent in water might affect the phase separation of *in situ*-formed implants [194]. In such study, a PLGA/solvent formulation was prepared and solvents with lower water miscibility would delay the phase separation process, which resulted in more fluid polymer matrices. Both EtOH and DMSO are miscible in water; however, PC shows a partial solubility in water (8.3%) [208]. Such characteristic might also explain the slow release of PC related to the poor increase in viscosity of the corresponding CarboCells.

Furthermore, in a study using a SAIB-based delivery system, it was reported that EtOH had the fastest efflux rate when compared to DMSO and NMP. The authors proposed that the difference in efflux rate was correlated to the intrinsic viscosity of the solvents as well as to solvent-matrix interactions. Regarding the former, the authors observed that a solvent with a lower viscosity would diffuse more rapidly from the depot. [121]. The dynamic viscosities at 20°C of EtOH, DMSO and PC are 1.22, 2.47 and 2.76 m·Pas, respectively [121], [209], which follows the sequence observed for the increase of viscosity (EtOH > DMSO > PC). An additional explanation might be given by the solvent-matrix interactions. SuBen is more soluble in DMSO and PC than in EtOH. Once the CarboCell is injected, EtOH would have more affinity for water than for the SuBen matrix; therefore, EtOH would rapidly diffuse out from the depot resulting in the faster increase in viscosity of the CarboCell. Thus, solvent diffusion might not be governed by a single factor, but rather by a combination of the physico-chemical properties of the solvents and their interaction with the CarboCell.

To further understand the solvent diffusion kinetics, a possible next step would be to determine the actual amount of solvent being released into the buffer over time. This could be done by measuring the refractive index of the release media. Moreover, a limitation within the present study is that solvent

efflux was only occurring at the top of the CarboCell, where the CarboCell was in direct contact with PBS. The diffusion kinetics might be different if the CarboCell is injected into the buffer because there would be a greater surface contact area between the CarboCell and the surrounding media.

Effect of co-solvents and solvents on drug release

As exemplified in previous chapters, the CarboCell composition is a fundamental factor driving the drug release kinetics. Each component possesses intrinsic physico-chemical properties that contribute in different ways to the performance of the CarboCell. In this section, we evaluated the effect of different co-solvents (GTH, GTO) and solvents (EtOH, DMSO) in the release kinetics of R848. R848 was formulated in equal concentrations (1.2 mg/g) in various CarboCells (Table 7) and *in vitro* drug release studies were conducted.

Table 7. CarboCell compositions used to study the effect of different co-solvents and solvents on drug release.

CarboCell formulation	**Chemical components (w/w%)**				
	σ-SuBen	*GTO*	*GTH*	*EtOH*	*DMSO*
CC6	60	-	25	-	15
CC7	60	-	25	15	-
CC8	60	25	-	15	-

Regarding the overall drug release profile, it was observed that after 3 weeks, the percentage of released R848 was around 10% lower for the formulation containing GTO (CC8). At this time point, both CarboCells comprising GTH (CC6 and CC7) had displayed a similar cumulative drug release (49.2 ± 2.5% and 46.5 ± 0.9%, respectively) (Fig. 38A). While the co-solvent influenced the long-term drug release, it was found that the choice of solvent played a key role in the initial burst release. The burst release, measured 2 h after injection, was reduced by more than half when using DMSO as solvent. Despite containing different co-solvents, CC7 and CC8 showed the same burst release, determined as 7.2± 0.6% and 6.8 ± 0.7%, accordingly (Fig. 38B). Furthermore, the viscosity of the formulation was highly influenced by the solvent. When comparing CC6 to CC7, DMSO caused a 5-fold increase in viscosity at 37°C and a 7-fold increase at 25°C. The effect of the co-solvent in the CarboCell viscosity was not as drastic. In the case of CC7 and CC8, GTO increased the viscosity only between 10 and 30% (Fig. 38C).

In accordance with the results described in Chapter 4, the choice of co-solvent had an impact on the R848 release kinetics. GTO (log P= 8.3) is a more hydrophobic molecule than GTH (log P= 5.6). Moreover, the CarboCell containing GTO (CC8) had a higher viscosity than its counterpart with GTH (CC7). However, the increase in viscosity caused by GTO was not as drastic by the one caused by DMSO. Once EtOH leaves the CarboCell, it is expected that the depot containing GTO would also have a higher viscosity than the one with GTH. Therefore, the combination of a more hydrophobic co-solvent and a higher viscosity of the depot might explain the overall lower drug release from CC8.

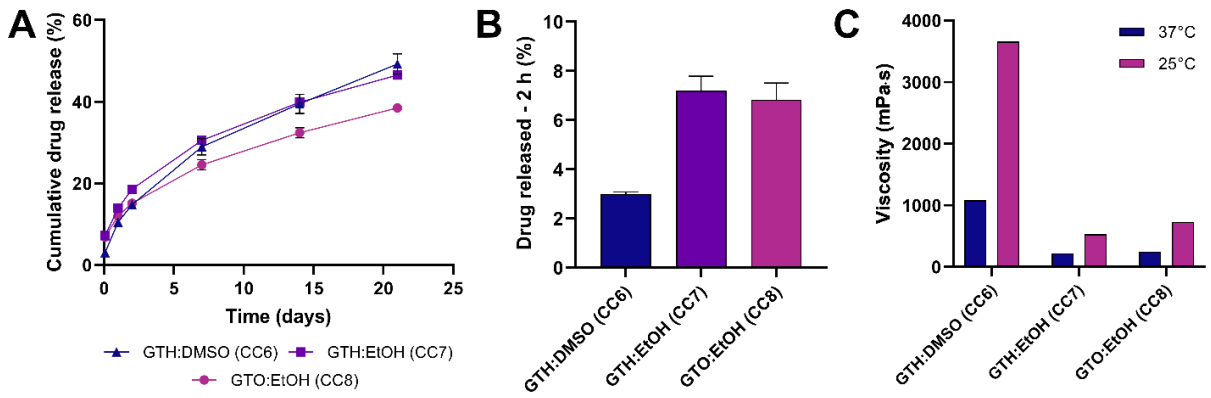

Figure 38. Effect of GTH/GTO and DMSO/EtOH on drug release. (**A**) *In vitro* drug release profile of R848 (1.2 mg/g) from different formulations over 3 weeks. (**B**) Percentage of drug released 2 h post-injection. (**C**) Viscosity of the CarboCells measured after preparation at 25°C and 37°C. Data is shown as mean ± SEM (n=3).

In addition, the choice of solvent can be an effective way to reduce the initial burst release. Other studies in SAIB-based systems have reported that EtOH caused a high burst release, while DMSO could lower it [117], [121]. Such phenomenon is likely related to the initial viscosity of the formulation and the diffusion of the solvent out from the depot. The viscosity at room temperature of CC6, which contained DMSO, was 5 times higher than its counterpart with EtOH (CC7). Thus, as discussed earlier, high viscosity might lower the diffusion of the drug. Based on our previous observations from other studies, we may assume that more EtOH than DMSO has been released into the media during the first hours after injection. When the solvent diffuses from the depot, some drug molecules leave within it thereby causing a higher burst release. Interestingly, after 7 days CC6 and CC7 displayed the same release profile (Fig. 38A). Once the solvent had been released from both CarboCells, the injected depots had the same fractions of SuBen and GTH. Therefore, the R848 release kinetics from both CarboCells eventually were the same. This finding highlights the importance of the solvent regarding the initial drug release.

The burst release is a critical aspect to control for intratumoral drug delivery systems. A high initial burst leads to the release of a large drug dose, which consequently can cause local or systemic toxicity [36], [171]. Moreover, if a high amount of drug is released initially, the release profile may be shortened thereby requiring more frequent dosing [171]. While DMSO could lower the initial burst release, it also caused a considerable increase in the viscosity of the CarboCell. If a formulation is too viscous, then the injectability can be negatively affected specially when using long and thin needles [199]. Thus, there is a fine balance between the type and amount of solvent needed to achieve a low burst release without compromising the injectability of the formulation.

Effect of σ-SuBen and π-SuBen on drug release

As described in Chapter 2, there are two types of SuBen available for the preparation of CarboCells: σ-SuBen and π-SuBen (Fig. 20). The former refers to the material supplied by Sigma-Aldrich that, besides octabenzoate, contains less esterified versions of SuBen including penta-, hexa- and hepta-

benzoate. π-SuBen refers to the material presenting only the fully esterified compound. In Chapter 2, it was described that the chemical stability of R848 was not affected by neither σ-SuBen nor π-SuBen. Nonetheless, the potential effect of the different types of SuBen on drug release kinetics had not been investigated. Hence, several CarboCells comprising either σ-SuBen or π-SuBen were prepared (Table 8) and the *in vitro* release of R848 (1.2 mg/g) was evaluated. In addition, formulations with varying amounts of DMSO were included to further assess the effect of DMSO on viscosity and burst release.

Table 8. CarboCell compositions to study the effect of σ-SuBen and π-SuBen on drug release.

CarboCell formulation	Chemical components (weight ratio)				
	σ-SuBen	*π-SuBen*	*CLA-8*	*GTH*	*DMSO*
CC5	60	-	-	20	20
CC6	60	-	-	25	15
CC9	60	-	-	20	25
CC10	50	-	10	20	20
CC11	-	50	10	20	20
CC12	-	50	10	20	25

In general, it was observed that over a 3-week period, a higher amount of R848 had been released from the CarboCells containing π-SuBen as matrix. For instance, after 3 weeks, CC11 had released 67.8 ± 0.7% of R848, whereas CC10 showed 40.3 ± 0.3 % of R848 release. In accordance with the results from the previous section, the formulations containing the same ratios of carbohydrate ester and co-solvent (e.g., CC11 and CC12) eventually showed the same release profile, despite having different amounts of solvent prior to injection (Fig. 39A). Regarding the burst release, formulations with π-SuBen also showed a higher initial release of R848. Moreover, the burst release increased when increasing the percentage of DMSO (Fig. 39C). Conversely, higher amounts of DMSO caused a decrease in the viscosity of the CarboCells. Also, CarboCells comprising π-SuBen had a lower viscosity than the ones containing σ-SuBen (Fig. 39D).

It is apparent that σ-SuBen promotes stronger intermolecular interactions in the CarboCell that results in an increased viscosity. This might be related to the presence of SuBen molecules with various degrees of esterification (e.g., penta-, hexa-, hepta-benzoate), which have free hydroxyl groups in contrast to π-SuBen that does not contain any. Besides the chemical differences between π-SuBen and σ-SuBen, these materials are physically different. σ-SuBen is a compact fine powder, while π-SuBen is a more crystalline and less dense material (Appendix V-S19). As discussed in the previous section, the faster drug release observed for CarboCells with π-SuBen is likely correlated to the lower viscosity of such formulations. Increasing the percentage of DMSO reduced the viscosity, which consequently can improve the injectability of the CarboCell. Nonetheless, it is important to consider that the initial drug release was higher as the amount of DMSO increased. Again, a balance between injectability and burst release needs to be considered during the development of the formulations. In the future, it would be interesting to test if different molecules than R848 would experience the same

effects. For instance, a more hydrophobic molecule than R848 might be less susceptible to a high burst release when increasing the percentage of DMSO. R848-C8, a molecule with a higher log P, may be used as a model since it displayed a lower initial release than R848 when formulated in the same CarboCell, as exemplified in Chapter 2 (Fig. 25A).

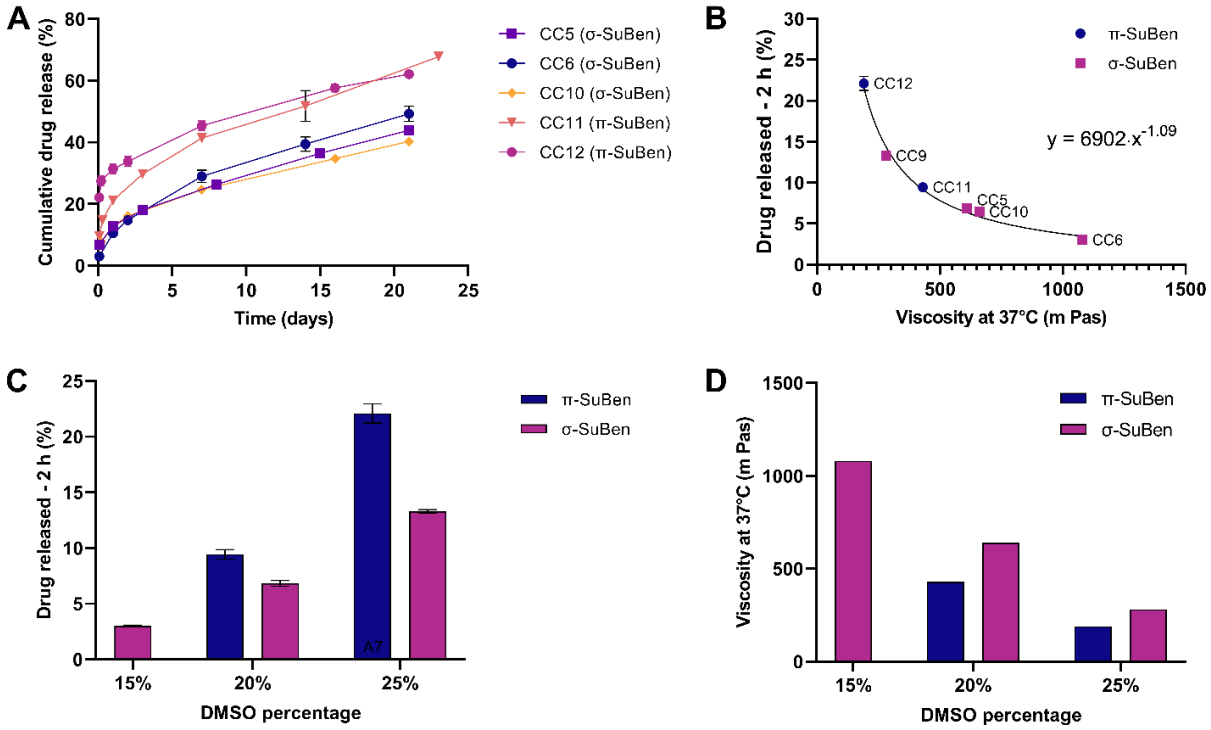

Figure 39. Differences between σ-SuBen and π-SuBen on drug release. (**A**) *In vitro* drug release profile of R848 (1.2 mg/g) from multiple formulations based on either σ-SuBen or π-SuBen. (**B**) Correlation between the burst release (i.e., percentage of drug released 2 h post-injection) and the viscosity at 37°C of CarboCells with the composition SuBen:GTH:DMSO. The fitted curve has and R^2 of 0.9772. (**C, D**) Effect of the percentage of DMSO in the (**C**) burst release and **(D**) viscosity of the formulations at 37°C. Drug release data is shown as mean ± SEM (n=3-4); viscosity data is shown as the mean of three measurements from a single replicate.

It was also found that there was a correlation between viscosity and the initial burst release (Fig. 39B). The data was fitted through a log transformation followed by a linear regression analysis. The resulting curve had an R^2 of 0.9772 with random residuals thus deeming the curve as an appropriate model (Appendix V-S20). It is expected that such correlation will be useful for predicting an estimated burst release of formulations with the composition SuBen:GTH:DMSO (with or without CLA-8) based on their viscosity at 37°C. Since the data was fitted using R848 as model molecule, the mathematical model might only apply to drugs with similar physico-chemical properties to R848.

Effect of injection volume on drug release

An injection volume of 50 µL has been the norm throughout the formulation development and pre-clinical testing of the CarboCell system. Such volume has been adequate for evaluation in mice; however, to further advance the CarboCell technology, the injection volume will need to be adjusted for larger animal species [210]. Hence, we investigated if increasing the injection volume would affect the drug release

profile. R848 was formulated in CC8 (Table 7) at a concentration of 1.2 mg/g; CarboCell was injected at different volumes and the *in vitro* release kinetics were determined.

The drug release curves showed the same overall profile regardless of the injection volume. Logically, the amount of released R848 was higher as the injected volume increased because the larger depots would contain more drug (Fig. 40A, B). Moreover, it was observed that at each time point there was a linear relationship between the surface area of the injected depot and the amount of released R848 (Fig. 40C). The surface areas were calculated assuming a spherical shape of the self-formed depot.

Since a low burst release is fundamental to minimize the risk of local and systemic toxicity, we next evaluated how the injection volume would influence the burst release *in vivo*. For this purpose, different volumes of CC8 with both R848 and RepSox were injected s.c. in mice, where the percentage of released drug was measured 5 h post-injection. Like in the *in vitro* release studies, a decrease in the percentage of released drug was observed when increasing the injection volume. This occurred for both RepSox and R848 alike (Fig. 40D).

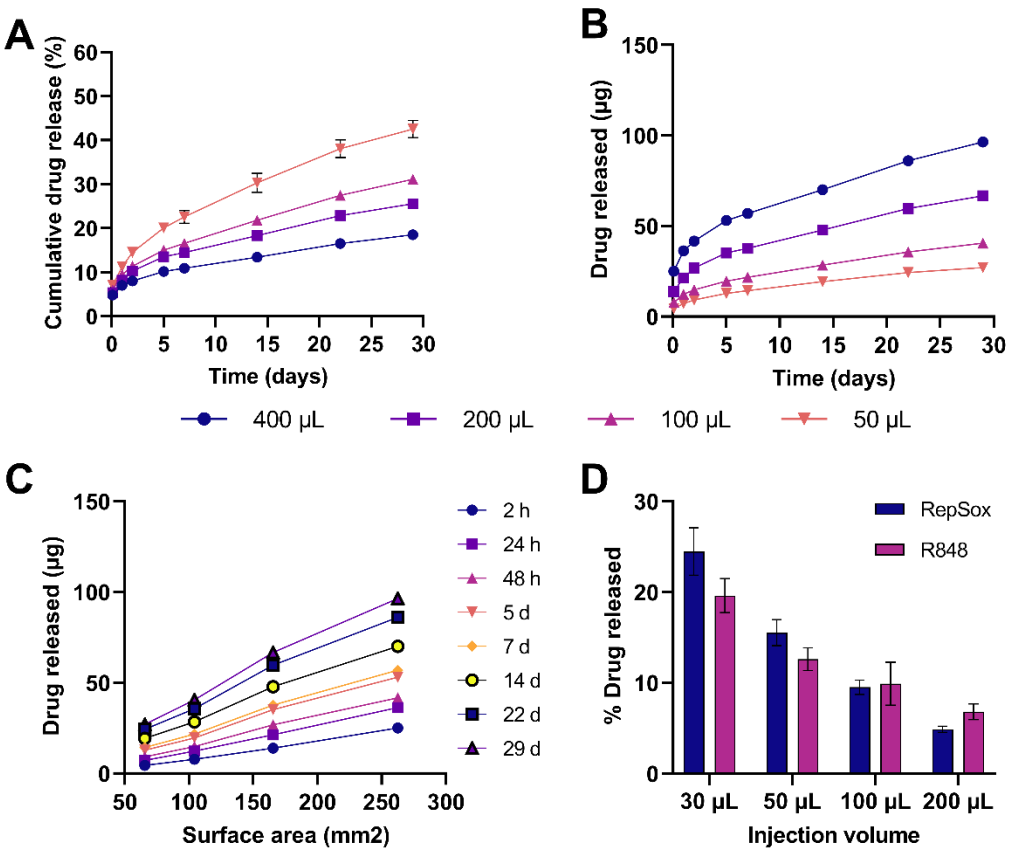

Figure 40. Effect of injection volume on drug release. (**A**) In vitro percentage of cumulative drug release and (**B**) total amount of released R848 from different injection volumes of CC8 (1.2 mg/g R848). (**C**) Total amount of R848 released *in vitro* as a function of the surface area of CarboCell at multiple time points. (**D**) *In vivo* release of R848 (1.2 mg/g) and RepSox (8 mg/g) after s.c. injection of different volumes of CC8. Data is shown as mean ± SEM (n=3-6).

In the previous chapter, we showed that the drug concentration does not affect the release profile. Therefore, both injection volume and drug concentration may be manipulated without a considerable impact on the drug release profile from the CarboCell. From a formulation perspective, we expect that the injection volume and dosing can be easily adjusted and escalated in the CarboCell thereby enabling its use in larger animal models. A major concern when increasing the injection volume is that the burst release will increase too [211], [212]. For instance, in the case of nanoparticles, it has been suggested that the burst release is related to the amount of drug present on the surface area. Noticeably, the *in vivo* burst release remained low despite increasing the surface area of the injected depot. Overall, increasing the injection volume should not have a noticeable effect in the performance of the CarboCell.

Evaluation of autoclave and gamma irradiation as sterilization methods

Sterilization is a fundamental process aimed at ensuring that the drug product is free of pathogens to safeguard the health of the patients. Depending on the sterilization method and conditions, the chemical and physical stability of a drug product might be affected [213], [214]. Thus, R848 and RepSox were formulated in various CarboCells (Table 9) and their chemical stability was evaluated after being subjected to autoclaving or gamma irradiation. Stability was determined by measuring the percentage AUC of drug-derived impurities compared to the AUC of the drugs.

Table 9. CarboCell formulations to study drug stability as a function of different sterilization procedures.

CarboCell formulation	**Chemical components (w/w%)**						
	σ-SuBen	*π-SuBen*	*CLA-8*	*GTO*	*GTH*	*EtOH*	*DMSO*
CC11	-	50	10	-	20	-	20
CC13	63	-	-	17	-	20	-
CC14	60.5	-	2.5	17	-	20	-
CC15	58	-	5	17	-	20	-
CC16	-	50	10	25	-	15	-
CC17	-	60	-	-	20	-	20

Overall, gamma irradiation was better at preserving drug stability in the CarboCells (Table 10). Gamma irradiation was particularly advantageous for the sterilization of CC11 as 100% of R848 remained intact, while around 10% of modified R848 molecules were detected after autoclaving. When comparing CC13 (0% CLA-8), CC14 (2.5% CLA-8) and CC15 (5 % CLA-8), it was observed that the percentage of intact drugs in the autoclaved samples slightly decreased with an increasing percentage of CLA-8 in the CarboCell. For the formulations containing CLA-8, R848-BAI was the most abundant impurity followed by R848-BA (their chemical structures can be found in Fig. 36). Moreover, all formulations were physically stable regardless of the sterilization method. The CarboCells remained clear and no signs of precipitation or phase separation were observed. Nonetheless, all CarboCells containing CLA-8 acquired a bright yellow coloration (Fig. 42), a phenomenon that will be further discussed later in the text.

Table 10. Effect of sterilization methods on drug stability. Percentage of intact drug measured in CarboCells after being subjected to autoclaving or gamma irradiation (30 kGy). All formulations contained 6 mg/g R848 and 20 mg/g RepSox, except CC11, which only contained 1.2 mg/g R848. A percentage of 100.0% indicates that no drug-derived impurities were detected. Data is shown as mean ± SEM (n=3) for autoclave samples, whereas n=1 for gamma irradiation.

CarboCell formulation	Percentage of intact drugs (%)	
	Autoclave	*Gamma irradiation*
CC11	91.1 ± 2.1	100.0
CC13	99.7 ± 0.0	100.0
CC14	99.0 ± 0.1	99.9
CC15	97.7 ± 0.1	99.9

Although being an effective method, steam sterilization can induce physico-chemical changes in both the drug and the drug delivery system due to the high temperatures involved. Some drugs are thermos-labile and experience degradation upon exposure to heat [215]. Also, several drug delivery systems are heat-sensitive. For instance, nanoparticles can aggregate and change in size, whereas hydrogels might experience modifications in their swelling properties [203], [214]. In the case of R848, we have shown in Chapter 2 that an increase in temperature can induce R848 to react with the carbohydrates esters in the CarboCell. Thus, it was not surprising that autoclaving caused a higher generation of impurities compared to gamma irradiation, in which the process temperature is much lower. Gamma irradiation has been widely recognized as an effective alternative to autoclaving for the sterilization of heat-sensitive drug products [204]. Therefore, its application to the CarboCell system was further investigated.

Next, we investigated the effect of the radiation dose on the stability of R848 and RepSox formulated in CC11 and CC16, both formulations containing 10% CLA-8. The formulations were then subjected to three different radiation doses: 10, 20 and 30 kGy. It was found that the drugs remained intact and no drug-derived molecules were detected irrespective of the radiation dose (Table 11). In all cases, the AUC percentages of R848 and RepSox remained constant (Fig. 41A). Nevertheless, a possible degradation product from CLA-8 was detected. After gamma irradiation, a newly formed peak was observed at 280 nm with an RT of 8.9 min. It was also noticed that the AUC of such peak increased as the radiation dose was higher (Fig. 41B). Unfortunately, the identity of the new chemical entity could not be determined by neither LC-MS nor MALDI-TOF. However, we are certain that the additional peak represents a molecule derived from CLA-8 because it was not detected in formulations without CLA-8 (Appendix V-S21). It has been estimated that CLA-8 and its derived impurity have a similar molar absorptivity at 280 nm (Appendix V-S23, S24). Therefore, based on the AUC percentage at 280 nm, we estimated that in average 1.3, 3.3 and 4.9 % of CLA-8 was modified in the samples receiving 10, 20 and 30 kGy, respectively. A typical dose for sterilization of pharmaceuticals is 25 kGy [203].So at this dose, we might expect around 4% of the CLA-8 derived impurity in CarboCells containing 10% CLA-8. As exemplified in Chapter 4, decreasing the amount of CLA-8 in the formulation can aid in reducing the percentage of related impurities.

Table 11. Effect of the dose of gamma irradiation on drug stability. Percentage of intact drug measured in CarboCells after being subjected to various doses of gamma irradiation. All formulations contained 1.2 mg/g R848 and 8 mg/g RepSox. A percentage of 100.0% indicates that no drug-derived impurities were detected (n=1).

CarboCell formulation	Percentage of intact drugs (%)		
	10 kGy	*20 kGy*	*30 kGy*
CC11	100.0	100.0	100.0
CC16	100.0	100.0	100.0

As previously mentioned, it was noticed that all formulations comprising CLA-8 became bright yellow after being subjected to gamma irradiation (Fig. 42). Moreover, as the radiation dose increased, the CarboCells became more yellow (Appendix V-S22). CLA-8 is a carbohydrate ester containing iodinated benzoate groups. Hence, we hypothesize that gamma irradiation caused the release of iodine from CLA-8 into the CarboCell [216], which consequently caused the yellow coloration of the formulation. Likewise, the impurity derived from CLA-8 may correspond to a less iodinated version of CLA-8.

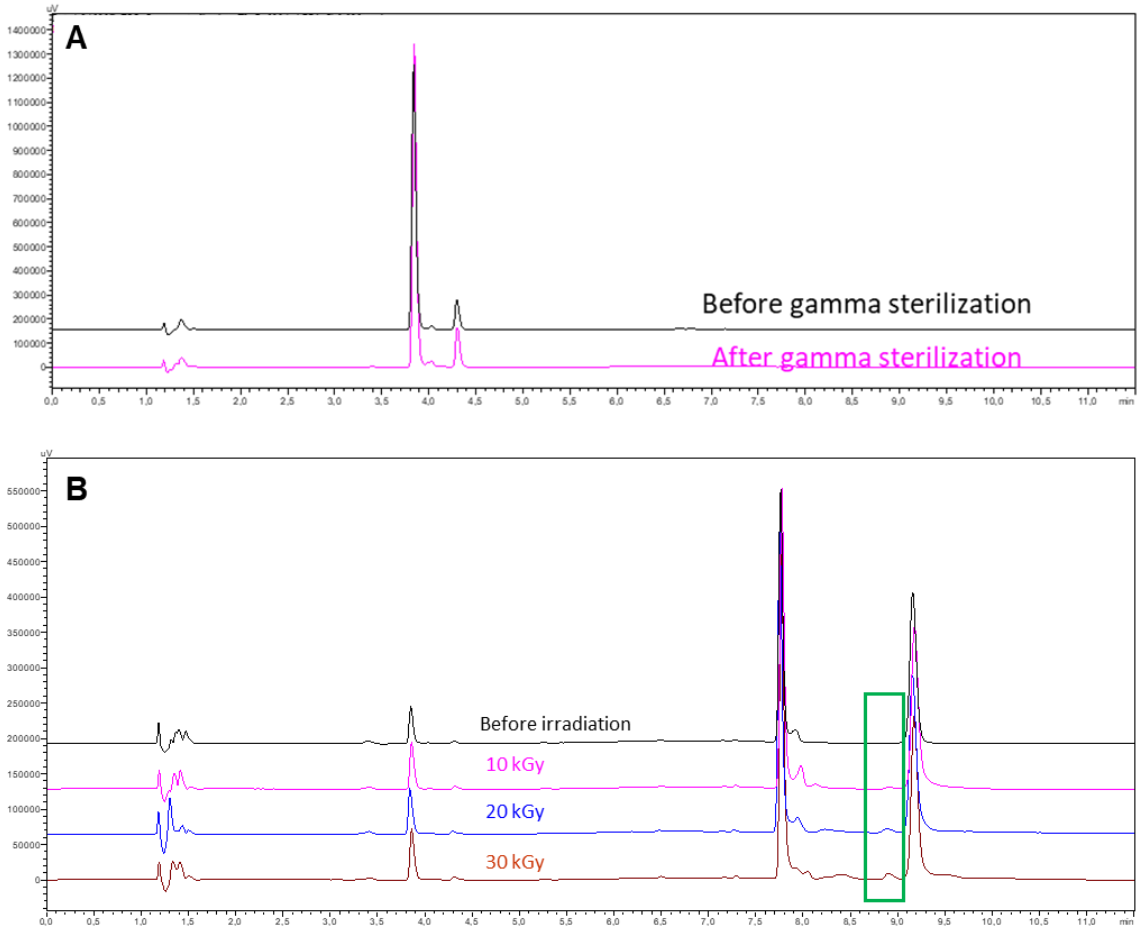

Figure 41. Effect of gamma irradiation on the chemical stability of the drugs and CLA-8. (**A**) Representative chromatogram of all formulations receiving gamma irradiation where drug-derived molecules were not detected. The chromatograms show the peaks corresponding to RepSox (RT= 3.8 min) and R848 (RT=4.3 min) before and after gamma sterilization. (**B**) Chromatogram of formulation CC11 before and after receiving various doses of gamma irradiation. A possible degradation of CLA-8 was observed (RT= 8.9 min, framed in green); octabenzoate and CLA-8 showed a RT of 7.8 min and 9.2 min, respectively. UV detection was done at (**A**) 320 nm and (**B**) 280 nm.

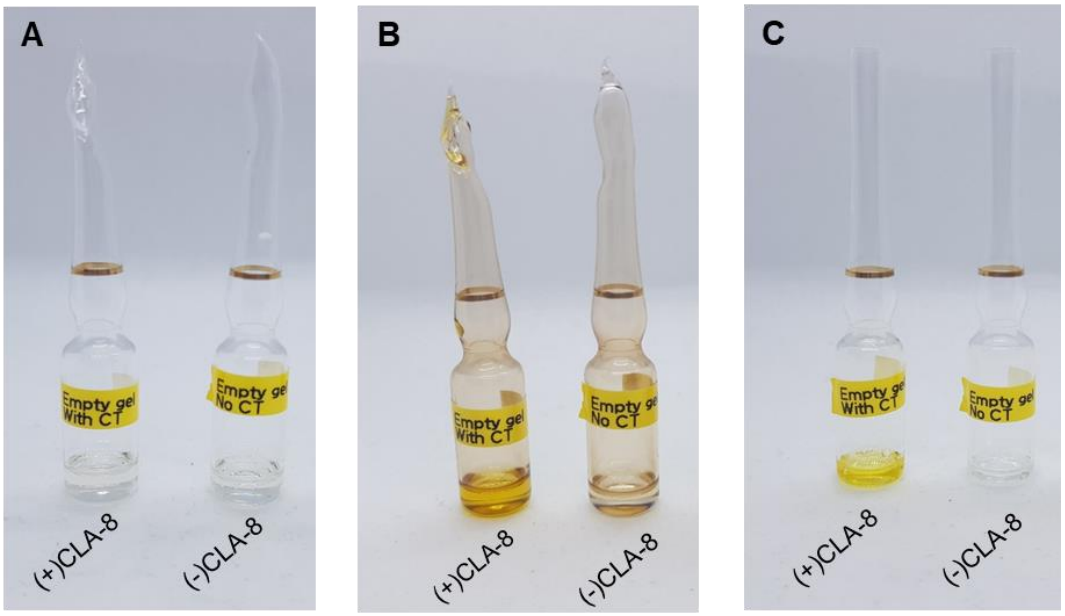

Figure 42. Visual evaluation of CarboCells subjected to gamma irradiation. Glass ampoules containing formulations with (+) and without (-) CLA-8 corresponding to C11 and C17, respectively. Pictures were taken (**A**) before irradiation, (**B**) after irradiation with 30 kGy and (**C**) after transferring the irradiated CarboCells to new ampoules. None of the formulations contained drug molecules.

Furthermore, the glass ampoules containing the CarboCells also experienced a change in color. After being subjected to the radiation, the vials displayed a brownish color (Fig. 42B). It is known that ionizing radiation might cause discoloration and degradation of certain packaging materials [217]–[219]. For instance, a study reported that Type I standard glass was very susceptible to discoloration from gamma irradiation. Cerium oxide (CeO) glass as well as cyclic olefin copolymer (COC) and cyclic olefin polymer (COP) plastic were suggested as alternative materials that better retain their optical clarity [219]. The glass ampoules used in this project are made of Type I standard glass, so using other packaging materials such as CeO glass might be an option for future studies.

Ionizing radiation is capable of creating and breaking bonds, so it has been reported that sterilization via gamma radiation might degrade the cross-linking in drug delivery polymers like hydrogels. In such cases, besides the morphology of the formulation, the drug release profiles may be affected as well [203], [220], [221]. Since the CarboCell platform is not based on polymers, an impact on the performance of the CarboCell is not expected. This is supported by the fact that although minimal degradation of CLA-8 was observed, the SuBen matrix of the CarboCell remained intact. Nonetheless, it would be recommended to measure the viscosity of the irradiated formulation and conduct an *in vitro* release study to verify that the performance of the CarboCell was not affected. Furthermore, to ensure that the CarboCells with CLA-8 remain stable after gamma irradiation, the samples should be stored at either 4°C or -20°C (previously determined as adequate temperatures) and the chemical stability of the drugs and CLA-8 should be monitored as well as the physical appearance of the CarboCell.

5.4 Concluding remarks and future perspectives

CarboCells with multiple compositions were tested to understand their correlation with viscosity, solvent diffusion and drug release. The type of solvent had a great effect on both the viscosity of the CarboCell and the initial burst release. DMSO increased the viscosity of the CarboCell, whereas EtOH decreased it. Conversely, at equal concentrations, the drug burst release was lower when using DMSO instead of EtOH as solvent. Accordingly, incorporating a higher percentage of DMSO in the formulation increased the viscosity of the CarboCells and decreased the burst release. Moreover, EtOH was the solvent released the fastest from the CarboCells, which might had contributed to the higher burst release. Nonetheless, the choice of solvent was not as influential for the long-term release profiles. It was observed that CarboCells with equal compositions, only differing in the solvent, would eventually display the same release profile despite having different burst releases. Regarding the co-solvents, GTO caused a slight increase in the viscosity of the CarboCell and a slower overall drug release from the CarboCell. The latter is likely linked to the increased viscosity and hydrophobicity of the self-formed depot once the solvent diffuses out from the system. In a comparable manner, using σ-SuBen instead of π-SuBen generated more viscous CarboCells that consequently displayed a lower drug release. Hence, we have shown that there are several ways to tailor the drug release profiles of the CarboCell, which exhibits the versatility of the system. Overall, the knowledge obtained in this project will be useful to aid and facilitate future formulation developments for additional drug substances and applications of the CarboCell technology.

It is important to highlight that this set of results were obtained using SuBen-based CarboCells. Therefore, it is uncertain if these observations would be fully translated to other carbohydrate esters. Each carbohydrate ester has unique physico-chemical properties that might contribute differently to the performance of the CarboCell. Therefore, in the future it would be interesting to extend the characterization testing to cover other carbohydrate esters (e.g., LacBen, LOIB, RaBen). Likewise, other drug molecules with different characteristics than R848 might be used as model molecules to expand our understanding on the CarboCell system.

Furthermore, it was observed that the injection volume did not affect the *in vitro* release profile from the CarboCells. Importantly, the *in vivo* burst release was not increased despite increasing the injection volume. Such finding is crucial since a high burst release might induce toxicity. Thus, it is expected that greater injection volumes can be used in larger animal models without compromising the drug release kinetics from the CarboCell.

Regarding the sterilization method, gamma irradiation was better than autoclaving at maintaining the stability of R848 and RepSox in the CarboCells. In the majority of the tested formulations, the drugs remained 100% intact after gamma irradiation. Nonetheless, a drawback of gamma irradiation is that it caused the release of small amounts of iodine from CLA-8 into the CarboCells thereby producing a yellow color in the formulation. Another side effect of gamma irradiation was the discoloration of the glass ampoules. However, this might be prevented by changing the packaging material. In the future, irradiated CarboCells should be monitored for long-term stability in addition to conducting general

characterization studies (e.g., viscosity measurement, in vitro drug release) to further ensure the integrity of the CarboCell.

5.5 Materials and methods

Chemicals

All chemicals were purchased from Sigma Aldrich, Merck unless stated otherwise. Ethanol (absolute), acetonitrile (MeCN) and dimethyl sulfoxide (DMSO) were purchased from VWR Chemicals. R848 was purchased from AmBeed and RepSox from Selleckchem. π-SuBen was purified as indicated in section 2.5. GTH was purchased from TCI. CLA-8 was synthesized as described in Appendix III.

Preparation of CarboCell

CarboCell formulations were prepared by mixing the carbohydrate esters (σ-SuBen, π-SuBen) with the co-solvents (GTO,GTH), solvents (EtOH, PC, DMSO) and contrast agent CLA-8, if applicable. The different compositions are indicated in Tables 6-9, and the corresponding amount of each compound was weighed into one vial. The mixture was placed in an ultrasonication bath at 70-80°C for 1-2 hours and occasionally vortexed to generate homogenous solutions, namely CarboCells, which were stored at 4 °C until further use. Drug molecules were incorporated into the formulation by proportionally adding CarboCell on top of a previously freeze-dried drug aliquot, until reaching the desired drug concentration. CarboCells were subjected to magnetic stirring at 40-50 °C until the drug was completely dissolved. The drug concentration in each CarboCell is stated in each of the results section.

Animal handling

All experimental procedures were approved by the Danish Experimental Animal Inspectorate. All female BALB/c Jrj mice were obtained at 6 weeks of age from Janvier and allowed to acclimatize for one week prior to starting the studies.

UHPLC method

HPLC analyses were done using a Shimadzu Nexera-X UHPLC instrument with a PDA detector. The samples were injected (5 µL for samples in DMSO/MeCN or 40 µL for samples in PBS) onto a Waters Terra BEH C8 column (2.5µm, 4.6x75mm, temperature 25°C) at a flow rate of 0.8 or 1 mL/min (for samples in DMSO/MeCN or in PBS, respectively). The solvent system consisted of mobile phase A (5% MeCN, 0.1% TFA in water) and mobile phase B (0.1% TFA in MeCN). For *in vitro* drug release studies, chromatographic separation was achieved using a gradient of 0 to 100% phase B in 5 min followed by 2.5 min at 100% B. For analysis of samples dissolved in DMSO (i.e., containing CLA-8), the employed gradient was 0 to 100% phase B in 5 min followed by 4 min at 100% B. Ultraviolet detection at 280 nm or 320 nm was used to identify the specified compounds.

Viscosity of CarboCells

Viscosity measurements were done using an EMS-1000 viscometer set at 1000 rpm. The measuring time varied depending on temperature and viscosity range. 1 mL of each tested formulations (without containing drug molecules) were individually pipetted into the instrument´s corresponding glass tube and a 1.2 mm aluminum sphere was placed inside the tube. Viscosities were determined at 25°C and 37°C with measurement times between 10 s and 1 min.

Viscosity as function of solvent release

CarboCells containing the same proportion of different solvents were prepared as indicated in Table 6. 0.5 mL of each formulation were placed inside a glass tube and a 4.7 mm aluminum sphere was added. The samples were incubated at 37°C for 2 h and then 5 mL of PBS were carefully added on top of the CarboCell in each tube. After 24 h 2 mL of PBS were removed and replaced with fresh buffer; afterwards this procedure was repeated every 5-7 days. Viscosity was measured at different time points at 37°C, with measuring times between 10 s and 5 min. Every 2-3 days, 2 mL of PBS were removed and replaced with fresh buffer.

In vitro drug release

Unless otherwise stated, 50 µL of each tested CarboCell were individually injected in 8-mL glass vials containing 2 mL PBS, for which the exact amount of injected CarboCell was weighed. The vials were incubated at 37 °C and at each sampling point 1 mL of PBS was taken. 1 mL of fresh buffer was added immediately to the vial to replace the taken sample. The samples were then analyzed by HPLC (UV detection at 320 nm) and the concentration of drug in the release media was calculated via a standard curve. The cumulative drug release was calculated according to equations 2 and 3.

In vivo drug release

For each CarboCell, 50 µL were injected s.c. in female BALB/c Jrj mice; mice were anesthetized using ~2% isoflurane during injections. At each sampling point, mice were euthanized and the CarboCell depots were collected. Such depots were immediately dissolved in 1 mL MeCN and incubated at room temperature overnight. The samples were then filtered using 0.45-µm pore, nylon syringe filters (Frisenette) and diluted eight times prior analysis. As reference, 10 µL of each CarboCell (non-injected) were dissolved in 1 mL MeCN, as described before. All samples were then analyzed by UHPLC.

The drug release percentage was determined by ratiometric analysis. The AUC values of R848 and RepSox (320 nm) and SuBen (280 nm) were measured to calculate the AUC ratios of drugs/SuBen in all samples. The percentage of released drug was calculated by comparing the AUC ratios in the collected CarboCells versus the corresponding ratios in the reference (non-injected) CarboCell (equation 1).

Effect of autoclaving and gamma irradiation on drug stability

CarboCells were prepared as described in Table 9 containing R848 and RepSox as specified. As time zero samples, approximately 25 µL of each CarboCell were dissolved in 500 µL DMSO. Then 25 µL of the resulting solution were diluted with 475 µL DMSO. Both samples (diluted and non-diluted) were analyzed by UHPLC. Next, around 300 µL of each formulation (in triplicates) were placed in 1 mL, pre-scored glass ampoules (Wheaton) and heat-sealed. To test steam sterilization, samples were placed in an autoclave at 121°C and 15 psi for 15 min. To test gamma irradiation, samples received 10, 20 or 30 kGy as radiation dose, where the process temperature was 25 ± 0.5°C. Gamma irradiation was conducted in a Gammacell using cylindrical ^{60}Co pencils as the radioactivity source as described in [222] and the process was carried out at DTU Center for Nuclear Technologies. After each sterilization process, the CarboCells were dissolved and analyzed following the same procedure as for time zero samples.

Statistical analyses

When required, statistical analyses were performed on GraphPad Prism 9. The correspondingly used statistical test is specified in figure legends. A p-value ≤0.05 was deemed as statistically significant.

Chapter 6.
Hydrophobic ion pairing, a useful formulation tool for the CarboCell

6.1 Background

As highlighted in previous chapters, CarboCell facilitates the easy formulation of water-insoluble drugs, which tends to be challenging particularly for parenteral administration. Hydrophobic drug substances can be simply added to the CarboCell without the need of any chemical modifications. While such feature is advantageous, it also represents an inherent limitation to the type of molecules that can be formulated in the CarboCell system. Hydrophobic ion pairing (HIP) represents an attractive strategy that can allow the incorporation of charged hydrophilic drugs into the CarboCell platform, thereby expanding the functionality and possible applications of the CarboCell. The modification of solubility enabled by HIP has allowed successful encapsulation of multiple hydrophilic drugs into diverse drug delivery systems originally optimized for hydrophobic molecules. Examples of molecules eligible for HIP complexation include peptides, RNA, antibodies, and small charged molecules [223]–[226].

HIP denotes the process of establishing ionic interactions between a charged hydrophilic molecule and a molecule with an opposing charge, referred as co-ion or counterion. A co-ion not only requires an opposite charge to the molecule of interest, but co-ions also need to have at least one hydrophobic domain; for this reason, many of the utilized co-ions in HIP are ionic surfactants [227], [228]. The pairing between the charged hydrophilic molecule and the co-ion can be stoichiometric or non-stoichiometric in terms of molar, mass or charge ratio (Fig. 43). The HIP process results in the formation of an ion pair or HIP complex, which is uncharged and water-insoluble. The increase in hydrophobicity results from masking the intrinsic charge of the molecule and because the hydrophobic moieties of the co-ion cover the original molecule thus excluding water and preventing the solvation of ionic-ionic interaction sites [227].

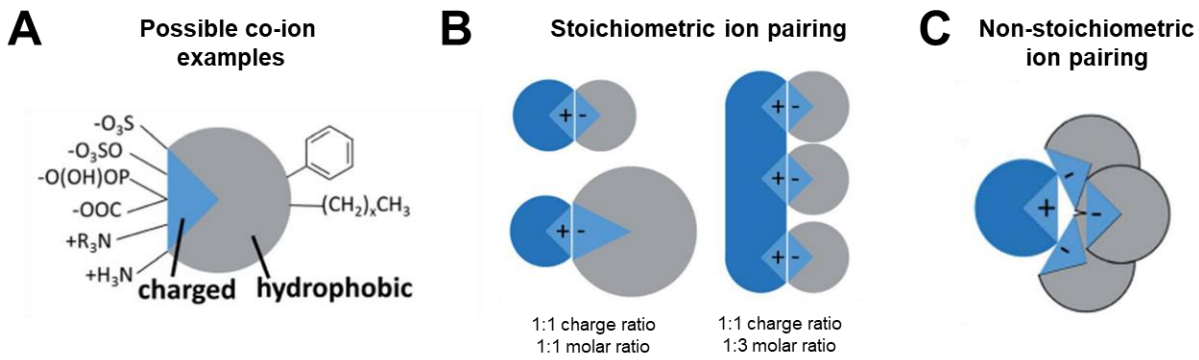

Figure 43. Schematic representation of hydrophobic ion pairing (HIP). (**A**) Examples of possible charged groups and hydrophobic domains present in a co-ion. (**B**) Stoichiometric HIP between a cationic hydrophilic drug molecule (blue) and an anionic co-ion (gray) indicating their charge and molar ratios. (**C**) Non-stoichiometric HIP. (Illustration adapted from [227]).

Importantly, the association between the molecule of interest and the co-ion is temporary and can be reversed. The HIP complex will remain hydrophobic until the involved molecules dissociate [227], [229]. De-complexation is generally driven by the pH or salts present in the surrounding medium. The former can modify the protonation state of the charged species thus promoting de-complexation. Salts can cause a counterion competition, which also leads to de-complexation. Once dissociated, the high ionic strength in the medium makes it difficult for the original species to form a complex again [227].

Solubility can also be modified by adding provisional hydrophobic domains to a hydrophilic drug, as exemplified by prodrug approaches using lipid anchors [230]. However, such strategies require chemical modifications of the covalent bonds in the original drug. From a regulatory perspective, HIP offers an advantage because prodrugs require a full FDA approval, while HIP complexation of already approved drugs might face less strict regulatory requirements [231].

To start exploring the HIP strategy and its possible application in the CarboCell system, we decided to use indocyanine green (ICG) as a surrogate molecule. ICG is a fluorescent dye approved by the FDA for intravenous injection, which is routinely used in the clinic for various surgical and imaging diagnostic methods such as sentinel lymph node mapping [232]. ICG is a symmetric small molecule with amphiphilic character; it is formed by two polycyclic parts (benzoindotricarbocyanin), linked by a carbon chain and that constitute the lipophilic domains of the molecule. Each polycyclic part is also bound to a sulfate group that promotes the solubility of ICG in water (Fig. 44) [233]. ICG is generally available in powder form as a sodium salt and it has an experimental log P value of -0.3 at pH 7.4 [234]. As ICG is a water-soluble anionic molecule, it makes it a suitable candidate for HIP complexation.

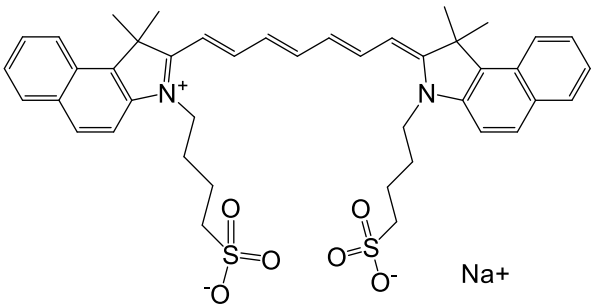

Figure 44. Chemical structure of indocyanine green (ICG), presented as a sodium salt.

Due to the negative charge of ICG, cationic co-ions are required for the HIP complexation. When selecting a co-ion, besides its charge, physico-chemical properties as the hydrophobicity and pK_a need to be considered. Regarding the former, it is normally expected that the higher the log P of a co-ion, the more hydrophobic the HIP complex will be [235]–[237]. In addition to the log P, the chemical structure of the hydrophobic domains in the co-ion play an important role during the complexation process and the release from the delivery vehicle. Steric hindrance and hydrophobic interactions can arise between the hydrophobic groups of the co-ion with (i) one another, (ii) other hydrophobic moieties in the drug of interest, and (iii) the drug delivery system [227], [238]. As previously stated, the co-ions have to be charged to form the HIP complex. Therefore, the pK_a of the co-ion and the pH of the solution are important factors to consider as they dictate the degree of ionization of a molecule [227]. In this project, cationic co-ions with diverse structures and physico-chemical properties were used to investigate HIP complexation with ICG (Table 12).

HIP complexes can be prepared before or after loading of the drug vehicle of interest. There are several techniques to prepare HIP complexes and the selection of the preparation method depends on factors such as the water solubility of the co-ions, the stability of the drug molecule and the type of drug delivery system [227]. Here, we investigated the application of the Bligh-Dyer method. Originally, the Bligh-Dyer method was developed to perform lipid extraction [239]. Nonetheless, such technique has proven to be useful for HIP complexation [240], [241]. Briefly, in the Bligh-Dyer method the HIP complex is produced in a mixture of water, methanol and chloroform, which results in a homogeneous solution. Then, by changing the ratios of the aforementioned components, a biphasic system is obtained comprising a water/methanol phase and a chloroform phase. The unbound compounds stay in the water/methanol phase, while the HIP complexes remain in the organic phase from where they can be isolated. Advantages of the Bligh-Dyer method include ease of preparation, allowing the use of water-insoluble co-ions, robustness towards high concentrations of co-ions and high product yields [240].

Table 12. Co-ions used for HIP complexation with ICG. The pKa, log P and log D values were estimated for each molecule using the ChemAxon® software.

Co-ion	Structure	pK_a	Log P	Log D (pH < 5)
Tetraethyl ammonium bromide (TEAB)	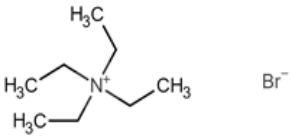	-	-2.6	-
Cetyltrimethyl ammonium bromide (CTAB)	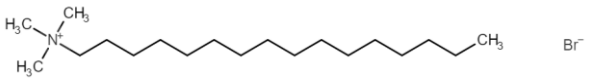	-	2.7	-
Benethamine (BENA)	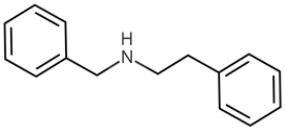	9.6	3.6	0.2
Dodecylamine (DDA)		10.2	4.3	0.3
Tetraoctyl ammonium bromide (TOAB)	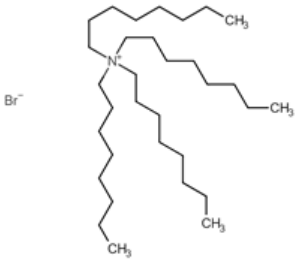	-	8.4	-

6.2 Objectives

In order to investigate hydrophobic ion pairing as a strategy to formulate hydrophilic molecules into the CarboCell system using ICG as a surrogate molecule, the following objectives were established:

- To evaluate the complexation efficiency of ICG with multiple co-ions via the Bligh-Dyer method.
- To assess the solubility of ICG-HIP complexes in the CarboCell
- To investigate the effect of HIP complexation on the stability and fluorescence properties of ICG
- To investigate the *in vitro* release kinetics of ICG as a function of the co-ion used for HIP complexation and the CarboCell formulation
- To conduct *in vivo* testing of one or more CarboCells containing ICG-HIP

6.3 Results and discussion

Screening of co-ions and complexation efficiency

HIP complexation of ICG with various co-ions covering a broad range of physico-chemical properties was investigated via the Bligh-Dyer method and qualitatively evaluated by visual inspection. The tests were initially performed using a 1:1 charge ratio; since ICG has two negative sulfonate groups, two positive co-ion molecules per ICG were added. Additionally, ICG was dissolved in either 0.01 M HCl or plain MQ to evaluate the effect of pH on HIP complexation.

The expected biphasic system resulting from the Bligh-Dyer method can be observed in Fig. 45A. ICG was efficiently complexed when using CTAB, BENA, DDA and TOAB as co-ions. The light green or colorless upper phase indicated that most of the ICG was present in the organic phase. In contrast, there was a noticeably higher amount of ICG in the water/methanol phase when using TEAB as co-ion, being almost the same as the control. TEAB is the least hydrophobic of the tested co-ions, which might explain its low complexation efficiency. In accordance with another study, it was reported that tetrabutylammonium bromide was not an effective co-ion for HIP complexation due to its short alkyl chains [238].

Moreover, pH did not have a visible effect on the complexation efficiency when using quaternary amines as co-ions. This result was expected since sulfonate anions and quaternary amines are permanently charged in aqueous media regardless of the pH. In the case of BENA and DDA, the complexation efficacy was noticeably decreased when ICG was dissolved in sole water rather than in 0.01 M HCl (Appendix VI-S25). When dissolved in water, BENA and DDA produce solutions with a pH around 9-10, which is very close to their pK_a values (9.6 and 10.2, respectively). Therefore, the addition of HCl lowers the pH and the majority of the co-ions become positively charged thereby increasing the complexation efficiency.

Next, the ICG-HIP complexes were isolated by recovering the organic phase and drying the chloroform under a gentle flow of nitrogen. Free ICG and ICG-HIP complexes were incorporated into a CarboCell to evaluate their solubility. CarboCells were formulated with approximately equal concentrations of ICG (2.5 mg/g) either as a HIP complex or in native form. All ICG-HIP complexes regardless of the co-ion were readily solubilized in the CarboCell resulting in bright green solutions with no visible particles (Fig. 45B, Appendix VI-S26). In contrast, free ICG was poorly dissolved in the CarboCell, which looked opaque and contained plenty of undissolved particles. These results indicate that the hydrophobicity of ICG was substantially increased due to HIP complexation.

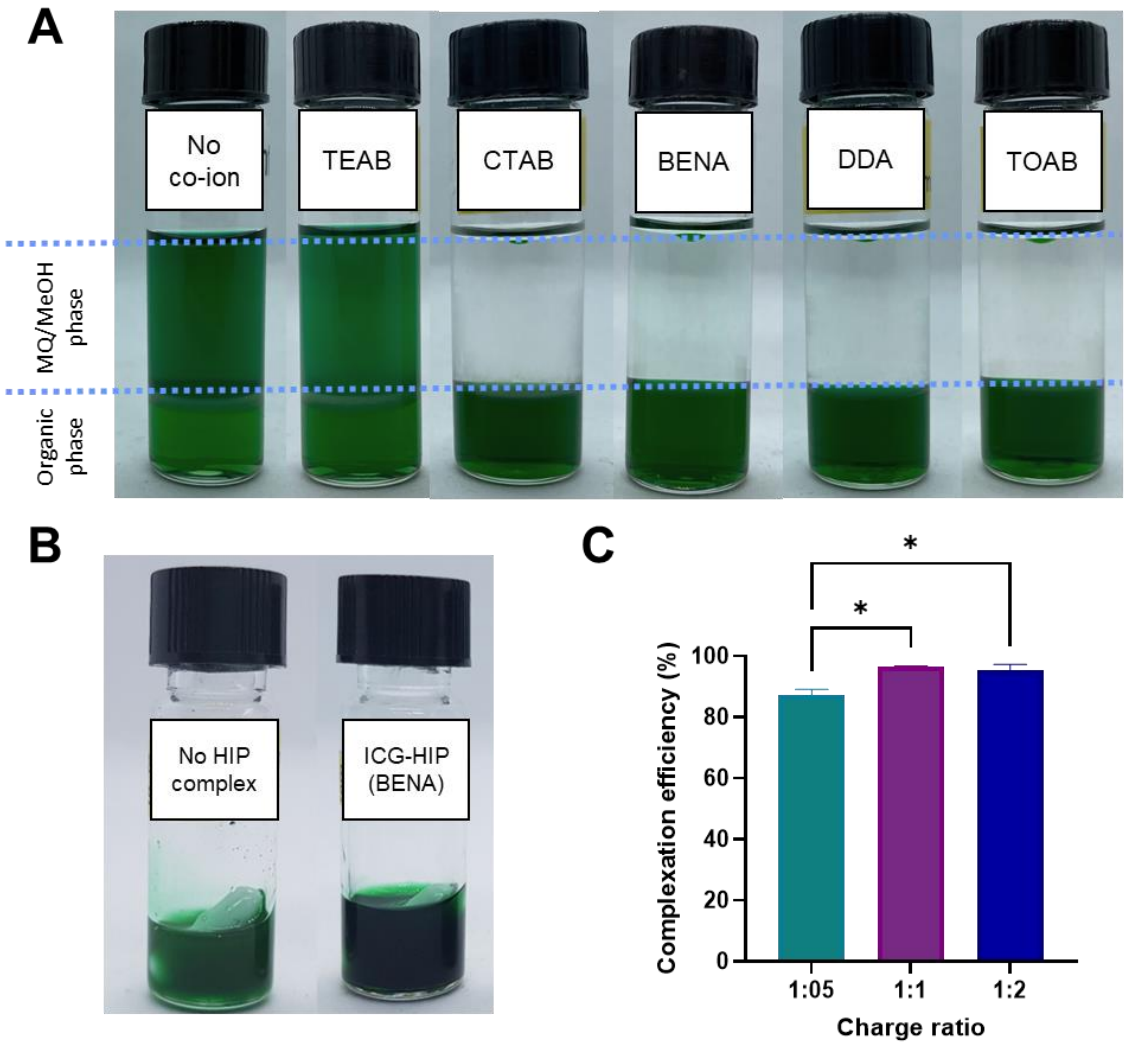

Figure 45. Screening of co-ions and HIP complexation efficiency. (**A**) HIP complexation of ICG with multiple co-ions; the ICG-HIP complex is solubilized in the organic phase, while the non-complexed ICG stays in the MQ/MeOH phase. (**B**) Comparison between a CarboCell (CC3, described in Table 13) containing < 2.5 mg/mL free ICG (left) and 2.5 mg/mL ICG-HIP complex (right). (**C**) Complexation efficiency of ICG with BENA at different charge ratios. Data is presented as mean ± SEM (n=3); the statistical analysis corresponds to a one-way ANOVA with Tukey multiple comparisons (* $p \leq 0.05$).

Then, complexation efficiency as a function of charge ratio was investigated using BENA as model co-ion. HIP complexation was done in charge ratios of 1:0.5, 1:1 and 1:2 (ICG:co-ion). The concentration of ICG in the organic phase was quantified by UHPLC to calculate the complexation percentage. At charge ratios of 1:1 and 1:2, the HIP complexation efficiency was around 95%. Complexation efficiency dropped to approximately 87% at a charge ratio of 1:0.5 (Fig. 45C). Subsequent HIP complexation studies with different charge ratios using the remaining co-ions (CTAB, TEAB, DDA, TOAB) displayed the same trends as ICG-BENA (Appendix VI-S27). In general, lower complexation efficiencies are expected when decreasing charge or molar ratios [227], [240]. Although the complexation decreased by less than 10%, a reduction on the charge ratio is generally associated

with a decrease in the log P of the HIP complex [240]. Thus, charge ratios can be an alternative way to modulate the hydrophobicity of the resulting HIP complex.

Several studies have reported a reduced complexation efficacy in the presence of excess co-ions, especially when using methods involving solely water [242]–[244]. In such methods, the co-ions and the drug molecules are mixed in water where they interact to form a HIP complex, which are later isolated after centrifugation of the solution. However, an excess of co-ions promotes the formation of micelles, thus there are less co-ions available to associate with the drug molecule. It has been suggested that techniques involving multiple solvents, like the Bligh-Dyer method, increase the critical micelle concentration (CMC) and hinder the formation of micelles thereby displaying consistent complexation efficiencies even at higher charge ratios [240], [245], [246].

Stability of free ICG and ICG-HIP complexes

ICG both as a free molecule and in a HIP complex was incubated in different solvents to investigate its stability. Drug stability was monitored by UHPLC. First, native ICG was dissolved in water, DMSO and EtOH and subsequently stored at room temperature and protected from light. After 7 days, extensive degradation of ICG in water was observed in the chromatogram at 780 nm, where the peak corresponding to ICG almost disappeared. The stability of ICG was substantially higher in DMSO and EtOH since the ICG peak is clearly visible after 7 days and the AUC only decreased by around 10% (Fig. 46).

Overall, ICG is a very sensitive molecule that degrades upon exposure to light, high temperature and in various solvents [247], [248]. Instability of ICG in aqueous solutions has been widely reported in literature [248]–[251]. For instance, when stored at 37°C, ICG remains stable only for 5 h [249]. Aggregation, irreversible degradation and decreased fluorescence are some of the changes experienced by ICG in aqueous media [250]. This represented a challenge for the analysis of ICG concentrations in studies as *in vitro* drug release, which will be further described later in the text. To verify that ICG-HIP complexes would be stable if dissolved in MeCN, HIP complexes of ICG with all the co-ions were prepared, dissolved in MeCN and stored at room temperature. No changes in AUC were observed after 24 h for any ICG-HIP complex, indicating that the ICG-HIP complexes were stable (Appendix VI-S28).

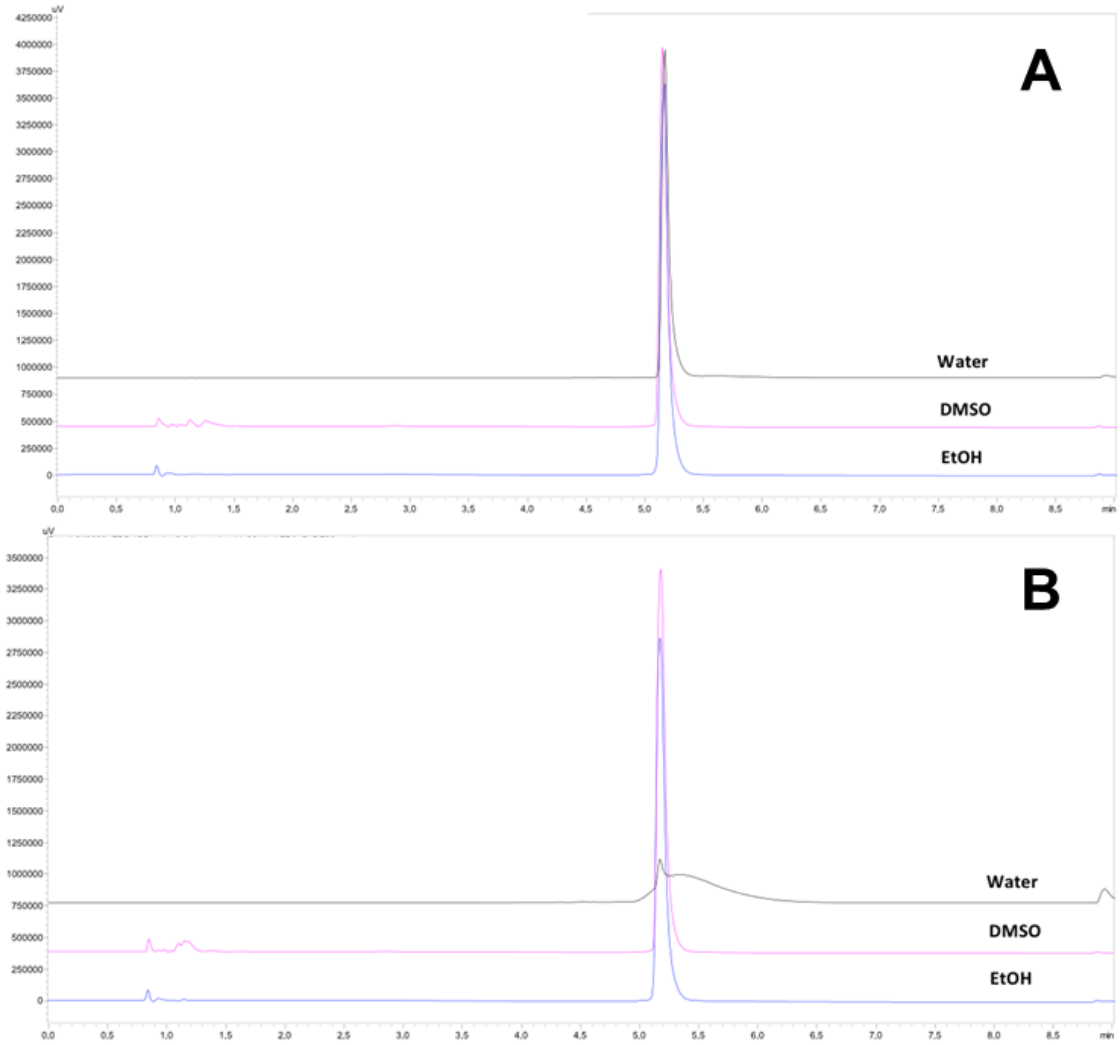

Figure 46. Stability of free ICG in various solvents. Chromatograms comparison of free ICG dissolved at a concentration of 40 µg/mL in water, DMSO and EtOH (**A**) 30 min after preparation and (**B**) after 7 days of incubation at room temperature protected from light. The chromatograms were recorded at 780 nm and ICG has a retention time of 5.2 min.

Assuming that all co-ions display similar stability, ICG-BENA was incubated in various solvents to evaluate if there was a difference with native ICG and to select the most adequate solvent for the stability of ICG-HIP in the CarboCell. The tested solvents were DMSO, EtOH, PC, acetone and BenOH. The target concentration of complexed ICG was 0.25 mg/mL, which was achieved for all the solvents except for acetone, in which ICG-BENA was only partially soluble. After 5 days at room temperature, the ICG peak retained its shape and there were no apparent changes in the AUC of ICG in DMSO, EtOH and PC. In constrast, ICG was visibly degraded following incubation of ICG-BENA in BenOH (Fig. 47). Comparable results were also observed when storing the samples at 37°C (Appendix VI-S29). Excluding BenOH, the ICG-BENA complex might be stable in the tested solvents due to their lower dielectric constant compared to water. As the dielectric constant decreases, the force holding ions together is increased, allowing the HIP complex to remain associated [227], [252]. A possible explanation for the ICG instability in BenOH might be the presence of impurities. It has been reported that commercial BenOH is exposed to the atmosphere, an oxidation process occurs resulting in the formation of benzaldehyde, benzaldehyde dibenzyl acetal and water [253]. Although these impurities

are usually present at trace levels, they might be affecting the stability of ICG. In fact, sole BenOH was analyzed by UHPLC and multiple peaks were detected at 210 nm, a wavelength where BenOH-derived impurities are visible (Appendix VI-S30). To confirm this hypothesis, the study would need to be repeated using a newly opened BenOH bottle.

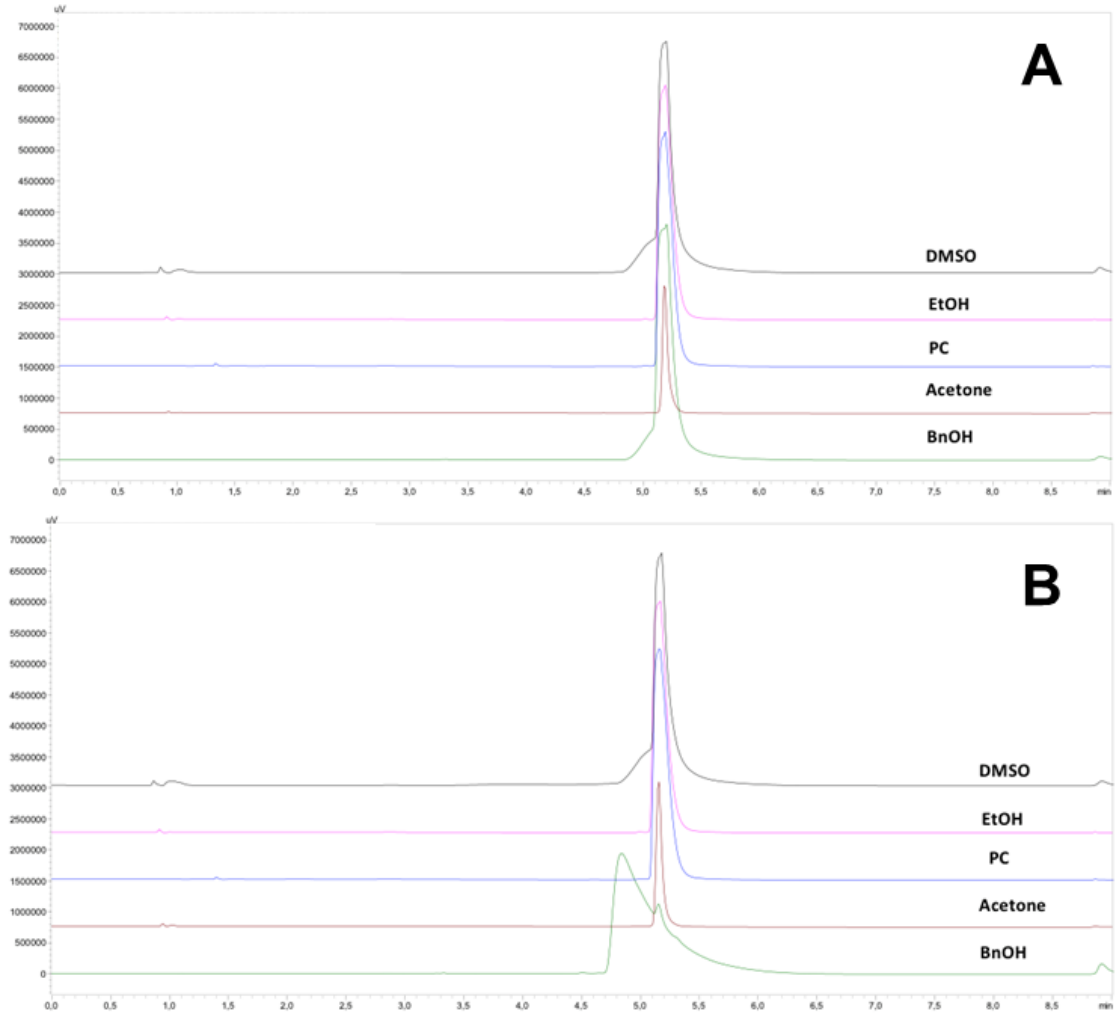

Figure 47. Stability of ICG in a HIP complex with BENA in various solvents. Chromatograms comparison of ICG-BENA dissolved at a concentration of 250 µg/mL in multiple solvents (**A**) 30 min after preparation and (**B**) after 5 days of incubation at room temperature protected from light. The chromatograms were recorded at 780 nm.

Effect of HIP complexation on the fluorescence of ICG

Next, the effect of HIP complexation on the fluorescence properties of ICG was evaluated. For this purpose, free ICG and ICG-HIP complexes with the different co-ions were dissolved in EtOH, a solvent in which ICG is stable, and their excitation and emission scans were recorded. TEAB was excluded from this and subsequent experiments due to its low complexation efficiency. In addition, serial concentrations of ICG both free and complexed were done to evaluate the self-quenching effect.

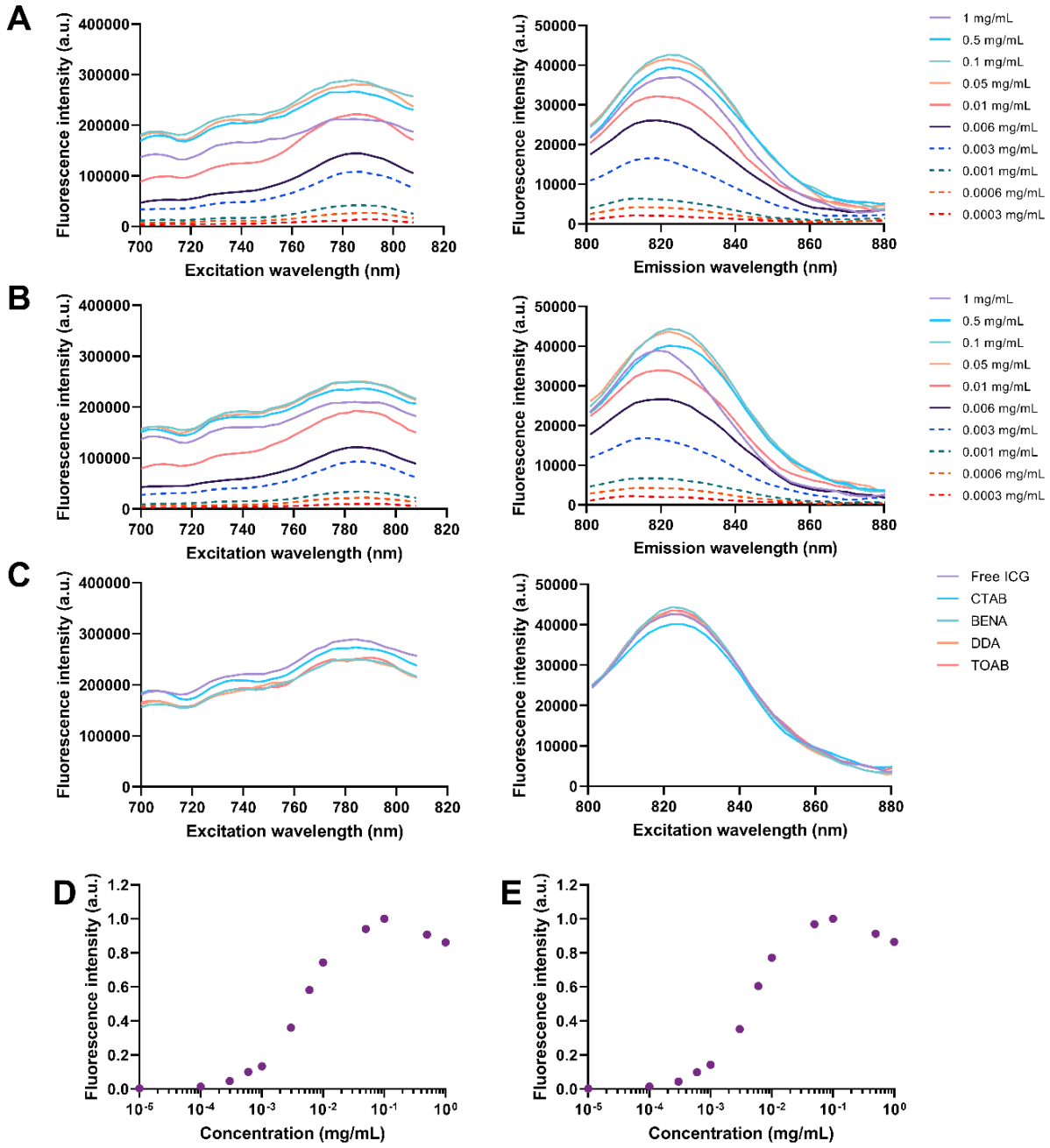

Figure 48. Fluorescence of ICG as a free molecule and in HIP complexes. (**A-B**) Fluorescence excitation and emission spectra of (**A**) free ICG and (**B**) ICG-BENA at varying concentrations. (**C**) Fluorescence excitation and emission spectra of ICG as a free molecule and in a HIP complex with various co-ions at a concentration of 0.1 mg/mL. (**D-E**) Fluorescence intensity of (**D**) free ICG and (**E**) ICG-BENA as a function of concentration. All solutions had EtOH as solvent and the fluorescence spectra of the rest of the ICG-HIP complexes can be found in Appendix VI-S31.

It was observed that the emission intensity of ICG, whether in the native form or in a HIP complex, gradually increased until reaching a concentration of 0.1 mg/mL. At this concentration, the excitation maxima was 785 nm, whereas the emission maxima was 822 nm. Above 0.1 mg/mL, the fluorescence intensity started decreasing as a consequence of ICG self-quenching (Fig. 48A,B). This was an expected phenomenon since quenching of ICG has been reported above 0.1 – 0.5 mg/mL ICG in plasma [254], [255]. Interestingly, the native ICG and ICG-HIP complexes showed the same excitation and emission spectra at concentrations below the self-quenching threshold (Fig. 48C, Appendix VI-S32). As further showed in Fig. 48D and 48E, using ICG-BENA as an example, there is no apparent effect of HIP complexation in the fluorescence intensity of ICG. If ICG-HIP were to be included in the CarboCell as a fluorescent marker, any co-ion could be used for the HIP complexation without any effect on the fluorescence properties of ICG.

In vitro burst release and drug release kinetics of ICG-HIP complexes

To investigate if different co-ions would have an effect on the burst release of ICG, ICG was complexed with either BENA or TOAB and formulated in CarboCells comprising various components and ratios (Table 13). Each CarboCell had a concentration of 0.1 mg/g ICG. The concentration of ICG in the release media (PBS) was measured by UHPLC 2.5 h after injection.

It was observed that the burst release depended on both the CarboCell formulation and the co-ion in the HIP complex (Table 13). Regarding the former, irrespective of the used co-ion, the sequence of percentage ICG released was CC1 > CC2 > CC3 > CC4. Interestingly, ICG-BENA could not be fully solubilized in CC1, in contrast with ICG-TOAB that was easily dissolved in such CarboCell. ICG was not detected in the release media from neither CC4 formulations. This is in line with previous observations on the effect of Et-Pal in drastically reducing drug release (Chapter 4). When comparing the burst release between ICG-BENA and ICG-TOAB, it appeared that slightly more ICG was released when using BENA as co-ion.

Table 13. In vitro burst release of ICG-HIP complexes. Percentage of ICG released 2.5 h post-injection in PBS of ICG-BENA and ICG-TOAB from different CarboCell formulations. Data is presented as mean ± SD (n=3). Note that ICG-BENA could not be dissolved in CC1. If ICG was not detected in the release media, this was reported as 0.0. The concentration of ICG in the CarboCells was 0.1 mg/g.

CarboCell	Composition (w/w%)	ICG released (%)	
		BENA	*TOAB*
CC1	LOIB:GTO:EtOH (82.5:7.5:10)	-	10.4 ± 0.4
CC2	SuBen:GTH:DMSO (60:20:20)	5.9 ± 0.6	3.0 ± 1.0
CC3	SuBen:GTO:EtOH (60:25:15)	3.3 ± 0.5	2.7 ± 0.3
CC4	SuBen:Et-Pal:EtOH (62.5:22.5:15)	0.0	0.0

Next, the effect of the co-ions and the concentration of ICG-HIP in the CarboCell on the ICG release profile over 14 days was studied. For this purpose, ICG was complexed with BENA or TOAB and then incorporated into CC2 with a final ICG concentration of 0.1 or 2.5 mg/g. Additionally, two different

concentrations of ICG in the Bligh-Dyer method were tested to investigate if such variable would have an effect on the ICG-HIP solubility or its release kinetics (Table 14). Due to the quick degradation of ICG in aqueous media, the percentage of released ICG was calculated based on the fraction of ICG left in the injected depot via ratiometric analysis.

Table 14. Experiment design to investigate the in vitro release kinetics of ICG-HIP complexes. ICG was complexed with either BENA or TOAB. All HIP complexes were formulated in CC2.

Formulation ID	ICG conc. for complexation	Co-ion	ICG conc. in CarboCell
A	5 mg/mL	BENA	0.1 mg/mL
B	5 mg/mL	TOAB	2.5 mg/mL
C	2.5 mg/mL	BENA	2.5 mg/mL
D	2.5 mg/mL	TOAB	0.1 mg/mL

It was found that both the co-ion and the ICG-HIP concentration influenced the release kinetics of ICG (Fig. 49A, B). At equal ICG concentrations, the release of ICG was faster when using BENA as complexation co-ion. Overall, more ICG was released when complexed with BENA rather than with TOAB. Importantly, the release of ICG was reduced for both types of co-ions when increasing the concentration of ICG-HIP in the CarboCell. For instance, the percentage of ICG released from CarboCells with ICG-BENA decreased by around 4-fold when increasing the concentration from 0.1 to 2.5 mg/g. At the latter concentration, the release of ICG was completely abolished from CarboCells containing ICG-TOAB. Moreover, the chromatograms did not show signs of ICG degradation in the injected depots, suggesting that the CarboCell protects ICG and enhances its stability.

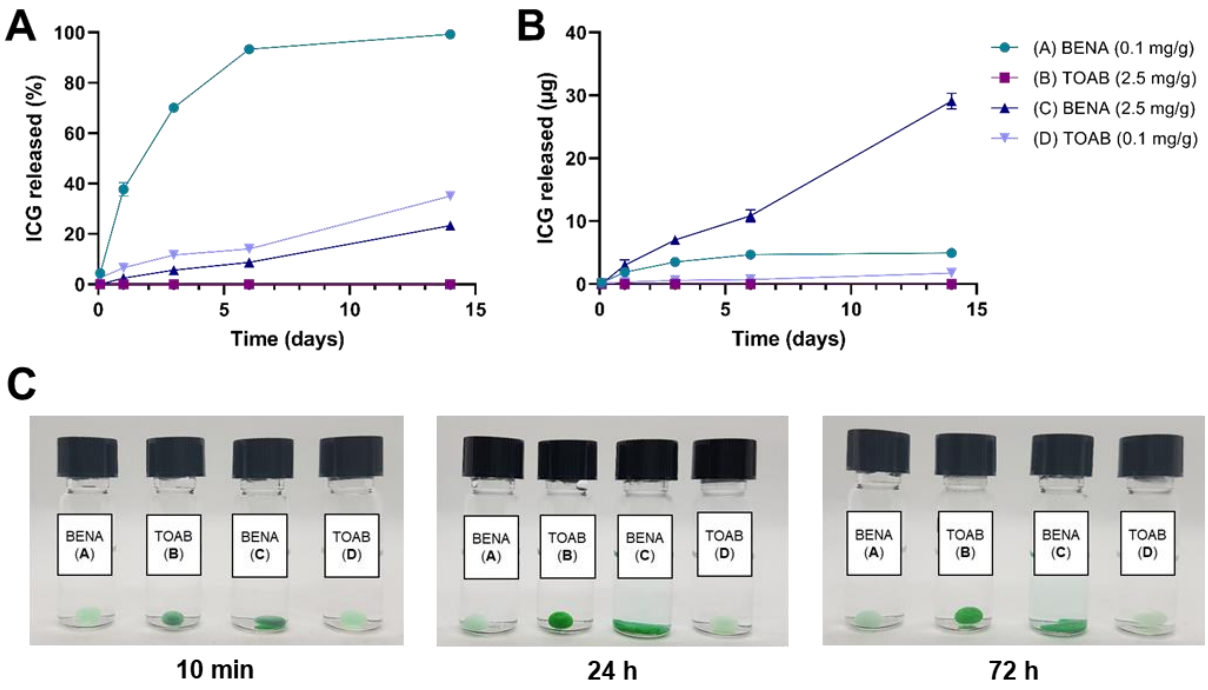

Figure 49. In vitro release of ICG when complexed with BENA or TOAB. (**A**) Percentage and (**B**) total amount of ICG released from CC2 after injection in PBS and incubation at 37 °C. (**C**) Self-formed depots of the tested CarboCells 10 min, 24 h and 72 h after injection. Refer to table 14 for the details of each formulation.

Interestingly, in the case of ICG-BENA, the concentration of the ICG-HIP complex also affected the morphology of the injected depot. It was noticed that the CarboCell depot flattened over time at a concentration of 2.5 mg/g, whereas such phenomenon did not occur at the lower concentration (Fig. 49C). The depot-flattening phenomenon had also been observed in other CarboCell formulations containing ICG-HIP complexes also at 2.5 mg/g (Appendix VI-S33). Furthermore, there was no apparent effect caused by the different concentrations of ICG used during the complexation method.

As described in Chapter 3, drug release from the CarboCell is influenced by the hydrophobicity of the drug, where more hydrophobic drug molecules are released more slowly. BENA and TOAB possess different log P values (3.6 and 8.4, respectively), with TOAB being the most hydrophobic co-ion. Although the log P of the ICG-HIP complexes is unknown, it is generally expected that the higher the log P of the co-ion, the higher the log P of the HIP complex [235], [236]. Therefore, if ICG-TOAB were more hydrophobic than ICG-BENA, then the former would be retained longer in the CarboCell scaffold thereby reducing the ICG release. Several studies have also reported that release from the delivery vehicle usually is reduced, as the log P of the co-ion increases [237], [256], [257].

However, it is unclear if ICG is being released as a complex or as a free molecule. The difference in release rates by different co-ions might alternatively be explained by the de-complexation of ICG-HIP. Generally, a HIP complex behaves as a hydrophobic molecule until it is exposed to salts or a pH that promote the dissociation of the complex [227]. Besides the solvent diffusing out of the CarboCell scaffold, previously we have shown that water pores form in the CarboCell depot once injected in PBS (Fig. 24). As PBS comes into contact with the HIP complexes in CarboCell, the ICG-HIP complex might dissociate both due to the high dielectric constant of water and the salts present in the buffer and. Although PBS has a pH of 7.4, it is expected that the majority of the BENA molecules (pK_a: 9.6) remain ionized. Unlike TOAB, BENA has smaller and less hydrophobic domains than TOAB, which may not be as efficient excluding salts and water from the ionic interactions in the complex. Therefore, ICG-BENA might be more prone to de-complexation once exposed to PBS. Once de-complexed, ICG can be more easily released from the CarboCell. In a future study, the release of ICG-HIP in release media with different salt concentrations could be studied to understand the role of ionic strength on the release kinetics of HIP complexes.

Unlike previous studies with other drugs namely R848 (Chapter 4), the concentration of ICG-HIP had a clear effect on the release profile of ICG. In the case of ICG-BENA, a correlation between decreased ICG release and depot flattening could be observed. Such depot flattening was likely a result from a decrease in the surface tension of CarboCell. At an increased concentration, there was a higher amount not only of ICG but also of the corresponding co-ion. The co-ions as surfactants have the ability to lower surface tension [258]. As a higher amount of BENA molecules could migrate to the surface of the CarboCell, the surface tension was lowered thereby causing the depot flattening. The CarboCell depot containing ICG-TOAB retained its shape throughout the study despite the increase on concentration. This difference might be explained by the chemical structure of the co-ions. It is evident that TOAB has a bulkier structure than BENA since the charged amine in TOAB is surrounded by four long alkyl chains (Table 12). The bulkiness of the TOAB molecule might difficult its arranging and interaction with water

molecules in the surface of the CarboCell; thus, TOAB was not as effective as BENA in reducing the surface tension. Moreover, the co-ions on the CarboCell surface probably act as a barrier that hampers the release of ICG, where TOAB restricts the diffusion of ICG due to its greater size/bulkiness than BENA [238], [256], [259].

Fluorescence of ICG-BENA in CarboCell

Due to the promising results formulating ICG-HIP in CarboCells, it was decided to explore the application of ICG to enhance the visibility of CarboCell. This way the CarboCell may be used as a localization marker for applications such as NIR fluorescence image-guided surgery and if ICG is released, then it may be useful for sentinel lymph node mapping. The highest ICG fluorescence intensity is desired to obtain the best visualization of the CarboCell after being injected. Thus, CarboCells containing serial concentrations of ICG-BENA were prepared to evaluate the fluorescence properties of ICG by recording their fluorescence spectra and by NIR fluorescence imaging of the formulations. BENA was chosen as a model co-ion since it showed a wider variety of release profiles than TOAB.

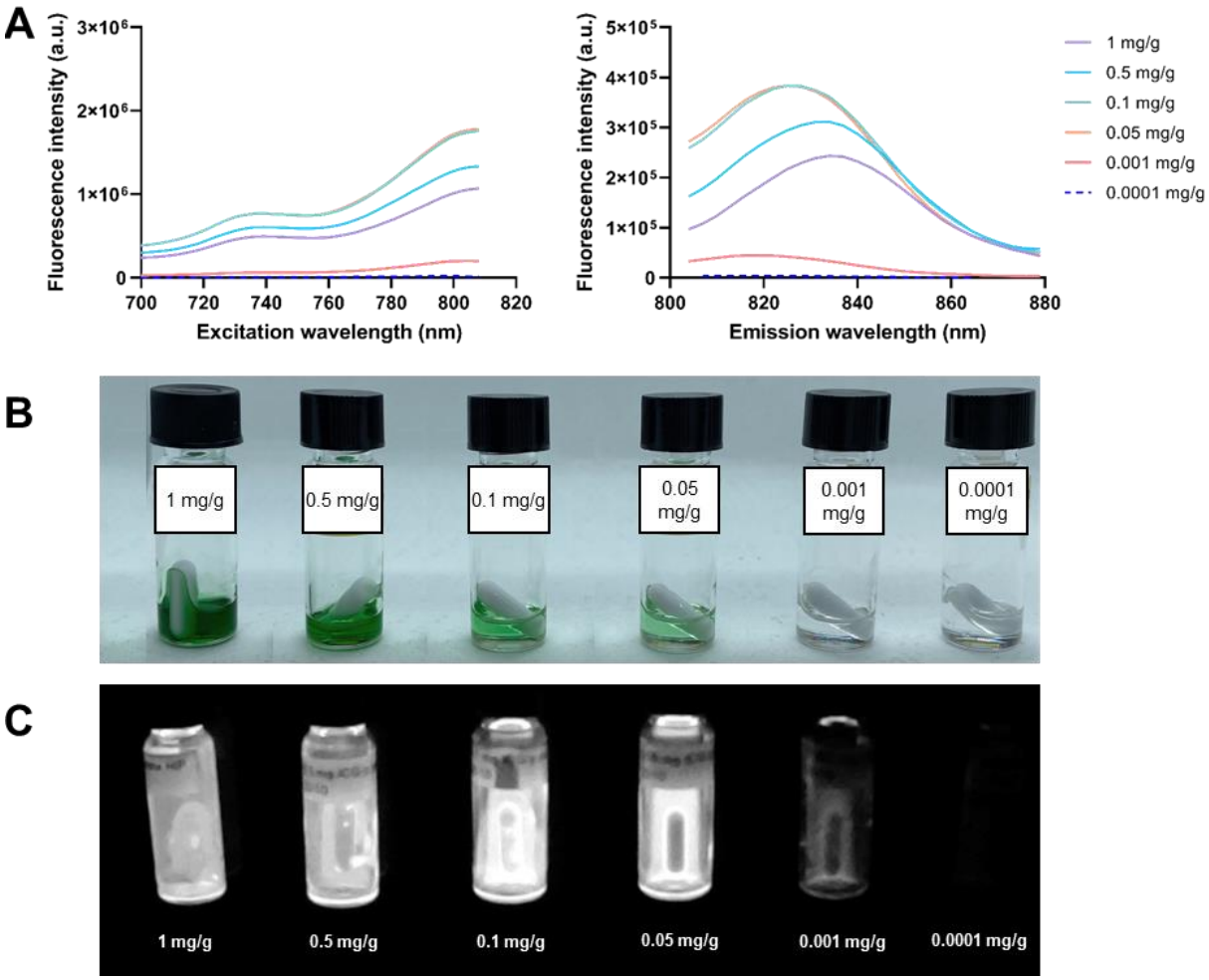

Figure 50. Fluorescence of ICG-BENA in a CarboCell. (**A**) Fluorescence and emission spectra of ICG-BENA in CC3 at varying concentrations. (**B**) Color and (**C**) NIR fluorescence images of ICG-BENA at various concentrations in CC3 when contained in glass vials.

Self-quenching of ICG occurred at the concentrations above 0.1 mg/g, resembling the observations from the earlier fluorescence study. The highest fluorescence intensity was obtained at 0.05 and 0.1 mg/g ICG-BENA (Fig. 50A). At these concentrations, the emission maxima was obtained at 825 nm, which is slightly higher than the emission maxima observed for ICG in EtOH. Such shift was not surprising since it is known that fluorescence can be affected by the solvent and environment surrounding the fluorophore [260]. As expected, the CarboCells containing 0.05 and 0.1 mg/g ICG-BENA displayed the best visibility via NIR imaging. A reduced fluorescence intensity was observed from the 0.5 and 1 mg/g ICG-BENA formulations, while the lowest concentrations showed a very low or non-existent signal (Fig. 50B, C). Therefore, it was decided to use 0.1 mg/g as the ICG-BENA concentration for the subsequent *in vivo* evaluation.

In vivo evaluation of ICG-BENA in CarboCells.

The in vivo studies were conducted using two CarboCell formulations, CC3 and CC4, which had shown different ICG release kinetics as per the previous in vitro release experiments. CC3 was injected into the right and left paw of a rat, while CC4 was injected into a single paw and deep into the thigh of a separate rat. CarboCells were visualized immediately after injection and 20 h post-injection using an in-house built NIR camera.

Both CarboCells were clearly visible and displayed a high NIR intensity after injection (Fig. 51A). After 20 h, it was found that CC3 had released ICG, which had migrated to the local draining lymph nodes (Fig. 51B). In the case of CC4, there was no signal of ICG in the local draining lymph nodes 20 h post-injection, not even after retracting the overlaying muscles. Instead, a high fluorescence intensity was only observed at the sites were CC4 was injected (Fig. 51C). These results were in agreement with the observations from the previous *in vitro* release experiments, where ICG was released from CC3 but not from CC4. Nonetheless, monitoring of additional time points are required to further examine the *in vivo* release kinetics of ICG and determine the period in which ICG remains visible at both the lymph nodes and in the injected depot.

Interestingly, when performing surgery on the rat receiving CC4, it was noticed that the CC4 depot had solidified (Fig. 51D). This is probably an effect of using Et-Pal as co-solvent. Thus, CC4 containing ICG-HIP at a concentration of 0.1 mg/g might be a potential palpable marker for NIR fluorescence image guided surgery [133].

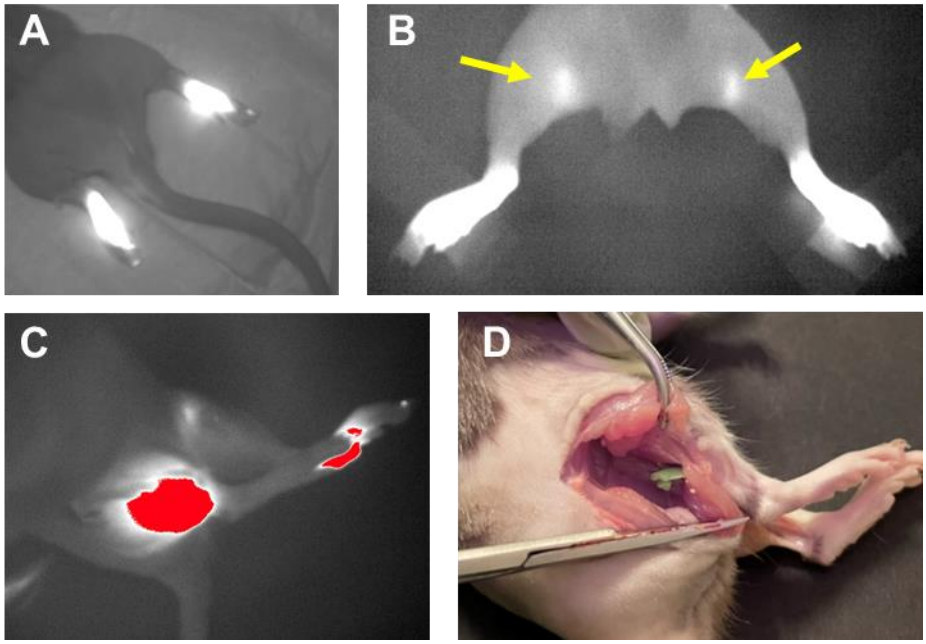

Figure 51. In vivo evaluation of CarboCells containing ICG-BENA. NIR fluorescence images of ICG-BENA in CC3 (**A**) immediately after injection in the rat's paws and (**B**) 20 h post-injection, where the yellow arrows point to the local draining lymph nodes. (**C**) NIR fluorescence image of the sites where CC4 containing ICG-BENA was injected (right thigh and left paw) taken 20 h post-injection; ICG was not visible in the local draining lymph nodes. (**D**) Image of the solidified depot of CC4.

6.4 Concluding remarks and future perspectives

HIP complexation represents a useful technique for the temporal modification of the solubility of a charged hydrophilic molecule. In this project, the Bligh-Dyer method was successfully applied to form HIP complexes of ICG with BENA, CTAB, TOAB and DDA. Using the aforementioned co-ions, the complexation efficiency was close to 100% at charge ratios of 1:1 and 1:2. Due to HIP complexation, the solubility of ICG in the CarboCell system was considerably increased. HIP via the Bligh-Dyer method might be applied to variety of ionizable molecules including proteins and peptides, which expands the amount and type of drug substances than can be formulated in the CarboCell platform. In the context of cancer treatment, HIP may enable the CarboCell to locally deliver molecules such as chemokines (proteins), peptide antigens and chemotherapeutics as doxorubicin (a cationic small molecule) [261], [262].

The Bligh-Dyer method proved to be an easy, efficient, scalable and robust technique for HIP complexation. Nevertheless, a potential drawback of the Bligh-Dyer method is the use of toxic solvents particularly chloroform. A prospective alternative has been reported in which methanol and chloroform were substituted with ethyl acetate and ethanol [263]. Such method should be evaluated in the future to investigate if similar results can be obtained using less toxic solvents.

Moreover, the release rate could be modulated depending on the CarboCell composition and the hydrophobicity of the co-ion, where a more hydrophobic co-ion (TOAB) caused a slower release from the CarboCell. However, it was not certain if ICG was released as a free molecule or as a HIP complex. Measuring the concentration of co-ions in the release media over time as well as in the injected depot

might help elucidate the release mechanism of HIP complexes from CarboCell. Also, using a more chemically stable molecule as model may facilitate the analysis.

Furthermore, it was found that a high concentration of co-ions and alternatively bulky co-ion molecules could also act as a barrier that decreases or abolishes drug diffusion out of the system. If using CarboCell solely as a localization marker, the retention of dyes or contrast agents might be beneficial to ensure a constant and enhanced visualization of the CarboCell scaffold. A high concentration of co-ions also lowered the surface tension *in vitro*, though it is unclear if such effect would be also observed after *in vivo* injections.

Interestingly, the fluorescence properties of ICG were not altered after HIP complexation. The expected self-quenching effect was observed and the highest fluorescence intensity of ICG-HIP was obtained at an ICG concentration of 0.05 – 1 mg/g both in EtOH and in a CarboCell. CarboCells in combination with ICG-HIP could be formulated to either retain or release ICG after injection *in vivo*. In particular, ICG-BENA in CC4 showed potential as a palpable marker for NIR image-guided surgery. For this purpose, long-term stability of ICG in the CarboCell would also need to be evaluated in the future.

6.5 Experimental section

Chemicals

Chemicals were purchased from Sigma Aldrich, Merck unless stated otherwise. EtOH (absolute), MeCN, MeOH, DMSO and chloroform were purchased from VWR Chemicals. LOIB and BENA were obtained from Carbosynth. BenOH was purchased from Fisher Scientific.

HIP via Bligh-Dyer method

ICG was dissolved in a 0.01 M HCl solution to a concentration of 2.5 mg/mL, unless otherwise stated. Each co-ion (BENA, DDA, CTAB, TEAB or TOAB) was dissolved in MeOH in a 1:1 molar ratio to ICG as to obtain a final 1:1 (ICG:co-ion) charge ratio, unless otherwise stated. In an 8-mL glass vial, 1 mL of chloroform, 2 mL of co-ion solution (MeOH), and 1 mL of ICG solution (water) were added in that order (methanol without co-ions was used as a control). The vials were gently shaken (i.e., slowly turned over 2-3 times) and incubated for 45 min at room temperature in the dark. Then 1 mL of water was added followed by 1 mL of chloroform to form a biphasic system. The vial was gently shaken again and incubated for 45 min at room temperature in the dark. The resulting HIP complex is present in the lower organic phase. To isolate the HIP complex, the chloroform phase was recovered and transferred to a new glass vial. Chloroform was then evaporated under a gentle flow of nitrogen.

Complexation efficiency

HIP complexation of ICG was done via Bligh-Dyer method as described above. However, to evaluate the charge ratios of 1:0.5 and 1:2, co-ions were dissolved in MeOH in 1:0.5 and 1:2 molar ratios (ICG:co-ion), respectively. After recovering the HIP complex from the organic phase, to quantify the

amount of recovered ICG a known volume of EtOH was added into the dried HIP complex and analyzed by UHPLC.

UHPLC method

HPLC analyses were done using a Shimadzu Nexera-X UHPLC instrument with a PDA detector. The samples were injected (10 µL) onto a Waters Terra BEH C8 column (2.5µm, 4.6x75mm, temperature 25°C) at a flow rate of 1 mL/min. For the *in vitro* stability studies, a Waters Terra BEH C18 column (2.5µm, 4.6x75mm) was used. The solvent system consisted of mobile phase A (5% MeCN, 0.1% TFA in water) and mobile phase B (0.1% TFA in MeCN). Chromatographic separation was achieved using a gradient of 0 to 100% phase B in 5 min followed by 1.5 min at 100% B. ICG was detected at 780 nm.

Preparation of CarboCell

CarboCell formulations were prepared by weighing and mixing the corresponding carbohydrate ester, co-solvent and solvent according to the compositions indicated in Table 13. The mixture was placed in an ultrasonication bath at 70-80°C for 1-2 hours and occasionally vortexed to generate homogenous solutions, namely CarboCells, which were stored at 4 °C until further use. ICG-HIP complexes were incorporated into the formulation by proportionally adding CarboCell on top of an aliquot of dried ICG-HIP complex, until reaching the desired ICG concentration. CarboCells were subjected to magnetic stirring at 40-50 °C until the ICG-HIP was completely dissolved.

In vitro stability studies

Native ICG was dissolved in MQ water, EtOH or DMSO at a final concentration of 0.04 mg/mL. Samples were then incubated in the dark at room temperature. Likewise, ICG-HIP complexes with either TEAB, CTAB, BENA, DDA or TOAB were dissolved in MeCN and incubated in the dark at room temperature. ICG-BENA complexes were dissolved in DMSO, EtOH, PC, acetone or BenOH at a concentration of 250 µg/mL and then incubated in the dark at room temperature or at 37°C. At the specified time points, samples were analyzed by UHPLC.

Fluorescence of ICG-HIP complexes in EtOH

Complexes of ICG with BENA, DDA, CTAB and TOAB were formed and solutions of the different ICG-HIP complexes were prepared in EtOH in a concentration range of 0.0003 – 1 mg/mL. Solutions of native ICG in EtOH were included as control. 100 µL of each sample and PBS (in duplicate) were placed in a 96-well black NUNC plate covered with a lid. Fluorescence emission and excitation spectra were recorded using a TECAN Spark multimode microplate reader with the following settings: excitation wavelength=790nm (for emission scan), emission wavelength=822 nm (for excitation scan), top reading, bandwidth=5 nm.

Fluorescence of ICG-BENA in CarboCell

ICG-BENA complex was prepared and dissolved in the CC2 formulation at a concentration of 1 mg/g. Serial dilutions were done to obtain CarboCells in the ICG concentration range of 0.0001 – 1 mg/g. Approximately 75 µL of each CarboCell (in duplicate) were placed in a 96-well black NUNC plate and fluorescence was measured as described previously though using a bandwidth of 7.5 nm.

In vitro release of ICG-HIP

To evaluate the *in vitro* burst release, ICG-HIP complexes were prepared and formulated in various CarboCells as indicated in Table 13. 50 µL of each CarboCell were injected in glass vials containing 2 mL PBS and they were incubated at 37°C protected from light. After 2.5 h, release media samples were analyzed by UHPLC using the previously described method.

To evaluate the general release profile, ICG-HIP complexes were prepared and formulated in various CarboCells as indicated in Table 14. 50 µL of each CarboCell were injected in glass vials containing 2 mL PBS and they were incubated at 37°C protected from light. At specified time points, PBS was carefully removed from the vials and the CarboCell depot was dissolved in DMSO and vortexed until dissolution. As reference, 10 µL of each CarboCell (non-injected) were dissolved in DMSO (n=4).

The ICG release percentage was determined by ratiometric analysis. The AUC values of ICG (780 nm) and SuBen (280 nm) were measured to calculate the AUC ratio of ICG/SuBen in all samples. The percentage of released ICG was calculated by comparing the AUC ratios in the collected CarboCells versus the corresponding ratios in the reference (non-injected) CarboCell (equation 1).

NIR imaging

CarboCells were imaged *in vitro* and *in vivo* using an in-house assembled NIR imaging lamp and camera, which were connected to an HP Windows computer (no special software needed). An 810 nm lamp and an X-Nite850 nm edge-pass filter were used (Appendix VI-S34).

In vivo evaluation

ICG-BENA complexes were formulated in CC3 and CC4 at a concentration of 0.1 mg/g ICG. Winstar female rats (350g), acquired from Janvier, were anesthetized with ~2% isoflurane. 30 and 50 µL of the CC3 formulation were injected s.c. in the right and left paw, respectively, of a single rat. 30 µL of the CC4 formulation were injected s.c. in the right paw of a separate rat, which also received a 100-µL injection deep in the thigh. All injections were performed using 23G needles. NIR imaging was done immediately after injection and after 20 h. All *in vivo* experiments were approved by the Danish National Animal Experiments Inspectorate.

Statistical analyses

When required, statistical analyses were performed on GraphPad Prism 9. The correspondingly used statistical test is specified in figure legends. A p-value ≤0.05 was deemed as statistically significant.

Chapter 7.
General conclusions and future perspectives

Despite the great advances on cancer immunotherapy, it still faces challenges in terms of efficacy and safety. Regarding the former, only a small portion of cancer patients are respondent to immunotherapy. ICIs, for example, are the largest category of approved immunotherapies and they target the adaptive arm of the immune system. However, most cancer patients have a deficient adaptive immune response against cancer cells. To surpass such obstacle, the administration of drugs aimed at activating an innate immune response and linking innate and adaptive immunity has received a lot of attention. Nevertheless, innate immune activating molecules, such as TLRas, do not only target immune cells that are cancer-specific. In this case, healthy cells throughout the body can also be susceptible to immune stimulation. Consequently, the systemic administration of innate immune activating molecules is associated with severe toxicity including autoimmune responses and cytokine release syndrome. Intratumoral immunotherapy is a practical strategy to achieve a local high drug concentration. Nevertheless, low injection reproducibility, drug leakage into systemic circulation and the rapid wash-out of drugs from tumors can compromise patient safety as well as an effective immune activation in the TME.

Our group developed the CarboCell, a novel drug delivery system aimed to address the aforementioned challenges. CarboCell is administered intratumorally and upon injection, it self-forms a depot that provides a sustained release of drugs activating the innate immune response and triggering an effective anti-cancer response. The intratumoral administration of the CarboCell can minimize systemic drug exposure and additionally, it enables the CarboCell to use the tumor as a source of antigens expressed across multiple cancer cell clones. Thus, CarboCell can also address the challenge of intra- and inter-tumoral cancer heterogeneity. In this project, several aspects of the CarboCell system were investigated including *in vitro* and *in vivo* characterization, drug stability, formulation development and therapeutic efficacy in murine models. The main drugs formulated in the CarboCell were TLR7/8 agonists (R848 and R848 prodrugs) and a TGF-β inhibitor (RepSox), all of which are small molecules and poorly soluble in water.

Drug stability is a critical quality attribute in any pharmaceutical formulation, so the chemical stability of R848 in the CarboCell was firstly investigated. It was found that R848 was reactive with some carbohydrate esters that are used as matrix of the CarboCell. The chemical modification of R848 was first observed in LOIB-based formulations, in which the primary amine in R848 acquired an isobutyrate group. It was found that the type of carbohydrate ester in the formulation highly influenced the stability

of R848. R848 was most stable in non-reducing carbohydrates esters comprising benzoate groups, indicating the key role of both the anomeric center of the sugars and steric hindrance. The importance of the anomeric center was demonstrated by blocking the anomeric center in LOIB through the addition of a methoxy group in its anomeric carbon. In this way, the reactivity towards R848 could be annulled and R848 maintained its chemical integrity. Moreover, it was observed that the reactivity of R848 was lower in both acidic conditions and low temperatures (≤ 4°C). Gardiquimod, another member of the imidazoquinolines family, was also prone to react with the carbohydrate esters in the CarboCell, while other drug molecules with different chemical structures were not. Thus, it is recommended that drug stability in the CarboCell should be assessed on a case-by-case basis. Overall, R848 displayed excellent short-term stability in π-SuBen and σ-SuBen. Due to its commercial availability, σ-SuBen was chosen as the main carbohydrate ester for subsequent formulations.

Inspired by the previous findings, five novel R848 prodrugs were synthesized. Different acyl groups were added in the primary amine of R848 to protect it from potential interactions with the carbohydrate esters in the CarboCell. Once released from the CarboCell, the prodrugs would exert their function as R848. The R848 prodrugs had a wide range of physico-chemical properties and all could be effortlessly solubilized in multiple CarboCell formulations, which shows the versatility of the system. R848 and R848 prodrugs showed sustained release profiles both *in vivo* and *in vitro*. Furthermore, the release profiles can be tailored depending on both the hydrophobicity of the drugs and the chemical composition of the CarboCell, where the latter can be easily modified. CarboCell was also able to provide a low burst release *in vitro* and also after both s.c. and i.t. injection in mice. The low burst release was correlated to a lower induction of IL-6 and a reduced weight loss, which indicated the potential of CarboCell to minimize drug spillover and systemic toxicity. To evaluate therapeutic efficacy, mice bearing CT26 tumors were treated with i.t. injections of CarboCells with R848 and R848 prodrugs. The treatment was well tolerated and the CarboCell significantly improved the MST of the mice. R848-IBA was determined as a potential alternative to R848 because it displayed a lower burst release, which might be advantageous for its tolerability in humans.

During the evaluation of the R848 prodrugs, the incorporation of the novel CT contrast CLA-8 into the CarboCell was investigated as well. CarboCell is intrinsically visible through ultrasound and MRI, and the addition of a CT contrast can further enhance its visibility across imaging technologies. CLA-8, an iodinated carbohydrate ester, could be formulated into CarboCells comprising SuBen, GTH and DMSO, up to a final concentration of 15%. CarboCells with CLA-8 showed excellent CT contrast before and after injection in mice. Therefore, CarboCell is an excellent localization marker to validate accurate and reproducible intratumoral injections, which is much needed in clinical practice. This CarboCell feature can be useful for image-guided injections and subsequent monitoring and planning of injections. However, it is unknown for how long the CarboCell depot will still be visible after injection. The visibility of the CarboCell over time might be reduced by the gradual biodegradation of its components, an aspect that has not been investigated yet. Thus, the long-term visibility and the biodegradability of the CarboCell should be evaluated in the future.

Next, the simultaneous formulation and co-delivery of R848 and RepSox was evaluated. Both drugs could be incorporated in CarboCells at concentrations as high as 12 mg/g R848 and 16 mg/g RepSox, but very likely the drug concentration can be further increased. The multi-target treatment was compared to R848 monotherapy, where the former induced an improved therapeutic response in mice bearing either CT26 or EMT-6 tumors. Again, the treatment was well tolerated, which underlines the ability of CarboCell to provide on-target drug delivery and small systemic spillover. Furthermore, the multi-drug treatment could induce a systemic anti-cancer immune response, which can be beneficial for the treatment of metastatic cancer.

Until now, the dosing schedule of the CarboCell treatment has consisted on four injections, each one done at a 7-day interval. In this project, a new formulation was developed to double the drug-releasing period and reduce the total number of injections from four to two injections per treatment. This was achieved by increasing the SuBen/GTO ratio in the CarboCell. In this way, the self-formed depot became more hydrophobic and viscous, both of which caused a slower drug release by hindering the diffusivity of the drug through the depot. It was also found that increasing the drug concentration in the CarboCell did not affect the overall release profile curves. The original CarboCell had a concentration of 3 mg/g R848 and 8 mg/g RepSox. In the new formulation for extended release, the drug concentration was doubled and mice treated with the new dose schedule (two injections given at a 14-day interval) showed a therapeutic response comparable to the original formulation and schedule. Reducing the frequency of injections can increase patient compliance and decrease the risk of organ injury or dissemination of cancer cells that may be associated with recurrent intratumoral injections. Afterwards, CLA-8 could also be incorporated in the formulation for extended release up to a final concentration of 5%. The addition of CLA-8 did not have an apparent impact neither in the drug release kinetics nor in the therapeutic efficacy of the CarboCell. Furthermore, the extended release formulation showed excellent stability after storage at both 4°C and -20°C, and it is expected to remain stable for the long-term.

We demonstrated that the CarboCell enables the simultaneous formulation and delivery of two different drugs, but we are confident that more drug molecules might be incorporated into the delivery system. Such feature is advantageous since the cancer-immunity cycle can be targeted in numerous ways and a combinatorial drug treatment may induce an enhanced therapeutic effect. An on-going phase I/II clinical trial (NCT04799054) has demonstrated encouraging early results that support the efficacy of the intratumoral administration of R848 as monotherapy. Therefore, we expect that the multi-target approach discussed in this project can have a successful clinical application. Moreover, as exemplified by the R848 prodrugs, we have also shown that drugs with different hydrophobicities can be released at different rates. Thus, overall, the CarboCell platform is very flexible and can enable the design of new immunotherapeutic strategies.

As part of the formulation development in this project, several characterization studies were performed to gain further knowledge and understanding of the CarboCell system. Various SuBen-based CarboCell compositions were tested to understand the correlation between viscosity, solvent diffusion and drug release. It was observed that both the amount and type of solvent were key factors influencing the drug burst release. In general, using DMSO as solvent produced a lower burst release and increased the viscosity of the formulation. A lower burst release may also be correlated to the slower diffusion of DMSO out of the system compared to EtOH. The burst release could be decreased by increasing the percentage of DMSO in the CarboCell. However, this also made the formulation more viscous, an important parameter that influences the injectability of the CarboCell. While the solvent was not as influential for the long-term release profiles, the choice of co-solvent and the sugar to co-solvent ratio played a key role in this aspect as previously exemplified for the extended release formulation. Moreover, using either σ-SuBen or π-SuBen as the CarboCell matrix also influenced the formulation viscosity and the overall drug release profile. σ-SuBen generated more viscous formulations than π-SuBen, which was also correlated to a slower drug release.

Importantly, the injection volume did not seem to affect the drug release profile from the CarboCells. Therefore, it is expected that greater injection volumes can be used in larger animal models without compromising the drug release kinetics. The sterilization process is another fundamental aspect for the advancement of the CarboCell. Gamma irradiation was a better method than autoclaving to preserve the chemical drug stability. However, gamma irradiation caused a degradation of ~1-5% of the CLA-8 present of the formulation, which caused the release of iodine and a change in coloration. It still needs to be evaluated if such side effects will have an impact on the long-term stability of the formulations.

A key characteristic of the CarboCell is its ability to solubilize hydrophobic drugs. However, this is also an inherent limitation on the type of molecules that can be incorporated into the CarboCell. HIP is a technique in which hydrophilic charged molecules interact with co-ions with an opposite charge to form temporal hydrophobic complexes. Thus, HIP was investigated, using ICG as model molecule, to expand the type and amount of drugs that can be formulated and delivered via CarboCell. The Bligh-Dyer method was an efficient, easy and robust technique to produce HIP complexes of ICG with a variety of co-ions (BENA, CTAB, TOAB, and DDA). The solubility of the ICG-HIP complexes was considerably higher in the CarboCells compared to the native ICG. Both the type and concentration of the co-ion influenced the release of ICG from the CarboCell. A high co-ion concentration as well as bulkier, hydrophobic co-ions caused a slower ICG release. Interestingly, the fluorescence properties of ICG were not affected due to the HIP complexation. Therefore, we explored the use of ICG-HIP as an additive to the CarboCell as localization marker for applications such as NIR image-guided surgery or lymph node mapping. The highest fluorescence intensity of ICG-HIP in a CarboCell was observed at an ICG concentration of 0.05 – 1 mg/g. CarboCells in combination with ICG-BENA were successfully formulated to either retain or release ICG after injection *in vivo*. Therefore, HIP via the Bligh-Dyer method might be applied to great variety of ionizable molecules like peptides, proteins, RNA and multiple hydrophilic small molecules, thereby expanding the applications of the CarboCell.

Overall, we have demonstrated the characteristics as well as the multiple advantages and benefits of the CarboCell technology for intratumoral immunotherapy. Throughout this PhD project, several formulation strategies and characterization studies of the CarboCell have been performed to serve as a foundation for further development of the system. In conclusion, we are confident that the CarboCell platform has great potential for future advancement as an effective and safe strategy for intratumoral immunotherapy.

References

[1] C. P. Wild, E. Weiderpass, and B. W. Stewart, *World Cancer Report: Cancer Research for Cancer Prevention*. 2020.

[2] H. Sung *et al.*, “Global Cancer Statistics 2020: GLOBOCAN Estimates of Incidence and Mortality Worldwide for 36 Cancers in 185 Countries,” *CA. Cancer J. Clin.*, vol. 71, no. 3, pp. 209–249, May 2021, doi: 10.3322/CAAC.21660.

[3] B. Vogelstein and K. W. Kinzler, “Cancer genes and the pathways they control,” *Nat. Med.*, vol. 10, no. 8, pp. 789–799, Aug. 2004, doi: 10.1038/NM1087.

[4] D. Hanahan and R. A. Weinberg, “The Hallmarks of Cancer,” *Cell*, vol. 100, no. 1, pp. 57–70, Jan. 2000, doi: 10.1016/S0092-8674(00)81683-9.

[5] D. Hanahan and R. A. Weinberg, “Hallmarks of cancer: The next generation,” *Cell*, vol. 144, no. 5, pp. 646–674, Mar. 2011, doi: 10.1016/J.CELL.2011.02.013.

[6] S. I. Grivennikov, F. R. Greten, and M. Karin, “Immunity, Inflammation, and Cancer,” *Cell*, vol. 140, no. 6, p. 883, Mar. 2010, doi: 10.1016/J.CELL.2010.01.025.

[7] Z. Abbas and S. Rehman, “An Overview of Cancer Treatment Modalities,” *Neoplasm*, Sep. 2018, doi: 10.5772/INTECHOPEN.76558.

[8] M. Arruebo *et al.*, “Assessment of the Evolution of Cancer Treatment Therapies,” *Cancers (Basel).*, vol. 3, no. 3, p. 3279, Sep. 2011, doi: 10.3390/CANCERS3033279.

[9] C. Y. Huang, D. T. Ju, C. F. Chang, P. Muralidhar Reddy, and B. K. Velmurugan, “A review on the effects of current chemotherapy drugs and natural agents in treating non-small cell lung cancer,” *BioMedicine*, vol. 7, no. 4, pp. 12–23, Dec. 2017, doi: 10.1051/BMDCN/2017070423.

[10] L. L. Bu *et al.*, “Advances in drug delivery for post-surgical cancer treatment,” *Biomaterials*, vol. 219, p. 119182, Oct. 2019, doi: 10.1016/J.BIOMATERIALS.2019.04.027.

[11] R. Demicheli, M. W. Retsky, W. J. M. Hrushesky, M. Baum, and I. D. Gukas, “The effects of surgery on tumor growth: a century of investigations,” *Ann. Oncol.*, vol. 19, no. 11, pp. 1821–1828, Nov. 2008, doi: 10.1093/ANNONC/MDN386.

[12] S. Tohme, R. L. Simmons, and A. Tsung, “Surgery for Cancer: A Trigger for Metastases,” *Cancer Res.*, vol. 77, no. 7, p. 1548, 2017, doi: 10.1158/0008-5472.CAN-16-1536.

[13] E. Dickens and S. Ahmed, “Principles of cancer treatment by chemotherapy,” *Surg.*, vol. 36, no. 3, pp. 134–138, Mar. 2018, doi: 10.1016/J.MPSUR.2017.12.002.

[14] M. Chiu, G. Taurino, M. G. Bianchi, M. S. Kilberg, and O. Bussolati, “Asparagine Synthetase in Cancer: Beyond Acute Lymphoblastic Leukemia,” *Front. Oncol.*, vol. 9, p. 1480, Jan. 2020, doi: 10.3389/FONC.2019.01480/BIBTEX.

[15] E. Evans and J. Staffurth, “Principles of cancer treatment by radiotherapy,” *Surg.*, vol. 36, no. 3, pp. 111–116, Mar. 2018, doi: 10.1016/J.MPSUR.2017.12.006.

[16] B. W. Goy, M. S. Soper, T. Chang, J. M. Slezak, H. A. Cosmatos, and M. Tome, “Treatment results of brachytherapy vs. external beam radiation therapy for intermediate-risk prostate cancer with 10-year followup,” *Brachytherapy*, vol. 15, no. 6, pp. 687–694, Nov. 2016, doi: 10.1016/J.BRACHY.2016.06.015.

[17] H. H. W. Chen and M. T. Kuo, “Improving radiotherapy in cancer treatment: Promises and challenges,” *Oncotarget*, vol. 8, no. 37, p. 62742, Sep. 2017, doi: 10.18632/ONCOTARGET.18409.

[18] F. M. Burnet, “The concept of immunological surveillance,” *Immunol. Asp. Neoplasia*, vol. 13, pp. 1–27, 1970.

[19] D. S. Chen and I. Mellman, “Oncology Meets Immunology: The Cancer-Immunity Cycle,” *Immunity*, vol. 39, no. 1, pp. 1–10, Jul. 2013, doi: 10.1016/J.IMMUNI.2013.07.012.

[20] R. Pio, D. Ajona, S. Ortiz-Espinosa, A. Mantovani, and J. D. Lambris, “Complementing the cancer-immunity cycle,” *Front. Immunol.*, vol. 10, no. APR, p. 774, 2019, doi: 10.3389/FIMMU.2019.00774/BIBTEX.

[21] K. Esfahani, L. Roudaia, N. Buhlaiga, S. V. Del Rincon, N. Papneja, and W. H. Miller, “A Review of Cancer Immunotherapy: From the Past, to the Present, to the Future,” *Curr. Oncol. 2020, Vol. 27, Pages 87-97*, vol. 27, no. s2, pp. 87–97, Apr. 2020, doi: 10.3747/CO.27.5223.

[22] A. D. Waldman, J. M. Fritz, and M. J. Lenardo, “A guide to cancer immunotherapy: from T cell basic science to clinical practice,” *Nat. Rev. Immunol. 2020 2011*, vol. 20, no. 11, pp. 651–668, May 2020, doi: 10.1038/s41577-020-0306-5.

[23] S. Pouliliou, C. Nikolaidis, and G. Drosatos, “Current trends in cancer immunotherapy: a literature-mining analysis,” *Cancer Immunol. Immunother.*, vol. 69, no. 12, pp. 2425–2439, Dec. 2020, doi: 10.1007/S00262-020-02630-8.

[24] A. Sharma, M. Campbell, C. Yee, S. Goswami, and P. Sharma, “Immunotherapy of Cancer,” *Clin. Immunol.*, pp. 1033-1048.e1, Jan. 2019, doi: 10.1016/B978-0-7020-6896-6.00077-6.

[25] A. Osipov, A. Murphy, and L. Zheng, “From immune checkpoints to vaccines: The past, present and future of cancer immunotherapy,” *Adv. Cancer Res.*, vol. 143, pp. 63–144, Jan. 2019, doi: 10.1016/BS.ACR.2019.03.002.

[26] A. J. Korman, S. C. Garrett-Thomson, and N. Lonberg, “The foundations of immune checkpoint blockade and the ipilimumab approval decennial,” *Nat. Rev. Drug Discov. 2021*, pp. 1–20, Dec. 2021, doi: 10.1038/s41573-021-00345-8.

[27] P. S. Linsley, J. A. L. Greene, W. Brady, J. Bajorath, J. A. Ledbetter, and R. Peach, “Human B7-1 (CD80) and B7-2 (CD86) bind with similar avidities but distinct kinetics to CD28 and CTLA-4 receptors,” *Immunity*, vol. 1, no. 9, pp. 793–801, 1994, doi: 10.1016/S1074-7613(94)80021-9.

[28] M. A. Postow, M. K. Callahan, and J. D. Wolchok, “Immune Checkpoint Blockade in Cancer Therapy,” *J. Clin. Oncol.*, vol. 33, no. 17, p. 1974, Jun. 2015, doi: 10.1200/JCO.2014.59.4358.

[29] K. M. Hargadon, C. E. Johnson, and C. J. Williams, “Immune checkpoint blockade therapy for cancer: An overview of FDA-approved immune checkpoint inhibitors,” *Int. Immunopharmacol.*, vol. 62, pp. 29–39, Sep. 2018, doi: 10.1016/J.INTIMP.2018.06.001.

[30] T. F. Nishijima, S. S. Shachar, K. A. Nyrop, and H. B. Muss, “Safety and Tolerability of PD-1/PD- L1 Inhibitors Compared with Chemotherapy in Patients with Advanced Cancer: A Meta- Analysis,” *Oncologist*, vol. 22, no. 4, p. 470, Apr. 2017, doi: 10.1634/THEONCOLOGIST.2016-0419.

[31] A. Haslam and V. Prasad, “Estimation of the Percentage of US Patients With Cancer Who Are Eligible for and Respond to Checkpoint Inhibitor Immunotherapy Drugs,” *JAMA Netw. Open*, vol. 2, no. 5, pp. e192535–e192535, May 2019, doi: 10.1001/JAMANETWORKOPEN.2019.2535.

[32] A. Marabelle, L. Tselikas, T. de Baere, and R. Houot, “Intratumoral immunotherapy: using the tumor as the remedy,” *Ann. Oncol.*, vol. 28, pp. xii33–xii43, Dec. 2017, doi: 10.1093/ANNONC/MDX683.

[33] Y. T. Liu and Z. J. Sun, “Turning cold tumors into hot tumors by improving T-cell infiltration,” *Theranostics*, vol. 11, no. 11, pp. 5265–5286, Mar. 2021, doi: 10.7150/THNO.58390.

[34] E. Appleton *et al.*, “Kickstarting Immunity in Cold Tumours: Localised Tumour Therapy Combinations With Immune Checkpoint Blockade,” *Front. Immunol.*, vol. 12, p. 4319, Oct. 2021, doi: 10.3389/FIMMU.2021.754436/BIBTEX.

[35] P. Sharma, S. Hu-Lieskovan, J. A. Wargo, and A. Ribas, “Primary, Adaptive and Acquired Resistance to Cancer Immunotherapy,” *Cell*, vol. 168, no. 4, p. 707, Feb. 2017, doi: 10.1016/J.CELL.2017.01.017.

[36] L. Milling, Y. Zhang, and D. J. Irvine, “Delivering safer immunotherapies for cancer,” *Adv. Drug Deliv. Rev.*, vol. 114, p. 79, May 2017, doi: 10.1016/J.ADDR.2017.05.011.

[37] F. S. Hodi *et al.*, “Improved survival with ipilimumab in patients with metastatic melanoma,” *N. Engl. J. Med.*, vol. 363, no. 8, pp. 711–723, Aug. 2010, doi: 10.1056/NEJMOA1003466.

[38] J. M. Michot *et al.*, “Immune-related adverse events with immune checkpoint blockade: A comprehensive review,” *Eur. J. Cancer*, vol. 54, pp. 139–148, Feb. 2016, doi: 10.1016/J.EJCA.2015.11.016.

[39] Y. Nouri, R. Weinkove, and R. Perret, “T-cell intrinsic Toll-like receptor signaling: implications for cancer immunotherapy and CAR T-cells,” *J. Immunother. Cancer*, vol. 9, no. 11, p. e003065, Nov. 2021, doi: 10.1136/JITC-2021-003065.

[40] S. Adams, “Toll-like receptor agonists in cancer therapy,” *Immunotherapy*, vol. 1, no. 6, p. 949, Nov. 2009, doi: 10.2217/IMT.09.70.

[41] Z. Urban-Wojciuk *et al.*, “The role of TLRs in anti-cancer immunity and tumor rejection,” *Front. Immunol.*, vol. 10, no. OCT, p. 2388, 2019, doi: 10.3389/FIMMU.2019.02388/BIBTEX.

[42] T. Kawasaki and T. Kawai, “Toll-Like Receptor Signaling Pathways,” *Front. Immunol.*, vol. 5, no. SEP, 2014, doi: 10.3389/FIMMU.2014.00461.

[43] S. Manicassamy and B. Pulendran, “Modulation of adaptive immunity with Toll-like receptors,” *Semin. Immunol.*, vol. 21, no. 4, pp. 185–193, Aug. 2009, doi: 10.1016/J.SMIM.2009.05.005.

[44] W. B. Coley, “The treatment of malignant tumors by repeated inoculations of erysipelas. With a report of ten original cases. 1893.,” *Clin. Orthop. Relat. Res.*, no. 262, pp. 3–11, Jan. 1991.

[45] B. Wiemann and C. O. Starnes, “Coley’s toxins, tumor necrosis factor and cancer research: a historical perspective,” *Pharmacol. Ther.*, vol. 64, no. 3, pp. 529–564, 1994, doi: 10.1016/0163-7258(94)90023-X.

[46] N. Jain, J. Hubbard, F. Vega, G. Vidal, G. Garcia-Manero, and G. Borthakur, “Spontaneous Remission of Acute Myeloid Leukemia: Report of Three Cases and Review of the Literature,” *Clin. Leuk.*, vol. 2, no. 1, pp. 64–67, 2008.

[47] M. Smith *et al.*, “Trial Watch: Toll-like receptor agonists in cancer immunotherapy,” *Oncoimmunology*, vol. 7, no. 12, Dec. 2018, doi: 10.1080/2162402X.2018.1526250.

[48] D. Varshney, S. Y. Qiu, T. P. Graf, and K. J. Mchugh, “Employing Drug Delivery Strategies to Overcome Challenges Using TLR7/8 Agonists for Cancer Immunotherapy,” *AAPS J. 2021 234*, vol. 23, no. 4, pp. 1–18, Jun. 2021, doi: 10.1208/S12248-021-00620-X.

[49] J. Kang, S. Demaria, and S. Formenti, “Current clinical trials testing the combination of immunotherapy with radiotherapy,” *J. Immunother. Cancer*, vol. 4, no. 1, pp. 1–20, Sep. 2016, doi: 10.1186/S40425-016-0156-7/TABLES/4.

[50] H. Zhang *et al.*, “Development of thermosensitive resiquimod-loaded liposomes for enhanced cancer immunotherapy,” *J. Control. Release*, vol. 330, pp. 1080–1094, Feb. 2021, doi: 10.1016/J.JCONREL.2020.11.013.

[51] A. H. Rook *et al.*, “Topical resiquimod can induce disease regression and enhance T-cell effector functions in cutaneous T-cell lymphoma,” *Blood*, vol. 126, no. 12, p. 1452, Sep. 2015, doi: 10.1182/BLOOD-2015-02-630335.

[52] A. L. Engel, G. E. Holt, and H. Lu, “The pharmacokinetics of Toll-like receptor agonists and the impact on the immune system,” *Expert Rev. Clin. Pharmacol.*, vol. 4, no. 2, p. 275, Mar. 2011, doi: 10.1586/ECP.11.5.

[53] M. Schön *et al.*, “Tumor-selective induction of apoptosis and the small-molecule immune response modifier imiquimod,” *J. Natl. Cancer Inst.*, vol. 95, no. 15, pp. 1138–1149, Aug. 2003, doi: 10.1093/JNCI/DJG016.

[54] S. Majewski, M. Marczak, B. Mlynarczyk, B. Benninghoff, and S. Jablonska, “Imiquimod is a strong inhibitor of tumor cell-induced angiogenesis,” *Int. J. Dermatol.*, vol. 44, no. 1, pp. 14–19, Jan. 2005, doi: 10.1111/J.1365-4632.2004.02318.X.

[55] C. D. Dumitru *et al.*, “NK1.1+ cells mediate the antitumor effects of a dual Toll-like receptor 7/8 agonist in the disseminated B16-F10 melanoma model,” *Cancer Immunol. Immunother.*, vol. 58, no. 4, pp. 575–587, Apr. 2009, doi: 10.1007/S00262-008-0581-7.

[56] F. Sato-Kaneko *et al.*, “Combination immunotherapy with TLR agonists and checkpoint inhibitors suppresses head and neck cancer,” *JCI Insight*, vol. 2, no. 18, Sep. 2017, doi: 10.1172/JCI.INSIGHT.93397.

[57] J. Zhu *et al.*, “Local administration of a novel Toll-like receptor 7 agonist in combination with doxorubicin induces durable tumouricidal effects in a murine model of T cell lymphoma,” *J. Hematol. Oncol.*, vol. 8, no. 1, pp. 1–10, Mar. 2015, doi: 10.1186/S13045-015-0121-9/TABLES/1.

[58] S. Schölch *et al.*, “Radiotherapy combined with TLR7/8 activation induces strong immune responses against gastrointestinal tumors,” *Oncotarget*, vol. 6, no. 7, pp. 4663–4676, Dec. 2014, doi: 10.18632/ONCOTARGET.3081.

[59] K. A. Michaelis *et al.*, “The TLR7/8 agonist R848 remodels tumor and host responses to promote survival in pancreatic cancer,” *Nat. Commun.*, vol. 10, no. 1, Dec. 2019, doi: 10.1038/S41467-019-12657-W.

[60] H. Chi *et al.*, “Anti-tumor Activity of Toll-Like Receptor 7 Agonists,” *Front. Pharmacol.*, vol. 8, no. MAY, May 2017, doi: 10.3389/FPHAR.2017.00304.

[61] L. I. Harrison, C. Astry, S. Kumar, and C. Yunis, “Pharmacokinetics of 852A, an imidazoquinoline Toll-like receptor 7-specific agonist, following intravenous, subcutaneous, and oral administrations in humans,” *J. Clin. Pharmacol.*, vol. 47, no. 8, pp. 962–969, Aug. 2007, doi: 10.1177/0091270007303766.

[62] P. J. Pockros *et al.*, “Oral resiquimod in chronic HCV infection: Safety and efficacy in 2 placebo-controlled, double-blind phase IIa studies,” *J. Hepatol.*, vol. 47, no. 2, pp. 174–182, Aug. 2007, doi: 10.1016/J.JHEP.2007.02.025.

[63] J. P. Vasilakos and M. A. Tomai, “The use of Toll-like receptor 7/8 agonists as vaccine adjuvants,” *Expert Rev. Vaccines*, vol. 12, no. 7, pp. 809–819, Jul. 2013, doi: 10.1586/14760584.2013.811208.

[64] J. A. Joyce and D. T. Fearon, “T cell exclusion, immune privilege, and the tumor microenvironment,” *Science (80-.).*, vol. 348, no. 6230, pp. 74–80, Apr. 2015, doi: 10.1126/science.aaa4971.

[65] F. R. Balkwill, M. Capasso, and T. Hagemann, “The tumor microenvironment at a glance,” *J. Cell Sci.*, vol. 125, no. 23, pp. 5591–5596, Dec. 2012, doi: 10.1242/JCS.116392.

[66] Q. Duan, H. Zhang, J. Zheng, and L. Zhang, “Turning Cold into Hot: Firing up the Tumor Microenvironment,” *Trends in Cancer*, vol. 6, no. 7, pp. 605–618, Jul. 2020, doi: 10.1016/J.TRECAN.2020.02.022.

[67] J. Galon and D. Bruni, “Approaches to treat immune hot, altered and cold tumours with combination immunotherapies,” *Nat. Rev. Drug Discov. 2018 183*, vol. 18, no. 3, pp. 197–218, Jan. 2019, doi: 10.1038/s41573-018-0007-y.

[68] M. Binnewies *et al.*, “Understanding the tumor immune microenvironment (TIME) for effective therapy,” *Nat. Med.*, vol. 24, no. 5, pp. 541–550, May 2018, doi: 10.1038/S41591-018-0014-X.

[69] C. Groeneveldt, T. van Hall, S. H. van der Burg, P. ten Dijke, and N. van Montfoort, “Immunotherapeutic Potential of TGF-β Inhibition and Oncolytic Viruses,” *Trends Immunol.*, vol. 41, no. 5, pp. 406–420, May 2020, doi: 10.1016/J.IT.2020.03.003.

[70] K. Ganesh and J. Massagué, “TGF-β Inhibition and Immunotherapy: Checkmate,” *Immunity*, vol. 48, no. 4, p. 626, Apr. 2018, doi: 10.1016/J.IMMUNI.2018.03.037.

[71] C. Neuzillet *et al.*, “Targeting the TGFβ pathway for cancer therapy,” *Pharmacol. Ther.*, vol. 147, pp. 22–31, Mar. 2015, doi: 10.1016/J.PHARMTHERA.2014.11.001.

[72] D. V. F. Tauriello *et al.*, “TGFβ drives immune evasion in genetically reconstituted colon cancer metastasis,” *Nat. 2018 5547693*, vol. 554, no. 7693, pp. 538–543, Feb. 2018, doi: 10.1038/nature25492.

[73] Y. Lan *et al.*, “Enhanced preclinical antitumor activity of M7824, a bifunctional fusion protein simultaneously targeting PD-L1 and TGF-,” *Sci. Transl. Med.*, vol. 10, no. 424, p. 5488, Jan. 2018, doi: 10.1126/SCITRANSLMED.AAN5488.

[74] B. G. Kim, E. Malek, S. H. Choi, J. J. Ignatz-Hoover, and J. J. Driscoll, “Novel therapies emerging in oncology to target the TGF-β pathway,” *J. Hematol. Oncol. 2021 141*, vol. 14, no. 1, pp. 1–20, Apr. 2021, doi: 10.1186/S13045-021-01053-X.

[75] M. S. Mitra *et al.*, “A Potent Pan-TGFβ Neutralizing Monoclonal Antibody Elicits Cardiovascular Toxicity in Mice and Cynomolgus Monkeys,” *Toxicol. Sci.*, vol. 175, no. 1, pp. 24–34, 2020, doi: 10.1093/toxsci/kfaa024.

[76] C. García-Fernández, A. Saz, C. Fornaguera, and S. Borrós, “Cancer immunotherapies revisited: state of the art of conventional treatments and next-generation nanomedicines,” *Cancer Gene Ther. 2021 289*, vol. 28, no. 9, pp. 935–946, Apr. 2021, doi: 10.1038/s41417-021-00333-5.

[77] R. S. Riley, C. H. June, R. Langer, and M. J. Mitchell, “Delivery technologies for cancer immunotherapy,” *Nat. Rev. Drug Discov.*, vol. 18, no. 3, p. 175, Mar. 2019, doi: 10.1038/S41573-018-0006-Z.

[78] D. Schmid *et al.*, “T cell-targeting nanoparticles focus delivery of immunotherapy to improve antitumor immunity,” *Nat. Commun. 2017 81*, vol. 8, no. 1, pp. 1–12, Nov. 2017, doi: 10.1038/s41467-017-01830-8.

[79] L. B. Kennedy and A. K. S. Salama, “A review of cancer immunotherapy toxicity,” *CA. Cancer J. Clin.*, vol. 70, no. 2, pp. 86–104, Mar. 2020, doi: 10.3322/CAAC.21596.

[80] V. Murthy, J. Minehart, and D. H. Sterman, “Local Immunotherapy of Cancer: Innovative Approaches to Harnessing Tumor-Specific Immune Responses,” *J. Natl. Cancer Inst.*, vol. 109, no. 12, Dec. 2017, doi: 10.1093/JNCI/DJX097.

[81] J. T. Wilson *et al.*, “pH-responsive nanoparticle vaccines for dual-delivery of antigens and immunostimulatory oligonucleotides,” *ACS Nano*, vol. 7, no. 5, pp. 3912–3925, May 2013, doi: 10.1021/NN305466Z.

[82] Y. Pan *et al.*, “Mechanogenetics for the remote and noninvasive control of cancer immunotherapy,” *Proc. Natl. Acad. Sci. U. S. A.*, vol. 115, no. 5, pp. 992–997, Jan. 2018, doi: 10.1073/PNAS.1714900115/VIDEO-1.

[83] K. Shao, S. Singha, X. Clemente-Casares, S. Tsai, Y. Yang, and P. Santamaria, “Nanoparticle-based immunotherapy for cancer,” *ACS Nano*, vol. 9, no. 1, pp. 16–30, Jan. 2015, doi: 10.1021/NN5062029.

[84] I. Melero, E. Castanon, M. Alvarez, S. Champiat, and A. Marabelle, “Intratumoural administration and tumour tissue targeting of cancer immunotherapies,” *Nat. Rev. Clin. Oncol. 2021 189*, vol. 18, no. 9, pp. 558–576, May 2021, doi: 10.1038/s41571-021-00507-y.

[85] D. Delcassian and A. K. Patel, “Nanotechnology and drug delivery,” *Bioeng. Innov. Solut. Cancer*, pp. 197–219, Jan. 2020, doi: 10.1016/B978-0-12-813886-1.00009-7.

[86] N. Bertrand, J. Wu, X. Xu, N. Kamaly, and O. C. Farokhzad, “Cancer nanotechnology: The impact of passive and active targeting in the era of modern cancer biology,” *Adv. Drug Deliv. Rev.*, vol. 66, pp. 2–25, Feb. 2014, doi: 10.1016/J.ADDR.2013.11.009.

[87] L. E. Gerlowski and R. K. Jain, “Microvascular permeability of normal and neoplastic tissues,” *Microvasc. Res.*, vol. 31, no. 3, pp. 288–305, May 1986, doi: 10.1016/0026-2862(86)90018-X.

[88] S. Wilhelm *et al.*, “Analysis of nanoparticle delivery to tumours,” *Nat. Rev. Mater.*, vol. 1, Apr. 2016, doi: 10.1038/NATREVMATS.2016.14.

[89] H. Cabral, H. Kinoh, and K. Kataoka, “Tumor-Targeted Nanomedicine for Immunotherapy,” *Acc. Chem. Res.*, vol. 53, no. 12, pp. 2765–2776, Dec. 2020, doi: 10.1021/ACS.ACCOUNTS.0C00518.

[90] S. E. Ackerman *et al.*, “Abstract 1559: TLR7/8 immune-stimulating antibody conjugates elicit robust myeloid activation leading to enhanced effector function and anti-tumor immunity in pre-clinical models,” *Cancer Res.*, vol. 79, no. 13 Supplement, pp. 1559–1559, Jul. 2019, doi: 10.1158/1538-7445.AM2019-1559.

[91] S. E. Ackerman *et al.*, “Immune-stimulating antibody conjugates elicit robust myeloid activation and durable antitumor immunity,” *Nat. Cancer 2020 21*, vol. 2, no. 1, pp. 18–33, Dec. 2020, doi: 10.1038/s43018-020-00136-x.

[92] F. Meric-Bernstam *et al.*, “Advances in HER2-Targeted Therapy: Novel Agents and Opportunities Beyond Breast and Gastric Cancer,” *Clin. Cancer Res.*, vol. 25, no. 7, p. 2033, Apr. 2019, doi: 10.1158/1078-0432.CCR-18-2275.

[93] M. Krishna and S. G. Nadler, “Immunogenicity to Biotherapeutics – The Role of Anti-drug Immune Complexes,” *Front. Immunol.*, vol. 7, no. FEB, p. 21, 2016, doi: 10.3389/FIMMU.2016.00021.

[94] A. Renner, M. Burotto, and C. Rojas, “Immune checkpoint inhibitor dosing: Can we go lower without compromising clinical efficacy?,” *J. Glob. Oncol.*, vol. 2019, no. 5, pp. 1–5, Jul. 2019, doi: 10.1200/JGO.19.00142.

[95] E. P. Goldberg *et al.*, “Intratumoral cancer chemotherapy and immunotherapy: opportunities for nonsystemic preoperative drug delivery,” *J. Pharm. Pharmacol.*, vol. 54, no. 2, pp. 159–180, Feb. 2002, doi: 10.1211/0022357021778268.

[96] C. Boutros *et al.*, “Safety profiles of anti-CTLA-4 and anti-PD-1 antibodies alone and in combination,” *Nat. Rev. Clin. Oncol. 2016 138*, vol. 13, no. 8, pp. 473–486, May 2016, doi: 10.1038/nrclinonc.2016.58.

[97] R. Govindan, “Attack of the clones,” *Science (80-.).*, vol. 346, no. 6206, pp. 169–170, Oct. 2014, doi: 10.1126/SCIENCE.1259926.

[98] L. Hammerich, A. Binder, and J. D. Brody, “In situ vaccination: Cancer immunotherapy both personalized and off- the- shelf,” *Mol. Oncol.*, vol. 9, no. 10, p. 1966, Dec. 2015, doi: 10.1016/J.MOLONC.2015.10.016.

[99] D. V Smirnov *et al.*, “Intratumoral immunotherapy with the TLR7/8 agonist 3M-052,” *J. Immunother. Cancer 2013 11*, vol. 1, no. 1, pp. 1–1, Nov. 2013, doi: 10.1186/2051-1426-1-S1-P138.

[100] D. Smirnov, J. J. Schmidt, J. T. Capecchi, and P. D. Wightman, “Vaccine adjuvant activity of 3M-052: An imidazoquinoline designed for local activity without systemic cytokine induction,” *Vaccine*, vol. 29, no. 33, pp. 5434–5442, Jul. 2011, doi: 10.1016/J.VACCINE.2011.05.061.

[101] J. Zalevsky, “NKTR-214 plus NKTR-262, a Scientifically-Guided Rational Combination Approach for Immune Oncology,” *Biology and Preclinical Development Nektar Therapeutics World*, 2017. https://www.nektar.com/application/files/9815/1741/9346/Zalevsky_WPC_June2017_FINAL.pdf (accessed Feb. 05, 2022).

[102] J. Ishihara *et al.*, “Matrix-binding checkpoint immunotherapies enhance antitumor efficacy and reduce adverse events,” *Sci. Transl. Med.*, vol. 9, no. 415, Nov. 2017, doi: 10.1126/SCITRANSLMED.AAN0401.

[103] F. R. Greten and S. I. Grivennikov, “Inflammation and Cancer: Triggers, Mechanisms and Consequences,” *Immunity*, vol. 51, no. 1, p. 27, Jul. 2019, doi: 10.1016/J.IMMUNI.2019.06.025.

[104] B. S. Graham *et al.*, “Immunization with Cocktail of HIV-Derived Peptides in Montanide ISA-51 Is Immunogenic, but Causes Sterile Abscesses and Unacceptable Reactogenicity,” *PLoS One*, vol. 5, no. 8, 2010, doi: 10.1371/JOURNAL.PONE.0011995.

[105] M. F. Fransen, T. C. Van Der Sluis, F. Ossendorp, R. Arens, and C. J. M. Melief, “Controlled local delivery of CTLA-4 blocking antibody induces CD8+ T-cell-dependent tumor eradication and decreases risk of toxic side effects,” *Clin. Cancer Res.*, vol. 19, no. 19, pp. 5381–5389, Oct. 2013, doi: 10.1158/1078-0432.CCR-12-0781.

[106] J. Li, Y. Luo, B. Li, Y. Xia, H. Wang, and C. Fu, “Implantable and Injectable Biomaterial Scaffolds for Cancer Immunotherapy,” *Front. Bioeng. Biotechnol.*, vol. 8, p. 1363, Nov. 2020, doi: 10.3389/FBIOE.2020.612950/BIBTEX.

[107] J. Li and D. J. Mooney, “Designing hydrogels for controlled drug delivery,” *Nat. Rev. Mater. 2016 112*, vol. 1, no. 12, pp. 1–17, Oct. 2016, doi: 10.1038/natrevmats.2016.71.

[108] L. Zuniga *et al.*, “A single dose of intratumoral TransCon™ TLR7/8 agonist monotherapy promoted sustained activation of antigen presenting cells resulting in CD4+ and CD8+ T cell activation and tumor growth inhibition,” *J. Immunother. Cancer*, vol. 9, no. Suppl 2, pp. A804–A804, Nov. 2021, doi: 10.1136/JITC-2021-SITC2021.769.

[109] Ascendis Pharma A/S, “TransCon technology,” Mar. 2019. https://ascendispharma.gcs-web.com/static-files/0c44cfef-cb29-4c88-a842-86f5d4e48974 (accessed Feb. 04, 2022).

[110] Ascendis Pharma Oncology Division A/S, “A Study of TransCon TLR7/8 Agonist With or Without Pembrolizumab in Patients With Advanced or Metastatic Solid Tumors ,” Mar. 16, 2021. https://clinicaltrials.gov/ct2/show/NCT04799054 (accessed Jan. 13, 2022).

[111] C. Wang *et al.*, “In situ formed reactive oxygen species-responsive scaffold with gemcitabine and checkpoint inhibitor for combination therapy,” *Sci. Transl. Med.*, vol. 10, no. 429, Feb. 2018, doi: 10.1126/SCITRANSLMED.AAN3682.

[112] R. A. Sheth *et al.*, “Assessment of Image-Guided Intratumoral Delivery of Immunotherapeutics in Patients With Cancer,” *JAMA Netw. open*, vol. 3, no. 7, Jul. 2020, doi: 10.1001/JAMANETWORKOPEN.2020.7911.

[113] N. M. Muñoz *et al.*, “Influence of injection technique, drug formulation and tumor microenvironment on intratumoral immunotherapy delivery and efficacy,” *J. Immunother. Cancer*, vol. 9, no. 2, p. e001800, Feb. 2021, doi: 10.1136/JITC-2020-001800.

[114] S. Kempe and K. Mäder, “In situ forming implants - an attractive formulation principle for parenteral depot formulations,” *J. Control. Release*, vol. 161, no. 2, pp. 668–679, Jul. 2012, doi: 10.1016/J.JCONREL.2012.04.016.

[115] W. B. Liechty, D. R. Kryscio, B. V. Slaughter, and N. A. Peppas, “Polymers for Drug Delivery Systems,” *Annu. Rev. Chem. Biomol. Eng.*, vol. 1, p. 149, Jul. 2010, doi: 10.1146/ANNUREV-CHEMBIOENG-073009-100847.

[116] A. Hatefi and B. Amsden, “Biodegradable injectable in situ forming drug delivery systems,” *J. Control. Release*, vol. 80, no. 1–3, pp. 9–28, Apr. 2002, doi: 10.1016/S0168-3659(02)00008-1.

[117] X. Lin *et al.*, “A novel risperidone-loaded SAIB-PLGA mixture matrix depot with a reduced burst release: Effects of solvents and PLGA on drug release behaviors in vitro/in vivo,” *J. Mater. Sci. Mater. Med.*, vol. 23, no. 2, pp. 443–455, Feb. 2012, doi: 10.1007/S10856-011-4521-2/FIGURES/8.

[118] Y. Lu, Y. Yu, and X. Tang, “Sucrose acetate isobutyrate as an in situ forming system for sustained risperidone release,” *J. Pharm. Sci.*, vol. 96, no. 12, pp. 3252–3262, 2007, doi: 10.1002/jps.21091.

[119] R. I. Jølck *et al.*, “Injectable Colloidal Gold in a Sucrose Acetate Isobutyrate Gelating Matrix with Potential Use in Radiation Therapy,” *Adv. Healthc. Mater.*, vol. 3, no. 10, pp. 1680–1687, Oct. 2014, doi: 10.1002/ADHM.201300668.

[120] X. Lin *et al.*, “A Uniform Ultra-Small Microsphere/SAIB Hybrid Depot with Low Burst Release for Long-Term Continuous Drug Release,” *Pharm. Res.*, vol. 32, no. 11, pp. 3708–3721, Nov. 2015, doi: 10.1007/S11095-015-1731-1/FIGURES/10.

[121] J. Guo *et al.*, “The Anti-Melanoma Efficiency of the Intratumoral Injection of Cucurbitacin-Loaded Sustained Release Carriers: In Situ-Forming Implants,” *AAPS PharmSciTech*, vol. 16, no. 4, pp. 973–985, Aug. 2015, doi: 10.1208/S12249-015-0292-2/FIGURES/11.

[122] F. W. Okumu *et al.*, “Sustained delivery of human growth hormone from a novel gel system: SABER,” *Biomaterials*, vol. 23, no. 22, pp. 4353–4358, 2002, doi: 10.1016/S0142-9612(02)00174-6.

[123] M. R. Moman *et al.*, “Long-term experience with transrectal and transperineal implantations of fiducial gold markers in the prostate for position verification in external beam radiotherapy; feasibility, toxicity and quality of life,” *Radiother. Oncol.*, vol. 96, no. 1, pp. 38–42, Jul. 2010, doi: 10.1016/J.RADONC.2010.02.027.

[124] G. F. Persson *et al.*, “Percutaneously implanted markers in peripheral lung tumours: report of complications,” *Acta Oncol.*, vol. 52, no. 6, pp. 1225–1228, 2013, doi: 10.3109/0284186X.2013.764009.

[125] P. A. Kupelian *et al.*, “Implantation and stability of metallic fiducials within pulmonary lesions,” *Int. J. Radiat. Oncol. Biol. Phys.*, vol. 69, no. 3, pp. 777–785, Nov. 2007, doi: 10.1016/J.IJROBP.2007.03.040.

[126] T. Harada *et al.*, “Real-time tumor-tracking radiation therapy for lung carcinoma by the aid of insertion of a gold marker using bronchofiberscopy,” *Cancer*, vol. 95, no. 8, pp. 1720–1727, Oct. 2002, doi: 10.1002/CNCR.10856.

[127] G. F. Persson *et al.*, “Stability of percutaneously implanted markers for lung stereotactic radiotherapy,” *J. Appl. Clin. Med. Phys.*, vol. 14, no. 5, pp. 187–195, 2013, doi: 10.1120/JACMP.V14I5.4337.

[128] M. Machiels *et al.*, “A Novel Liquid Fiducial Marker in Esophageal Cancer Image Guided Radiation Therapy: Technical Feasibility and Visibility on Imaging,” *Pract. Radiat. Oncol.*, vol. 9, no. 6, pp. e506–e515, Nov. 2019, doi: 10.1016/J.PRRO.2019.06.018.

[129] M. De Ridder, L. C. Gerbrandy, T. M. de Reijke, K. A. Hinnen, and M. C. C. M. Hulshof, “BioXmark® liquid fiducial markers for image-guided radiotherapy in muscle invasive bladder cancer: A safety and performance trial,” *Br. J. Radiol.*, vol. 93, no. 1111, Jul. 2020, doi: 10.1259/BJR.20200241.

[130] S. R. de Blanck *et al.*, “Long term safety and visibility of a novel liquid fiducial marker for use in image guided radiotherapy of non-small cell lung cancer,” *Clin. Transl. Radiat. Oncol.*, vol. 13, pp. 24–28, Nov. 2018, doi: 10.1016/J.CTRO.2018.07.004.

[131] L. M. Bruun, *Development of Novel Biomaterials for Potentiation of Radiotherapy*. DTU Nanotech, 2016.

[132] C. Moreton, “Poor Solubility – Where Do We Stand 25 Years after the ‘Rule of Five’? | American Pharmaceutical Review - The Review of American Pharmaceutical Business & Technology,” Feb. 18, 2021. https://www.americanpharmaceuticalreview.com/Featured-Articles/573402-Poor-Solubility-Where-Do-We-Stand-25-Years-after-the-Rule-of-Five/ (accessed Oct. 05, 2021).

[133] A. E. Hansen *et al.*, “Multimodal soft tissue markers for bridging high-resolution diagnostic imaging with therapeutic intervention,” *Sci. Adv.*, vol. 6, no. 34, Aug. 2020, doi: 10.1126/SCIADV.ABB5353.

[134] J. Chang *et al.*, “A robotic system for 18F-FMISO PET-guided intratumoral pO2 measurements,” *Med. Phys.*, vol. 36, no. 11, p. 5301, 2009, doi: 10.1118/1.3239491.

[135] W. Wang *et al.*, “Carbohydrate based biomarkers enable hybrid near infrared fluorescence and 64 Cu based radio-guidance for improved surgical precision,” *Nanotheranostics*, vol. 5, no. 4, pp. 448–460, 2021, doi: 10.7150/NTNO.60295.

[136] K. Newick, S. O’Brien, E. Moon, and S. M. Albelda, “CAR T Cell Therapy for Solid Tumors,” *Annu. Rev. Med.*, vol. 68, pp. 139–152, Jan. 2017, doi: 10.1146/ANNUREV-MED-062315-120245.

[137] J. M. Michot *et al.*, “Immune-related adverse events with immune checkpoint blockade: a comprehensive review,” *Eur. J. Cancer*, vol. 54, pp. 139–148, Feb. 2016, doi: 10.1016/J.EJCA.2015.11.016.

[138] C. Pasare and R. Medzhitov, “Toll-like receptors: linking innate and adaptive immunity,” *Adv. Exp. Med. Biol.*, vol. 560, pp. 11–18, 2005, doi: 10.1007/0-387-24180-9_2.

[139] J. J. Wu, D. B. Huang, and S. K. Tyring, “Resiquimod: a new immune response modifier with potential as a vaccine adjuvant for Th1 immune responses,” *Antiviral Res.*, vol. 64, no. 2, pp. 79–83, Nov. 2004, doi: 10.1016/J.ANTIVIRAL.2004.07.002.

[140] M. A. Tomai *et al.*, “Immunomodulating and antiviral activities of the imidazoquinoline S-28463,” *Antiviral Res.*, vol. 28, no. 3, pp. 253–264, Nov. 1995, doi: 10.1016/0166-3542(95)00054-P.

[141] Z. Wu, “Drug stability testing and formulation strategies,” *Pharm Dev Technol.*, vol. 23, no. 10, p. 941, Nov. 2018, doi: 10.1080/10837450.2018.1548742.

[142] J. Conner *et al.*, “The Biomanufacturing of Biotechnology Products,” *Biotechnol. Entrep. Starting, Manag. Lead. Biotech Co.*, pp. 351–385, Jan. 2014, doi: 10.1016/B978-0-12-404730-3.00026-9.

[143] M. Jamrógiewicz, “Consequences of New Approach to Chemical Stability Tests to Active Pharmaceutical Ingredients,” *Front. Pharmacol.*, vol. 7, no. FEB, Feb. 2016, doi: 10.3389/FPHAR.2016.00017.

[144] K. Pilaniya, H. K. Chandrawanshi, U. Pilaniya, P. Manchandani, P. Jain, and N. Singh, “Recent trends in the impurity profile of pharmaceuticals,” *J. Adv. Pharm. Technol. Res.*, vol. 1, no. 3, p. 302, Jul. 2010, doi: 10.4103/0110-5558.72422.

[145] R. J. Ouellette and J. D. Rawn, “Carbohydrates,” *Org. Chem.*, pp. 889–928, Jan. 2018, doi: 10.1016/B978-0-12-812838-1.50028-1.

[146] D. Harris, “Quantitative chemical analysis,” *Chem List*, vol. 98, pp. 871–872, 2004.

[147] I. H. T. Guideline, “Stability testing of new drug substances and products,” *Q1A (R2), Curr. step*, vol. 4, pp. 1–24, 2003.

[148] J. R. Murphy and J. D. Hofer, “Establishing Shelf Life, Expiry Limits, and Release Limits,” *Drug Inf. J. DIJ / Drug Inf. Assoc. 2002 364*, vol. 36, no. 4, pp. 769–781, Dec. 2002, doi: 10.1177/009286150203600407.

[149] A. Mann, “Conformational Restriction and/or steric hindrance in medicinal chemistry,” *Pract. Med. Chem. Second Ed.*, pp. 233–250, Jan. 2003, doi: 10.1016/B978-012744481-9/50019-2.

[150] T. L. Andresen, J. Rosager Henriksen, A. E. Hansen, C. F. Melander, E. Serrano Chávez, and L. M. Bruun, “Dissacharide formulations for controlled drug release,” Dec. 17, 2020.

[151] G. Alatrash, H. Jakher, P. D. Stafford, and E. A. Mittendorf, “Cancer immunotherapies, their safety and toxicity,” *Expert Opin. Drug Saf.*, vol. 12, no. 5, pp. 631–645, Sep. 2013, doi: 10.1517/14740338.2013.795944.

[152] R. Baluna and E. S. Vitetta, “Vascular leak syndrome: a side effect of immunotherapy,” *Immunopharmacology*, vol. 37, no. 2–3, pp. 117–132, Oct. 1997, doi: 10.1016/S0162-3109(97)00041-6.

[153] G. Suntharalingam *et al.*, “Cytokine Storm in a Phase 1 Trial of the Anti-CD28 Monoclonal Antibody TGN1412,” *N. Engl. J. Med.*, vol. 355, no. 10, pp. 1018–1028, Sep. 2006, doi: 10.1056/NEJMOA063842.

[154] I. Sagiv-Barfi *et al.*, “Eradication of spontaneous malignancy by local immunotherapy,” *Sci. Transl. Med.*, vol. 10, no. 426, p. 31, Jan. 2018, doi: 10.1126/SCITRANSLMED.AAN4488.

[155] B. Kwong, S. A. Gai, J. Elkhader, K. D. Wittrup, and D. J. Irvine, “Localized immunotherapy via liposome-anchored anti- CD137 + IL-2 prevents lethal toxicity and elicits local and systemic antitumor immunity,” *Cancer Res.*, vol. 73, no. 5, pp. 1547–1558, Mar. 2013, doi: 10.1158/0008-5472.CAN-12-3343.

[156] B. Kwong, H. Liu, and D. J. Irvine, “Induction of potent anti-tumor responses while eliminating systemic side effects via liposome-anchored combinatorial immunotherapy,” *Biomaterials*, vol. 32, no. 22, pp. 5134–5147, Aug. 2011, doi: 10.1016/J.BIOMATERIALS.2011.03.067.

[157] M. Singh *et al.*, “Effective Innate and Adaptive Antimelanoma Immunity through Localized TLR7/8 Activation,” *J. Immunol.*, vol. 193, no. 9, pp. 4722–4731, Nov. 2014, doi: 10.4049/JIMMUNOL.1401160/-/DCSUPPLEMENTAL.

[158] S. Y. Kim *et al.*, “Lyophilizable and Multifaceted Toll-like Receptor 7/8 Agonist-Loaded Nanoemulsion for the Reprogramming of Tumor Microenvironments and Enhanced Cancer Immunotherapy,” *ACS Nano*, vol. 13, no. 11, pp. 12671–12686, Nov. 2019, doi: 10.1021/ACSNANO.9B04207.

[159] A. Fakhari *et al.*, “Thermosensitive Gel-Based Formulation for Intratumoral Delivery of Toll-Like Receptor 7/8 Dual Agonist, MEDI9197,” *J. Pharm. Sci.*, vol. 106, no. 8, pp. 2037–2045, Aug. 2017, doi: 10.1016/J.XPHS.2017.04.041.

[160] F. Vohidov *et al.*, “ABC triblock bottlebrush copolymer-based injectable hydrogels: design, synthesis, and application to expanding the therapeutic index of cancer immunochemotherapy,” *Chem. Sci.*, vol. 11, no. 23, pp. 5974–5986, Jun. 2020, doi: 10.1039/D0SC02611E.

[161] C.-H. Huang *et al.*, “Immunostimulatory TLR7 Agonist-Nanoparticles Together with Checkpoint Blockade for Effective Cancer Immunotherapy,” *Adv. Ther.*, vol. 3, no. 6, p. 1900200, Jun. 2020, doi: 10.1002/ADTP.201900200.

[162] L. Liu *et al.*, “A Biomimetic Polymer Magnetic Nanocarrier Polarizing Tumor-Associated Macrophages for Potentiating Immunotherapy,” *Small*, vol. 16, no. 38, p. 2003543, Sep. 2020, doi: 10.1002/SMLL.202003543.

[163] S. R. De Blanck *et al.*, “Feasibility of a novel liquid fiducial marker for use in image guided radiotherapy of oesophageal cancer,” *Br. J. Radiol.*, vol. 91, no. 1092, 2018, doi: 10.1259/BJR.20180236.

[164] K. A. Ryu, L. Stutts, J. K. Tom, R. J. Mancini, and A. P. Esser-Kahn, “Stimulation of innate immune cells by light-activated TLR7/8 agonists,” *J. Am. Chem. Soc.*, vol. 136, no. 31, pp. 10823–10825, Aug. 2014, doi: 10.1021/JA412314J.

[165] H. Tanji, U. Ohto, T. Shibata, K. Miyake, and T. Shimizu, “Structural reorganization of the Toll-like receptor 8 dimer induced by agonistic ligands,” *Science*, vol. 339, no. 6126, pp. 1426–1429, Mar. 2013, doi: 10.1126/SCIENCE.1229159.

[166] Z. Zhang *et al.*, “Structural Analysis Reveals that Toll-like Receptor 7 Is a Dual Receptor for Guanosine and Single-Stranded RNA,” *Immunity*, vol. 45, no. 4, pp. 737–748, Oct. 2016, doi: 10.1016/J.IMMUNI.2016.09.011.

[167] W. J. Heerink, G. H. de Bock, G. J. de Jonge, H. J. M. Groen, R. Vliegenthart, and M. Oudkerk, “Complication rates of CT-guided transthoracic lung biopsy: meta-analysis,” *Eur. Radiol.*, vol. 27, no. 1, p. 138, Jan. 2017, doi: 10.1007/S00330-016-4357-8.

[168] M. Gao *et al.*, “Preparation and characterization of curcumin thermosensitive hydrogels for intratumoral injection treatment,” *Drug Dev Ind Pharm*, vol. 40, no. 11, pp. 1557–1564, Nov. 2014, doi: 10.3109/03639045.2013.838579.

[169] G. Jianbo *et al.*, “The Anti-Melanoma Efficiency of the Intratumoral Injection of Cucurbitacin-Loaded Sustained-Release Carriers: A PLGA Particle System,” *J. Pharm. Sci.*, vol. 102, no. 8, pp. 2550–2563, Aug. 2013, doi: 10.1002/JPS.23604.

[170] M. Thing, C. Larsen, J. Østergaard, H. Jensen, and S. W. Larsen, “In vitro release from oil injectables for intra-articular administration: Importance of interfacial area, diffusivity and partitioning,” *Eur. J. Pharm. Sci.*, vol. 45, no. 3, pp. 351–357, Feb. 2012, doi: 10.1016/J.EJPS.2011.12.006.

[171] X. Huang and C. S. Brazel, “On the importance and mechanisms of burst release in matrix-controlled drug delivery systems,” *J. Control. Release*, vol. 73, no. 2–3, pp. 121–136, Jun. 2001, doi: 10.1016/S0168-3659(01)00248-6.

[172] B. Bahmani *et al.*, “Intratumoral immunotherapy using platelet-cloaked nanoparticles enhances antitumor immunity in solid tumors,” *Nat. Commun. 2021 121*, vol. 12, no. 1, pp. 1–12, Mar. 2021, doi: 10.1038/s41467-021-22311-z.

[173] W. H. Fridman, F. Pagès, C. Sauts-Fridman, and J. Galon, “The immune contexture in human tumours: impact on clinical outcome,” *Nat. Rev. Cancer 2012 124*, vol. 12, no. 4, pp. 298–306, Mar. 2012, doi: 10.1038/nrc3245.

[174] R. Cristescu *et al.*, “Pan-tumor genomic biomarkers for PD-1 checkpoint blockade-based immunotherapy,” *Science*, vol. 362, no. 6411, Oct. 2018, doi: 10.1126/SCIENCE.AAR3593.

[175] Ascendis Pharma, “Virtual R&D Program Update,” Dec. 14, 2021. https://investors.ascendispharma.com/static-files/5d94248d-2d7a-4825-893b-b47184140e5f (accessed Mar. 11, 2022).

[176] M. Z. Jin and W. L. Jin, “The updated landscape of tumor microenvironment and drug repurposing,” *Signal Transduct. Target. Ther. 2020 51*, vol. 5, no. 1, pp. 1–16, Aug. 2020, doi: 10.1038/s41392-020-00280-x.

[177] R. Baghban *et al.*, “Tumor microenvironment complexity and therapeutic implications at a glance,” *Cell Commun. Signal. 2020 181*, vol. 18, no. 1, pp. 1–19, Apr. 2020, doi: 10.1186/S12964-020-0530-4.

[178] R. A. Flavell, S. Sanjabi, S. H. Wrzesinski, and P. Licona-Limón, “The polarization of immune cells in the tumour environment by TGFβ,” *Nat. Rev. Immunol. 2010 108*, vol. 10, no. 8, pp. 554–567, Jul. 2010, doi: 10.1038/nri2808.

[179] M. J. Smyth, M. W. L. Teng, J. Swann, K. Kyparissoudis, D. I. Godfrey, and Y. Hayakawa, “CD4+CD25+ T regulatory cells suppress NK cell-mediated immunotherapy of cancer,” *J. Immunol.*, vol. 176, no. 3, pp. 1582–1587, Feb. 2006, doi: 10.4049/JIMMUNOL.176.3.1582.

[180] J. Park *et al.*, “Combination delivery of TGF-β inhibitor and IL-2 by nanoscale liposomal polymeric gels enhances tumour immunotherapy,” *Nat. Mater.*, vol. 11, no. 10, p. 895, 2012, doi: 10.1038/NMAT3355.

[181] M. Pickup, S. Novitskiy, and H. L. Moses, “The roles of TGFβ in the tumour microenvironment,” *Nat. Rev. Cancer*, vol. 13, no. 11, p. 788, 2013, doi: 10.1038/NRC3603.

[182] J. Peng *et al.*, “Inhibition of TGF-β signaling in combination with TLR7 ligation re-programs a tumoricidal phenotype in tumor-associated macrophages,” *Cancer Lett.*, vol. 331, no. 2, pp. 239–249, May 2013, doi: 10.1016/J.CANLET.2013.01.001.

[183] J. S. Jørgensen, *A Preclinical Evaluation of Cancer Treatments*. DTU Health Technology, 2018.

[184] Food and Drug Administration (FDA), “LIPIODOL ® (Ethiodized Oil) Injection FOR INTRAUTERINE AND INTRALYMPHATIC ADMINISTRATION ONLY,” Mar. 2014. https://www.accessdata.fda.gov/drugsatfda_docs/label/2014/009190s021lbl.pdf (accessed Feb. 16, 2022).

[185] M. J. Anderton *et al.*, “Induction of heart valve lesions by small-molecule ALK5 inhibitors,” *Toxicol. Pathol.*, vol. 39, no. 6, pp. 916–924, Oct. 2011, doi: 10.1177/0192623311416259.

[186] A. J. Stauber, K. M. Credille, L. L. Truex, W. J. Ehlhardt, and J. K. Young, “Nonclinical Safety Evaluation of a Transforming Growth Factor β Receptor I Kinase Inhibitor in Fischer 344 Rats and Beagle Dogs,” *J. Clin. Toxicol.*, vol. 4, no. 3, pp. 1–10, 2014, doi: 10.4172/2161-0495.196.

[187] H. Wang *et al.*, “Development of small molecule inhibitors targeting TGF-β ligand and receptor: Structures, mechanism, preclinical studies and clinical usage,” *Eur. J. Med. Chem.*, vol. 191, p. 112154, Apr. 2020, doi: 10.1016/J.EJMECH.2020.112154.

[188] R. Park, L. Lopes, C. R. Cristancho, I. M. Riano, and A. Saeed, “Treatment-Related Adverse Events of Combination Immune Checkpoint Inhibitors: Systematic Review and Meta-Analysis,” *Front. Oncol.*, vol. 10, Mar. 2020, doi: 10.3389/FONC.2020.00258.

[189] K. Wu, M. Yi, S. Qin, Q. Chu, X. Zheng, and K. Wu, “The efficacy and safety of combination of PD-1 and CTLA-4 inhibitors: A meta-analysis,” *Exp. Hematol. Oncol.*, vol. 8, no. 1, pp. 1–12, Oct. 2019, doi: 10.1186/S40164-019-0150-0/TABLES/2.

[190] M. Serpico and R. White, “Oil, fat and wax,” *Anc. Egypt. Mater. Technol.*, p. 390, 2000.

[191] A. Lančaričová, M. Havrlentová, D. Muchová, and A. Bednárová, “Oil content and fatty acids composition of poppy seeds cultivated in two localities of Slovakia,” *Agriculture*, vol. 62, no. 1, pp. 19–27, Apr. 2016, doi: 10.1515/AGRI-2016-0003.

[192] A. J. Williams *et al.*, “The CompTox Chemistry Dashboard: A community data resource for environmental chemistry,” *Journal of Cheminformatics*, Nov. 28, 2017. https://comptox.epa.gov/dashboard/chemical/details/DTXSID5059406 (accessed Feb. 17, 2022).

[193] “Lipids.” Michigan State University, [Online]. Available: https://chem.libretexts.org/@go/page/1211.

[194] K. J. Brodbeck, J. R. DesNoyer, and A. J. McHugh, “Phase inversion dynamics of PLGA solutions related to drug delivery: Part II. The role of solution thermodynamics and bath-side mass transfer,” *J. Control. Release*, vol. 62, no. 3, pp. 333–344, Dec. 1999, doi: 10.1016/S0168-3659(99)00159-5.

[195] J. Parasrampuria, L. C. Li, A. Dudleston, and H. Zhang, “The Impact of an Autoclave Cycle on the Chemical Stability of Parenteral Products,” *PDA J. Pharm. Sci. Technol.*, vol. 47, no. 4, 1993.

[196] F. Gellibert *et al.*, “Identification of 1,5-naphthyridine derivatives as a novel series of potent and selective TGF-β type I receptor inhibitors,” *J. Med. Chem.*, vol. 47, no. 18, pp. 4494–4506, Aug. 2004, doi: 10.1021/JM0400247.

[197] M. J. Groves, *Parenteral technology manual: an introduction to formulation and production aspects of parenteral products*. Interpharm Press Incorporated, 1985.

[198] R. P. Watt, H. Khatri, and A. R. G. Dibble, “Injectability as a function of viscosity and dosing materials for subcutaneous administration,” *Int. J. Pharm.*, vol. 554, pp. 376–386, Jan. 2019, doi: 10.1016/J.IJPHARM.2018.11.012.

[199] F. Cilurzo *et al.*, “Injectability Evaluation: An Open Issue,” *AAPS PharmSciTech*, vol. 12, no. 2, p. 604, Jun. 2011, doi: 10.1208/S12249-011-9625-Y.

[200] S. Moondra, N. Raval, K. Kuche, R. Maheshwari, M. Tekade, and R. K. Tekade, “Sterilization of Pharmaceuticals: Technology, Equipment, and Validation,” *Dos. Form Des. Parameters*, vol. 2, pp. 467–519, Jan. 2018, doi: 10.1016/B978-0-12-814421-3.00014-2.

[201] S. Singh and D. Mehta, “Sterilization of pharmaceutical dosage forms,” *Drug Deliv. Asp.*, pp. 169–190, Jan. 2020, doi: 10.1016/B978-0-12-821222-6.00008-7.

[202] E. Ruel-Gariépy and J. C. Leroux, “In situ-forming hydrogels--review of temperature-sensitive systems,” *Eur. J. Pharm. Biopharm.*, vol. 58, no. 2, pp. 409–426, Sep. 2004, doi: 10.1016/J.EJPB.2004.03.019.

[203] J. M. Halpern, C. A. Gormley, M. A. Keech, and H. A. Von Recum, “Thermomechanical Properties, Antibiotic Release, and Bioactivity of a Sterilized Cyclodextrin Drug Delivery System,” *J. Mater. Chem. B. Mater. Biol. Med.*, vol. 2, no. 18, p. 2764, May 2014, doi: 10.1039/C4TB00083H.

[204] E. Memisoglu-Bilensoy and A. A. Hincal, “Sterile, injectable cyclodextrin nanoparticles: Effects of gamma irradiation and autoclaving,” *Int. J. Pharm.*, vol. 311, no. 1–2, pp. 203–208, Mar. 2006, doi: 10.1016/J.IJPHARM.2005.12.013.

[205] K. A. da Silva Aquino, “Sterilization by gamma irradiation,” *Gamma Radiat.*, vol. 9, pp. 172–202, 2012.

[206] S. Turker, A. Yekta Özer, E. Kiliç, M. Özalp, S. Çolak, and M. Korkmaz, “Gamma-irradiated liposome/niosome and lipogelosome/niogelosome formulations for the treatment of rheumatoid arthritis,” *Interv. Med. Appl. Sci.*, vol. 5, no. 2, pp. 60–69, 2013.

[207] P. M. Armenante and O. Akiti, “Sterilization processes in the pharmaceutical industry,” *Chem. Eng. Pharm. Ind. Drug Prod. Des. Dev. Model.*, pp. 311–379, 2019.

[208] J. Busch, “Final report on the safety assessment of propylene carbonate,” *J. Am. Coll. Toxicol.*, vol. 6, no. 1, pp. 23–51, 1987.

[209] European Chemicals Agency (ECHA), “Registration Dossier - Propylene carbonate.” https://echa.europa.eu/registration-dossier/-/registered-dossier/16088/4/23 (accessed Mar. 04, 2022).

[210] A. B. Nair and S. Jacob, “A simple practice guide for dose conversion between animals and human,” *J. Basic Clin. Pharm.*, vol. 7, no. 2, p. 27, 2016, doi: 10.4103/0976-0105.177703.

[211] G. J. S. Dawes, L. E. Fratila-Apachitei, K. Mulia, I. Apachitei, G. J. Witkamp, and J. Duszczyk, “Size effect of PLGA spheres on drug loading efficiency and release profiles,” *J. Mater. Sci. Mater. Med.*, vol. 20, no. 5, pp. 1089–1094, May 2009, doi: 10.1007/S10856-008-3666-0.

[212] J. Yoo and Y. Y. Won, “Phenomenology of the Initial Burst Release of Drugs from PLGA Microparticles,” *ACS Biomater. Sci. Eng.*, vol. 6, no. 11, pp. 6053–6062, Nov. 2020, doi: 10.1021/ACSBIOMATERIALS.0C01228.

[213] R. Galante, T. J. A. Pinto, R. Colaco, and A. P. Serro, “Sterilization of hydrogels for biomedical applications: A review,” *J. Biomed. Mater. Res. Part B Appl. Biomater.*, vol. 106, no. 6, pp. 2472–2492, 2018.

[214] M. A. Vetten, C. S. Yah, T. Singh, and M. Gulumian, “Challenges facing sterilization and depyrogenation of nanoparticles: Effects on structural stability and biomedical applications,” *Nanomedicine Nanotechnology, Biol. Med.*, vol. 10, no. 7, pp. 1391–1399, Oct. 2014, doi: 10.1016/J.NANO.2014.03.017.

[215] G. Alibrandi, S. Coppolino, N. Micali, and A. Villari, “Thermal sterilization of heat- sensitive products using high- temperature short- time sterilization,” *J. Pharm. Sci.*, vol. 90, no. 3, pp. 275–287, Mar. 2001, doi: 10.1002/1520-6017.

[216] D. Cubicciotti and J. H. Davies, “The release of iodine from iodide salts by gamma radiolysis,” *Nucl. Sci. Eng.*, vol. 60, no. 3, pp. 314–319, 1976.

[217] S. Shang, M. T. K. Ling, S. P. Westphal, and L. Woo, “Radiation sterilization compatibility of medical packaging materials,” *J. Vinyl Addit. Technol.*, vol. 4, no. 1, pp. 60–64, 1998.

[218] M. Haji-Saeid, M. H. O. Sampa, and A. G. Chmielewski, “Radiation treatment for sterilization of packaging materials,” *Radiat. Phys. Chem.*, vol. 76, no. 8–9, pp. 1535–1541, Aug. 2007, doi: 10.1016/J.RADPHYSCHEM.2007.02.068.

[219] D. Matagne, N. Delbar, H.-J. Hartmann, M. Gray, and M. Stickelmeyer, “Development of a process using electron beam for a terminal sterilization for parenteral formulations of pharmaceuticals,” *Radiat. Phys. Chem.*, vol. 71, no. 1–2, pp. 421–424, Sep. 2004, doi: 10.1016/J.RADPHYSCHEM.2004.03.041.

[220] A. San Juan *et al.*, “Degradation of chitosan-based materials after different sterilization treatments,” *IOP Conf. Ser. Mater. Sci. Eng.*, vol. 31, no. 1, p. 012007, Feb. 2012, doi: 10.1088/1757-899X/31/1/012007.

[221] S. Çalş, S. Bozda, H. S. Kaş, M. Tunçay, and A. A. Hncal, “Influence of irradiation sterilization on poly(lactide-co-glycolide) microspheres containing anti-inflammatory drugs,” *Farm.*, vol. 57, no. 1, pp. 55–62, Jan. 2002, doi: 10.1016/S0014-827X(01)01171-5.

[222] J. G. Hjørringgaard, C. Ankjærgaard, M. Bailey, and A. Miller, “Alanine pellet dosimeter efficiency in a 40 kV x-ray beam relative to cobalt-60,” *Radiat. Meas.*, vol. 136, p. 106374, Aug. 2020, doi: 10.1016/J.RADMEAS.2020.106374.

[223] H. L. Wong, R. Bendayan, A. M. Rauth, and X. Y. Wu, “Development of solid lipid nanoparticles containing ionically complexed chemotherapeutic drugs and chemosensitizers,” *J. Pharm. Sci.*, vol. 93, no. 8, pp. 1993–2008, 2004, doi: 10.1002/JPS.20100.

[224] H. D. Lu, P. Rummaneethorn, K. D. Ristroph, and R. K. Prud’Homme, “Hydrophobic Ion Pairing of Peptide Antibiotics for Processing into Controlled Release Nanocarrier Formulations,” *Mol. Pharm.*, vol. 15, no. 1, pp. 216–225, Jan. 2018, doi: 10.1021/ACS.MOLPHARMACEUT.7B00824.

[225] A. Patel, R. Gaudana, and A. K. Mitra, “A novel approach for antibody nanocarriers development through hydrophobic ion-pairing complexation,” *J. Microencapsul.*, vol. 31, no. 6, pp. 542–550, 2014, doi: 10.3109/02652048.2014.885606.

[226] H. M. Abdelaziz, A. O. Elzoghby, M. W. Helmy, M. W. Samaha, J. Y. Fang, and M. S. Freag, “Liquid crystalline assembly for potential combinatorial chemo-herbal drug delivery to lung cancer cells,” *Int. J. Nanomedicine*, vol. 14, pp. 499–517, 2019, doi: 10.2147/IJN.S188335.

[227] K. D. Ristroph and R. K. Prud’homme, “Hydrophobic ion pairing: encapsulating small molecules, peptides, and proteins into nanocarriers,” *Nanoscale Adv.*, vol. 1, no. 11, pp. 4207–4237, Nov. 2019, doi: 10.1039/C9NA00308H.

[228] J. D. Meyer and M. C. Manning, “Hydrophobic ion pairing: altering the solubility properties of biomolecules,” *Pharm. Res.*, vol. 15, no. 2, pp. 188–193, 1998, doi: 10.1023/A:1011998014474.

[229] L. Feng, A. De Dille, V. J. Jameson, L. Smith, W. S. Dernell, and M. C. Manning, “Improved potency of cisplatin by hydrophobic ion pairing,” *Cancer Chemother. Pharmacol.*, vol. 54, no. 5, pp. 441–448, Nov. 2004, doi: 10.1007/S00280-004-0840-Z.

[230] S. M. Ansell *et al.*, “Modulating the therapeutic activity of nanoparticle delivered paclitaxel by manipulating the hydrophobicity of prodrug conjugates,” *J. Med. Chem.*, vol. 51, no. 11, pp. 3288–3296, Jun. 2008, doi: 10.1021/JM800002Y.

[231] V. J. Stella, “Prodrugs: Some Thoughts and Current Issues,” *J. Pharm. Sci.*, vol. 99, no. 12, pp. 4755–4765, Dec. 2010, doi: 10.1002/JPS.22205.

[232] J. T. Alander *et al.*, “A review of indocyanine green fluorescent imaging in surgery,” *Int. J. Biomed. Imaging*, vol. 2012, 2012, doi: 10.1155/2012/940585.

[233] T. Desmettre, J. M. Devoisselle, and S. Mordon, “Fluorescence Properties and Metabolic Features of Indocyanine Green (ICG) as Related to Angiography,” *Surv. Ophthalmol.*, vol. 45, no. 1, pp. 15–27, Jul. 2000, doi: 10.1016/S0039-6257(00)00123-5.

[234] National Center for Biotechnology Information, “PubChem Annotation Record for INDOCYANINE GREEN, Source: Hazardous Substances Data Bank (HSDB),” 2022. https://pubchem.ncbi.nlm.nih.gov/source/hsdb/3413#section=Human-Health-Effects (accessed Feb. 24, 2022).

[235] H. Zhou *et al.*, “Hydrophobic Ion Pairing of Isoniazid Using a Prodrug Approach,” *J. Pharm. Sci.*, vol. 91, no. 6, pp. 1502–1511, Jun. 2002, doi: 10.1002/JPS.10116.

[236] T. Satoh *et al.*, “Encapsulation of the synthetic retinoids Am80 and LE540 into polymeric micelles and the retinoids’ release control,” *J. Control. Release*, vol. 136, no. 3, pp. 187–195, Jun. 2009, doi: 10.1016/J.JCONREL.2009.02.024.

[237] Y. H. Song *et al.*, “A novel in situ hydrophobic ion pairing (HIP) formulation strategy for clinical product selection of a nanoparticle drug delivery system,” *J. Control. Release*, vol. 229, pp. 106–119, May 2016, doi: 10.1016/J.JCONREL.2016.03.026.

[238] W. Yin, Z. Dong, X. Chen, N. Finn, and M. Z. Yates, “Hydrophobic ion pairing to enhance encapsulation of water-soluble additives into CO2-swollen polymer microparticles,” *J. Supercrit. Fluids*, vol. 41, no. 2, pp. 293–298, Jun. 2007, doi: 10.1016/J.SUPFLU.2006.09.009.

[239] E. G. Bligh and W. J. Dyer, “A rapid method of total lipid extraction and purification,” *Can. J. Biochem. Physiol.*, vol. 37, no. 8, pp. 911–917, 1959.

[240] R. Wibel, J. D. Friedl, S. Zaichik, and A. Bernkop-Schnürch, “Hydrophobic ion pairing (HIP) of (poly)peptide drugs: Benefits and drawbacks of different preparation methods,” *Eur. J. Pharm. Biopharm.*, vol. 151, pp. 73–80, Jun. 2020, doi: 10.1016/J.EJPB.2020.04.004.

[241] D. D. Stuart and T. M. Allen, “A new liposomal formulation for antisense oligodeoxynucleotides with small size, high incorporation efficiency and good stability,” *Biochim. Biophys. Acta - Biomembr.*, vol. 1463, no. 2, pp. 219–229, Feb. 2000, doi: 10.1016/S0005-2736(99)00209-6.

[242] V. Jain *et al.*, “Ciprofloxacin surf-plexes in sub-micron emulsions: A novel approach to improve payload efficiency and antimicrobial efficacy,” *Int. J. Pharm.*, vol. 409, no. 1–2, pp. 237–244, May 2011, doi: 10.1016/J.IJPHARM.2011.02.020.

[243] H. Yuan, S. P. Jiang, Y. Z. Du, J. Miao, X. G. Zhang, and F. Q. Hu, “Strategic approaches for improving entrapment of hydrophilic peptide drugs by lipid nanoparticles,” *Colloids Surfaces B Biointerfaces*, vol. 70, no. 2, pp. 248–253, May 2009, doi: 10.1016/J.COLSURFB.2008.12.031.

[244] J. Griesser, G. Hetényi, M. Moser, F. Demarne, V. Jannin, and A. Bernkop-Schnürch, “Hydrophobic ion pairing: Key to highly payloaded self-emulsifying peptide drug delivery systems,” *Int. J. Pharm.*, vol. 520, no. 1–2, pp. 267–274, Mar. 2017, doi: 10.1016/J.IJPHARM.2017.02.019.

[245] H. N. Singh, S. M. Saleem, R. P. Singh, and K. S. Birdi, “Micelle formation of ionic surfactants in polar nonaqueous solvents,” *J. Phys. Chem.*, vol. 84, no. 17, pp. 2191–2194, 2002, doi: 10.1021/J100454A016.

[246] S. K. Shah, S. K. Chatterjee, and A. Bhattarai, “The Effect of Methanol on the Micellar Properties of Dodecyltrimethylammonium Bromide (DTAB) in Aqueous Medium at Different Temperatures,” *J. Surfactants Deterg.*, vol. 19, no. 1, pp. 201–207, Jan. 2016, doi: 10.1007/S11743-015-1755-X.

[247] E. Engel *et al.*, “Light-induced decomposition of indocyanine green,” *Invest. Ophthalmol. Vis. Sci.*, vol. 49, no. 5, pp. 1777–1783, Apr. 2008, doi: 10.1167/IOVS.07-0911.

[248] W. Holzer *et al.*, “Photostability and thermal stability of indocyanine green,” *J. Photochem. Photobiol. B Biol.*, vol. 47, no. 2–3, pp. 155–164, Dec. 1998, doi: 10.1016/S1011-1344(98)00216-4.

[249] S. Mindt, I. Karampinis, M. John, M. Neumaier, and K. Nowak, “Stability and degradation of indocyanine green in plasma, aqueous solution and whole blood,” *Photochem. Photobiol. Sci. 2018 179*, vol. 17, no. 9, pp. 1189–1196, Oct. 2020, doi: 10.1039/C8PP00064F.

[250] V. Saxena, M. Sadoqi, and J. Shao, “Degradation Kinetics of Indocyanine Green in Aqueous Solution,” *J. Pharm. Sci.*, vol. 92, no. 10, pp. 2090–2097, Oct. 2003, doi: 10.1002/JPS.10470.

[251] R. Philip, A. Penzkofer, W. Bäumler, R. M. Szeimies, and C. Abels, “Absorption and fluorescence spectroscopic investigation of indocyanine green,” *J. Photochem. Photobiol. A Chem.*, vol. 96, no. 1–3, pp. 137–148, May 1996, doi: 10.1016/1010-6030(95)04292-X.

[252] S. C. Moldoveanu and V. David, “Mobile Phases and Their Properties,” *Essentials Mod. HPLC Sep.*, pp. 363–447, Jan. 2013, doi: 10.1016/B978-0-12-385013-3.00007-0.

[253] A. M. Abend, L. Chung, R. T. Bibart, M. Brooks, and D. G. McCollum, “Concerning the stability of benzyl alcohol: formation of benzaldehyde dibenzyl acetal under aerobic conditions,” *J. Pharm. Biomed. Anal.*, vol. 34, no. 5, pp. 957–962, Mar. 2004, doi: 10.1016/J.JPBA.2003.11.007.

[254] B. Hollins, B. Noe, and J. M. Henderson, “Fluorometric determination of indocyanine green in plasma.,” *Clin. Chem.*, vol. 33, no. 6, pp. 765–768, Jun. 1987, doi: 10.1093/CLINCHEM/33.6.765.

[255] S. Mordon, J. M. Devoisselle, S. Soulie-Begu, and T. Desmettre, “Indocyanine Green: Physicochemical Factors Affecting Its Fluorescence in Vivo,” *Microvasc. Res.*, vol. 55, pp. 146–152, 1998.

[256] G. Carneiro *et al.*, “Formation of ion pairing as an alternative to improve encapsulation and anticancer activity of all-trans retinoic acid loaded in solid lipid nanoparticles,” *Int. J. Nanomedicine*, vol. 7, pp. 6011–6020, 2012, doi: 10.2147/IJN.S38953.

[257] B. K. Poudel *et al.*, “Development of polymeric irinotecan nanoparticles using a novel lactone preservation strategy,” *Int. J. Pharm.*, vol. 512, no. 1, pp. 75–86, Oct. 2016, doi: 10.1016/J.IJPHARM.2016.08.018.

[258] D. Attwood and A. T. Florence, “Surfactants,” in *FASTtrack Physical Pharmacy*, Pharmaceutical Press, 2012, pp. 55–78.

[259] L. Battaglia *et al.*, “Solid lipid nanoparticles for potential doxorubicin delivery in glioblastoma treatment: preliminary in vitro studies,” *J. Pharm. Sci.*, vol. 103, no. 7, pp. 2157–2165, 2014, doi: 10.1002/JPS.24002.

[260] J. R. Lakowicz, *Principles of fluorescence spectroscopy*. Springer, 2006.

[261] T. Mohan, W. Zhu, Y. Wang, and B. Z. Wang, “Applications of chemokines as adjuvants for vaccine immunotherapy,” *Immunobiology*, vol. 223, no. 6–7, pp. 477–485, Jun. 2018, doi: 10.1016/J.IMBIO.2017.12.001.

[262] D. Nobuoka *et al.*, “Intratumoral peptide injection enhances tumor cell antigenicity recognized by cytotoxic T lymphocytes: a potential option for improvement in antigen-specific cancer immunotherapy,” *Cancer Immunol. Immunother.*, vol. 62, no. 4, p. 639, Apr. 2013, doi: 10.1007/S00262-012-1366-6.

[263] C. Breil, M. Abert Vian, T. Zemb, W. Kunz, and F. Chemat, “‘Bligh and Dyer’ and Folch Methods for Solid–Liquid–Liquid Extraction of Lipids from Microorganisms. Comprehension of Solvatation Mechanisms and towards Substitution with Alternative Solvents,” *Int. J. Mol. Sci. 2017, Vol. 18, Page 708*, vol. 18, no. 4, p. 708, Mar. 2017, doi: 10.3390/IJMS18040708.

[264] D. Kushwah, H. B. Patel, P. K. Sinha, and P. K. Jana, “Practical approach for the determination of response factors of impurities in drugs by HPLC,” *E-Journal Chem.*, vol. 8, no. 4, pp. 1504–1511, 2011, doi: 10.1155/2011/462364.

Appendices

Appendix I. SuBen as internal reference

There are two ways to calculate the percentage of drug released from a CarboCell. In *in vitro* release studies, the concentration of drug in the release media namely PBS is measured at different time points and compared to the known amount of drug that was injected. However, such an approach is not possible when performing *in vivo* drug release studies. In this case, at each time point, the injected scaffold in the mice has to be collected in order to calculate the percentage of drug left in the depot. In contrast to the *in vitro* studies, it is not possible to know the precise amount of CarboCell that was injected. Thus, the percentage of drug left in the CarboCell is calculated based on a ratiometric analysis, as described in for example sections 3.3 and 4.5. Hence, we validated that SuBen could be used as a reference for such ratiometric analysis.

SuBen was chosen as an internal reference due to its high hydrophobicity, as it does not partition to the aqueous phase and remains in the self-formed CarboCell scaffold. Therefore, the AUC of SuBen remains constant relative to the AUC of the drug, which decreases as the drug is being released. To validate this approach, the cumulative release of R848 was calculated in an *in vitro* drug release study and afterwards the CarboCells were dissolved to independently determine the percentage of R848 left in the depots using the ratiometric analysis.

After the HPLC analysis, the ratios between the R848 AUC and sucrose octa-benzoate AUC area were calculated. Next, by comparing to a non-injected CarboCell sample (containing 100% of drug) it was possible to calculate the percentage of drug left in the depots (see Box 1). It was determined that on average 38.1% of R848 remained in the gel, which means a drug release of 61.9%. This result is similar to the drug release calculated using the drug concentration in the release media, which is 63.4% (Fig. S1). Thus, ratiometric analysis can also be used to calculate total drug release.

Box 1. Example of calculation of the percentage of drug remaining inside a CarboCell

$$\frac{AUC\ R848}{AUC\ SuBen}\ in\ a\ CarboCell\ containing\ 100\%\ of\ drug = 0.52 \rightarrow Constant\ ratio$$

$$\frac{AUC\ R848}{AUC\ SuBen}\ in\ a\ collected\ CarboCell\ sample = 0.20 \rightarrow Sample\ ratio$$

$$Percentage\ of\ drug\ in\ the\ CarboCell = 100 * \frac{Sample\ ratio}{Constant\ ratio}$$

$$Percentage\ of\ drug\ in\ the\ CarboCell\ (\%) = 100 * \frac{0.20}{0.052} = 38.5\%$$

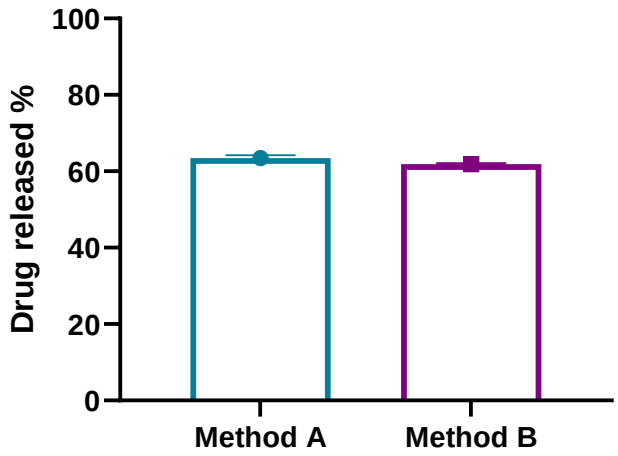

Figure S1. In-vitro release percentage of R848 obtained in two different ways: (method A) by calculating the amount of drug released to the media at different sampling points during 7 weeks and (method B) by calculating the percentage of drug left in the depot at the end of the study. Data is presented as mean ± SD (n=3)

Appendix II. Supplementary information to Chapter 2

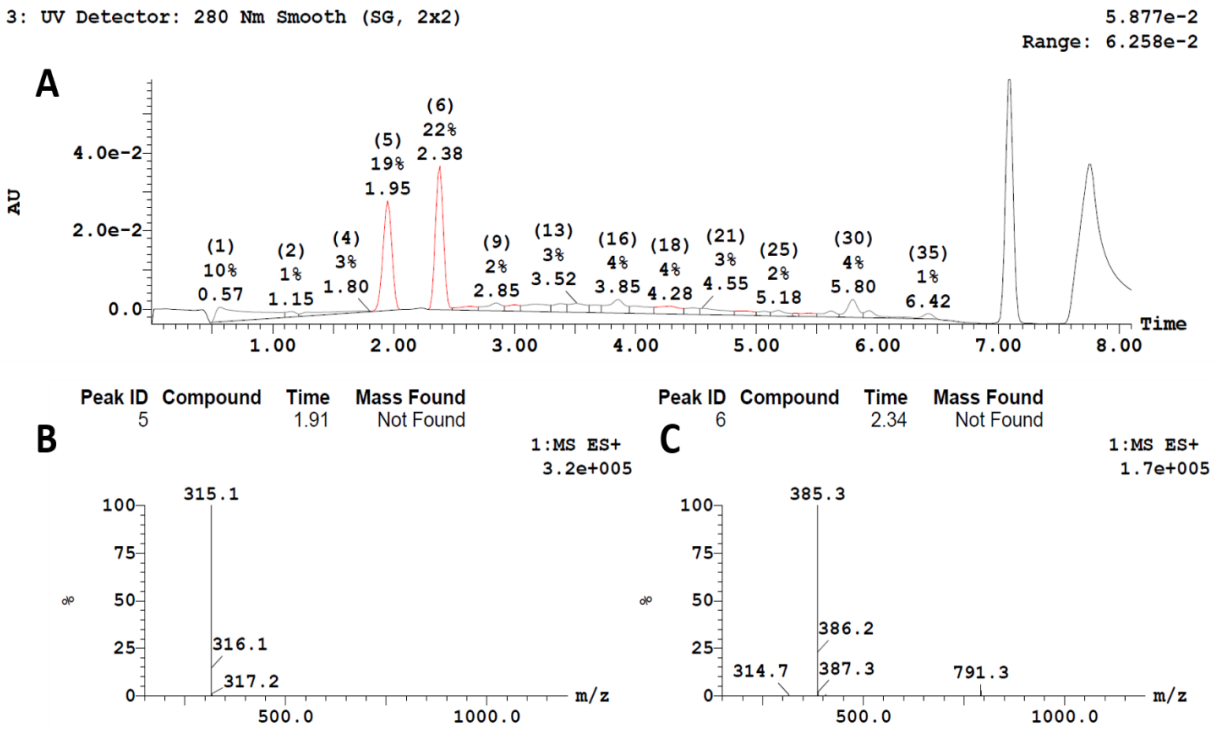

Figure S2. LC-MS analysis results of a sample containing R848 in R2 CC after incubation at 37°C. (**A**)The highlighted peak (5) and peak (6) correspond to R848 and R848-IBA. (**B-C**) m/z values of R848 (**B**) and R84-IBA (**C**).

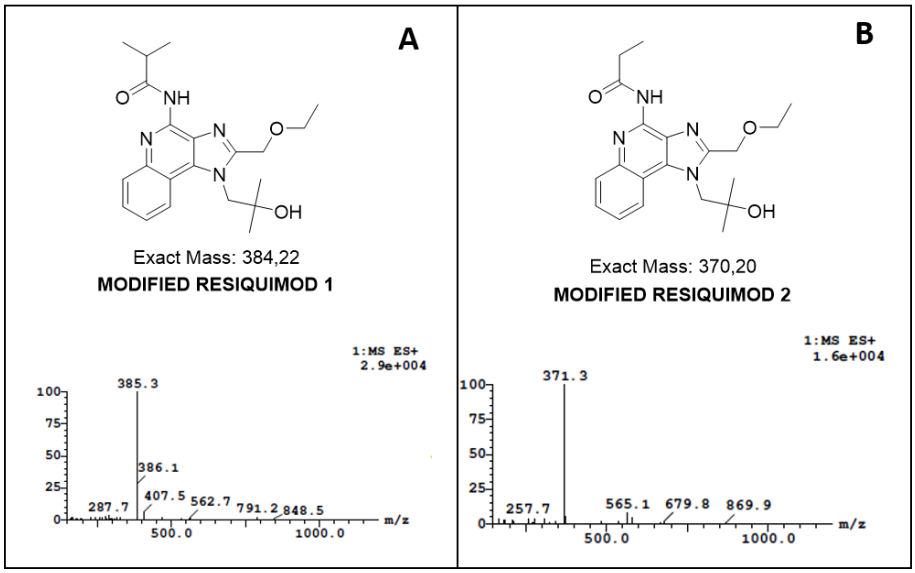

Figure S3. Molecular structure and m/z values measured by LC-MS of the modified versions of R848, which form in (**A**) LOIB- and SAIB-based CarboCells, as well as in (**B**) LAP-based gels formulation.

A

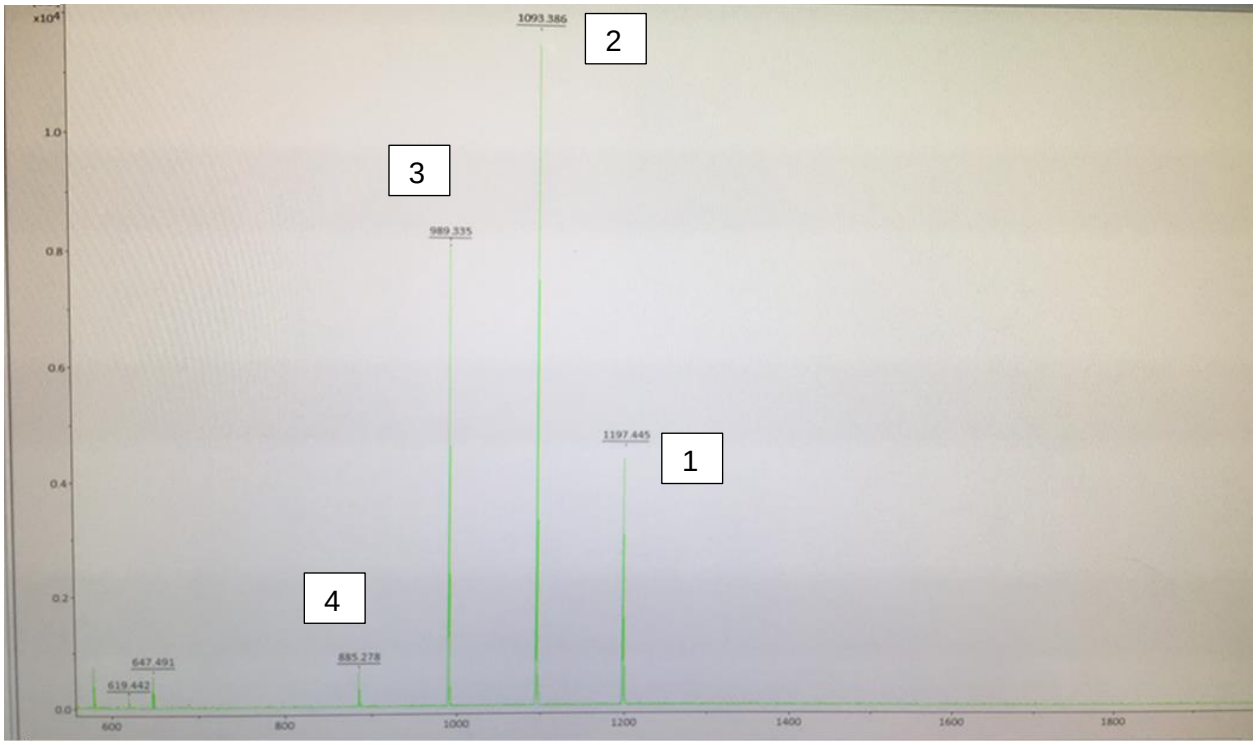

B

Compound	M + 1	M + Na	Peak number
Sucrose octabenzoate	1175.1	1197.4	1
Sucrose heptabenzoate	1071.3	1093.4	2
Sucrose hexabenzoate	967.3	989.3	3
Sucrose pentabenzoate	863.3	885.3	4

Figure S4. Molecular species identified by MALDI-TOF in an σ-SuBen sample. (**A**) Peaks detected by MALDI-TOF, which correspond to sucrose (1) octa-, (2) hepta-, (3) hexa- and (4) penta-benzoate. (**B**) Table specifying the exact mas (M+1) and the detected masses (M+Na).

Appendix III – Supplementary information to Chapter 3

Supplementary materials and methods

Synthesis of R848 prodrugs

All chemicals were purchased from Sigma-Aldrich unless otherwise stated. *O*-(7-azabenzotriazol-1-yl)-1,1,3,3-tetramethyluronium hexafluorophosphate (HATU) used for the solid phase peptide synthesis were purchased from Iris Biotech GmbH. R848 was purchased from Ambeed. All chemicals and reagents were of analytical grade and used without further purification.

Reactions were monitored by thin layer chromatography (TLC); visualization was carried out by UV-light exposure (254 and 365 nm), Cemol and KMnO4-stain. Automated flash column chromatography both reverse- and normal-phase was done on a Büchi Reveleris autoflash. Mass spectra were recorded on a Waters UPLC ESI-MS (Acquity UPCL system with a TUV detector and a QDa single quadrupole MS with ESI detector) by employing a Waters Acquity UPLC® BEH C_{18} (1.7 µm, 2.1 × 50 mm) column. RP-UPLC MS Eluent A consisted of 0.1 % FA in water; Eluent B consisted of 0.1 % FA in CH_3CN. Analytical RP-UHPLC was performed on a UHPLC Shimadzu Nexera-X2 (SPD-M20A PDA detector) using the following columns: (A) Waters XTerra® C_8 (5 µm, 4.6×150 mm) and (B) Waters XTerra® C_{18} (5 µm, 4.6×150 mm). The following analytical gradient was used: 5-100% MeCN in water with 0.1% TFA over 15 min, 1 mL/min.

Preparative HPLC was performed on a Thermo Fisher Ultimate 3000 using a Phenomenex GeminiC18 (5 µm, 110 Å, 30 × 250 mm or 21.2 x 250 mm) column. Preparative HPLC analysis was monitored using UV/VIS detection at 220/280 nm. RP-Prep. HPLC Eluent A consisted of 0.1 % TFA in water; Eluent B consisted of 0.1 % TFA in CH_3CN. NMR spectra were recorded on a Varian Mercury 400 MHz Spectrometer. ^1H and ^{13}C NMR were recorded at 400 and 100 MHz, respectively. Chemical shifts (δ) are reported in ppm relative to the solvents signal peak.

R848-IBA

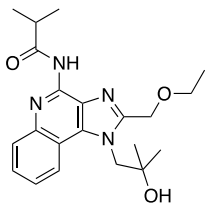

Resiquimod (31.2 mg, 0.099 mmol) was dissolved in dry CH_2Cl_2 (4 mL) in a flame dried round bottom flask fitted with nitrogen atmosphere and a magnetic stirbar. Iso-butyryl chloride (12.5 µL, 0.119 mmol) in CH_2Cl_2 (1 mL) was added to the solution. Triethylamine (27.7 µL, 0.198 mmol) and DMAP (0.6 mg, 0.005 mmol) in CH_2Cl_2 (0.2 µL) was added to the solution and let to react o/n at rt. The reaction was analyzed by UPLC-MS (BEH-C18, 5-100% CH_3CN in H_2O with 0.1% FA over 6 min). The solvent was

evaporated in vacuo. The crude compound was dissolved in CH_3OH (3 mL) and purified by RP-Prep chromatography on an automated Büchi Reveleris system (Prep-C18, 5-50% CH_3CN in H2O with 0.1% FA over 20min, UV-vis: 220, 254 and 280nm, ELSD, Rf-value: 13.5 min). The pure fractions were pooled and lyophilized to a white powder (28 mg, 74% yield). Purity was tested to >98% at both 220/280 nm by analytical UHPLC using column A and eluent gradient 1. ESI MS (*m/z*): Calc. mass $C_{21}H_{28}N_4O_3$ 384.2; found mass $[M+H]^+$ 385.2. ^{1}H NMR (400 MHz, DMSO-d_6) δ ppm: 10.01 (s, 1H), 8.53 (dd, *J* = 8.4, 1.4 Hz, 1H), 7.93 (dd, *J* = 8.3, 1.4 Hz, 1H), 7.62 (ddd, *J* = 8.3, 6.9, 1.3 Hz, 1H), 7.54 (ddd, *J* = 8.3, 6.9, 1.4 Hz, 1H), 5.23 – 4.54 (m, 5H), 3.55 (q, *J* = 7.0 Hz, 2H), 3.13 (hept, *J* = 6.8 Hz, 1H), 1.38 – 1.06 (m, 15H). ^{13}C NMR (101 MHz, DMSO-d_6), *δ* (ppm): 175.54, 143.15, 135.48, 128.61, 126.78, 124.23, 121.55, 116.82, 65.26, 64.65, 54.75, 33.88, 27.42, 19.18, 14.75.

R848-BA

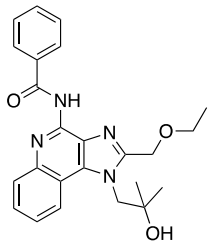

Resiquimod (29.9mg, 0.095 mmol) was dissolved in dry CH2Cl2 (4 mL) in a flame dried round bottom flask fitted with nitrogen atmosphere and a magnetic stirbar. Benzoyl chloride (16.1 µL, 0.14 mmol) in CH2Cl2 (1 mL) was added to the solution. Triethylamine (27 µL, 0.19 mmol) and DMAP (0.5 mg, 4.8 µmol) in CH2Cl2 (0.5 mL) was added to the solution and let to react o/n at rt. The reaction was analyzed by UPLC-MS (BEH-C18, 5-100% CH3CN in H2O with 0.1% FA over 6 min). The reaction was stopped by evaporating the solvent in vacuo. The crude compound was dissolved in CH3OH and purified by RP-Prep chromatography on an automated Büchi Reveleris system (Prep-C18, 5-50% CH3CN in H2O with 0.1% FA over 20min, UV-vis: 220, 254 and 280nm, ELSD). The pure fractions were pooled and lyophilized to a white powder (34 mg, 85% yield). Purity was tested to >98% at both 220/280 nm by analytical UHPLC using column A and eluent gradient 1. ESI MS (*m/z*): Calc. mass $C_{24}H_{26}N_4O_3$ 418.2; found mass $[M+H]^+$ 419.3. ^{1}H NMR (400 MHz, DMSO), δ (ppm): 10.87 (bs, 1H), 8.62 (d, *J* = 8.3 Hz, 1H), 8.10 (d, *J* = 7.6 Hz, 2H), 8.02 (dd, *J* = 8.4, 1.4 Hz, 2H), 7.72 – 7.52 (m, 5H), 4.88 – 4.84 (m, 4H), 3.52 (q, *J* = 7.0 Hz, 2H), 1.21 (s, 6H), 1.13 (t, *J* = 7.0 Hz, 3H). ^{13}C NMR (101 MHz, DMSO), δ (ppm): 132.00, 128.45, 128.15, 127.38, 124.97, 122.16, 70.70, 65.50, 64.96, 54.98, 27.62, 14.99.

R848-C4

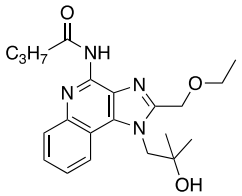

Butyric acid (42 mg, 0.48 mmol) was dissolved in dry DMF (3 mL) and activated with PyBOP (243 mg, 0.47 mmol) for 2 min in a flame dried round bottom flask fitted with nitrogen atmosphere and a magnetic stir bar. Then, a mixture of Resiquimod (50 mg, 0.16 mmol and triethylamine (222 µL, 1.59 mmol) in dry DMF (3 mL) was added and the mixture was stirred for 2 h. The reaction was analyzed by UPLC-MS (BEH-C18, 5-100% CH_3CN in H_2O with 0.1% FA over 6 min). The reaction was left overnight after with the starting material was fully converted and the solvent was evaporated in vacuo. The crude compound was purified by preparative HPLC using a TF prep. system (Phenomenex GeminiC18 (5 µm, 110 Å, 250 x 21.2 mm), 5-100% CH_3CN in H_2O with 0.1% TFA over 20 min, UV-Vis: 220/280nm). The pure fractions were pooled and lyophilized to a white powder (58 mg, 95% yield). Purity was tested to >96% at both 220/280 nm by analytical UHPLC using column A and eluent gradient 1. ESI MS (*m/z*): Calc. mass $C_{21}H_{28}N_4O_3$ 384.2; found mass $[M+H]^+$ 385.3. ^{1}H NMR (400 MHz, DMSO-d_6), δ (ppm): 11.80 (bs, 1H), 8.69 (d, *J* = 8.4 Hz, 1H), 8.26 (d, *J* = 8.4 Hz, 1H), 7.84 – 7.76 (m, 1H), 7.70 (ddd, *J* = 8.4, 7.0, 1.3 Hz, 1H), 5.19 – 4.65 (m, 4H), 3.57 (q, *J* = 7.0 Hz, 2H), 2.76 (t, *J* = 7.3 Hz, 2H), 1.71 (h, *J* = 7.3 Hz, 2H), 1.25 – 1.12 (m, 9H), 0.99 (t, *J* = 7.4 Hz, 3H). ^{13}C NMR (101 MHz, DMSO-d_6), δ (ppm): 175.02, 157.99, 157.67, 154.49, 143.62, 138.33, 129.25, 126.37, 126.06, 124.09, 122.85, 115.78, 70.69, 65.71, 64.57, 55.24, 37.96, 27.57, 18.00, 14.98, 13.57.

R848-C8

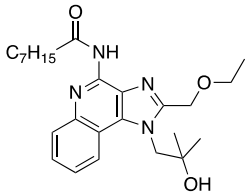

Octanoic acid (68.8 mg, 0.48 mmol) was dissolved in dry DMF (3 mL) and activated with PyBOP (243 mg, 0.47 mmol) for 2 min in a flame dried round bottom flask fitted with nitrogen atmosphere and a magnetic stir bar. Then, a mixture of Resiquimod (50 mg, 0.16 mmol and triethylamine (222 µL, 1.59 mmol) in dry DMF (3 mL) was added and the mixture was stirred for 2 h. The reaction was analyzed by UPLC-MS (BEH-C18, 5-100% CH_3CN in H_2O with 0.1% FA over 6 min). The reaction was left overnight after with the starting material was fully converted and the solvent was evaporated in vacuo. The crude compound was purified by preparative HPLC using a TF prep. system (Phenomenex GeminiC18 (5 µm, 110 Å, 250 x 21.2 mm), 5-100% CH_3CN in H_2O with 0.1% TFA over 20 min, UV-Vis: 220/280nm). The pure fractions were pooled and lyophilized to a white powder (67 mg, 96% yield). Purity was tested to >96% at both 220/280 nm by analytical UHPLC using column A and eluent gradient 1. ESI MS (m/z): Calc. mass $C_{25}H_{36}N_4O_3$ 440.3; found mass [M+H]+ 441.4. ^{1}H NMR (400 MHz, DMSO-d_6), δ (ppm):

11.91 (bs, 1H), 8.70 (d, *J* = 8.4 Hz, 1H), 8.27 (d, *J* = 8.4 Hz, 1H), 7.81 (t, *J* = 7.7 Hz, 1H), 7.71 (t, *J* = 7.7 Hz, 1H), 5.14 – 4.72 (m, 4H), 3.57 (q, *J* = 7.0 Hz, 2H), 2.78 (t, *J* = 7.4 Hz, 2H), 1.67 (q, *J* = 7.2 Hz, 2H), 1.44 – 1.22 (m, 8H), 1.20 (s, 6H), 1.15 (t, *J* = 7.0 Hz, 3H), 0.93 – 0.82 (m, 3H). ^{13}C NMR (101 MHz, DMSO-d_6), δ (ppm): 175.41, 158.03, 157.70, 154.63, 143.57, 129.38, 126.16, 122.91, 115.69, 70.69, 65.72, 64.55, 55.25, 45.88, 45.84, 36.05, 31.17, 28.50, 28.47, 27.59, 25.95, 25.87, 24.48, 22.08, 14.97, 13.96.

R848-C12

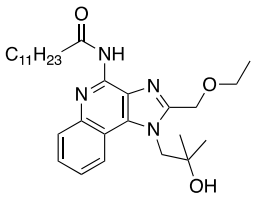

Dodecanoic acid (95.6 mg, 0.48 mmol) was dissolved in dry DMF (3 mL) and activated with PyBOP (243 mg, 0.47 mmol) for 2 min in a flame dried round bottom flask fitted with nitrogen atmosphere and a magnetic stir bar. Then, a mixture of Resiquimod (50 mg, 0.16 mmol and triethylamine (222 µL, 1.59 mmol) in dry DMF (3 mL) was added and the mixture was stirred for 2 h. The reaction was analyzed by UPLC-MS (BEH-C18, 5-100% CH_3CN in H_2O with 0.1% FA over 6 min). The reaction was left overnight after with the starting material was fully converted and the solvent was evaporated in vacuo. The crude compound was purified by preparative HPLC using a TF prep. system (Phenomenex GeminiC18 (5 µm, 110 Å, 250 x 21.2 mm), 5-100% CH_3CN in H_2O with 0.1% TFA over 20 min, UV-Vis: 220/280nm). The pure fractions were pooled and lyophilized to a white powder (66 mg, 84% yield). Purity was tested to >98% at both 220/280 nm by analytical UHPLC using column A and eluent gradient 1. ESI MS (m/z): Calc. mass $C_{29}H_{44}N_4O_3$ 496.3; found mass $[M+H]^+$ 497.4. ^{1}H NMR (400 MHz, DMSO) δ ppm: 11.66 (bs, 1H), 8.67 (d, *J* = 8.4 Hz, 1H), 8.23 (d, *J* = 8.4 Hz, 1H), 7.79 (t, *J* = 7.7 Hz, 1H), 7.69 (t, *J* = 7.7 Hz, 1H), 5.14 – 4.69 (m, 4H), 3.68 (bs, 1H), 3.56 (q, *J* = 7.0 Hz, 2H), 2.77 (t, *J* = 7.3 Hz, 2H), 1.67 (p, *J* = 7.3 Hz, 2H), 1.44 – 1.10 (m, 25H), 0.84 (t, *J* = 6.7 Hz, 3H). ^{13}C NMR (101 MHz, DMSO) δ ppm: 176.75, 157.95, 157.87, 155.97, 143.68, 138.32, 129.11, 126.27, 125.96, 124.53, 122.77, 115.86, 70.69, 65.68, 64.59, 55.22, 36.05, 31.29, 29.03, 29.00, 28.93, 28.80, 28.71, 28.54, 27.56, 24.52, 22.09, 14.97, 13.95.

Synthesis of CT contrast agent CLA-8 (α,β Lactose octa para-iodobenzoate)

Dry solvents were purchased from Acros Organics (AcroSeal, extra dry over molecular sieves). All other chemicals were purchased from Sigma Aldrich and were used as received.

All reactions were carried out under inert atmosphere (N_2). Water sensitive liquids and solutions were transferred via syringe. Water used for washing of the isolated products was in all cases MilliQ water. Organic solutions were concentrated by rotary evaporation at 30-80˚C at 200-0 mbar. TLC was carried out using aluminum sheets pre-coated with silica 60F (Merck 5554). The TLC plates were inspected

under UV light or developed using a cerium ammonium sulphate solution (1% cerium (IV) sulphate $(CeSO_4)_2$ and 2.5% hexa-ammonium molybdate in a 10% sulfuric acid solution).

Nuclear Magnetic Resonance (NMR) was conducted on a Bruker Ascend™ 400 MHz - operating at 401.3 MHz for ^{1}H nmr- with a 5 mm H – Broadband Dual Channel z-gradient Prodigy cryoprobe at 298 K using the residual solvent as internal standard. All coupling constants (*J*) are expressed in Hz. The FID files were processed in Mnova Suite. In ^{1}H-NMR spectra of α,β anomeric mixtures, the integral of H-1 of the most abundant anomer (H-1 β), was set to 1.0 (in case the peaks could be clearly resolved from nearby multiplets), and the percentage of each anomeric species was calculated from the integral ratio of H-1 α and H-1 β. MALDI-TOF MS was conducted on a Bruker Autoflex Speed™ mass spectrometer. The matrix used for MALDI-TOF was a mixture of 2,5 dihydroxy benzoic acid (DHB) spiked with sodium trifluoroacetate in ethanol (60mg/mL). Mass detection of species that could not be detected by MALDI-TOF MS was performed in positive mode on an ESI micrOTOF-Q III (Bruker Daltonics, Bremen, Germany) with a sample flow rate of 180 µL/h. The ions were scanned in the range 50 - 3,000 *m*/*z* with the following settings: Capillary 4,500 V; end plate offset -500 V; nebulizer 0.3 bar; dry gas 4 L/min at 200 °C. The instrument was calibrated prior to the analysis using a solution of 2.5 mM NaOH, 2.25 mM formic acid in 90% *i*-PrOH/water. Preparative flash and prep chromatography was conducted on a Buchi Reveleris™ system generally utilizing Ecoflex 40 g C18 cartridges with a standard gradient of acetonitrile, water and 0.1% Formic acid (FA). Freezedrying was performed on a Cool Safe CS110-4 Pro™ freezedrier, and liquid N_2 was utilized to freeze the samples.

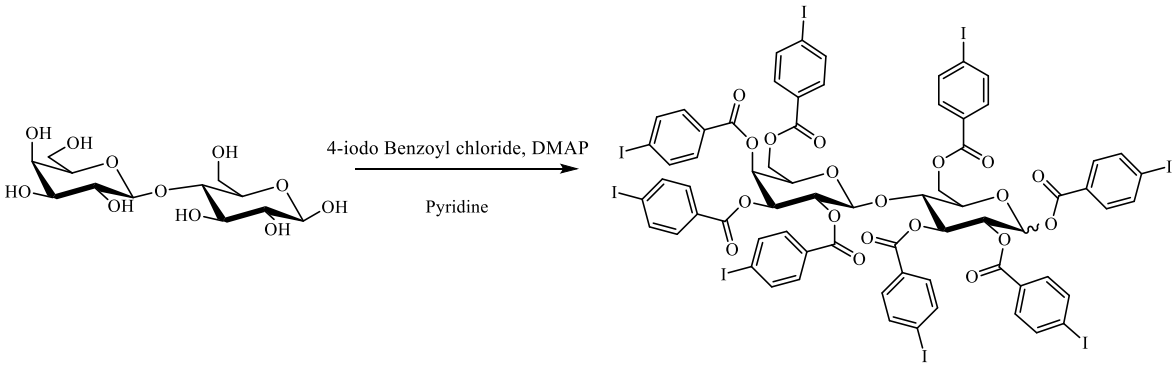

β-lactose (3.4g, 10 mmol) was suspended in dry pyridine (100 mL) under inert atmosphere (N_2). Hereafter para-iodobenzoyl chloride (25 g, 95 mmol, 1.2 eq. pr. hydroxyl group) was carefully added. Then, a catalytic amount of DMAP (121 mg, 0.1 eq.) was added, and the mixture was sonicated under inert atmosphere at 50^{0}C for 20 minutes for complete dissolution of all reagents. Then the reaction was heated to 65˚C and continued overnight, whereafter TLC (5% acetone, toluene) and QTOF-MS showed complete acylation of the starting material. The reaction was cooled down to room temperature and a precipitate formed, which was filtered off through suction filtration. The supernatant was then cooled to 2^{0}C and further precipitate was filtered off, whereafter the supernatant was concentrated under reduced pressure. The concentrate was dissolved in dichloromethane and washed with $NaHCO_3$ (aq.) (8 x 100 mL), brine (1 x 100 mL) and water (1 x 100 mL). The organic phase was dried with $MgSO_4$ (s), filtered, concentrated under reduced pressure and dried *in vacuo.* The solid was recrystallized from dichloromethane:ethanol 1:5 to give a white crystalline compound. Yield: 12.9 g (60%) (~25% alpha,

~75% beta anomer). ^{1}H NMR (400 MHz, DMSO-d6) δ 7.99 (d, J = 8.4 Hz, 1H), 7.94 – 7.42 (m, 37H), 7.28 (dd, J = 8.6, 2.9 Hz, 3H), 6.60 (d, J = 3.7 Hz, 0.3H), 6.40 (d, J = 8.0 Hz, 1H), 6.06 (t, J = 9.0 Hz, 1H), 5.95 (t, J = 9.7 Hz, 0.3H), 5.86 – 5.72 (m, 1H), 5.64 (dd, J = 7.5, 3.5 Hz, 1H), 5.56 (dd, J = 10.1, 3.8 Hz, 0.3H), 5.50 (t, J = 8.7 Hz, 1H), 5.43 – 5.31 (m, 3H), 4.69 – 4.41 (m, 4H), 4.39 – 4.27 (m, 3H), 3.99 (dd, J = 11.2, 6.6 Hz, 1H), 3.87 – 3.70 (m, 1H). QTOF-MS: Calculated mass $[M+ Na]^{+}$: 2204.50. Found: 2204.40.

Solubility test

1 mL of PBS, PBS with 5% DMSO or PBS with 8% DMSO were added to aliquots containing 3 mg of drug (R848, R848-IBA, R848-C4 or R848-C8). A magnetic stirrer was placed inside each vial and the solutions were stirred (100 rpm) at room temperature for 24 h. Afterwards, the solutions were filtered using a 0.45 µm nylon filter and a 1-mL syringe and the samples were analysed by UHPLC. The analysis were performed in a Shimadzu Nexera-X UHPLC with a PDA detector using the following settings. Samples were injected (5 µL) onto a Waters Terra XBridge® BEH C8 column (2.5 µm, 4.6x75mm, temperature 25 °C) at a flow rate of 0.8 mL/min. The solvent system consisted of mobile phase A (5% MeCN, 0.1% TFA in water) and mobile phase B (0.1% TFA in MeCN). The gradient was 0% B for 1 min, 0 to 100% B in 5 min, 100% B for 1.5 min, 100% B to 0% B in 0.5 min, 0% B for 1 min. UV detection at 240 nm was used to measure the AUC of each drug molecule and the drug concentration was calculated with a standard curve.

Stability of R848 prodrugs in different solvents

A stock solution of each prodrug was made (0.5 mg/mL) in dimethyl sulfoxide (DMSO), propylene carbonate (PC), benzyl alcohol (BnOH) and ethanol (EtOH). Aliquots of 300 µL were made of the stock solutions in HPLC vials. The HPLC aliquots were loaded into a Shimadzu Nexera-X2 UHPLC (PDA detector) and stored at 40°C in the autosampler for the accelerated stability study. At each time point, 10µL of each aliquot were analyzed by UHPLC using a Waters XTerra® C_8 (5 µm, 4.6×150 mm) column with the following method settings: Eluent A consisted of 0.1 % TFA and 5 % CH_3CN in MilliQ water; HPLC Eluent B consisted of 0.1 % TFA in CH_3CN; gradient: 5-100% B over 15 min; column oven: 40°C. The AUC at 280 nm and 320 nm was measured and the prodrug stability was evaluated by comparing the AUC of the parent compound relative to the AUC of generated impurities over a period of 0 h to minimum 40 h.

Stability studies

CarboCells (CC1, CC2 and CC3) were prepared as described in the “Materials and methods” section. The SuBen:PC and SuBen:DMSO formulations had a weight ratio of 60:40. All tested solutions and CarboCells had equimolar drug concentrations (R848-IBA (1.47 mg/g), R848-C4 (1.47 mg/g), R848-C8 (1.68 mg/g), R848-C12 (1.90 mg/g)). After drug loading, the resulting formulation was divided in equal parts and each sealed aliquot was incubated at either 40, 4 or -20°C. At each sampling point, 25 µL of

each vial were taken and dissolved in 500 µL of DMSO (for CC3 formulations) or acetonitrile. Samples were analyzed on a Shimadzu Nexera-X UHPLC. Samples were injected (5 µL) onto a Waters Terra XBridge® BEH C18 column (2.5 µm, 4.6x75mm, temperature 40 °C) at a flow rate of 0.8 mL/min. The solvent system consisted of mobile phase A (5% MeCN, 0.1% TFA in water) and mobile phase B (0.1% TFA in MeCN). The gradient was 0% B for 1 min, 0 to 100% B in 5 min, 100% B for 8 min, 100% B to 0% B in 0.5 min, 0% B for 1 min. UV detection at 320 nm was used to measure the AUC of the drug molecules and any related impurities. Since R848 is a product from the prodrug's activation, prodrug stability is reported as the AUC percentage of the corresponding prodrug in a given sample.

In vivo release (intratumoral injection)

CT26 tumors were established in 7 weeks old female BALB/c Jrj mice as done for the *in vivo* mouse therapy study. R848 (1.2 mg/g), R848-IBA (1.47 mg/g) and R848-C8 (1.68 mg/g) were formulated in CC1 CarboCells. For each CarboCell, 50 µL were injected intratumorally in the mice (mice were anesthetized using ~3-5% sevoflurane during injections). At each sampling point, mice were euthanized and the CarboCell depots were collected. Such depots were immediately dissolved in 1 mL acetonitrile and incubated at room temperature overnight. Sample preparation, UHPLC analysis and calculation of the percentage of released drug was done as described for the *in vivo* release study in the "Materials and methods" section.

Supplementary tables and figures

Table S5. Solubility of R848 and R848 prodrugs in different solvents at 25°C.

Drug molecule	Solubility in PBS (µg/mL)	Solubility in PBS, 5% DMSO (µg/mL)	Solubility in PBS, 8% DMSO (µg/mL)
R848	≥ 1000	≥ 1000	≥ 1000
R848-IBA	280	390	480
R848-C4	160	240	280
R848-C8	20	50	120

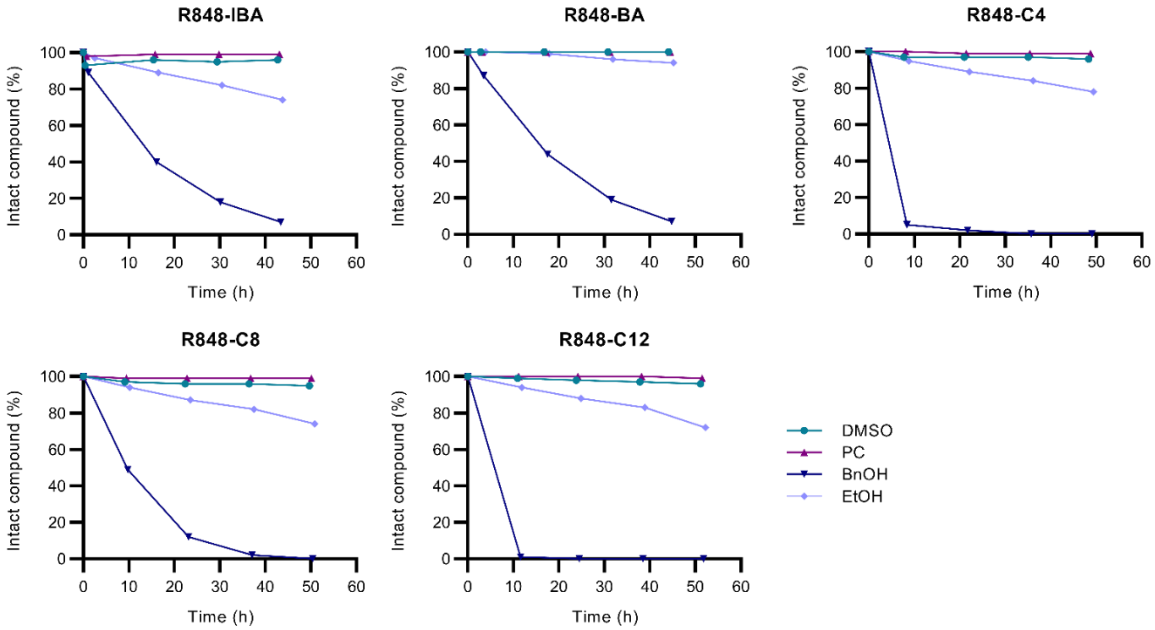

Figure S6. Accelerated stability of R848 prodrugs in DMSO, PC, BnOH and EtOH. 300-µL aliquots with a concentration of 0.5 mg/mL drug were incubated at 40°C in the autosampler tray of a Shimadzu Nexera-X2 UHPLC; 10 µL samples were taken at specified time points and analyzed by UHPLC. Results are shown as the percentage of intact prodrug in different solvents overtime (calculated as the AUC of the prodrug relative to the AUC of generated activation/degradation products measured at 320 nm).

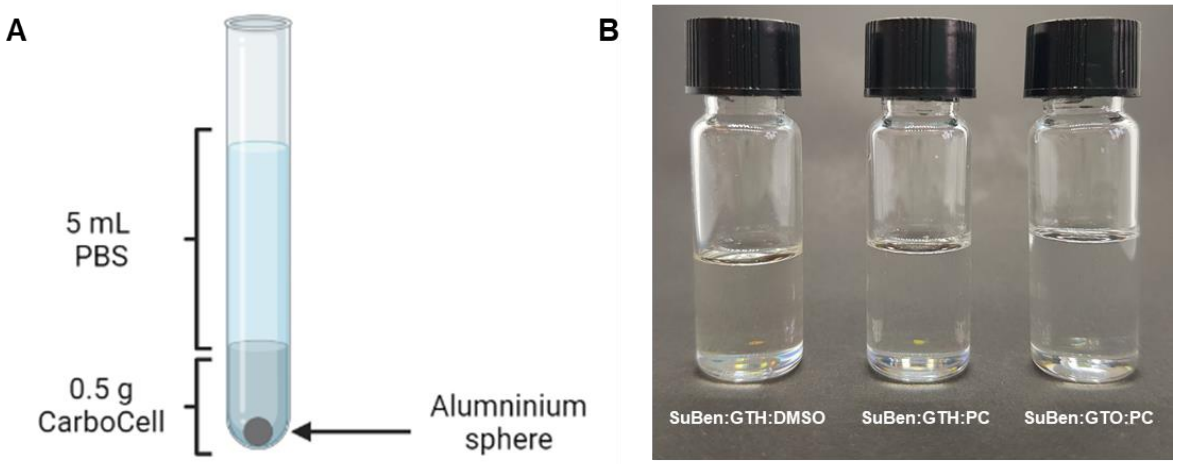

Figure S6. (**A**) Schematic illustration of the experimental setup to evaluate the viscosity of the CarboCell as an effect of solvent release over time. (**B**) Appearance of the tested CarboCell formulations, all with a composition of 60:20:20.

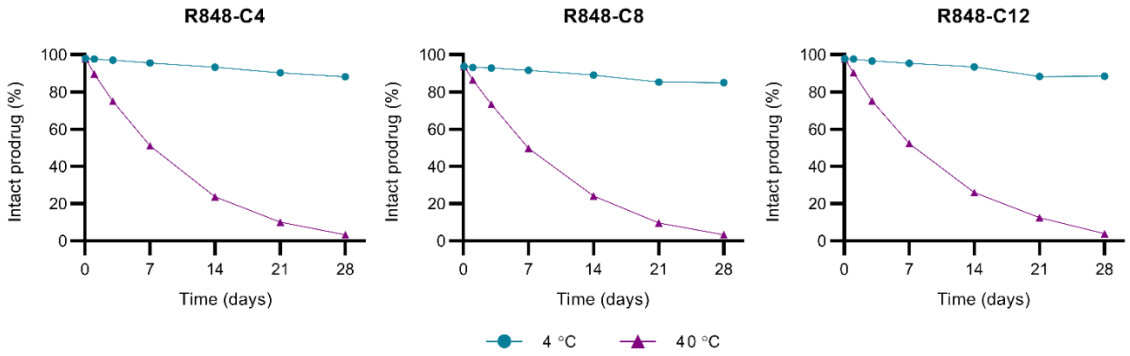

Figure S7. Stability of R848-C4, R848-C8 and R848-C12 formulated in equimolar concentrations (1.47 mg/g, 1.68 mg/g and 1.90 mg/g, respectively) in CC1 formulation. Aliquots of each formulation were stored either at 40°C or 4°C during 4 weeks and samples were taken at the designated time points. The percentage of intact prodrug was calculated as the AUC of the prodrug relative to the AUC of generated activation/degradation products measured at 320 nm by UHPLC.

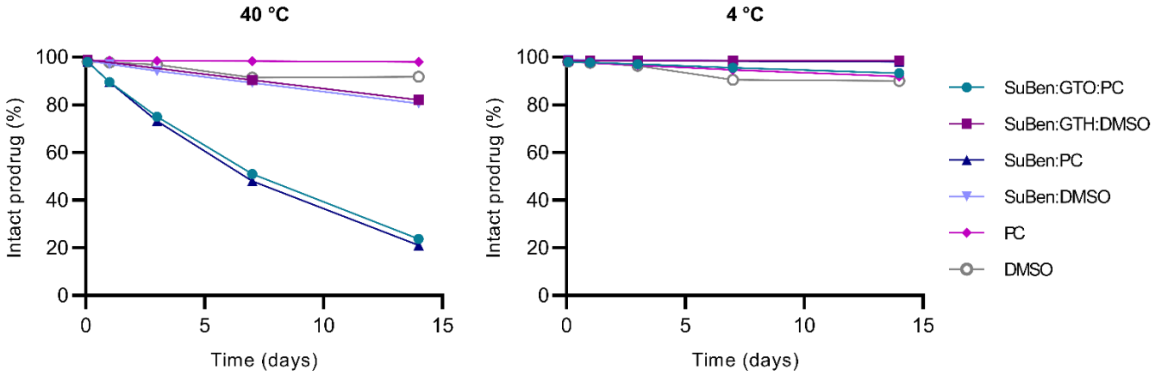

Figure S8. Stability of 1.47 mg/g R848-C4 at 40°C and 4°C in CarboCell CC1 and CC2, CarboCell without co-solvents (SuBen:PC and SuBen:DMSO), and in sole solvents (PC and DMSO). The percentage of intact prodrug was calculated as the AUC of the prodrug relative to the AUC of generated activation/degradation products measured at 320 nm by UHPLC.

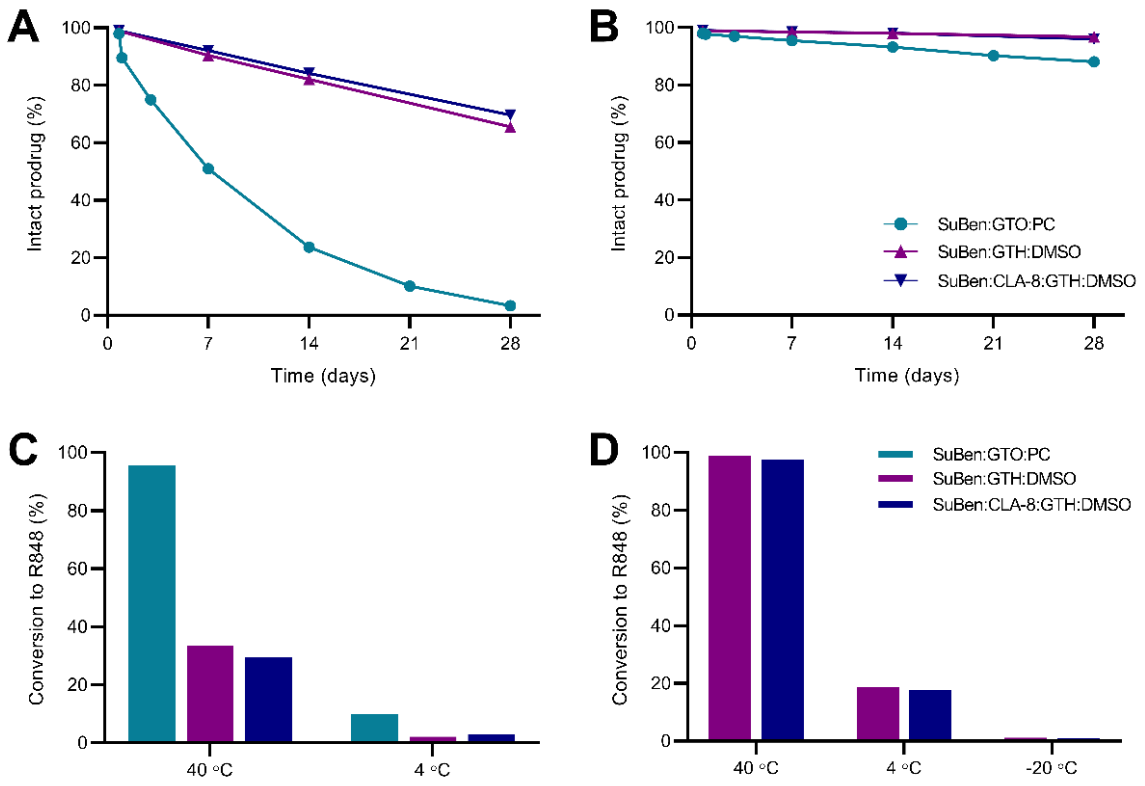

Figure S9. Stability of 1.47 mg/g R848-C4 in CC1, CC2 and CC3. (**A**) Percentage of intact R848-C4 in CarboCell formulations incubated at 40°C during 4 weeks. (**B**) Percentage of intact R848-C4 in CarboCell formulations incubated at 4°C during 4 weeks. (**C**) Percentage of R848-C4 that was converted into R848 after 4 weeks of incubation at either 40°C or 4°C. (**D**) Percentage of R848-C4 that was converted into R848 after 9 months of incubation at either 40°C, 4°C or -20°C. The percentage of R848-C4 was calculated as the AUC of the prodrug relative to the AUC of generated activation/degradation products measured at 320 nm.

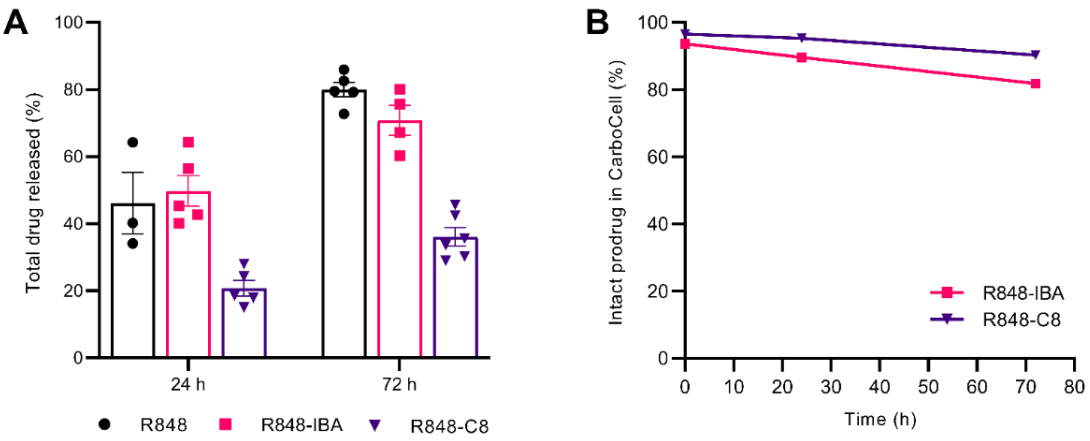

Figure S10. In-vivo release profiles and stability of R848, R848-IBA and R848-C8 from CC1 after i.t. injection in mice. (**A**) Percentage of R848 and prodrugs released from CarboCells calculated from the amount of drug retained in the collected depots. (**B**) Percentage of intact prodrug (R848-IBA and R848-C8) present in the CarboCell depots collected from the mice. The AUC of R848 and the prodrugs was measured by HPLC (UV detection at 320 nm) and the reported values correspond to the AUC percentage of prodrug in a given sample. Data points are shown as mean ± SEM (n=3-5).

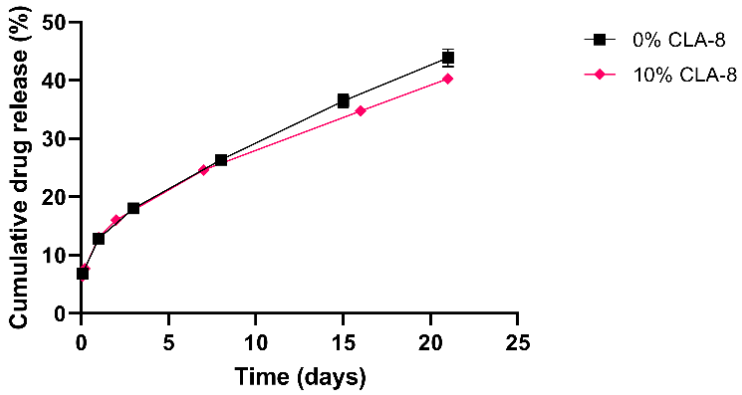

Figure S11. In vitro release profile of 1.2 mg/g R848 formulated in CarboCell containing either 0% (CC2) or 10% CLA-8 (CC3). Data is shown as mean ± SEM (n=3).

Appendix IV. Supplementary information to Chapter 4

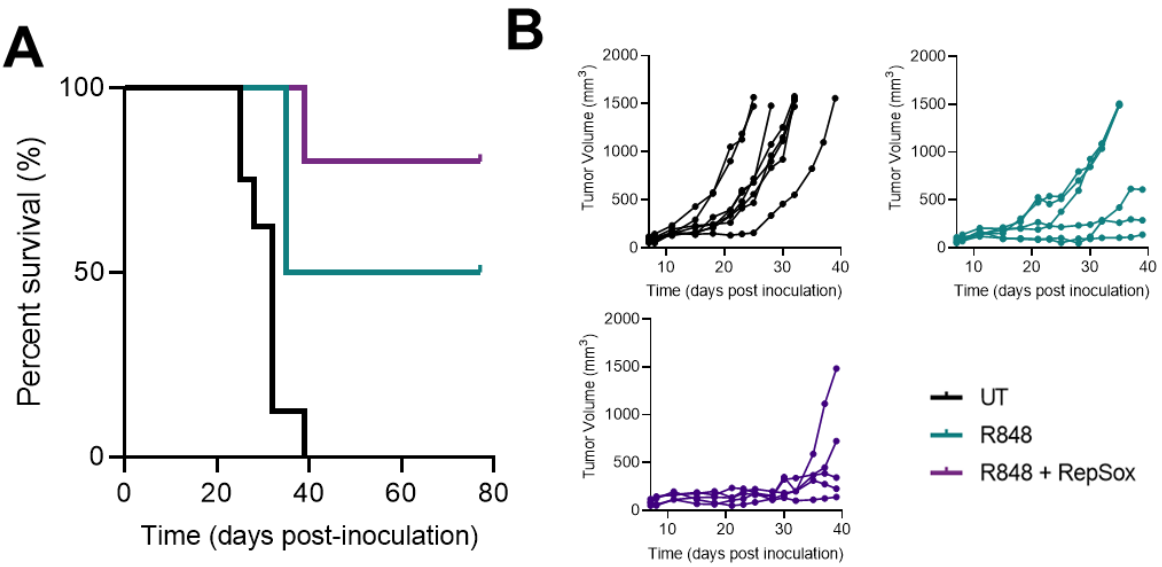

Figure S12. Therapeutic efficacy of N1 CC in mice bearing EMT-6 tumors. Mice were treated weekly four times with N1 CC for a dosing of 7.5 mg/kg R848 or 7.5 mg/kg R848 plus 8 mg/kg RepSox. (**A**) Kaplan-Meyer plot of mice survival for treatment groups and control. (**B**) Individual tumor growth curves. Abbreviations: UT=untreated.

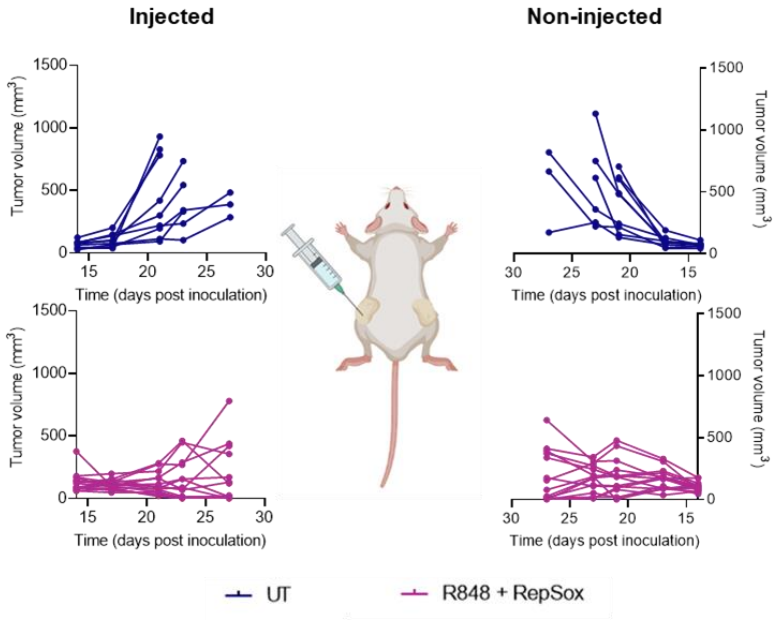

Figure S13. Individual tumor growth curves of mice bearing CT26 tumors. Mice were treated weekly four times with the N1 CC containing R848 and RepSox (7.5 mg/kg and 20 mg/kg, respectively), though only one tumor was injected. An untreated (UT) group was included as control.

Table S14. Estimated viscosity of the self-formed depots of different CarboCell formulations. The viscosity was determined following the procedure described in section 3.3.

Formulation components	Composition (w/w%)	Sugar / co-solvent ratio	Viscosity of final depots (mPa·s)
σ-SuBen:CLA-8:GTH:DMSO	50:10:20:20	3	343000
π-SuBen:CLA-8:GTH:DMSO	50:10:20:20	3	269000
σ-SuBen:GTO:EtOH	60:25:15	*2.4*	202000
σ-SuBen:GTH:EtOH	60:25:15	*2.4*	56800

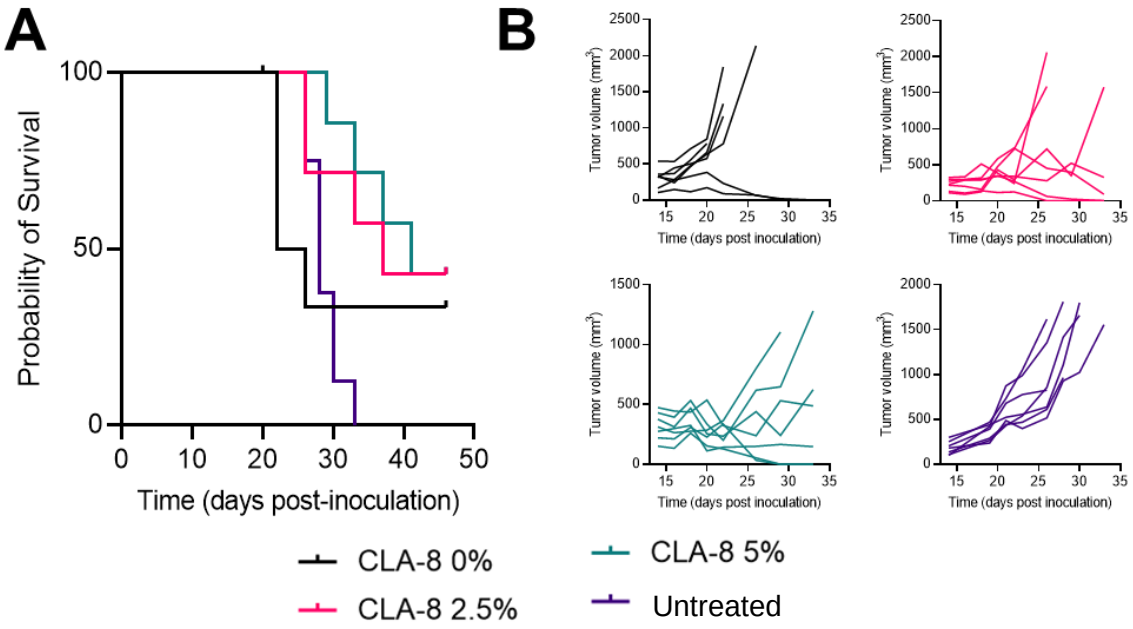

Figure S15. Therapeutic efficacy of CC11, CC12 and CC13 in mice. Mice bearing CT26 tumors were treated biweekly two times with CC11 (0% CLA-8), CC12 (2.5% CLA-8) and CC13 (5% CLA-8) with a concentration of 3 mg/g R848 + 16 mg/kg RepSox. (**A**) Kaplan-Meyer plot of mice survival for treatment groups and control. (**B**) Individual tumor growth curves.

Table S16. Stability of the N1 CC formulation containing 3 mg/g R848 and 8 mg/g RepSox after being subjected to steam autoclaving. The stability is reported as the AUC percentage of potential modified drug substances present in the formulation. If the molecule was not detected, this is reported as 0.0.

	R848-BA	RepSox-BA
Before autoclave	0.0	0.0
After autoclave	0.5	0.0

Table S17. Stability of the N1 CC formulation containing 3 mg/g R848 and 8 mg/g RepSox after incubation at either 40°C or 4°C. The stability is reported as the AUC percentage of potential modified drug substances present in the formulation at the time of measurement. If the molecule was not detected, this is reported as 0.0.

Time	40 °C		4 °C	
	R848-BA	*RepSox-BA*	*R848-BA*	*RepSox-BA*
T0	0.0	0.0	0.0	0.0
4 months	0.3	0.0	0.0	0.0
5 months	0.3	0.0	0.0	0.0
6 months	0.3	0.0	0.0	0.0
7 months	0.5	0.0	0.0	0.0
13 months	0.5	0.2	< 0.1	0.0

Table S18. Stability of the CC11 formulation containing 12 mg/g R848 and 16 mg/g RepSox after incubation at either 40°C or 4°C. The stability is reported as the AUC percentage of potential modified drug substances present in the formulation at the time of measurement. If the molecule was not detected, this is reported as 0.0.

Time	40 °C		4 °C	
	R848-BA	*RepSox-BA*	*R848-BA*	*RepSox-BA*
T0	0.0	0.0	0.0	0.0
1 month	0.5	0.0	0.0	0.0
2 months	0.8	0.5	0.0	0.0
3 months	1.1	0.6	0.0	0.0
9 months	2.5	0.4	< 0.1	0.0

Appendix V. Supplementary information to Chapter 5

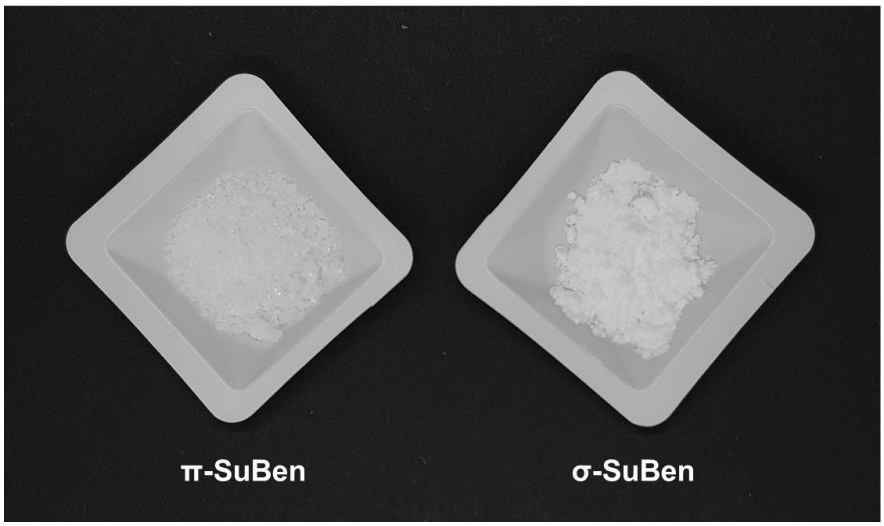

Figure S19. Physical appearance of π-SuBen and σ-SuBen. The former is a crystalline powder, while the latter is a compact powder. σ-SuBen is supplied by Sigma Aldrich and π-SuBen is obtained from the purification of such material.

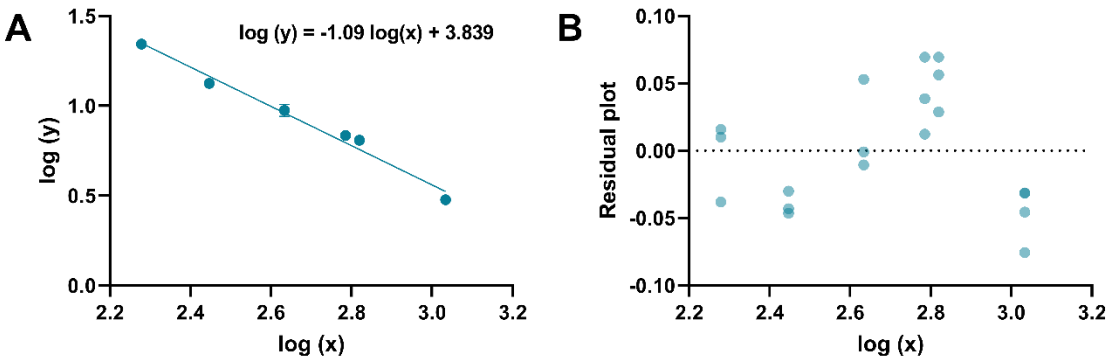

Figure S20. Correlation between viscosity and burst release for SuBen:GTH:DMSO formulations with or without CLA-8. (**A**) Linear regression analysis from the data log transformation in which y= percentage of drug released 2 h post-injection and x= viscosity at 37°C. (**B**) Random residuals graphs of the fitted function.

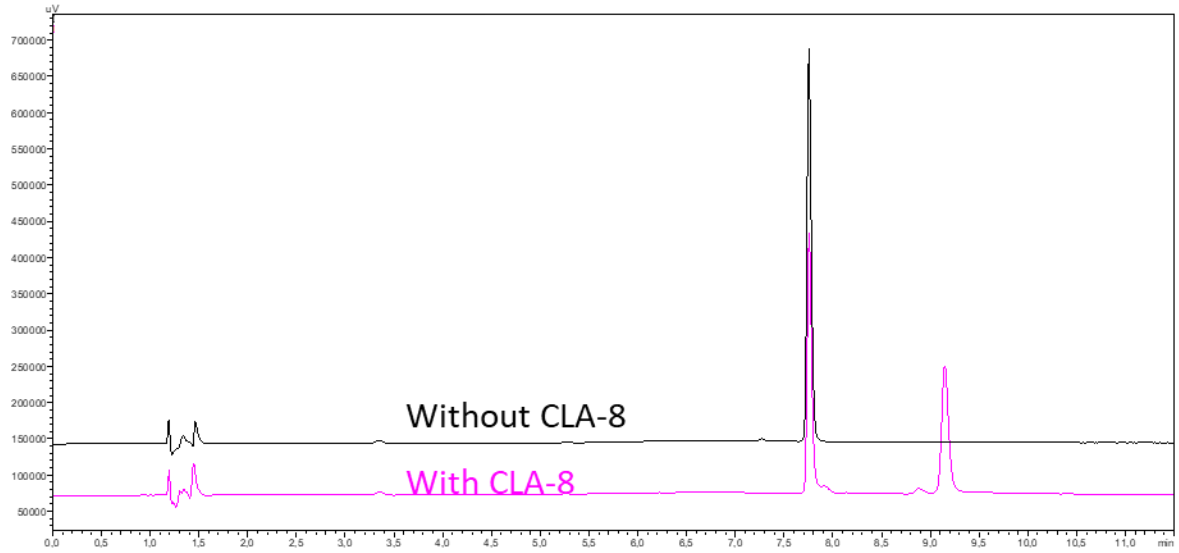

Figure S21. Comparison of individual chromatograms of CC11 (with CLA-8) and CC17 (without CLA-8) after irradiation of 30 kGy. SuBen and CLA-8 have a retention time of 7.7 min and 9.2, respectively. A possible degradation product from CLA-8 is observed at 8.9 min. Detection wavelength: 280 nm.

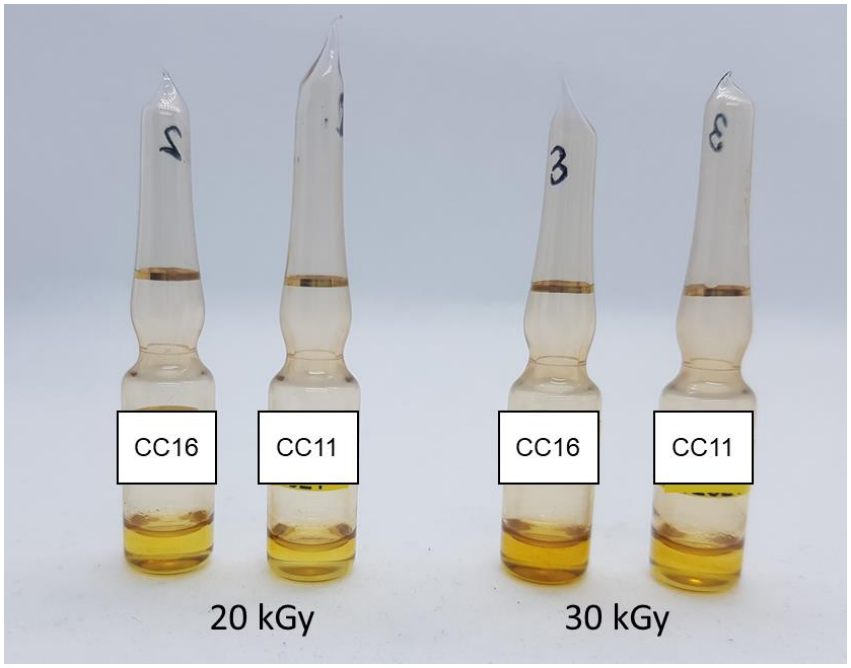

Figure S22. Glass ampoules containing formulations CC11 and CC16 (1.2 mg/g R848 + 8 mg/g RepSox) after irradiation at 20 kGy and 30 kGy.

Estimation of response factor for the CLA-8 derived impurity

In chromatography, a response factor (RF) is defined as the ratio between the AUC of an analyte and the amount of such molecule present in the sample. Usually, the response factor is calculated using a standard a calibration curve for the molecule of interest. However, in our case, there are no reference standards for the impurity derived from CLA-8. So, in order to see if CLA-8 and the CLA-8-derived impurity display similar UV responses at 280 nm, dilutions of a sample containing both molecules were done and then analyzed by HPLC. If both molecules had the same extinction coefficient, then the percentage of AUC corresponding to the impurity would remain constant throughout the dilutions. Samples of dissolved CarboCells subjected to 30 kGy of radiation were diluted with DMSO and analyzed by UHPLC (method specified in section 5.5). The RF was calculated using equation 3, shown below [264].

$$Response\ factor\ (RF) = \frac{Theoretical\ AUC\ \%\ (undiluted\ samples)}{Actual\ AUC\%\ (diluted\ samples)} \qquad \text{(Equation 3)}$$

Table S23. Estimation of the RF of the CLA-8 derived impurity in CC11. Previously dissolved samples of CC11 subjected to 30 kGy of irradiation were diluted in DMSO in the ratios indicated in the table. The AUC percentage corresponding to the CLA-8 impurity were obtained from the UHPLC chromatogram at 280 nm.

Sample solution	% Impurity AUC	RF value	Mean RF value
CC11 (100%)	3.85		
CC11 (75%) + DMSO (25%)	3.78	1.018	
CC11 (50%) + DMSO (50%)	4.04	0.952	0.965
CC11 (25%) + DMSO (75%)	4.16	0.925	

Table S24. Estimation of the RF of the CLA-8 derived impurity in CC16. Previously dissolved samples of CC16 subjected to 30 kGy of irradiation were diluted in DMSO in the ratios indicated in the table. The AUC percentage corresponding to the CLA-8 impurity were obtained from the UHPLC chromatogram at 280 nm.

Sample solution	% Impurity AUC	RF value	Mean RF value
CC16 (100%)	5.69		
CC16 (75%) + DMSO (25%)	5.29	1.075	
CC16 (50%) + DMSO (50%)	5.57	1.022	1.025
CC16 (25%) + DMSO (75%)	5.83	0.977	

The average RF value from both samples was 0.995 (Tables X and X). Since the RF value is very close to 1.0, we might assume that the CLA-8 derived impurity has comparable UV properties as CLA-8 at 280 nm.

Appendix VI. Supplementary information to Chapter 6

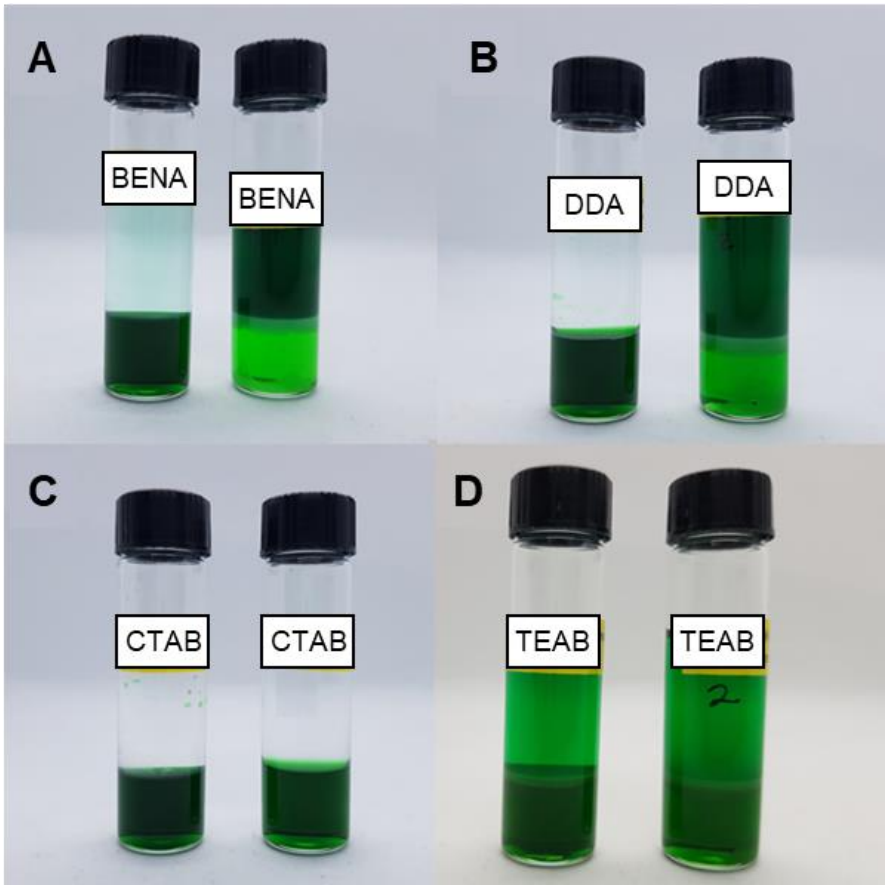

Figure S25. Effect of pH on complexation efficiency. HIP complexation of ICG with the co-ions (**A**) BENA, (**B**) DDA, (**C**) CTAB and (**D**) TEAB using the Bligh-Dyer method. HIP complexing was done using either ICG dissolved in 0.01 M HCl (vials on the left) or in sole MQ (vials on the right).

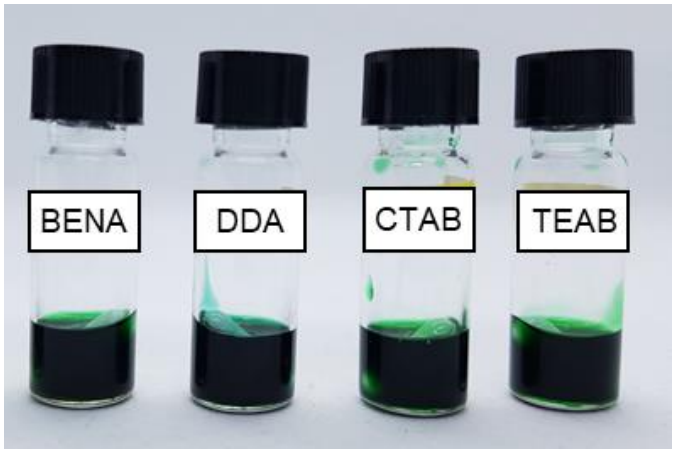

Figure S26. Solubilization of ICG-HIP complexes in CarboCell. ICG complexed with different co-ions (BENA, DDA, CTAB, TEAB) was incorporated into a CC3 formulation (SuBen:GTO:EtOH (60:25:15)). The approximate concentration of ICG was 2.5 mg/g.

Table S27. Complexation efficiency of ICG at different charge ratios. ICG was complexed with various co-ions at multiple charge ratios via the Bligh-Dyer method (n=1).

Charge ratio (ICG:co-ion)	Complexation efficiency (%)			
	TEAB	*CTAB*	*DDA*	*TOAB*
1:0.5	35.9	94.1	96.2	92.5
1:1	48.9	99.4	98.9	103.5
1:2	50.6	96.6	97.4	98.2

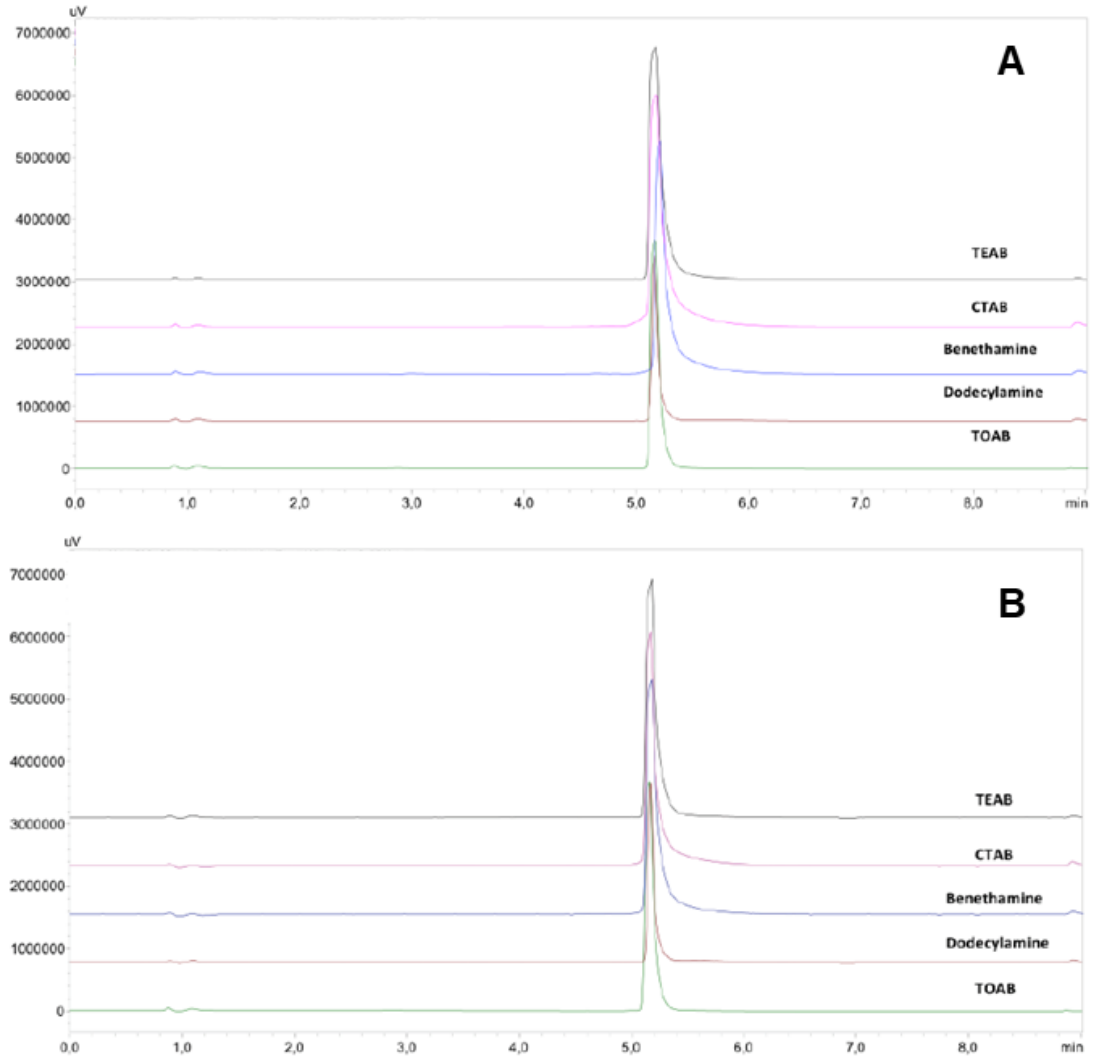

Figure S28. Stability of ICG-HIP complexes in MeCN. Chromatograms comparison of ICG complexed with different co-ions dissolved in MeCN (**A**) 30 min after preparation and (**B**) after 24 h of incubation at room temperature protected from light. The ICG concentration was 0.04 mg/mL and the chromatograms were recorded at 780 nm.

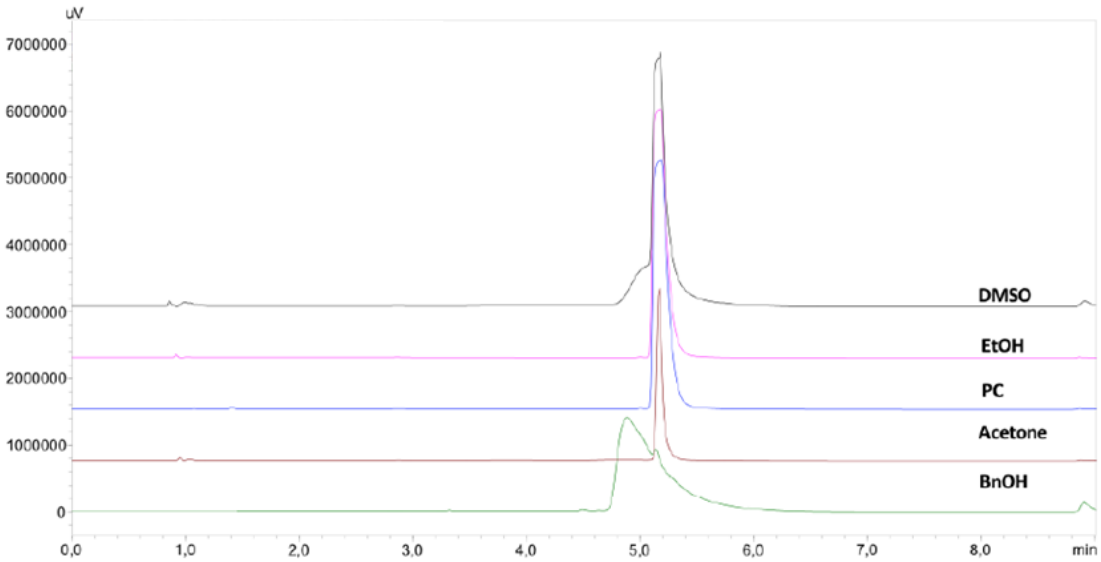

Figure S29. Stability of ICG in a HIP complex with BENA in various solvents. Chromatograms comparison of ICG-BENA dissolved at a concentration of 250 µg/mL in multiple solvents (**A**) 30 min after preparation and (**B**) after 5 days of incubation at 37°C protected from light. The chromatograms were recorded at 780 nm.

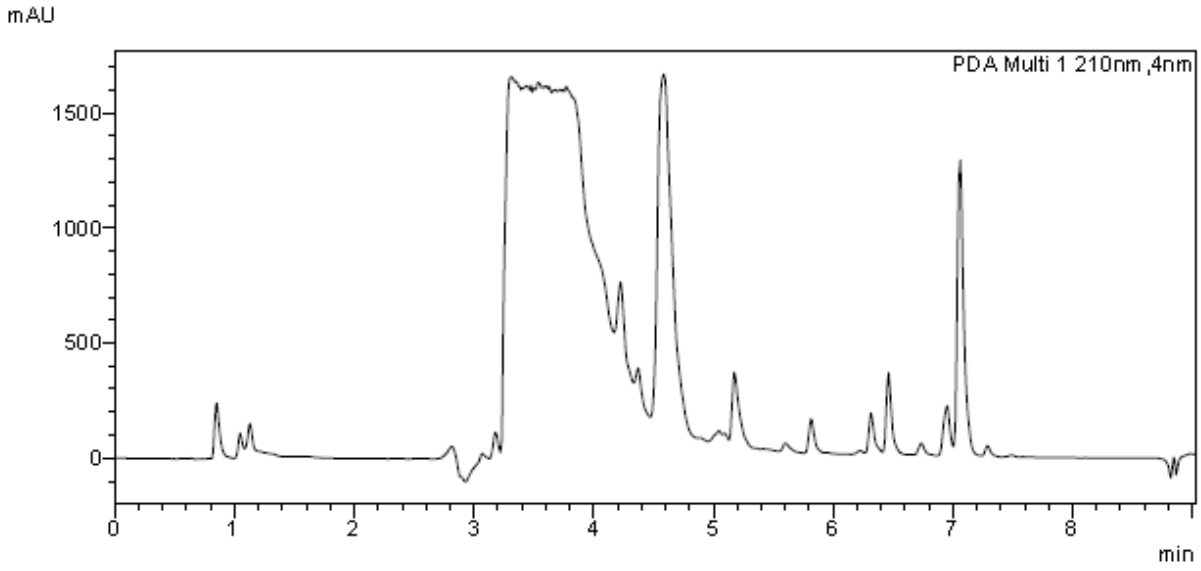

Figure S30. Analysis of BenOH. Pure BenOH was analyzed by UHPLC using the same method as for the other studies; the chromatogram was recorded at 210 nm.

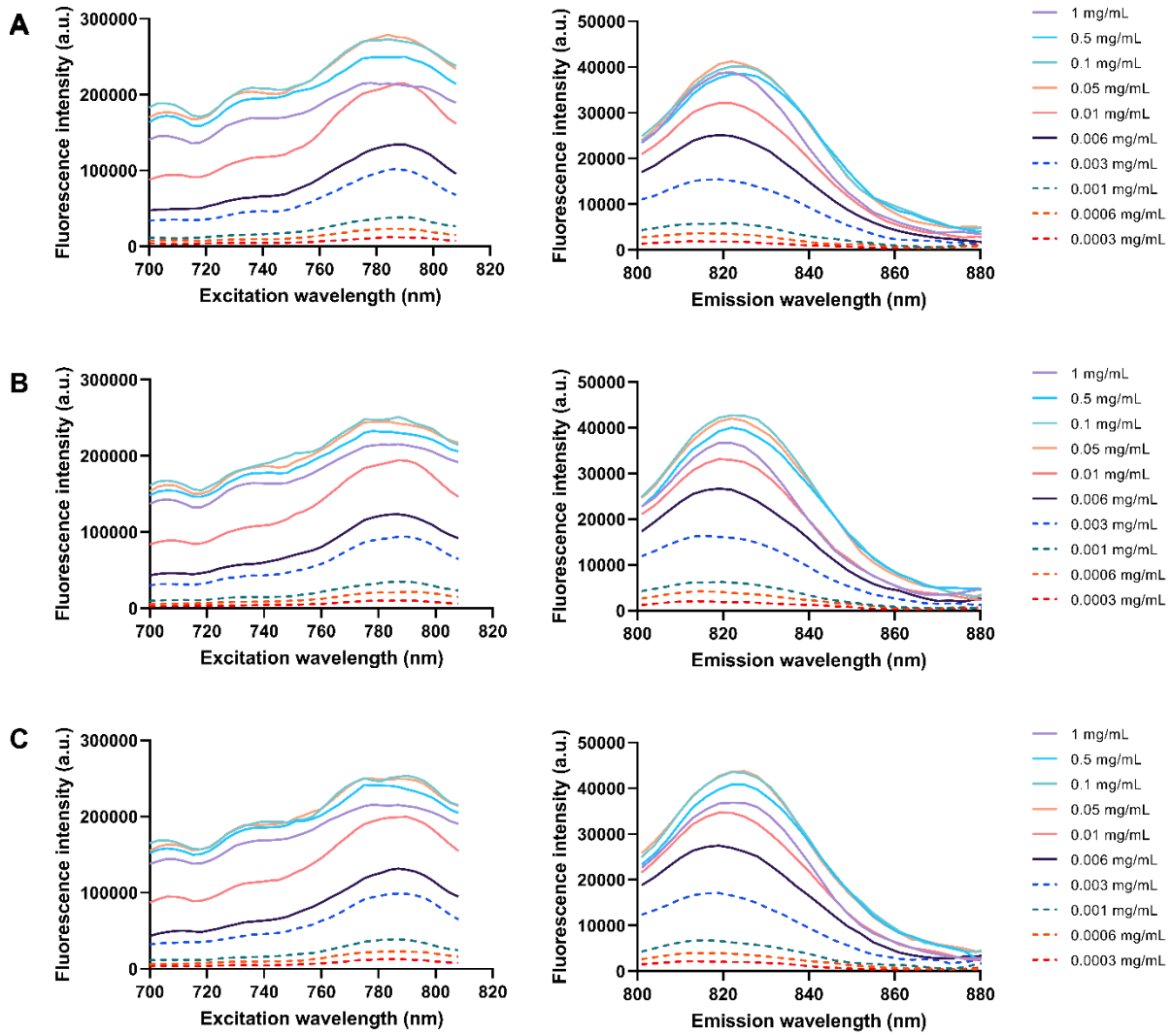

Figure S31. Fluorescence of ICG-HIP complexes as a function of concentration. Fluorescence excitation and emission spectra of (**A**) ICG-CTAB (**B**) ICG-DDA and (**C**) ICG-TOAB at varying concentrations. All solutions had EtOH as solvent.

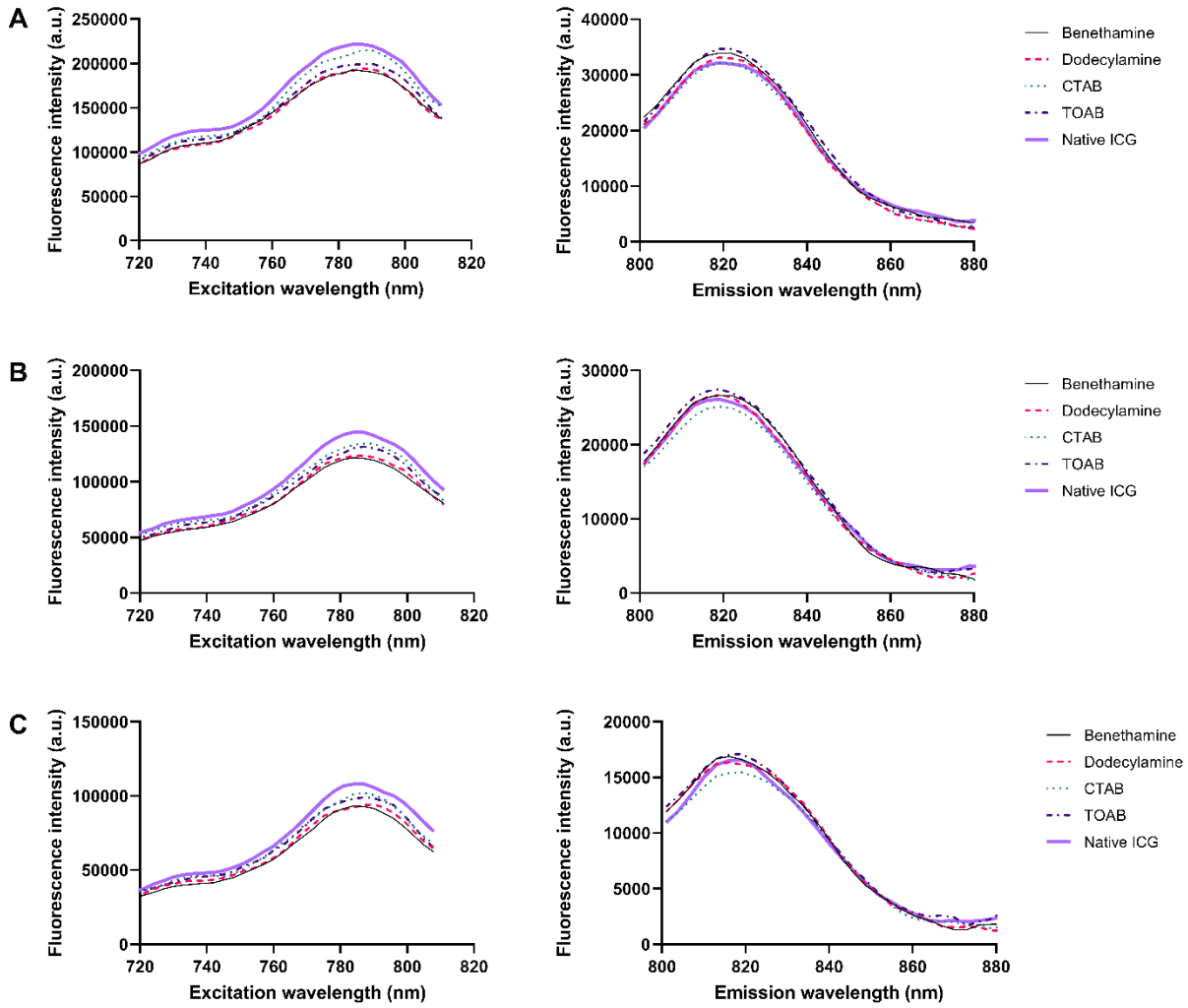

Figure S32. Fluorescence of ICG-HIP complexes as a function of co-ions. Fluorescence excitation and emission spectra of ICG-HIP complexes with multiple co-ions at concentrations of (**A**) 0.01 mg/g, (**B**) 0.006 mg/g, and (**C**) 0.001 mg/g.

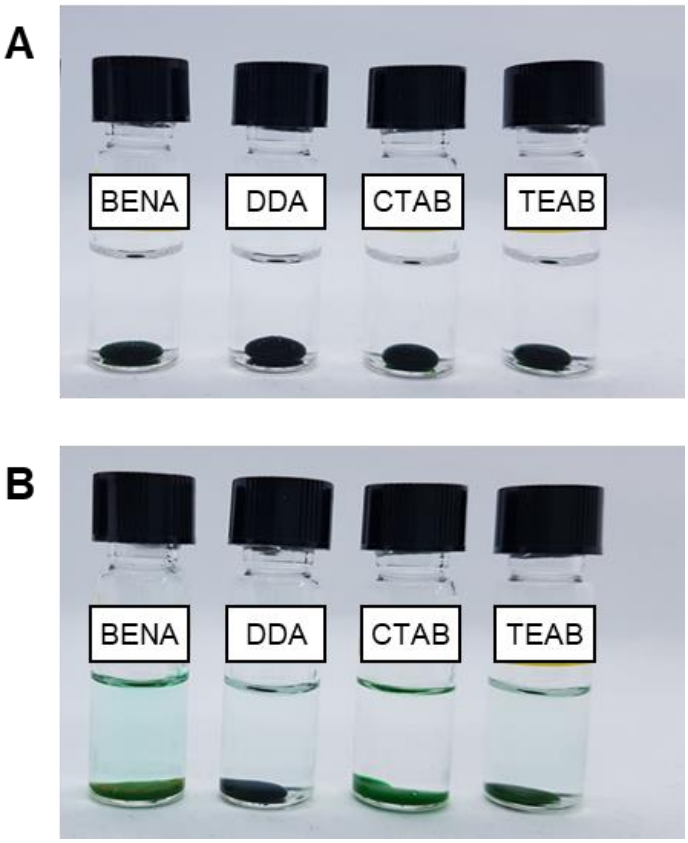

Figure S33. Morphology of injected depots. Images of injected CarboCell of ICG-HIP complexes with different co-ions (**A**) immediately after injection and (**B**) 72 h post-injection. All formulations had an approximate concentration of 2.5 mg/g ICG.

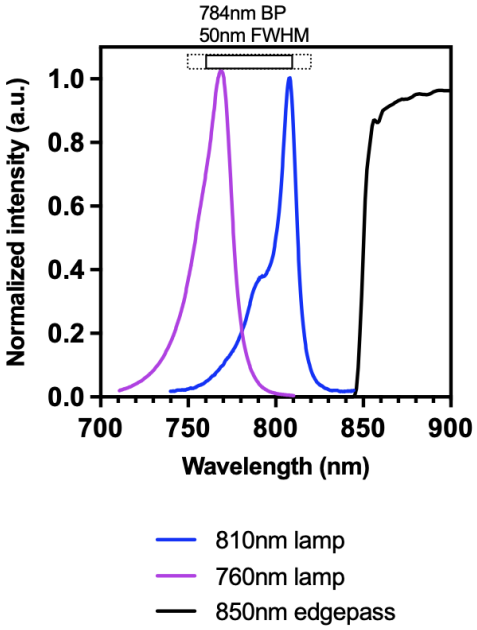

Figure S34. Spectral response of the NIR camera used for imaging in Chapter 6, including the X-Nite850 nm edge